OPTICAL CHARACTERIZATION OF CDTE, CDMGTE, AND CDTE/CDMGTE DOUBLE HETEROSTRUCTURES

By

Elizabeth G. LeBlanc, B.S.

A thesis submitted to the Graduate Council of
Texas State University in partial fulfillment
of the requirements for the degree of
Master of Science
with a Major in Physics
May 2016

Committee Members:

Thomas Myers, Chair

Mark Holtz

Alexander Zakhidov

FAIR USE AND AUTHOR'S PERMISSION STATEMENT

Fair Use

Duplication Permission

ACKNOWLEDGEMENTS

Special thanks to the Texas State University FPACE II research team, to collaborating FPACE II research groups at NREL, First Solar, ASU, CSU, CSOM, and WSU, Dr. Holtz' group for providing TRPL data, and to Dr. Zakhidov and James Shook for providing coding assistance.

TABLE OF CONTENTS

Page

LIST OF TABLES

Table **Page**

LIST OF FIGURES

Figure **Page**

1. INTRODUCTION

1.1 Introduction and Motivation

In an environment of growing energy consumption, cost effective and efficient approaches to renewable energy are rapidly becoming a major priority for the US Department of Energy (DoE). One of the leading possible alternatives is solar cell technology. In the US, the most efficient solar cell technologies are currently made of Gallium Arsenide (GaAs), however, due to high manufacturing costs, it is only used in space-based (or some Department of Defense) operations. In 2013, silicon (Si), in its various forms, dominated the global market share at over 93% of photovoltaic (PV) technologies.[1] While silicon is a fairly cheap material to use, it is not very efficient. It has been shown that thin film PV devices made of Cadmium Telluride, (CdTe) are more efficient than devices made of silicon, but only holds about 4% of the global market share.[1,2] In an effort to boost the use of CdTe in solar cell applications, the DoE launched the SunShot Initiative, a national collaborative effort to make solar energy cost-competitive with other forms of electricity by the end of the decade.[3] As part of the Initiative, the DoE has funded the FPACE II project which focuses on researching single crystal CdTe for PV applications. This project is a large collaboration effort involving research groups from the National Renewable Energies Laboratory (NREL), First Solar, Colorado School of Mines, Arizona State University, Colorado State University, Washington State University, and Texas State University.

CdTe is a II-VI semiconductor and has been shown to be a successful thin film solar cell material. However, much of its success has been due to art, not science. In

particular, it has recently been shown that photoluminescence intensity measurements done on bare CdTe epitaxially grown on a CdTe substrate were 4 orders of magnitude lower than CdTe/CdMgTe double heterostructures, indicating that interfacial recombination dominated the photoluminescence signal in the bare CdTe, contrary to previous conclusions that bulk recombination was dominant.[4] Based on this understanding, minority carrier lifetimes have been demonstrated in CdTe roughly 4 orders of magnitude higher than previously measured.

Each research group involved in the FPACE II project has a different focus, but the goal of the overall research is to approach the Shockley-Queisser limit for CdTe. The Shockley-Queisser limit is a theoretical efficiency ceiling for solar cells based on a single p-n junction.[5] There are three main factors that affect solar cell efficiency: blackbody radiation, radiative recombination, and spectral loss. The efficiency of a solar cell is described by the following

$$\eta = \frac{qV(\phi_s - \phi_r)}{\sigma T_{sun}^4} \quad (1)$$

Where q is the electric charge, V is the voltage across the device, ϕ_s is the incident photon flux entering the device, ϕ_r is the radiating photon flux leaving the device, σ is the Stefan-Boltzmann constant, and T_{sun} is the temperature of the sun.[6]

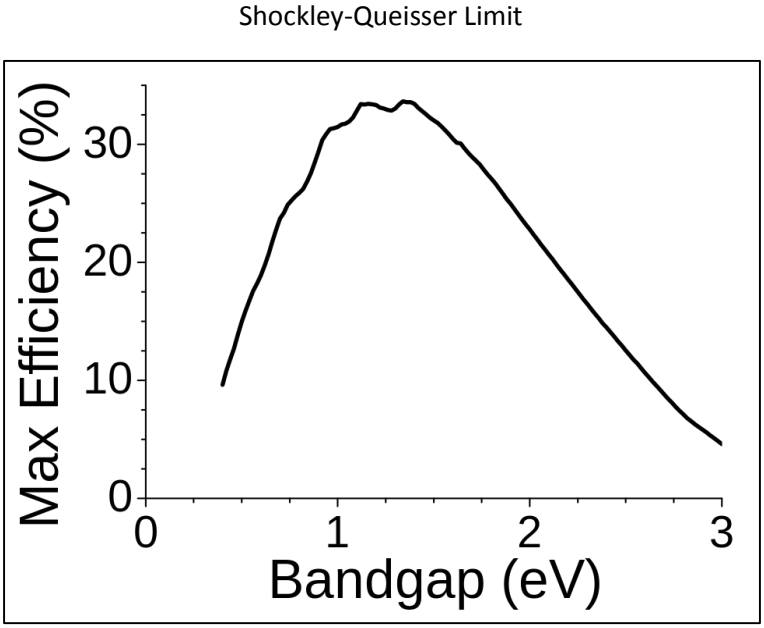

Figure 1. Depiction of the Shockley-Queisser limit. *CdTe has a band gap of about 1.5eV, putting it very near the optimal energy for maximum efficiency*[5]

The choice of CdTe was not an arbitrary one. Due to a band gap energy (to be discussed in detail later) of about 1.5eV, CdTe is a good candidate for achieving the maximum efficiency as described by the Shockley-Queisser limit as shown in Fig. 1.[7] The band gap of CdTe is only one of the advantages of this material for PV applications. CdTe also has a high absorption coefficient for incident photons.[8] This, in conjunction with the fact that its band gap is direct, allows photons with energy greater than the band gap to be absorbed within a few micrometers of the active layer. Because of this, less material is needed for the absorber layer in a device, leading to manufacturing cost savings. In addition, CdTe also permits both n and p-type doping.

The challenges involved in CdTe offer some insight as to why the material is not more widely used. One issue with CdTe has been the challenge in achieving high doping

concentrations (doping is the intentional introduction of impurities in an effort to increase the number of charge carriers in a semiconductor). This stems from the fact that many II-IV semiconductors exhibit self-compensating behavior, which is when charge carriers are used to satisfy broken bonds in the lattice structure, rather than contributing to the free carrier concentration. Another major challenge in CdTe PV devices is the formation of an Ohmic contact, which has proven to be difficult. Instead, a Schottky contact is often formed, limiting the ability of the device to produce the desired current-voltage characteristics.[9,10]

Texas State's involvement in the FPACE II project focuses on studying and developing growth processes via Molecular Beam Epitaxy (MBE) that reliably produce high crystalline quality CdTe samples. In order to qualify the crystalline structure of the samples that are grown via MBE, a number of optoelectronic characterization methods are used. These characterization techniques currently include Photoluminescence Intensity Measurements (PLI), Confocal Photoluminescence Imaging (c-PL), Spectral Ellipsometry, and Time-Resolved Photoluminescence (TRPL). This study will focus on these characterizations.

1.2 Band gaps and Photoluminescence

Before we start to discuss these techniques, a brief introduction to the physics behind how a solar cell works is needed. A solar cell, regardless of the specific material to be used, is based on semiconductor physics. Semiconductors are a special class of crystalline material with specific electrical properties, the most important of which for this study is a small energy band gap. The term band gap refers to an energy range where

electrons are forbidden to be due to quantum effects, and is the energy difference between the top of the valence band and the bottom of the conduction band. In the valence band electrons are bound to their atoms, while in the conduction band electrons are free to move throughout the material. It is possible for electrons to transition from one band to the other, if it has been given the requisite energy; namely, the band gap energy. Semiconductors differ from insulators in that insulators have very large band gaps; large enough that it is practically impossible for electrons to transition into the conduction band. Conductors on the other hand typically have extremely small or no band gaps, allowing electrons to flow freely. This band gap is different in each material and is determined by the material's unique molecular structure. An electron can gain the requisite amount of energy through heat (phonons) or light (photons).

Photons (quanta of light) have energy given by the relation

$$E_{photon} = \frac{hc}{\lambda} \tag{2}$$

Where h is Planck's contant, c is the speed of light, and λ is the wavelength of the light in vacuum. If a photon with energy greater than or equal to the band gap of a semiconductor strikes an electron in the valence band, then the photon can transfer its energy to the electron, allowing the electron to jump into the conduction band, leaving behind a hole in the valence band. This process is known as carrier generation. Both the electron in the conduction band, and the hole in the valence band, act as charge carriers in the material and can contribute to the overall current if the material is part of a device. However, the electron and hole are of opposite electrical charge, and are therefore attracted to each other. Recombination is the process of an electron falling back into the

valence band where a hole was. When the electron falls it loses energy in the form of a photon of energy equal to the band gap. This process of generating photons is called photoluminescence. Solar cells are able to generate current through the creation of electron-hole pairs (free charge carriers) and are specifically designed to prevent recombination. However, when studying the material properties of semiconductors, studying photoluminescence is an effective way of also studying how well the material will generate electron-hole pairs and thus is a measure of the efficacy of the material for photovoltaic applications.

1.3 Double Heterostructures

When studying material properties for use in PV applications, it is often useful to study double heterostructures (DHs or DH for singular). A heterostructure is a stack of dissimilar crystalline semiconductors. A few examples of heterostructures are shown in Fig. 2.

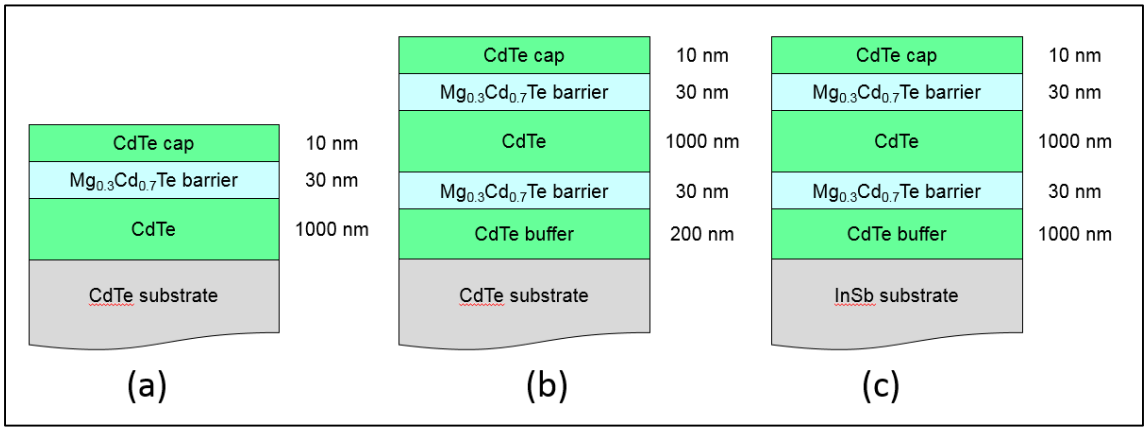

Figure 2. Depiction of heterostructures used in this study. *(a) A Single Heterostructure, composed of a single CdMgTe barrier. (b) A CdTe/CdMgTe DH grown on a CdTe substrate. (c) A CdTe/CdMgTe DH grown on an InSb substrate. In all cases, the CdTe cap is to prevent oxidation of the CdMgTe surface.*

A DH is a particular structure of semiconductor layers that is formed when two dissimilar semiconductors are grown into a "sandwich". The outer layers of this structure are made of a material with a larger band gap than the material in the middle. This particular structure confines charge carriers to the region of the semiconductor with the smaller band gap due to the discontinuity in the energy bands as shown in Fig. 3. The use of heterostructures is vital to solar cell design.[11] The reason for the use of DHs in this study will be made clear in proceeding discussions.

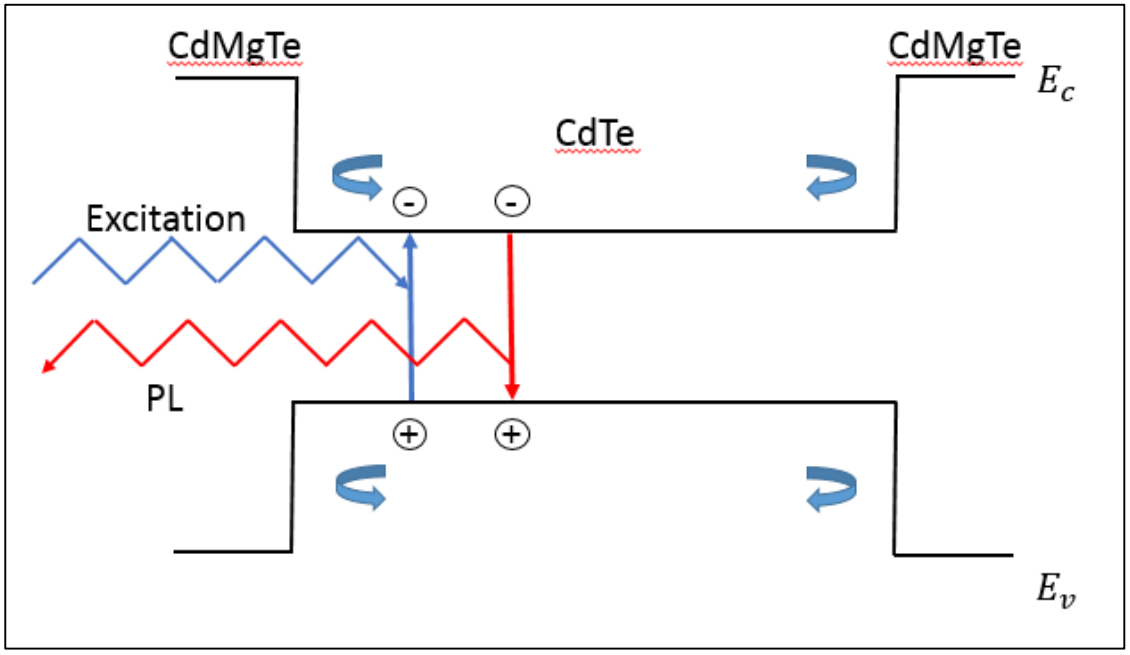

Figure 3. Depiction of the Energy Band structure in a CdTe/CdMgTe DH. *The larger band gap of the CdMgTe layers acts like a barrier for both electrons and holes that they cannot readily cross. This acts to confine the charge carriers to the CdTe layer. Also shown are excitation of carriers and subsequent photoluminescence. Note that neither photon is at its actual energy location relative to the bands shown, but are merely a depiction of the processes.*

2. DYNAMICS OF PHOTOLUMINESCENCE*

2.1 Generation and Recombination Mechanisms

To help better understand the basis for the measurements in my study, I will look at the fundamental physics of the dynamics of excess charge carriers involved in PLI measurements, and a comparison with TRPL measurements. In general, this leads to complicated modeling where simplified analytic expressions can only be derived in special cases. In order to gain some insight in interpretation of PLI and TRPL results, this section looks at one of these special cases. Both TRPL and PLI when we consider the low input intensity regime, are examples of low-injection conditions.

To begin, we need to develop the dynamics of charge carriers in a semiconductor. Through thermal or other means, electron-hole pairs are always being generated and are continually recombining in any semiconductor material. With no outside excitation source, and in thermal equilibrium, then the rate at which pairs are generated and the rate at which they recombine must be equal. The generation rate is defined as the number of electron-hole pairs generated per unit volume per unit time as a result of breakage of covalent bonds within the material. The recombination rate is defined as the number of recombination events per unit volume per unit time, and is related to the mean time between generation of an electron-hole pair and the subsequent recombination, often referred to as the mean carrier lifetime. In thermal equilibrium, we call the concentration

* The formalism in this chapter closely follows that found in many textbooks on the subject. For example, see [32] and [33].

of electrons n_0 and the concentration of holes p_0, which are functions of space. In this scenario, we may say that

$$g_{0n} = \frac{n_0}{\tau_{n_0}} \qquad \text{and} \qquad g_{0p} = \frac{p_0}{\tau_{p_0}} \tag{3}$$

Where g_{0n} and g_{0p} are the thermal generation rates of electrons and holes respectively, and τ_{n_0} and τ_{p_0} are the mean electron and hole lifetimes respectively. In every situation, the generation rates and the recombination rates of the two carriers must be equal

$$g_n = g_p \qquad \text{and} \qquad \frac{n}{\tau_n} = \frac{p}{\tau_p} \tag{4}$$

Where g_n and g_p are the actual generation rates (no longer thermal equilibrium), n and p are the local concentration and τ_n and τ_p are the lifetimes of the carriers. Note that in the general case, $\tau_{n,p}$ can be a function of n and p.

Recombination can occur through a number of different mechanisms. In the preceding discussion, we have used $\frac{p}{\tau_p}$ to define the recombination rate, however, a more general expression can be written as

$$\frac{dp}{dt} = \frac{dn}{dt} = -R(n,p) \tag{5}$$

Where

$$R(n,p) = r(n,p)[np - n_i^2] \tag{6}$$

The recombination rate $R(n,p)$ has units of $(cm^{-3}s^{-1})$ and $r(n,p)$ is a volume recombination rate function specific to a particular recombination mechanism and has units of cm^3/s. The intrinsic carrier concentration is given by n_i. There are three main

mechanisms for recombination: Shockley-Read-Hall (SRH), Auger, and Radiative recombination. In CdTe, Auger recombination does not play a significant role, and so, will not be investigated here. We will begin by examining SRH recombination

SRH recombination, also known as trap-assisted recombination, involves minority-carrier capture at defects in a semiconductor that have quantum levels in the band gap of the sample. The SRH recombination rate is given by

$$R_{SRH} = \frac{\sigma_p \sigma_n v_{th} N_t [pn - n_i^2]}{\sigma_n \left[n + n_i \, exp\left(\frac{E_t - E_i}{kT}\right)\right] + \sigma_p \left[p + n_i \, exp\left(\frac{E_i - E_t}{kT}\right)\right]} \tag{7}$$

Here, N_t is the volume density of deep level states; σ_p and σ_n are the hole and electron capture cross sections respectively; E_t is the energy level of the trap and E_i is the midpoint of the band gap. The electron and hole concentrations are n and p respectively and v_{th} is the thermal velocity of the electron or hole. From this, we see that the volume recombination rate function will of course be given by

$$r(n,p)_{SRH} = \frac{\sigma_p \sigma_n v_{th} N_t}{\sigma_n \left[n + n_i \, exp\left(\frac{E_t - E_i}{kT}\right)\right] + \sigma_p \left[p + n_i \, exp\left(\frac{E_i - E_t}{kT}\right)\right]} \tag{8}$$

If we now consider the introduction of injected (excess) holes, Δp (which is typically assumed to be equal to Δn), then the instantaneous values of n and p can be written as

$$\begin{aligned} p &= p_0 + \Delta p \\ n &= n_0 + \Delta p \end{aligned} \tag{9}$$

Let's now turn our attention to the case of an n-type semiconductor material ($n_0 \gg p_0$). In this case, we can derive the recombination rate for holes at a single energy level at E_t

in the forbidden energy gap. Here, we let $n_0 = N_D$, where N_D is the concentration of n-type dopants, and we approximate p_0 as zero, yielding

$$R_{SRH} = \frac{\sigma_p \sigma_n v_{th} N_t [\Delta p N_D - \Delta p^2]}{\sigma_n \left[N_D + \Delta p + n_i \, exp\left(\frac{E_t - E_i}{kT}\right)\right] + \sigma_p \left[\Delta p + n_i \, exp\left(\frac{E_i - E_t}{kT}\right)\right]} \quad (10)$$

If we instead consider a p-type semiconductor ($p_0 \gg n_0$), then we can derive a similar expression for the recombination rate of electrons at an energy level E_t in the forbidden gap. This time we let $p_0 = N_A$, where N_A is the concentration of p-type dopants, and we approximate n_0 as zero, yielding, with which we find

$$R_{SRH} = \frac{\sigma_p \sigma_n v_{th} N_t [\Delta p N_A - \Delta p^2]}{\sigma_n \left[\Delta p + n_i \, exp\left(\frac{E_t - E_i}{kT}\right)\right] + \sigma_p \left[N_A + \Delta p + n_i \, exp\left(\frac{E_i - E_t}{kT}\right)\right]} \quad (11)$$

A plot of the SRH recombination rate versus the trap energy E_t is shown below.

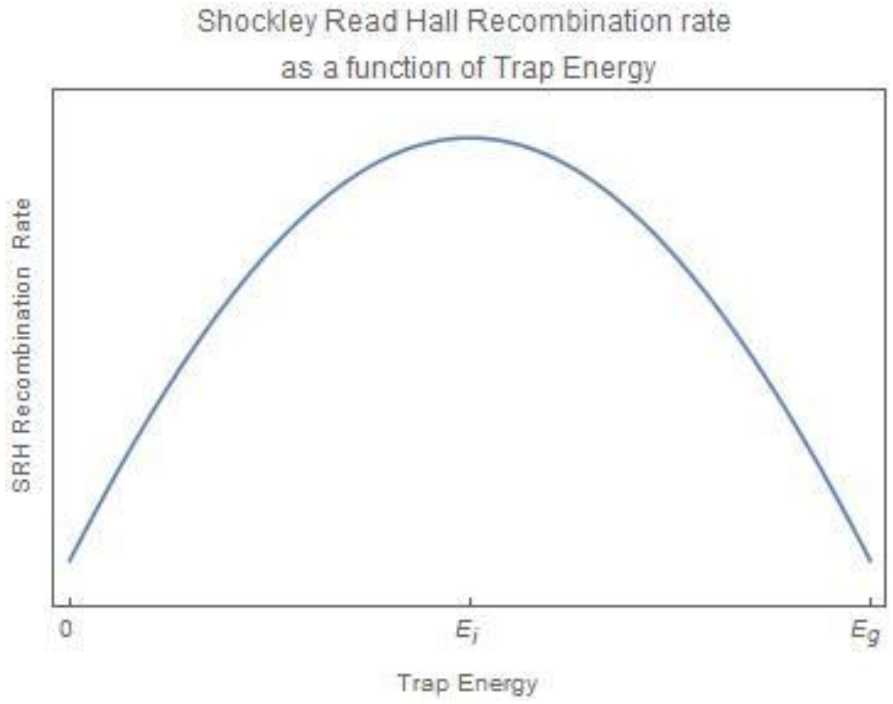

Figure 4. Plot of Shockley Read Hall Recombination rate versus Trap Energy.

Here, we see a peak at $E_t = E_i$, indicating that the maximum recombination rate occurs at defect levels at or near the midgap. In general, as $E_t \to E_i$, the SRH recombination rate increases. When the defect level lies near the conduction band or the valence band, then thermal emission of carriers in those traps causes the recombination rate to decrease. Specifically, when the defect level is near the valence band, the denominator term, $n_i exp\left(\frac{E_i - E_t}{kT}\right)$ becomes very large. This term describes the emission of captured holes to the valence band. Because of hole emission, the hole occupancy of the trap is small and the SRH recombination rate is decreased, or quenched. Depending on the value $|E_i - E_t|$, we can describe two different types of defects. When this energy difference is approximately half the band gap, i.e. when E_t lies near the conduction or valence band, then the defect is called a trap. However, when the energy level lies near the midgap, E_i, then the SRH recombination rate becomes very large and recombination is the most probable event. Thus, midgap centers where $E_i \sim E_t$ are very effective recombination sites, and these types of defects are called recombination centers.

We now turn to an investigation of surface recombination. Surface recombination is really a form of SRH recombination because the surface of a semiconductor is an inherent source of deep-level defect states caused by the dangling bonds at the crystal surface that result from the interruption of the periodicity in the lattice. This causes the surface to have a very high recombination rate, and because of this the concept of surface recombination velocity (SRV) was introduced. The states induced in the energy gap of a semiconductor by the surface are called surface states. Besides breaking the periodicity of the lattice, the surface is also likely to pick up impurities such as atmospheric gases and metals. The removal of dangling bonds and their associated surface states is called

passivation. The term interface is used to describe the effects of the semiconductor boundary. Thus, sometimes the terms surface and interface are used interchangeably. The semiconductor interfaces play a heavy role in minority carrier transport in PV devices, so their study is crucial. It has been shown that the potential barrier at semiconductor interfaces can be more controlled by charges in the interface states than by the contact potential difference of the materials.

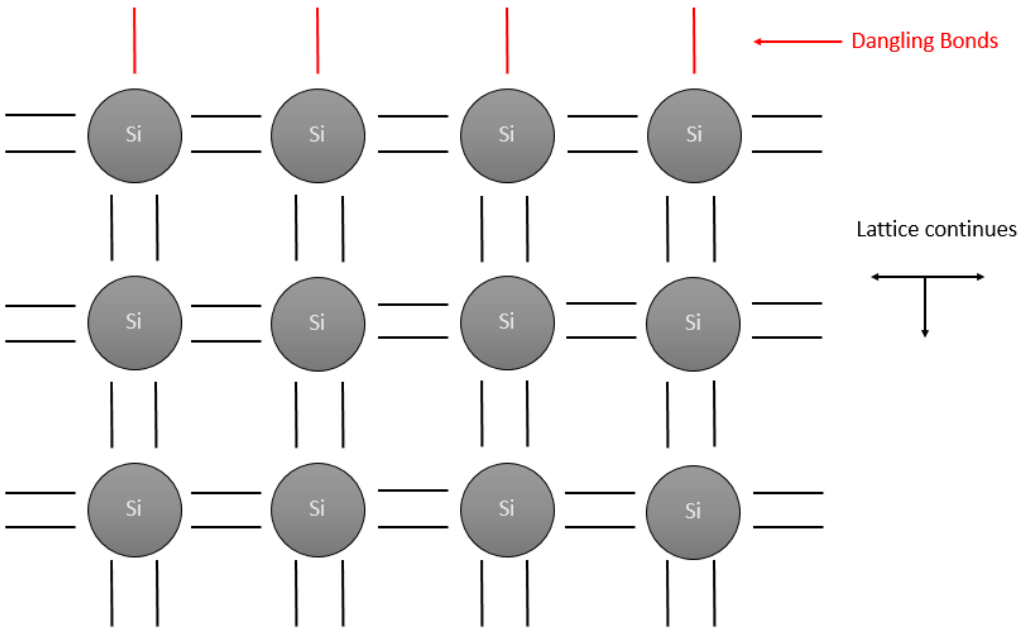

Figure 5. Depiction of dangling bonds on the surface of a semiconducting lattice structure. *Here, the surface of Si is shown, however for a real Si surface oxygen will bond with the dangling bonds very quickly.*

Early measurements of minority carrier lifetime in GaAs indicated that bulk lifetimes were dominated by the surface effects. In order to reduce the dominating effects of the large SRV, the introduction of a confinement structure occurred. This confinement structure was a GaAs/AlGaAs DH. Confinement was produced by the upward band

bending in the active layer, thus creating a "surface free" absorber layer. Only once this occurred were larger lifetime measurements observed, and AlGaAs became essential to GaAs technology. Because initial lifetime measurements of CdTe also produced poor results, it was decided to investigate DHs to determine if surface effects were dominating the measurements. The surface or interface recombination velocity is important in the operation of most compound semiconductors.

Surface states are usually represented by a continuum of states in the forbidden gap. However, using a model that has a single level at energy E_t is useful in describing the recombination effects. With this model, when analyzing the surface or interface, one can assume that these single-level SRH defects lie in a two dimensional plane bounding the semiconductor. We can derive this model by beginning with the assumption that all recombination centers lie in two thin sheets of unit (1 cm^2) cross-sectional area and thickness Δt. The fractional active volume containing defect centers is $\Delta t/d$, where d is the total thickness of the active region. The recombination rate for the volume containing the defects can be written generically as

$$R = \sigma v_{th} N_t \frac{2\Delta t}{d} \frac{\rho}{1 + \frac{2n_i}{N} \cosh\left(\frac{E_t - E_i}{kT}\right)} \tag{12}$$

Where ρ is the excess minority carrier density, and N is the majority carrier density. The defect containing volume becomes a surface upon shrinking Δt to 0. In this limit, we write

$$\lim_{\Delta t \to 0} \left| \frac{d\rho_s}{dt} = \sigma v_{th} N_t \frac{2\Delta t}{d} \frac{\rho_s}{1 + \frac{2n_i}{N} \cosh\left(\frac{E_t - E_i}{kT}\right)} \right|$$

(13)

Here, we note that the excess volume density ρ became ρ_s, the excess density (cm^{-3}) at the surface. One can define a planar density N_{st} (surface traps) as the limiting value of the product $N_t \Delta t$ as Δt goes to 0. The previous relation was an average over the entire volume, but recombination only happens at the surface, thus

$$R_{vs} = \frac{2}{d} \frac{\rho_s \sigma v_{th} N_{st}}{1 + \frac{2n_i}{N} \cosh\left(\frac{E_t - E_i}{kT}\right)} \qquad (cm^{-3}s^{-1}) \tag{14}$$

Where we have renamed the recombination rate to be R_{vs} to express that this rate is valid in the volume near the surface. We can use this expression to define the surface recombination R_s and the SRV:

$$R_{vs} = \frac{2}{d} R_s = \frac{2s}{d} \rho_s \tag{15}$$

From which we see that the surface recombination rate $(cm^{-2}s^{-1})$, is clearly equal to $\rho_s s$, where s is the SRV. We also see that

$$s = \frac{\sigma v_{th} N_{st}}{1 + \frac{2n_i}{N} \cosh\left(\frac{E_t - E_i}{kT}\right)} \tag{16}$$

And has units of (cm/s). For most real surfaces, s involves a summation over a number of near mid-gap states, however, this will suffice for our purposes.

We now turn to radiative recombination which is the process by which a conduction band electron and a valence band hole recombine to produce a photon of energy $hv \sim E_g$. Band to Band luminescence is referred to by a number of terms, depending on the source of excitation. For our purposes, we will focus on photoluminescence, which is the common term for the optical generation of

recombination luminescence. Photoluminescence intensity is much greater for direct band gap semiconductors as opposed to indirect band gap semiconductors. The photon emission rate for band to band transition is given by

$$R_L = r_{rad} np = B_{rad}(np - n_i^2) \tag{17}$$

And has units of $(cm^{-3}s^{-1})$. Here, p is the hole density, n is the electron density and B_{rad} is the radiative recombination coefficient which is a term that comes from summing the dipole matrix elements connecting the valence and conduction bands (beyond the scope of this study). B_{rad} has units of cm^3/s and is the specific recombination mechanism for radiative recombination (the r in the first definition of recombination). It is important to note that this equation gives the light output per unit volume L of a semiconductor with n electrons and p holes per cubic meter. For a semiconductor under illumination, a density of $\rho(r)$ electron-hole pairs is generated and the general expression for the net photoluminescence from the volume V is written in terms of an integral:

$$I_{PL} = B \int \left[\left(p_0 + \rho(r)\right)\left(n_0 + \rho(r)\right) - n_i^2\right] dV \tag{18}$$

$$= B \int [\rho(r)^2 + \rho(r)(p_0 + n_0)] dV \tag{19}$$

Under steady state, $\rho(r)$ remains constant in time, and therefore, so does I_{PL}.

2.2 Developing the Continuity Equations

Now that we have discussed recombination mechanisms, we return to developing the charge carrier dynamics in a semiconductor. By considering the change in the particle

flux in a crystal with rectangular geometry, and realizing that there will be g_p holes generated and p/τ_p holes lost in a given volume per unit time, we can arrive at an expression for the change in the number of holes per unit time. When put into mathematical form, this consideration results in the following relations

$$-\nabla \cdot \boldsymbol{J_p} + \ g_p - \frac{p}{\tau_p} = \frac{\partial p}{\partial t} \qquad \text{for holes}$$

$$-\nabla \cdot \boldsymbol{J_n} + \ g_n - \frac{n}{\tau_n} = \frac{\partial n}{\partial t} \qquad \text{for electrons}$$

Where the first term in both expressions describes the change in particle flux. These equations form what are called the continuity equations. The solutions of these equations, under appropriate boundary conditions describe the distribution of the electron and hole concentrations as a function of space and time. The solutions also give a complete description of the transport behavior of electrons and holes in the semiconductor under non-equilibrium conditions. In order to determine specific solutions to these equations, it is necessary to express the current in terms of carrier concentration. Current may be written as a sum of diffusion flux density and drift current density

$$\begin{aligned} \boldsymbol{J}_p &= -D_p \nabla p + p\mu_p \boldsymbol{E} \\ \boldsymbol{J}_n &= -D_n \nabla n - n\mu_n \boldsymbol{E} \end{aligned} \tag{21}$$

Where D is the diffusion coefficient or diffusivity, ∇p and ∇n are the concentration gradients and μ is the mobility of the carrier. Here, the first term describes diffusive current and is analogous to heat flow in the presence of a temperature gradient. The second term describes drift current as caused by the presence of an electric field $\boldsymbol{E}$.

Substituting these expressions for the particle flux density into the continuity equations yields

$$D_p\nabla^2 p - \mu_p\nabla\cdot(p\boldsymbol{E}) + g_p - \frac{p}{\tau_p} = \frac{\partial p}{\partial t}$$
$$D_n\nabla^2 n - \mu_n\nabla\cdot(n\boldsymbol{E}) + g_n - \frac{n}{\tau_n} = \frac{\partial n}{\partial t} \tag{22}$$

We can transform the divergence terms (terms involving $\nabla\cdot\boldsymbol{E}$) using the vector identity which states

$$\nabla\cdot(c\boldsymbol{A}) = \boldsymbol{A}\cdot\nabla c + c\nabla\cdot\boldsymbol{A} \tag{23}$$

At the same time, we can also define the generation rate as the sum of the thermal generation rate and excess generation rate:

$$g = g_0 + g' \tag{24}$$

Where g' is the excess generation rate. Using the vector identity (6), the resulting generation rate (7) and knowing that the thermal generation rate can be expressed as

$$g_{0n} = \frac{n_0}{\tau_{n_0}} \text{ and } g_{0p} = \frac{p_0}{\tau_{p_0}} \tag{25}$$

The continuity equations (22) take the form

$$D_p\nabla^2 p - \mu_p(\boldsymbol{E}\cdot\nabla p + p\nabla\cdot\boldsymbol{E}) + g_p' - \left(\frac{p}{\tau_p} - \frac{p_0}{\tau_{p_0}}\right) = \frac{\partial p}{\partial t}$$
$$D_p\nabla^2 p - \mu_p(\boldsymbol{E}\cdot\nabla p + p\nabla\cdot\boldsymbol{E}) + g_p' - \left(\frac{p}{\tau_p} - \frac{p_0}{\tau_{p_0}}\right) = \frac{\partial p}{\partial t} \tag{26}$$

At this point, one must be careful to realize that we have two equations, but three unknowns, $n, p,$ and $\boldsymbol{E}$. We can think of the electric field as the sum of an applied field and an internal field, which arises from the fact that the diffusivity of the electrons and holes may be different. In order to move forward with a determination of solutions to the continuity equations, we need a third equation. We can get an expression for the electric field using Poisson's equation relating the electric filed and the net charge density $e(p - n + N_d - N_a + p_a - n_d)$:

$$\nabla \cdot \boldsymbol{E} = \frac{4\pi\rho}{\kappa} = \frac{4\pi e(p - n + N_d - N_a + p_a - n_d)}{\kappa} \tag{27}$$

Where $N_d,$ and N_a are the doping density of donors and acceptors respectively, and p_a and n_d are the concentrations of available mobile holes and electrons, respectively. Because the applied field has no internal sources or sinks, its divergence is zero, and therefore, the divergence of $\boldsymbol{E}$ is just the divergence of the internal field.

We now have three equations and three unknowns, however, there is no way to solve these equations in a straightforward analytical manner. Therefore we must make some reasonable physical approximation which will allow us to arrive at a solution which will be adequate for most cases of practical importance. To begin, we will make the assumption of electrical neutrality or Charge Balance, which is the assumption that the excess electron density $\Delta n = n - n_0$ is exactly balanced by the excess hole density, $\Delta p = p - p_0$. Put another way

$$\Delta n = \Delta p = n - n_0 = p - p_0 \tag{28}$$

This assumption will only be used for the charge transport equations. Recall that the divergence of the electric field was given by the divergence of the internal field, which arises precisely because the concentrations of the holes and electrons are not the same, so we will therefore not apply this assumption to the divergence of the electric field equation. We will also assume that the sample is homogeneous, where the impurity density is uniform throughout. For such samples, the equilibrium carrier concentrations, p_0 and n_0 are constants. Therefore the gradients and time derivatives of the local concentrations, n and p, are equal to the gradients and derivatives for the excess concentrations, Δn and Δp. Recall that generation must occur in pairs. With this in mind, we realize that

$$g'_p = g'_n = g' \tag{29}$$

Rearranging the expression for the excess carriers (11), we find

$$n = \Delta n + n_0 \text{ and } p = \Delta p + p_0$$

$$\text{And} \tag{30}$$

$$n - p = n_0 - p_0$$

With these results, we find that the continuity equations (26) become

$$\begin{aligned} D_p \nabla^2(\Delta p) - \mu_p(\boldsymbol{E} \cdot \nabla(\Delta p) + p\nabla \cdot \boldsymbol{E}) + g' - \left(\frac{p_0 + \Delta p}{\tau_p} - \frac{p_0}{\tau_{p_0}}\right) &= \frac{\partial(\Delta p)}{\partial t} \\ D_n \nabla^2(\Delta p) - \mu_n(\boldsymbol{E} \cdot \nabla(\Delta p) + n\nabla \cdot \boldsymbol{E}) + g' - \left(\frac{p_0 + \Delta p}{\tau_p} - \frac{p_0}{\tau_{p_0}}\right) &= \frac{\partial(\Delta p)}{\partial t} \end{aligned} \tag{31}$$

We can eliminate the divergence terms by multiplying the first equation by $n\mu_n$, multiplying the second equation by $p\mu_p$ and adding the two equations together to get

$$\frac{n\mu_n D_p + p\mu_p D_n}{n\mu_n + p\mu_p}\nabla^2(\Delta p) - \frac{\mu_n\mu_p(n_0 - p_0)}{n\mu_n + p\mu_p}\boldsymbol{E}\cdot\nabla(\Delta p) + g' - \left(\frac{p_0 + \Delta p}{\tau_p} - \frac{p_0}{\tau_{p_0}}\right) = \frac{\partial(\Delta p)}{\partial t} \tag{32}$$

From here, we may use the Einstein relations, which are valid in all systems which obey Boltzmann statistics and state

$$D_p = \frac{\mu_p kT}{e} \quad \text{and} \quad D_n = \frac{\mu_n kT}{e} \tag{33}$$

Through this relation of the mobilities and the diffusivity coefficients, we arrive at a simplification of the form of the continuity equation

$$D^*\nabla^2(\Delta p) - \mu^*\boldsymbol{E}\cdot\nabla(\Delta p) + g' - \frac{\Delta p}{\tau} = \frac{\partial(\Delta p)}{\partial t} \tag{34}$$

Where

$$D^* = \frac{(n+p)D_n D_p}{nD_n + pD_p} = \frac{(n_0 + p_0 + 2\Delta p)D_n D_p}{(n_0 + \Delta p)D_n + (p_0 + \Delta p)D_p} \tag{35}$$

$$\mu^* = \frac{(n_0 - p_0)\mu_n\mu_p}{n\mu_n + p\mu_p} = \frac{(n_0 - p_0)\mu_n\mu_p}{(n_0 + \Delta p)\mu_n + (p_0 + \Delta p)\mu_p} \tag{36}$$

And τ, the excess carrier lifetime, is defined by

$$\frac{\Delta p}{\tau} = \frac{p_0 + \Delta p}{\tau_p} - \frac{p_0}{\tau_{p_0}} \tag{37}$$

The quantities D^* and μ^* are called the ambipolar diffusivity and mobility respectively, and, in general depend on the excess carrier concentration. The ambipolar coefficients are important for the high-injection case, which will be discussed later.

Once again, with the continuity equation above (34), we have arrived at an expression that is impossible to solve analytically, and we must proceed using approximate or numerical methods. If the excess carrier concentration, Δp, is much less than the larger of the equilibrium concentrations, n_0 or p_0, then the diffusivity, D^*, and the mobility, μ^*, are practically constant and analytic solutions to the continuity equation can be obtained. This is often called the low-injection case

$$\Delta p \ll (n_0, p_0) \tag{38}$$

Now let's turn our attention to lifetimes in the low-injection case. Recall that the equilibrium generation rate is defined by

$$g_{n0} = \frac{n_0}{\tau_{n0}} = \frac{p_0}{\tau_{p0}} \tag{39}$$

Now consider the following

$$\Delta p \ll n_0,$$

$$n_0 \gg p_0,$$

$$\Delta p \cong p_0$$

Then, the generation rate is expressed by

$$g = \frac{n_0 + \Delta p}{\tau_n} = \frac{p_0 + \Delta p}{\tau_p} \tag{40}$$

After generation, the density of electrons is basically unchanged ($n_0 + \Delta p \cong n_0$). This means that the probability per unit time that an individual hole will encounter an electron is also practically unchanged. This in turn means that the hole lifetime is independent of Δp and is unchanged. However, the density of holes has essentially doubled. This means that the probability per unit time that an electron will encounter a hole has doubled. Therefore, the electron lifetime is dependent on Δp and in this case, has decreased by half. To summarize, the lifetime of the minority carrier is basically independent of Δp, while the majority carrier is not. Based on the excess carrier lifetime, defined as

$$\frac{\Delta p}{\tau} = \frac{p_0 + \Delta p}{\tau_p} - \frac{p_0}{\tau_{p_0}} = \frac{n_0 + \Delta p}{\tau_n} - \frac{n_0}{\tau_{n_0}} \tag{41}$$

We arrive at the following

For strongly n-type ($\Delta p \ll n_0$): $\tau_p = \tau_{p_0} \quad \rightarrow \quad \tau = \tau_{p_0}$

For strongly p-type ($\Delta p \ll p_0$): $\tau_n = \tau_{n_0} \quad \rightarrow \quad \tau = \tau_{n_0}$

From here, we see that the excess carrier lifetime τ, simply reduces to the minority carrier lifetime in the low-injection condition. The diffusivity and mobility also reduce and simplify the continuity equation.

<u>For n-type ($\Delta p \ll n_0$)</u>

$$D^* \rightarrow D_p$$

$$\mu^* \rightarrow \mu_p \tag{42}$$

$$D_p \nabla^2(\Delta p) - \mu_p \boldsymbol{E} \cdot \nabla(\Delta p) + g' - \frac{\Delta p}{\tau} = \frac{\partial(\Delta p)}{\partial t}$$

For p-type ($\Delta p \ll p_0$)

$$D^* \rightarrow D_n$$

$$\mu^* \rightarrow \mu_n \tag{43}$$

$$D_n \nabla^2(\Delta p) - \mu_n \boldsymbol{E} \cdot \nabla(\Delta p) + g' - \frac{\Delta p}{\tau} = \frac{\partial(\Delta p)}{\partial t}$$

2.3 At the Surface

Up until this point we have focused on the charge dynamics in the bulk of the material. In order to continue with our analysis of the continuity equation as it pertains to this study, we need to examine what is happening at the surface of the material. It may be tempting to say that the boundary conditions arising from the surface would simply be to confine carriers, and that the electron and hole currents must vanish at the surface. However, the situation is not that simple, as carriers can recombine at the surface through mechanisms that are independent of the mechanisms that regulate the recombination rate in the bulk such as surface recombination. Based on this, one might say that there should be a deficiency of carriers at the surface because they are recombining, which would cause a diffusive current of carriers towards the surface. Once again, the situation is not that simple because thermal generation of carriers also takes place at the surface. And, if we are considering the case of thermal equilibrium, then the generation rate must precisely equal the recombination rate at the surface. Therefore, in thermal equilibrium, there is no net flux of carriers towards the surface and no change in the carrier concentrations in the region near the surface. This situation is an example of a general

principle of statistical mechanics called the Principle of Detailed Balancing or Microscopic Reversibility, which simply states that in thermal equilibrium any given microscopic process and the reverse process must proceed at the same rate. It is important to realize that the surface generation rate, which is a function of temperature only and is independent of the local charge carrier concentration, and the surface recombination rate, which depends directly upon the local carrier concentrations, must be equal in thermal generation.

To study the effect of surface recombination, we begin by considering the flux interchange between the surface and the interior region of the sample. Consider the figure below:

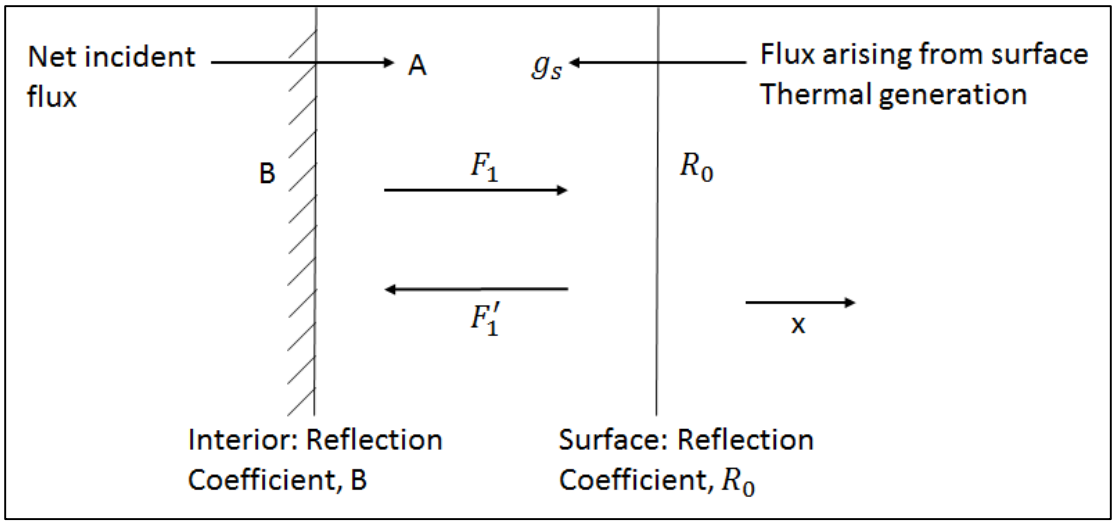

Figure 6. Diagram of the particle flux interchange between the bulk and the surface, in the region near the surface

First, we need to define a few parameters. R_0 is the surface relection coefficient which describes the probability that a single carrier collision with the surface will be sent back

to the bulk. The term $1 - R_0$ describes the probability that a particle will recombine at the surface. B is the bulk reflection coefficient which describes the probability that a carrier will reappear at the surface. The total flux flowing from the interior towards the surface, F_1, is made up of the incident flux, A, plus that part of the reverse flux which is reflected by the bulk. The total flux flowing from the surface towards the interior, F_1', is made up of the flux arising from the surface thermal generation, g_s, plus that part of the reverse flux which is reflected by the surface. So then, we can say that

$$F_1 = A + BF_1' \tag{44}$$

and

$$F_1' = g_s + R_0 F_1 \tag{45}$$

Which can be solved simultaneously, yielding

$$F_1 = \frac{A + Bg_s}{1 - R_0 B} \tag{46}$$

And

$$F_1' = \frac{g_s + AR_0}{1 - R_0 B} \tag{47}$$

From here, we can use the Boltzmann result that concludes that for a distribution of free particles which obey Boltzmann statistics, the number of particles per unit time crossing a plane surface of unit area in either direction is just $pv_{th}/4$, where p is the local particle concentration. With this, we can conclude

$$F_1 = F_1' = \frac{p_0 v_{th}}{4} \tag{48}$$

We can then use this result to obtain expressions for the thermal generation rate and the value of the incident flux A_0, under thermal equilibrium

$$g_s = \frac{p_0 v_{th}}{4}(1 - R_0) \tag{49}$$

$$A_0 = \frac{p_0 v_{th}}{4}(1 - B) \tag{50}$$

Because we are not just interested in the case of thermal equilibrium, we shall now assume a small departure from equilibrium, such that the Boltzmann distribution is still approximately correct. In this case, the two fluxes will no longer be equal. If we are considering a point x_0, then we can perform a Taylor Expansion on the previous definitions of the two fluxes to obtain

$$F_1 = \left[p(x_0) - \alpha\lambda\left(\frac{\partial p}{\partial x}\right)_{x_0}\right]\frac{v_{th}}{4} \tag{51}$$

$$F_1' = \left[p(x_0) + \alpha\lambda\left(\frac{\partial p}{\partial x}\right)_{x_0}\right]\frac{v_{th}}{4} \tag{52}$$

Where α is a constant of the order of unity and λ is the mean free path. The quantity in brackets represents the local concentration of particles at the place where the flux arriving at x_o originated. If we sum these two expressions and are considering the flux near the surface, then it is clear that

$$F_1 + F_1' = \frac{p_s v_{th}}{2} \tag{53}$$

Where p_s represents the concentration in the region near the surface. Making some substitutions into this expression (53) for the fluxes in the surface region (46) and (47),

including our expression for the thermal generation rate (49), we can obtain an expression for A, whose magnitude depends upon the nature of the excess carrier distribution which may be present in the bulk:

$$A = \frac{p_s v_{th}}{2}\frac{1 - R_0 B}{1 + R_0} - \frac{p_0 v_{th}}{4}\frac{(1 - R_0)(1 + B)}{1 + R_0} \tag{54}$$

The difference between the two fluxes is the net flux of carriers, which, if there is no electric field present, is equal to the net diffusion current evaluated at the surface. After some rather tedious algebra, it may be shown that

$$F_1 - F_1' = \frac{A(1 - R_0)}{1 - R_0 B} - \frac{g_s(1 + B)}{1 - R_0 B} = \frac{(p_s - p_0)v_{th}}{2}\frac{1 - R_0}{1 + R_0} = -D_p\left(\frac{\partial(\Delta p)}{\partial x}\right)_s \tag{55}$$

This is a statement of the surface boundary condition which must be applied to the continuity equation. The condition may be written in a more convenient form as

$$-D_p\left(\frac{\partial(\Delta p)}{\partial x}\right)_s = s \cdot (\Delta p)_s \tag{56}$$

Where the s subscripts indicate quantities to be evaluated at the surface, and s is the SRV. We see that we now have a second definition of the SRV, this time in terms of reflection probabilities, which can be expressed as

$$s = \frac{v_{th}}{2}\frac{1 - R_0}{1 + R_0} \tag{57}$$

The surface boundary condition can be written in a more general vector form as

$$-D_p[\boldsymbol{n} \cdot \nabla(\Delta p)]_s = s \cdot (\Delta p)_s \tag{58}$$

Where $\boldsymbol{n}$ is a unit surface normal vector pointing outwards.

2.4 The Steady State

Now that we have considered the effects of the surface of the material, let us now consider a uniform semiconductor sample which is illuminated with light of a wavelength such that the absorption coefficient of the material is small. In this case, the illumination may be consider to be approximately uniform through the crystal, and will lead to a constant generation rate that is proportional to the intensity of the light. We will call this the steady-state condition, and is a good representation of PLI measurements when performed at low input intensities, such that we are still considering the low-injection case. The sample geometry will be a large, thin rectangle as shown in Fig. 7.

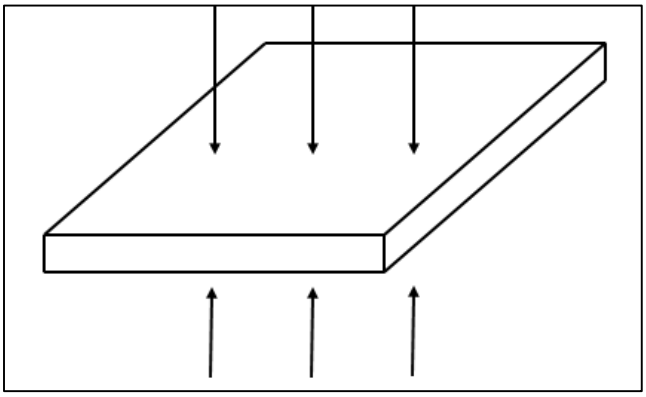

Figure 7. Semiconducting sample geometry for consideration in Steady and Transient State conditions.

At first glance, the DHs that we study here do not look like the geometry shown. However, because of the band bending that occurs due to the differences in band gap between CdTe and CdMgTe, the CdMgTe layers act as barriers that the charge carriers cannot cross, confining the carrier to the CdTe layer, thus simulating this geometry so that it is appropriate for analysis. From here we will construct the appropriate continuity

equation based on the geometry at hand. If we call the direction of incident light the x direction, and the y and z dimensions of the sample are sufficiently large, then the excess carrier concentration varies essentially only along the x-direction. With this, we may reduce the general continuity equation to a single dimension:

$$D_p \frac{d^2\Delta p}{dx^2} - \mu_p \boldsymbol{E} \cdot \nabla(\Delta p) + g' - \frac{\Delta p}{\tau_p} = \frac{\partial(\Delta p)}{\partial t} \tag{59}$$

We may reduce it further with the assumption that there is no electric field and that for the steady-state condition, there is no change in excess carrier concentration with respect to time ($\partial(\Delta p)/\partial t = 0$). So then, this becomes

$$\frac{d^2\Delta p}{dx^2} - \frac{\Delta p}{L_p^2} = -\frac{g'}{D_p} \tag{60}$$

Where L_p is the diffusion length of the carrier and is defined as

$$L_p^2 = D_p \tau_p \tag{61}$$

In the continuity expression above, we are assuming that we are dealing with an extrinsic n-type material where Δp is small compared to the majority carrier density. The solution to this inhomogeneous second order differential equation will be given by the solution to the corresponding homogeneous equation plus the particular solution. Here, the particular solution will simply be given by

$$\Delta p = \frac{g' L_p^2}{D_p} = g' \tau_p \tag{62}$$

And the general solutions to the homogeneous equation are given by

$$\Delta p_1 = A' e^{\frac{x}{L_p}} \quad and \quad \Delta p_2 = B' e^{-\frac{x}{L_p}} \tag{63}$$

Because any linear combination of solutions is itself a solution, for reasons that will become obvious momentarily, we may write the general solution for the excess carrier density profile as

$$\Delta p(x) = A cosh\left(\frac{x}{L_p}\right) + B sinh\left(\frac{x}{L_p}\right) + g'\tau_p \tag{64}$$

From the symmetry of the of the sample we are considering, we see that $\Delta p(x)$ must be an even function, and therefore the coefficient of the sinh function, B, must equal zero, so that our general solution to the differential equation becomes

$$\Delta p(x) = A cosh\left(\frac{x}{L_p}\right) + g'\tau_p \tag{65}$$

Where the particular solution describes the carrier density in the bulk of the material. From here, we can apply the surface boundary condition

$$-D_p\left(\frac{\partial(\Delta p)}{\partial x}\right)_s = s \cdot (\Delta p)_s \tag{66}$$

At either surface $\left(x = \frac{\pm x_0}{2}\right)$, to the above expression, rearrange, and find that

$$A = \frac{-sg'\tau_p}{s\, cosh\frac{x_0}{2L_p} + \frac{D_p}{L_p} sinh\frac{x_0}{2L_p}} \tag{67}$$

With this result, we arrive at a final solution

$$\Delta p(x) = g'\tau_p \left[1 - \frac{s\,cosh\frac{x}{L_p}}{s\,cosh\frac{x_0}{2L_p} + \frac{D_p}{L_p} sinh\frac{x_0}{2L_p}}\right] \tag{68}$$

This expression describes the excess charge carrier concentration profile within the sample. Unfortunately, this expression is not very intuitive, but we can see that it depends on the SRV. We can also see that when the SRV is zero, then the carrier concentration is constant and therefore uniform throughout the sample.

Now that we have this result, we can begin to talk about Photoluminescence. Recall that PLI is proportional to the Radiative Recombination rate defined as

$$R_L = B_{rad} np \tag{69}$$

In low-injection, this reduces to

$$R_L \approx B_{rad} n_0 \Delta p \tag{70}$$

Where the first two terms are approximately constant. The PLI is then given by

$$PLI = \int R_L dx = \int B_{rad} n_0 \Delta p\, dx = B_{rad} n_0 \int \Delta p\, dx \tag{71}$$

With this we can say that

$$PLI \sim \int \Delta p(x)\, dx \tag{72}$$

To get a better sense of what is going on here, the excess carrier concentration was plotted for CdTe in Mathematica© using appropriate values for D_p and L_p and various values of SRV. The exact material parameters used are shown in Table 1.

Table 1. Material parameters for CdTe used in calculations

Parameter	Value
μ_e	1000 cm^2/Vs
μ_h	100 cm^2/Vs
D_e	25.88 cm^2/s
D_h	2.588 cm^2/s
τ_{bulk}	2 μs
L_e	71.9 μm
L_h	22.7 μm

The excess carrier concentration was normalized such that

$$\frac{\Delta p(x)}{g'\tau_p} = 1 \tag{73}$$

When the SRV is zero. The normalized excess carrier concentrations were then integrated over the length of the sample to give a representative PLI that was then normalized such that

$$PLI(SRV = 0) = 1 \tag{74}$$

These results where then plotted against SRV. This was done for both N-type and P-type CdTe, with layer thicknesses of 0.5μm and 5μm, the results of which are shown below, starting with N-type CdTe with thickness of 0.5μm.

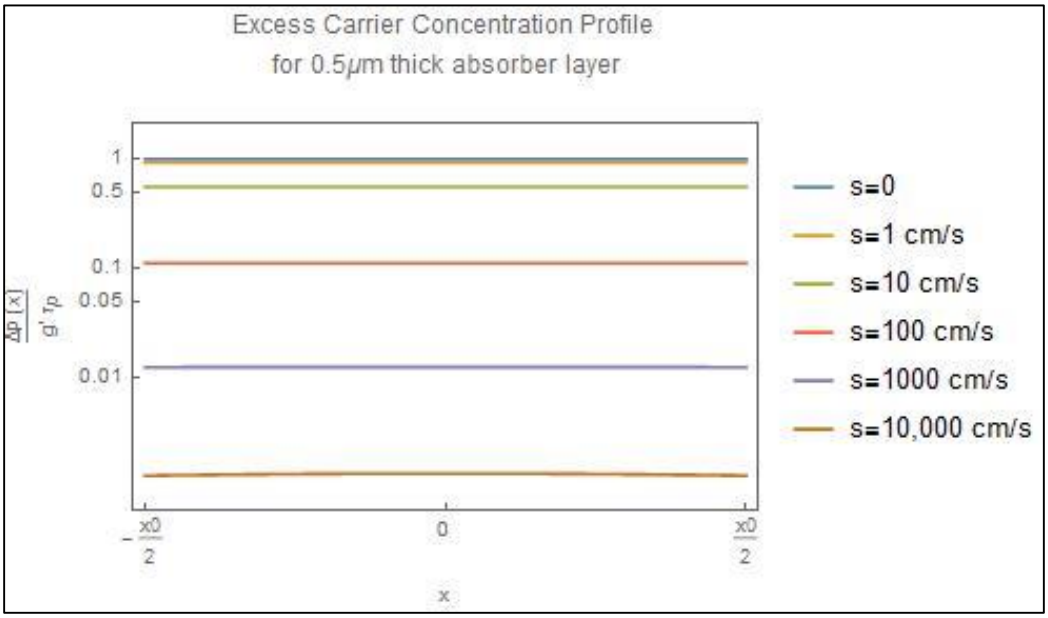

Figure 8. Plot of the excess carrier concentration profile within an N-type CdTe sample of length x0=0.5μm with various values of SRV.

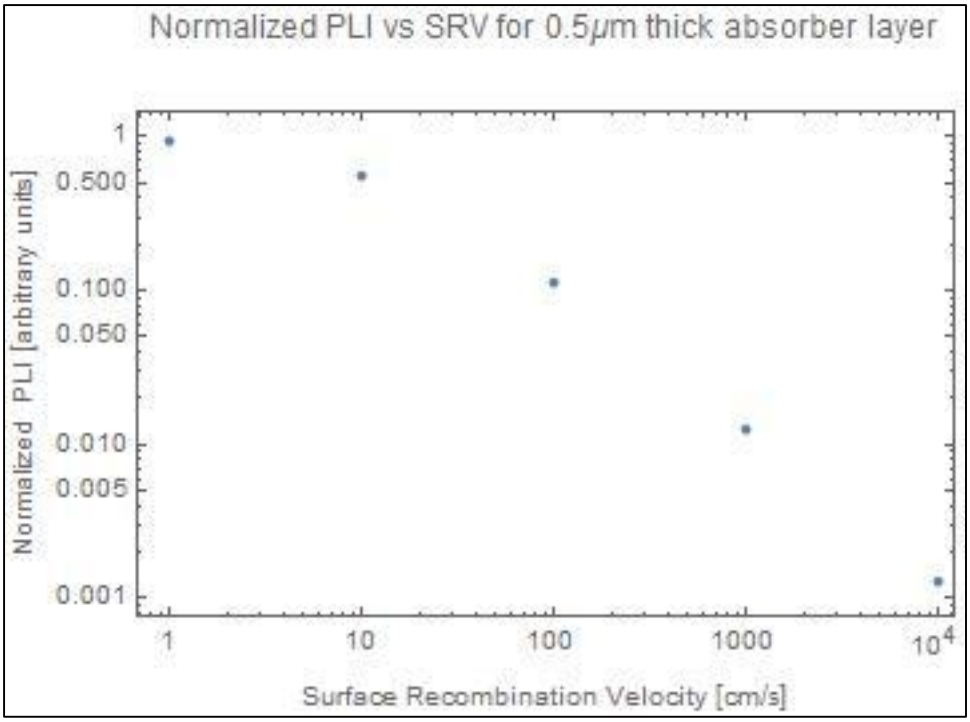

Figure 9. Plot of the Normalized PLI vs SRV for an N-type CdTe sample of length x0=0.5μm

From Fig. 8, we see that the excess carrier concentration does not vary much throughout the sample. This is due to the diffusion length being so long in comparison with the thickness of the sample. We also see that as SRV increases, the concentration of excess carriers decreases. We also see from Fig. 9 that as SRV increases by four orders of magnitude, the PLI decreases by three orders.

For an N-type CdTe sample that was 5μm thick,

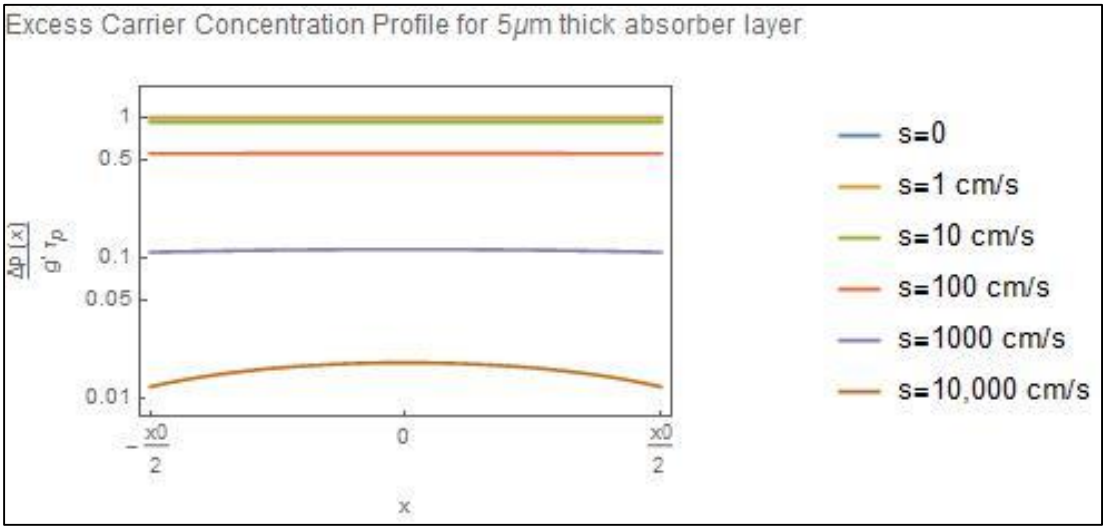

Figure 10. Plot of the excess carrier concentration profile within an N-type CdTe sample of length x0=5μm with various values of SRV.

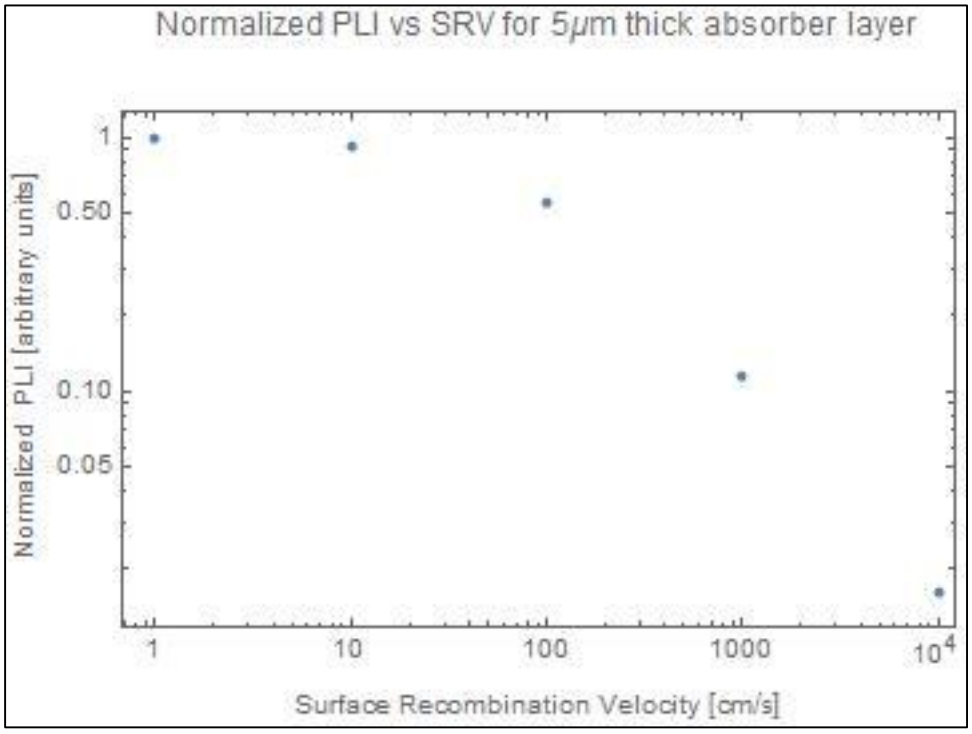

Figure 11. Plot of the Normalized PLI vs SRV for an N-type CdTe sample of length x0=5μm

From Fig. 10, we again see that the excess carrier concentration does not vary much throughout the sample, however this time we do see that at high values of SRV, there is a higher concentration of excess carriers in the middle of the sample than closer to the surfaces, indicating that in this case, the surface has a higher effect on the variation in the excess carrier concentration. It is also important to note that for this sample, which is an order of magnitude thicker than the previous, the excess carrier concentrations for the highest values of SRV are also an order of magnitude higher than the previous. We also see from Fig. 11 that the previous trend is still true, namely that as SRV increases, PLI decreases, although this time it is less quickly. We should also note that our values for PLI are also an order of magnitude larger for the highest values of SRV.

The same exploration was also done for P-type CdTe Samples

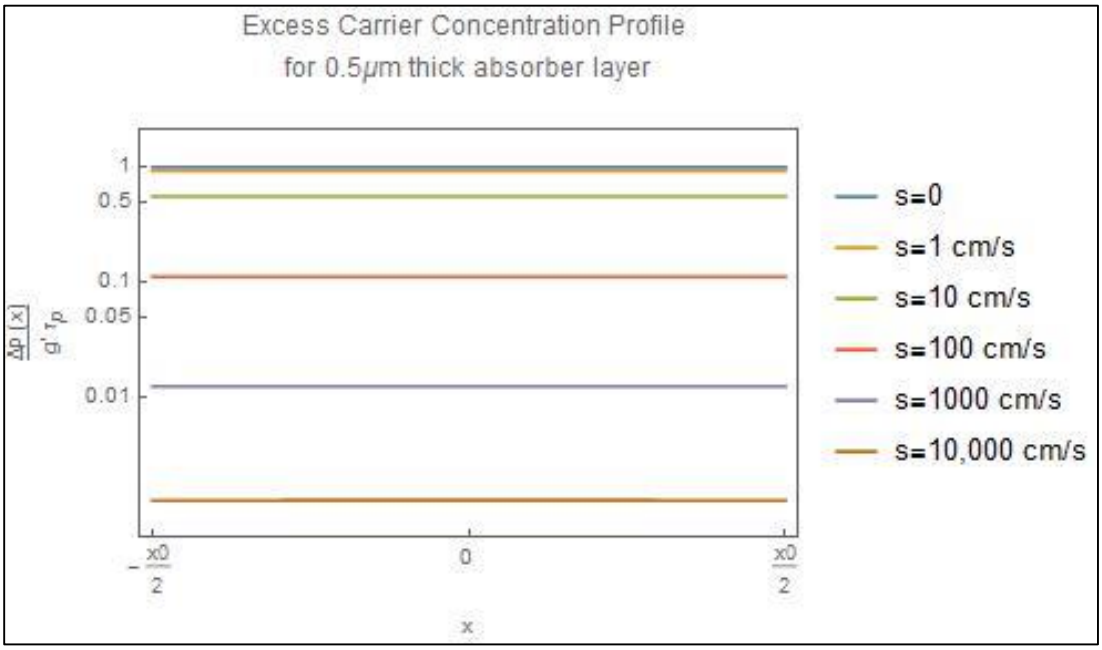

Figure 12. Plot of the excess carrier concentration profile within a P-type CdTe sample of length x0=0.5μm with various values of SRV.

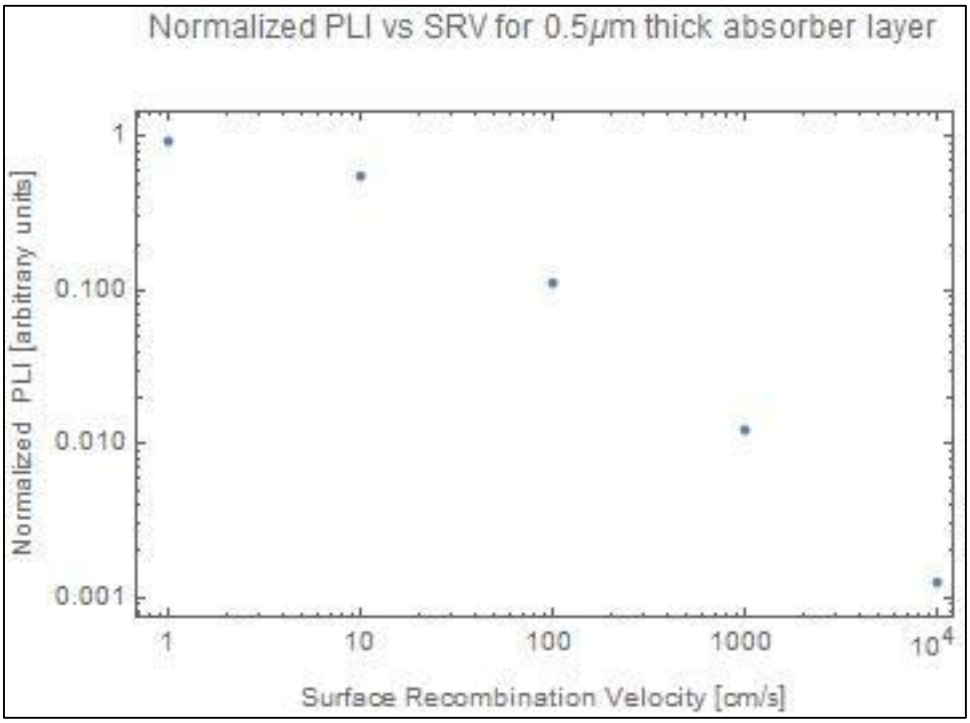

Figure 13. Plot of the Normalized PLI vs SRV for a P-type CdTe sample of length x0=0.5μm

Here, we see similar trends as we did for the N-type sample of the same size. From Fig. 12 we see very little variation in concentration throughout the sample and we also see that the carrier concentration decreases with increasing SRV. From Fig. 13 we again see that the PLI decreases by about 3 orders of magnitude with a four order of magnitude increase in SRV.

We now turn our attention to a P-type CdTe sample that was 5μm thick

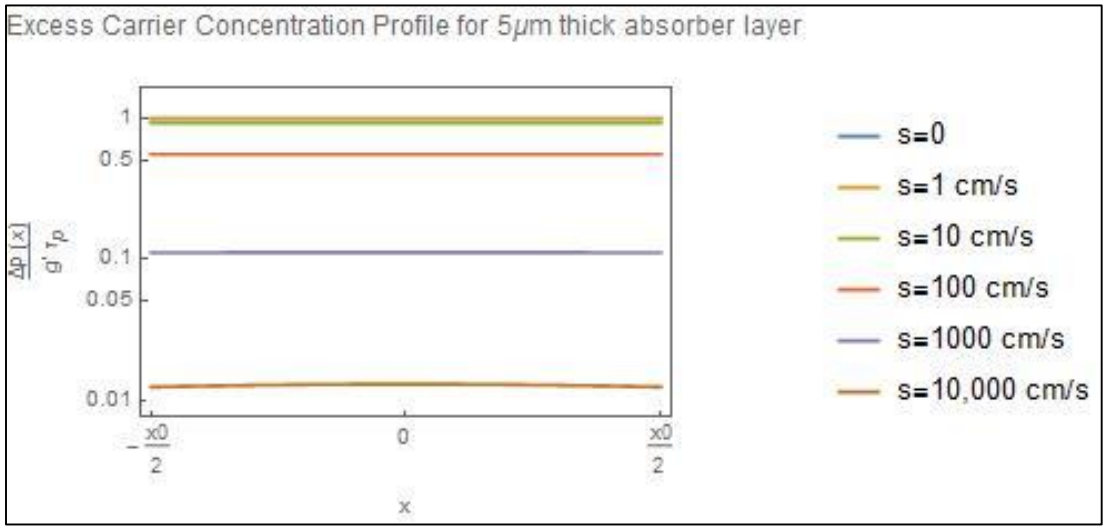

Figure 14. Plot of the excess carrier concentration profile within a P-type CdTe sample of length x0=5μm with various values of SRV.

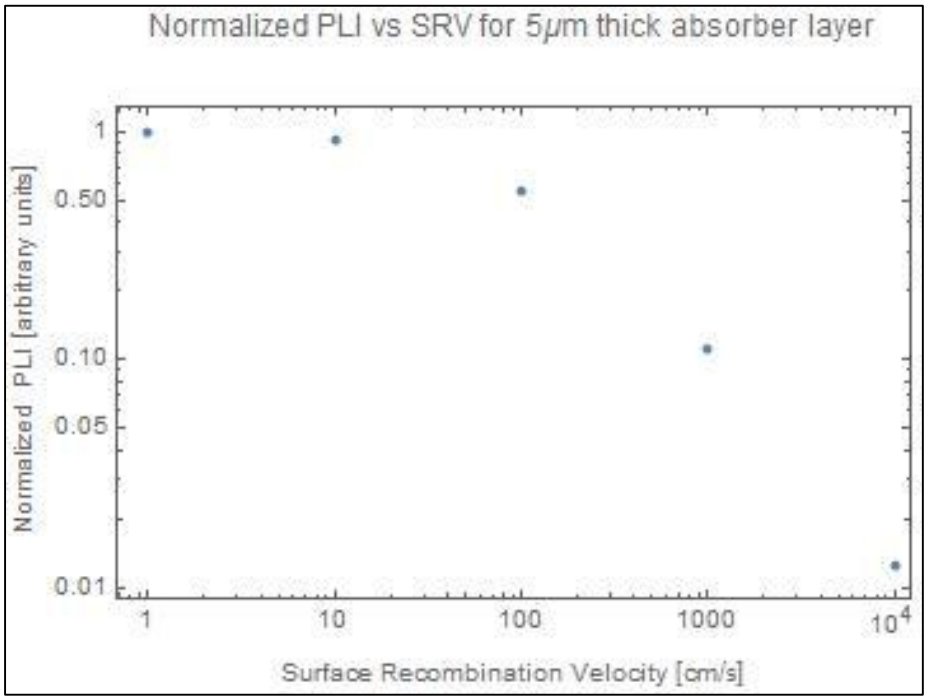

Figure 15. Plot of the Normalized PLI vs SRV for a P-type CdTe sample of length x0=5μm

Again we see similar trends here as we did for the N-type sample of the same thickness, with one major difference. We see from Fig. 14 that even at high SRV values, the excess carrier concentration is still fairly uniform throughout the sample, and as with the N-type sample, the concentration for the highest values of SRV are about an order of magnitude higher than the thinner P-type sample. From Fig. 15, we see that as we increase the SRV four orders of magnitude, the PLI only decreases by two orders of magnitude. As indicated by the exact values found in Appendices A and B, the PLI in the 5 μm thick n-type sample was about 25% larger than the corresponding p-type sample for the largest SRV. This, as well as the flatter profiles found in the p-type material is indicative of the higher diffusion velocity of the minority electron in p-type material compared to that of the minority hole in n-type CdTe.

From these investigations we can conclude that a thicker active layer will have a higher excess carrier concentration and higher PLI. This makes sense because there is a smaller surface area to volume ratio in the thicker samples, meaning that carriers are less likely to interact with the surface, because they must diffuse farther. We also see that a p-type sample is likely to have a more uniform excess charge carrier concentration than an N-type sample, and interacts with the surface less. It is because of this that absorber layers are typically p-type. The Mathematica codes used to generate these plots are available in Appendices A and B.

2.5 The Transient State

Now that we have looked at steady state illumination in low-injection, let us now turn our attention to the transient state, which allows a description of TRPL measurements. To begin, let us consider the same scenario as the steady state condition, with the exception that the light source will generate a uniform carrier density p_1 everywhere in the sample at time $t = 0$, at which instant the excitation source is abruptly turned off. This will be called the transient state condition, and this time the continuity equation

$$D_p \frac{d^2\Delta p}{dx^2} - \mu_p \boldsymbol{E} \cdot \nabla(\Delta p) + g' - \frac{\Delta p}{\tau_p} = \frac{\partial(\Delta p)}{\partial t} \tag{75}$$

takes the form of

$$D_p \frac{d^2\Delta p}{dx^2} - \frac{\Delta p}{\tau_p} = \frac{\partial(\Delta p)}{\partial t} \tag{76}$$

Now we must impose our conditions, the first of which will be the surface boundary conditions which are

$$-D_p\left(\frac{\partial(\Delta p)}{\partial x}\right)_{\frac{x_0}{2}} = s\cdot\Delta p\left({}^{x_0}/_{2},\, t\right) \tag{77}$$

And

$$D_p\left(\frac{\partial(\Delta p)}{\partial x}\right)_{-x_0/2} = s\cdot\Delta p\left(-{}^{x_0}/_{2},\, t\right) \tag{78}$$

In addition to the geometrical conditions, we must also impose initial and final conditions on the excess carrier concentration. The initial condition will be that at time $t = 0$, we require that $\Delta p(x,0) = p_1 = const$. The final condition will be that as $t \to \infty$, we require that $\lim_{t\to\infty} \Delta p(x,t) = 0$.

Before we impose our conditions, let's first make a substitution into our differential equation that will make subsequent calculations easier. If we make the substitution

$$\Delta p(x,t) = e^{-t/\tau_p}\, u(x,t) \tag{79}$$

Then the continuity equation becomes

$$D_p e^{-t/\tau_p}\frac{\partial^2 u(x,t)}{\partial x^2} - \frac{e^{-t/\tau_p}\, u(x,t)}{\tau_p} = -\frac{e^{-t/\tau_p}\, u(x,t)}{\tau_p} + e^{-t/\tau_p}\frac{\partial u(x,t)}{\partial t} \tag{80}$$

Which simplifies to

$$D_p\frac{\partial^2 u}{\partial x^2} = \frac{\partial u}{\partial t} \tag{81}$$

This substitution also changes the boundary and initial conditions to

$$-D_p\left(\frac{\partial u}{\partial x}\right)_{\frac{x_0}{2}} = s \cdot u\left(x_0/2\,,\ t\right) \tag{82}$$

$$D_p\left(\frac{\partial u}{\partial x}\right)_{x_0/2} = s \cdot u\left(-x_0/2\,,\ t\right) \tag{83}$$

$$u(x,0) = p_1 = const \tag{84}$$

From here, we will use the Separation of Variables technique to solve the continuity equation and we will seek solutions of the form

$$u(x,t) = X(x)T(t) \tag{85}$$

Substituting this back in the continuity equation, we find that

$$D_p\frac{\partial^2\left(X(x)T(t)\right)}{\partial x^2} = \frac{\partial\left(X(x)T(t)\right)}{\partial t} \tag{86}$$

$$D_pT(t)\frac{d^2X}{dx^2} = X(x)\frac{dT}{dt} \tag{87}$$

$$\frac{1}{X(x)}\frac{d^2X}{dx^2} = \frac{1}{D_pT(t)}\frac{dT}{dt} \tag{88}$$

The only way for this final expression to be true is if both sides of the equation are separately equal to a constant, because that is the only way for a function of only x and a function of only t to be equal for all possible values of x and t. We will call this constant $-\phi^2$, so that for all values of ϕ the constant will be negative; this is required to insure that as $t \to \infty$, $\Delta p \to 0$, which will soon become evident. So then, we now have

$$\frac{1}{X(x)}\frac{d^2X}{dx^2} = \frac{1}{D_p T(t)}\frac{dT}{dt} = -\phi^2 = const \tag{89}$$

Now we can consider each side of the equation separately. Let's start with $T(t)$, for which we find

$$\frac{1}{D_p T(t)}\frac{dT}{dt} = -\phi^2 \tag{90}$$

$$\frac{dT}{dt} = -\phi^2 D_p T(t) \tag{91}$$

Which has the solution

$$T(t) = e^{-\phi^2 D_p t} \tag{92}$$

It is here that we see that the constant must be negative so that the final condition is satisfied. Moving to the spatial dependence, $X(x)$, we find

$$\frac{1}{X(x)}\frac{d^2X}{dx^2} = -\phi^2 \tag{93}$$

$$\frac{d^2X}{dx^2} = -\phi^2 X(x) \tag{94}$$

Which has the solution

$$X(x) = A\cos\phi x + B\sin\phi x \tag{95}$$

Once again, based on the symmetry of the scenario at hand, we know that the excess carrier concentration must be an even function of x. Therefore, we know that $B = 0$. With our definition of $u(x,t)$, we find that a suitable solution to the continuity equation may be written as

$$u(x,t) = A\, e^{-\phi^2 D_p t} \cos \phi x \tag{96}$$

While this satisfies the differential equation, it does not satisfy the boundary conditions. However, we may form a linear superposition of solutions which will satisfy the differential equation and the boundary conditions

$$u(x,t) = \sum_n u_n(x,t) = \sum_n A_n\, e^{-\phi_n^2 D_p t} \cos \phi_n x \tag{97}$$

Where we may choose the values of A_n and ϕ_n so that the boundary conditions are satisfied by the superposition. Now we can apply the surface boundary conditions, which in order to satisfy, we require that each term in the summation satisfies

$$-D_p \left(\frac{\partial u_n}{\partial x}\right)_{x_0/2} = s \cdot u_n\left(x_0/2\,,\, t\right) \tag{98}$$

Substituting our expression for u_n, we find

$$-D_p \frac{\partial}{\partial x}\left[A_n\, e^{-\phi_n^2 D_p t} \cos(\phi_n x)\right]_{\frac{x_0}{2}} = s \cdot A_n\, e^{-\phi_n^2 D_p t} \cos\left(\frac{\phi_n x_0}{2}\right) \tag{99}$$

$$\phi_n A_n D_p e^{-\phi_n^2 D_p t}\, sin\left(\frac{\phi_n x_0}{2}\right) = s \cdot A_n\, e^{-\phi_n^2 D_p t} \cos\frac{\phi_n x_0}{2} \tag{100}$$

Rearranging, we find that

$$ctn\left(\frac{\phi_n x_0}{2}\right) = \frac{\phi_n D_p}{s} \tag{101}$$

Which can be manipulated such that both sides are functions of $\phi_n x_0/2$ by multiplying the right hand side by 1 in the form of

$$ctn\left(\frac{\phi_n x_0}{2}\right) = \frac{\phi_n D_p}{s}\frac{x_0}{x_0}\frac{2}{2} = \frac{2D_p}{s x_0}\left(\frac{\phi_n x_0}{2}\right) \tag{102}$$

In order to satisfy the boundary conditions, we must choose the values of ϕ_n that satisfy the above relation. The roots of this equation may be obtained numerically or graphically as the intersection of the two curves, shown below in Fig. 16.

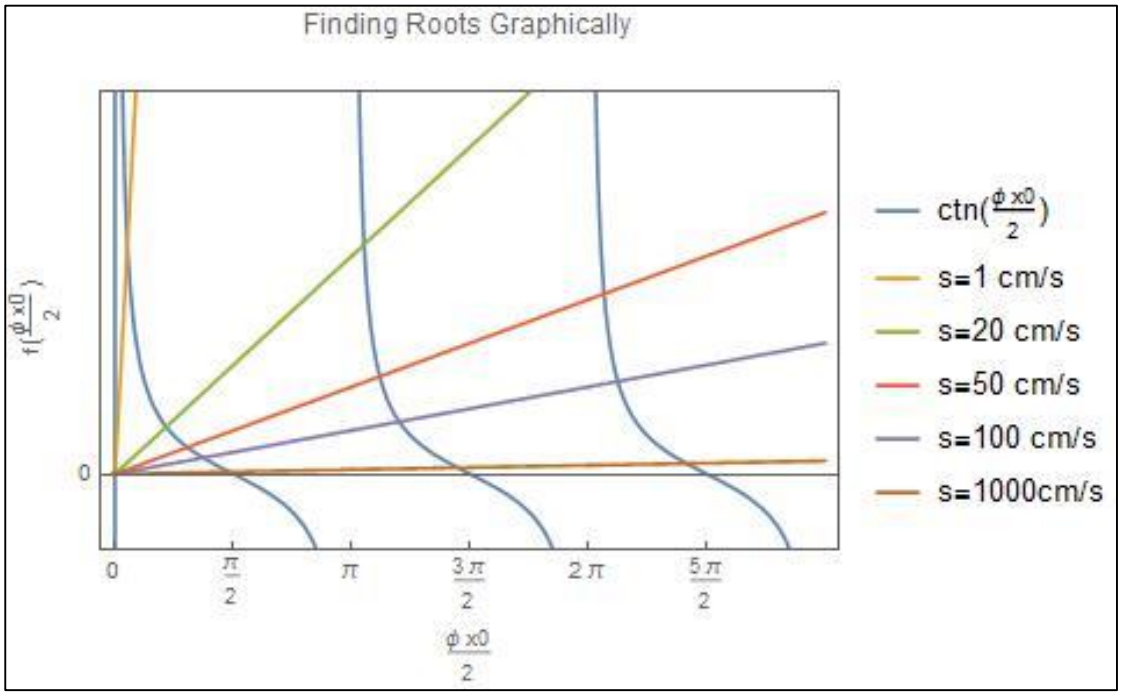

Figure 16. Finding Transient State roots graphically. *Plot of* $ctn\left(\frac{\phi_n x_0}{2}\right)$ *and* $\frac{2D_p}{sx_0}\left(\frac{\phi_n x_0}{2}\right)$ *for various values of SRV. Here, the values of* ϕ_n *can be determined from the intersections of the curves.*

Now we want to apply the initial condition that at $t = 0$, we require that $u(x, 0) = p_1 = const$. To accomplish this, let's assume that $u(x, 0)$ is an arbitrary even function $f(x)$, such that

$$u(x, 0) = \sum_{n=0}^{\infty} A_n \cos(\phi_n x) = f(x) \tag{103}$$

Multiplying both sides of this equation by $\cos(\phi_m x)$ and integrating over the interval $\left(-\frac{x_0}{2} < x < \frac{x_0}{2}\right)$, we get

$$\sum_{n=0}^{\infty} \int_{-\frac{x_0}{2}}^{\frac{x_0}{2}} A_n \cos(\phi_n x) \cos(\phi_m x)\, dx = \int_{-\frac{x_0}{2}}^{\frac{x_0}{2}} f(x) \cos(\phi_m x)\, dx \tag{104}$$

Based on the identity

$$\int_0^{2\pi} \cos(nx) \cos(mx)\, dx = \frac{\delta_{n,m}}{2} \tag{105}$$

Which defines orthogonality for the set of functions $\{\cos nx\}$ on an even interval, then we know that for the previous expression only the integral where $n = m$ on the left had side will contribute. So then, setting $n = m$, the summation collapses to a single integral, which can be evaluated as

$$\int_{-\frac{x_0}{2}}^{\frac{x_0}{2}} A_m \cos(\phi_m x) \cos(\phi_m x)\, dx = A_m \left[\frac{\phi_m x_0 + \sin \phi_m x_0}{2\phi_m}\right] \tag{106}$$

And with this, we can now solve for A_m

$$A_m \left[\frac{\phi_m x_0 + \sin \phi_m x_0}{2\phi_m}\right] = \int_{-\frac{x_0}{2}}^{\frac{x_0}{2}} f(x) \cos(\phi_m x)\, dx \tag{107}$$

$$A_m = \left[\frac{2\phi_m}{\phi_m x_0 + \sin \phi_m x_0}\right] \int_{-\frac{x_0}{2}}^{\frac{x_0}{2}} f(x) \cos(\phi_m x)\, dx \tag{108}$$

Recall that $f(x)$ was defined as $f(x) = u(x, 0) = p_1 = const.$ Inputting this into our expression for A_n $(n = m)$, we arrive at

$$A_n = \left[\frac{2\phi_n}{\phi_n x_0 + \sin \phi_n x_0}\right] \int_{-\frac{x_0}{2}}^{\frac{x_0}{2}} p_1 \cos(\phi_n x)\ dx \tag{109}$$

$$A_n = \frac{4p_1 \sin \frac{\phi_n x_0}{2}}{\phi_n x_0 + \sin \phi_n x_0} \tag{110}$$

Now recall our previous result for $u(x,t)$

$$u(x,t) = \sum_n A_n\, e^{-\phi_n^2 D_p t} \cos \phi_n x \tag{111}$$

Now we can substitute our result for A_n

$$u(x,t) = 4p_1 \sum_{n=0}^{\infty} \frac{\sin \frac{\phi_n x_0}{2} \cos(\phi_n x)}{\phi_n x_0 + \sin \phi_n x_0} e^{-\phi_n^2 D_p t} \tag{112}$$

Once again, recall that we defined the time dependent excess carrier concentration profile as

$$\Delta p(x,t) = e^{-t/\tau_p}\, u(x,t) \tag{113}$$

So then with our previous result, we arrive at a final solution which satisfies all of our conditions

$$\Delta p(x,t) = 4p_1 e^{-t/\tau_p} \sum_{n=0}^{\infty} \frac{\sin \frac{\phi_n x_0}{2} \cos(\phi_n x)}{\phi_n x_0 + \sin \phi_n x_0} e^{-\phi_n^2 D_p t} \tag{114}$$

Again, this is not necessarily very intuitive, but we can make some inferences. As $s \to 0$, the slope of the line in Fig. 15 becomes extremely large and the eigenvalues $\{\phi_n a\}$ approach $(0, 2\pi, 4\pi \ldots)$. For this set of values, $\sin(\phi_0 a/2) = 0$ for all values of ϕ_n except for the first. In the limit that $\{\phi_0 x_0\}$ goes to zero, then the term

$$\frac{\sin\left(\frac{\phi_0 x_0}{2}\right)}{\phi_0 x_0 + \sin(\phi_0 x_0)} \tag{115}$$

Reduces to 1/4 and the excess carrier concentration is given as

$$\Delta p(x,t) = p_1 e^{-t/\tau_p} \tag{116}$$

From which we see that at every instant, t, the excess carrier profile is constant throughout the sample and decays with time.

For $s \neq 0$, $\Delta p(x,t)$ exhibits a complex, multi-exponential decay at first, but because the ϕ_n values grow very quickly, eventually this decay will reduce to

$$e^{-\left(\frac{1}{\tau_p}+\phi_0^2 D_p\right)t} \tag{117}$$

From which we can define an effective lifetime such that

$$\frac{1}{\tau_{eff}} = \frac{1}{\tau_p} + \phi_0^2 D_p \tag{118}$$

Once again, now that we have a result for the excess charge carrier concentration, we can begin to talk about PL using the same relation as before

$$PL \sim \int \Delta p(x)\, dx \tag{119}$$

Again, the excess carrier concentration was plotted for CdTe in Mathematica© using appropriate values for D_p. This time however, because of the nature of our expression for the excess carrier concentration, an investigation of how many terms were significant needed to occur. To do this, the excess carrier density with varying numbers of terms (one through five) were plotted at $t = 0$. This was done for N-type and P-type CdTe with

thickness of 0.5μm and 5μm, with SRV =100 cm/s and SRV=1000 cm/s. To illustrate that for values of n greater than zero the effective lifetime is not significantly affected, the values of $1/\phi_n^2 D$ (s) are given for each scenario that we investigate.

We begin with N-type CdTe of 0.5 μm layer thickness

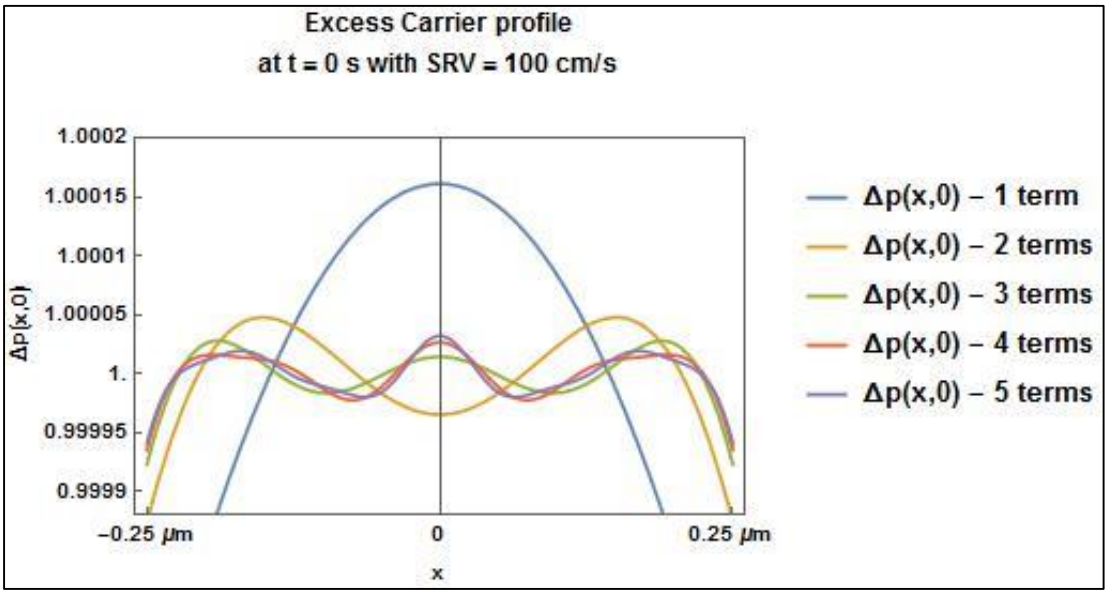

Figure 17. Excess carrier concentration profile for an N-type CdTe sample 0.5 µm thick with SRV = 100 cm/s. *Comparison of expressions with increasing number of terms included.*

And for the above scenario, the values of $1/\phi_n^2 D_p$ are shown below in Table 2.

Table 2. Contribution of higher order terms to effective lifetime for N-type CdTe with a 0.5µm thick active layer and SRV = 100 cm/s

n	$\frac{1}{\phi_n^2 Dp}$
0	$2.50\ x\ 10^{-7}\ s$
1	$2.44\ x\ 10^{-11}\ s$
2	$6.12\ x\ 10^{-12}\ s$
3	$1.53\ x\ 10^{-12}\ s$
4	$6.80\ x\ 10^{-13}\ s$

And again with SRV = 1000 cm/s

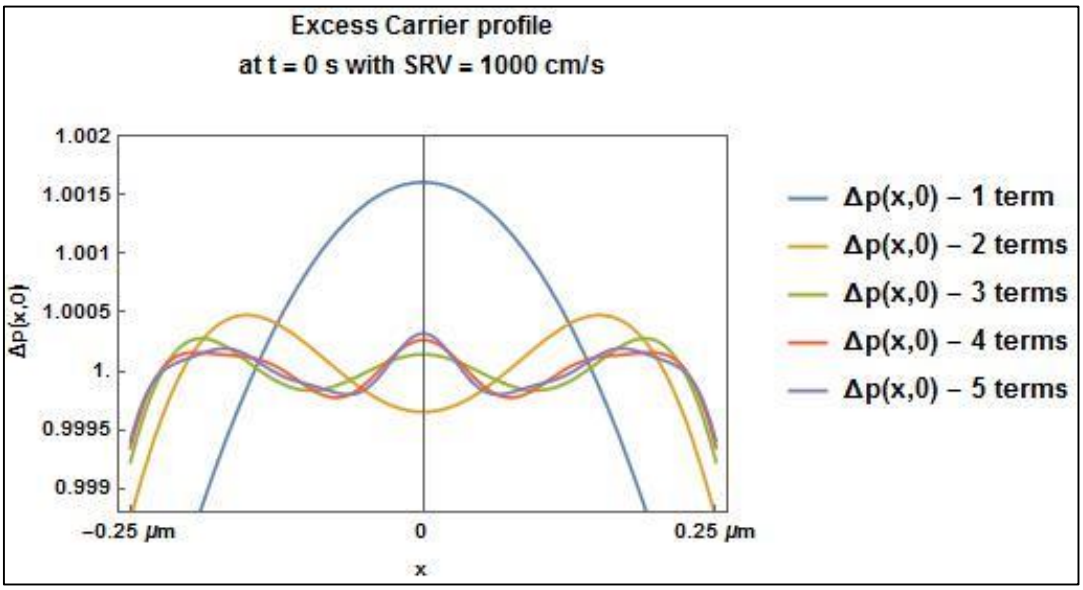

Figure 18. Excess carrier concentration profile for an N-type CdTe sample 0.5 µm thick with SRV = 1000 cm/s. *Comparison of expressions with increasing number of terms included.*

Where

Table 3. Contribution of higher order terms to effective lifetime for N-type CdTe with a 0.5µm thick active layer and SRV = 1000 cm/s

n	$\frac{1}{\phi_n^2 Dp}$
0	$2.51\ x\ 10^{-8}\ s$
1	$2.44\ x\ 10^{-11}\ s$
2	$6.12\ x\ 10^{-12}\ s$
3	$1.53\ x\ 10^{-12}\ s$
4	$6.80\ x\ 10^{-13}\ s$

Now we explore N-Type CdTe with 5 μm layer thickness

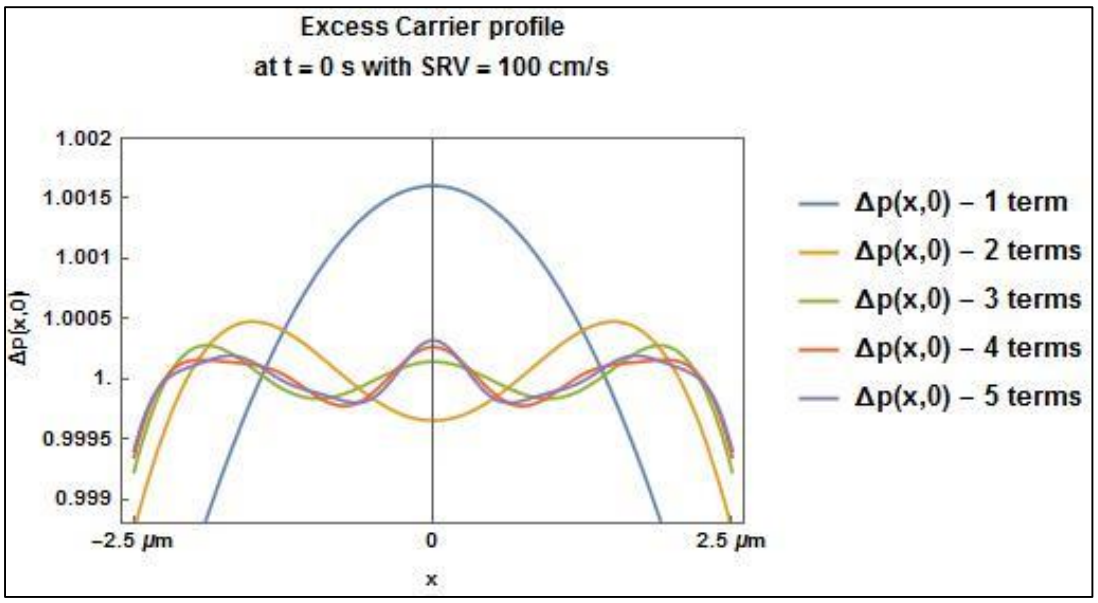

Figure 19. Excess carrier concentration profile for an N-type CdTe sample 5 µm thick with SRV = 100 cm/s. *Comparison of expressions with increasing number of terms included.*

Where

Table 4. Contribution of higher order terms to effective lifetime for N-type CdTe with a 5µm thick active layer and SRV = 100 cm/s

n	$\frac{1}{\phi_n^2 Dp}$
0	$2.51\ x\ 10^{-6}\ s$
1	$2.44\ x\ 10^{-9}\ s$
2	$6.12\ x\ 10^{-10}\ s$
3	$1.53\ x\ 10^{-10}\ s$
4	$6.80\ x\ 10^{-11}\ s$

And again with SRV = 1000 cm/s

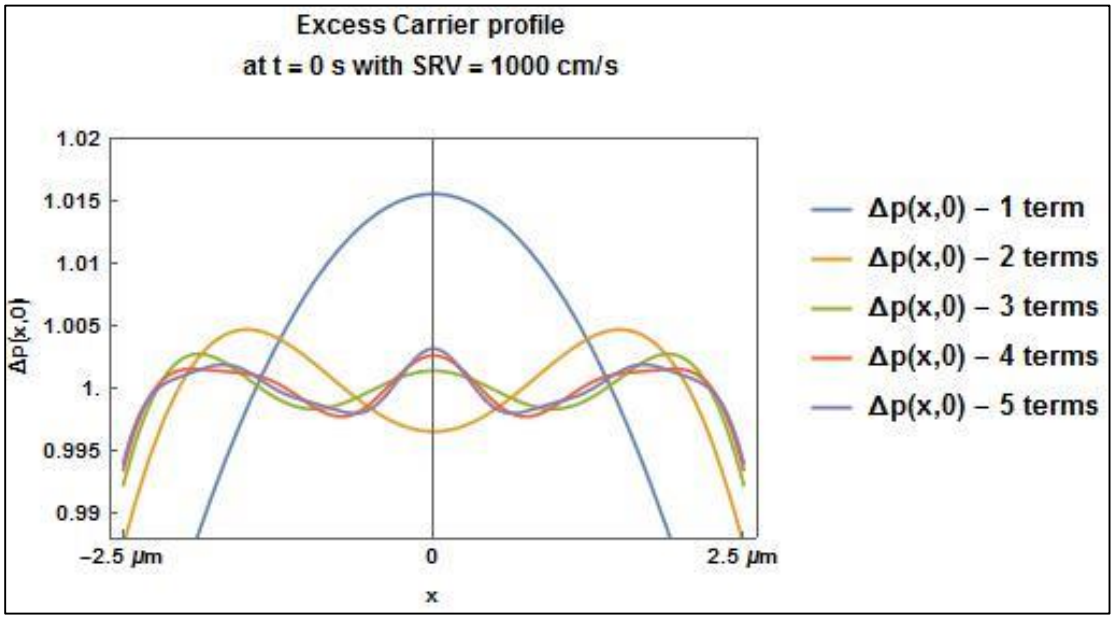

Figure 20. Excess carrier concentration profile for an N-type CdTe sample 5 µm thick with SRV = 1000 cm/s. *Comparison of expressions with increasing number of terms included.*

Where

Table 5. Contribution of higher order terms to effective lifetime for N-type CdTe with a 5µm thick active layer and SRV = 1000 cm/s

n	$\frac{1}{\phi_n^2 Dp}$
0	$2.58\ x\ 10^{-7}\ s$
1	$2.40\ x\ 10^{-9}\ s$
2	$6.09\ x\ 10^{-10}\ s$
3	$1.53\ x\ 10^{-10}\ s$
4	$6.79\ x\ 10^{-11}\ s$

For P-type CdTe with 0.5 μm layer thickness

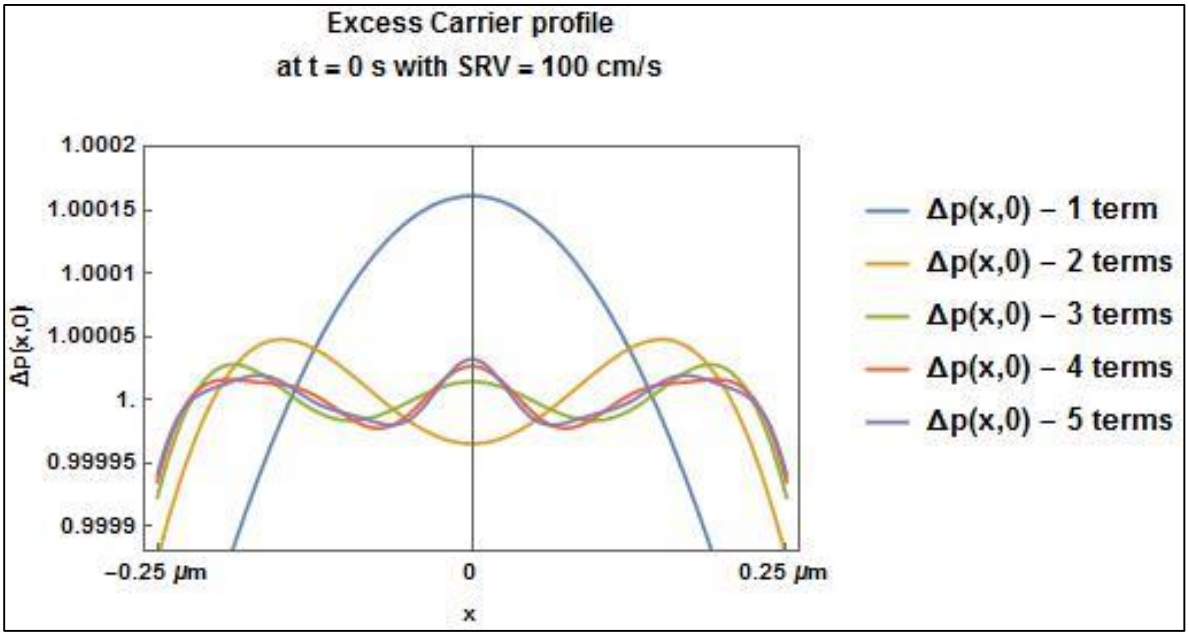

Figure 21. Excess carrier concentration profile for a P-type CdTe sample 0.5 µm thick with SRV = 100 cm/s. *Comparison of expressions with increasing number of terms included.*

Where

Table 6. Contribution of higher order terms to effective lifetime for P-type CdTe with a 0.5µm thick active layer and SRV = 100 cm/s

n	$\frac{1}{\phi_n^2 D_n}$
0	$2.50\ x\ 10^{-7}\ s$
1	$2.45\ x\ 10^{-11}\ s$
2	$6.12\ x\ 10^{-12}\ s$
3	$1.53\ x\ 10^{-12}\ s$
4	$6.80\ x\ 10^{-13}\ s$

And with SRV = 1000 cm/s

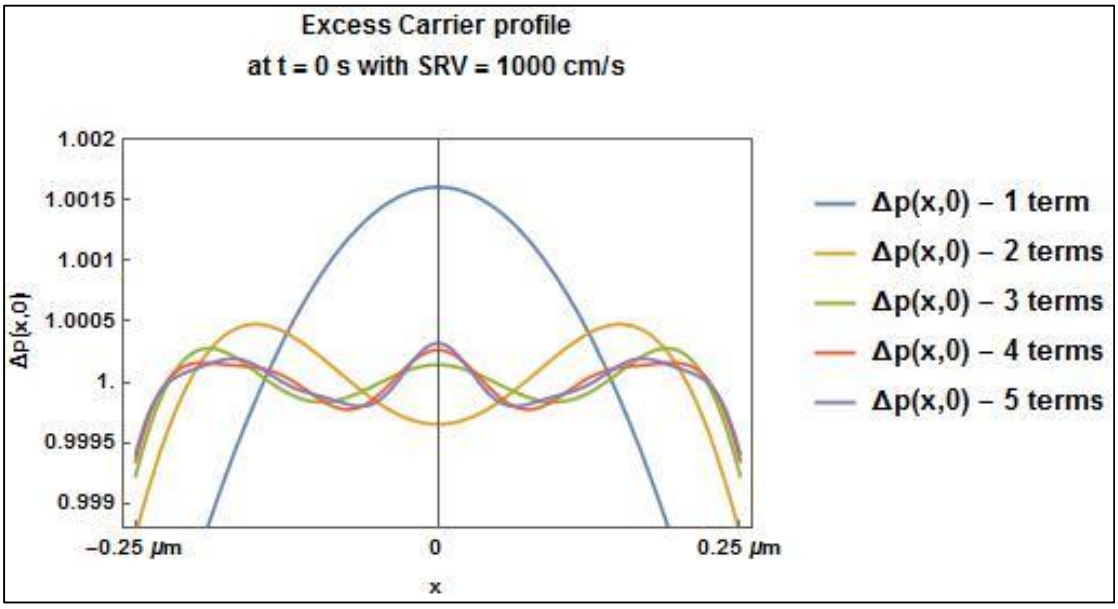

Figure 22. Excess carrier concentration profile for a P-type CdTe sample 0.5 µm thick with SRV = 1000 cm/s*. Comparison of expressions with increasing number of terms included.*

Where

Table 7. Contribution of higher order terms to effective lifetime for P-type CdTe with a 0.5µm thick active layer and SRV = 1000 cm/s

n	$\frac{1}{\phi_n^2 D_n}$
0	$2.51\ x\ 10^{-8}\ s$
1	$2.44\ x\ 10^{-11}\ s$
2	$6.12\ x\ 10^{-12}\ s$
3	$1.53\ x\ 10^{-12}\ s$
4	$6.80\ x\ 10^{-13}\ s$

And now for P-type CdTe with 5 μm layer thickness

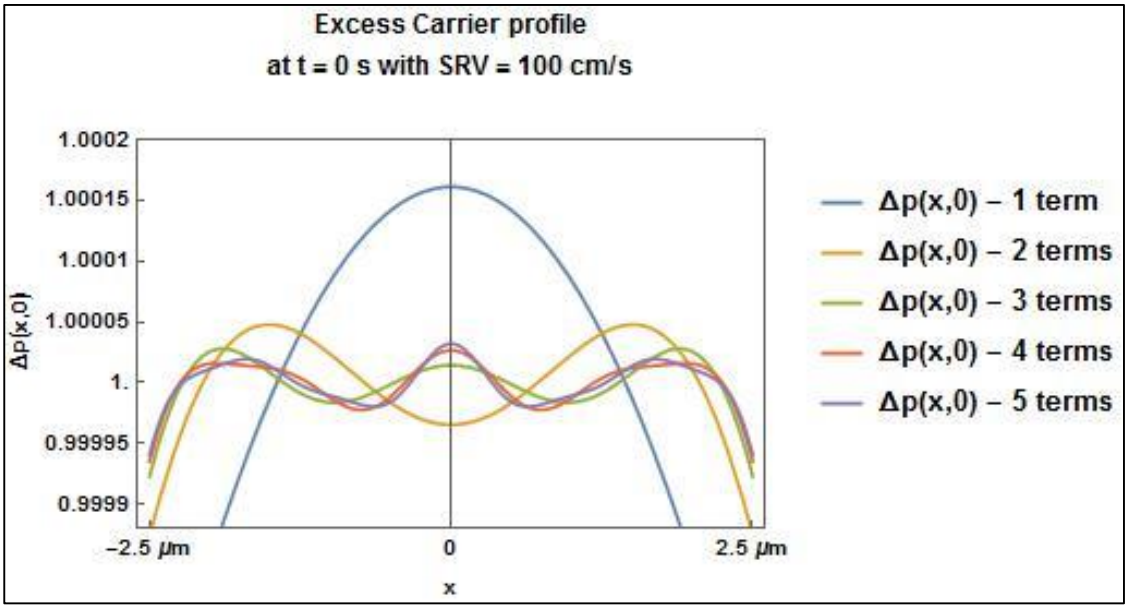

Figure 23. Excess carrier concentration profile for a P-type CdTe sample 5 µm thick with SRV = 100 cm/s. *Comparison of expressions with increasing number of terms included.*

Where

Table 8. Contribution of higher order terms to effective lifetime for P-type CdTe with a 5µm thick active layer and SRV = 100 cm/s

n	$\frac{1}{\phi_n^2 D_n}$
0	$2.76\ x\ 10^{-6}\ s$
1	$2.95\ x\ 10^{-9}\ s$
2	$7.40\ x\ 10^{-10}\ s$
3	$1.85\ x\ 10^{-10}\ s$
4	$8.23\ x\ 10^{-11}\ s$

And with SRV = 1000 cm/s

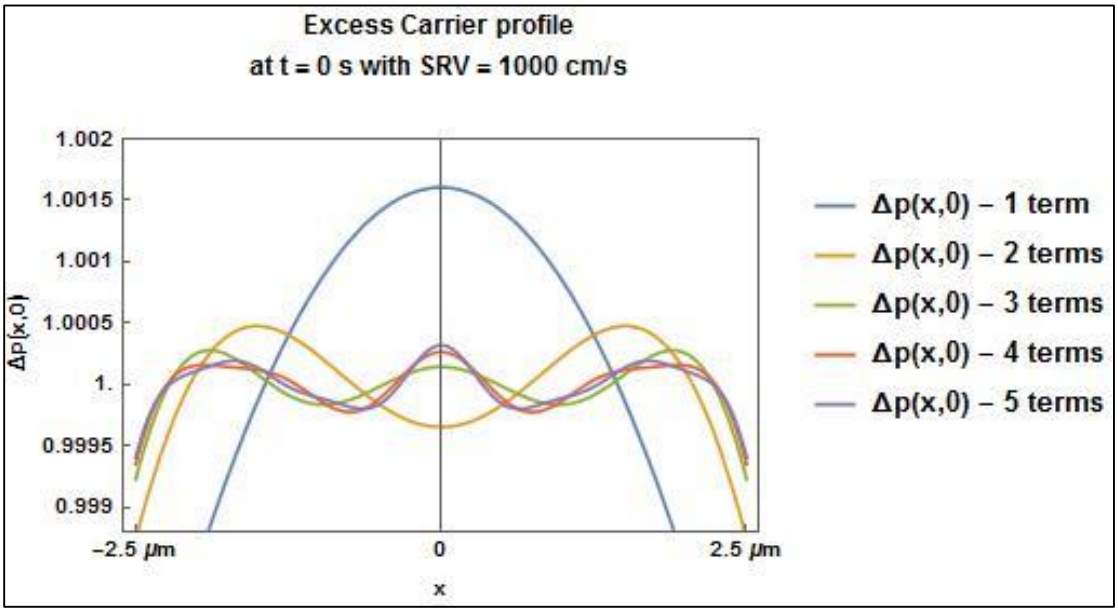

Figure 24. Excess carrier concentration profile for a P-type CdTe sample 5 µm thick with SRV = 1000 cm/s. *Comparison of expressions with increasing number of terms included.*

Where

Table 9. Contribution of higher order root terms to effective lifetime for P-type CdTe with a 5µm thick active layer and SRV = 1000 cm/s

n	$\frac{1}{\phi_n^2 D_n}$
0	$2.85\ x\ 10^{-7}\ s$
1	$2.90\ x\ 10^{-9}\ s$
2	$7.36\ x\ 10^{-10}\ s$
3	$1.85\ x\ 10^{-10}\ s$
4	$8.22\ x\ 10^{-11}\ s$

From these results, it was determined that 5 terms would be appropriate for this study. With this determined, the excess carrier density was then integrated over the length of the sample to obtain a time dependent expression for the PLI. This integral was then normalized so that

$$PLI(t = 0) = 1 \tag{120}$$

and plotted against time. This was also done for N-type and P-type CdTe of layer thickness 0.5 and 5 μm, with SRV =100 cm/s and SRV=1000 cm/s. We begin with the N-type results with layer thickness 0.5 μm

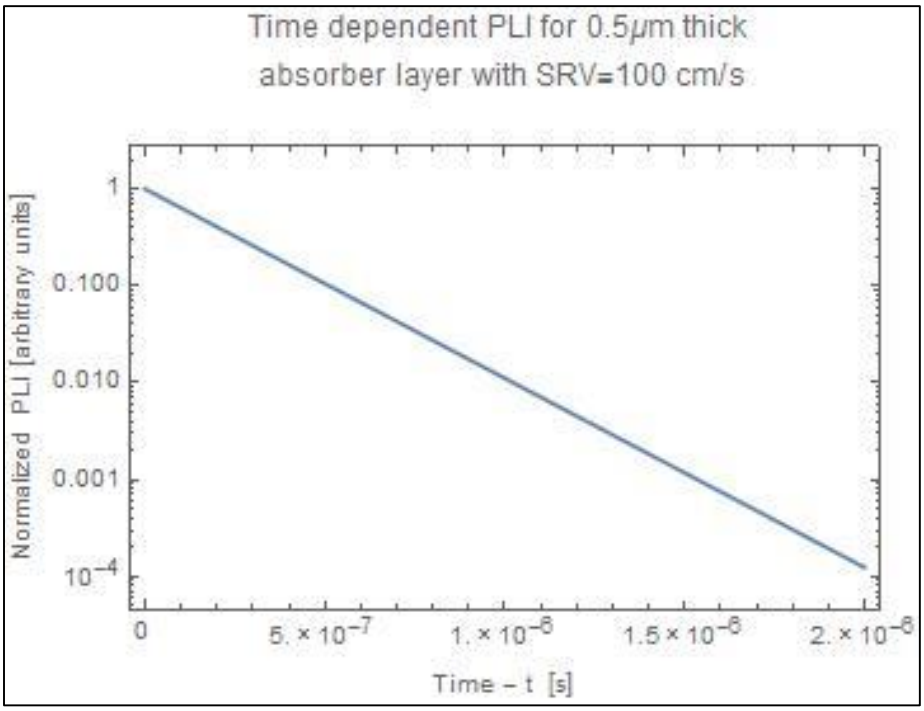

Figure 25. PL response to illumination that has been cut off for an N-type CdTe sample 0.5 µm thick with SRV=100 cm/s

Here, the effective lifetime as defined in equation (118) was found to be 0.22 μs.

When the SRV was set to 1000 cm/s, we found

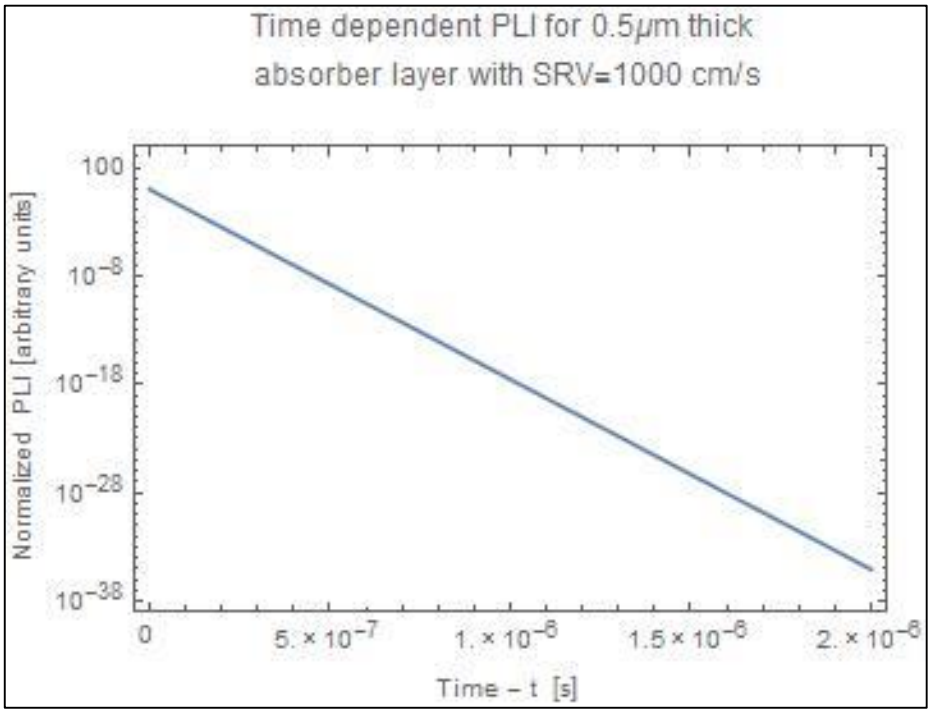

Figure 26. PL response to illumination that has been cut off for an N-type CdTe sample 0.5 µm thick with SRV=1000 cm/s

Where the effective lifetime was found to be 24.8 ns. From this, we see that the PLI drops off much quicker than previously, and thus we see that as SRV increases, we should expect the effective lifetime to decrease.

Exploring the 5 μm thick N-Type CdTe, we found

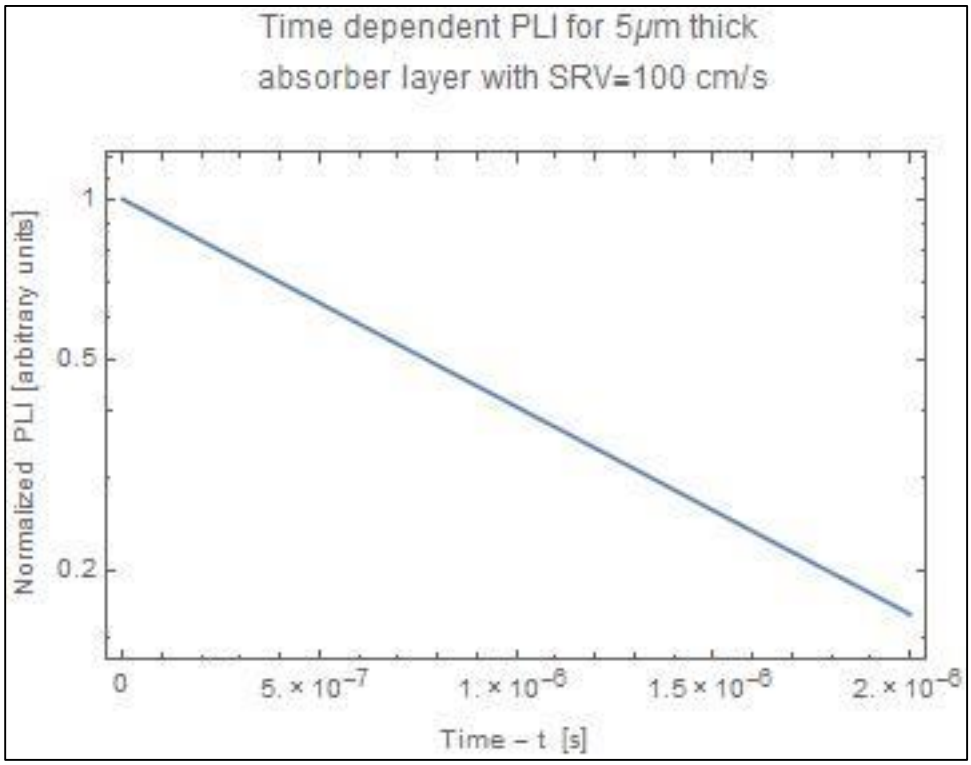

Figure 27. PL response to illumination that has been cut off for an N-type CdTe sample 5 μm thick with SRV=100 cm/s

Where the effective lifetime was found to be 1.11 μs.

When the SRV was increased, we found

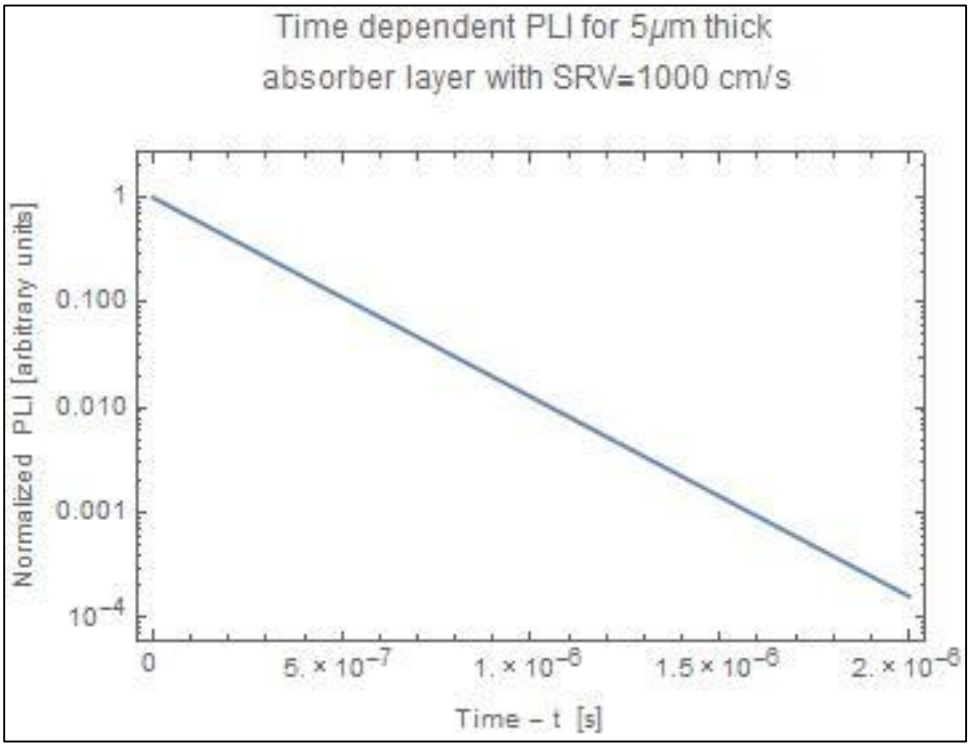

Figure 28. PL response to illumination that has been cut off for an N-type CdTe sample 5 μm thick with SRV=1000 cm/s

Where the effective lifetime was found to be 0.23 μs. From these two results, we see the same trend as before. Note though that the effective lifetime here is the approximately the same as the effective lifetime for the 0.5 μm thick N-type CdTe sample with SRV = 100 cm/s. This is indicative of the S/d nature of lifetime in a surface limited structure, where S is the SRV, and d is the active layer thickness, as discussed in detail in Chapter 3.4. Here we see that as we increase the layer thickness, we should expect an increase in the effective lifetime.

The same investigations were done for P-Type CdTe, beginning with a layer thickness of 0.5 μm

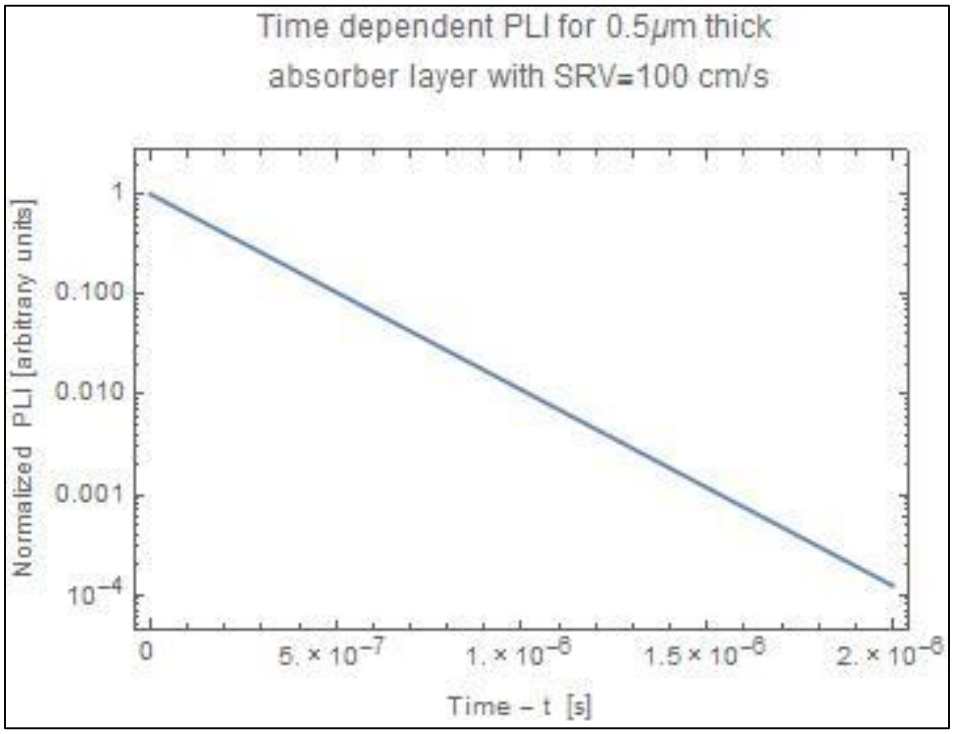

Figure 29. PL response to illumination that has been cut off for a P-type CdTe sample 0.5 μm thick with SRV=100 cm/s

Where the effective lifetime was found to be 0.22 μs.

When the SRV was increased, we found

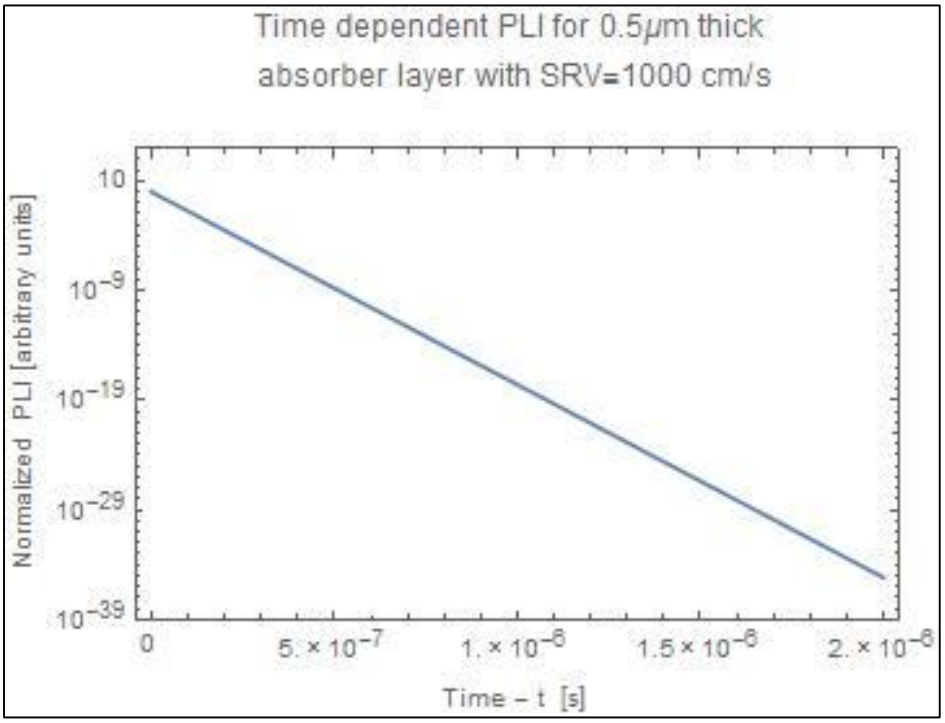

Figure 30. PL response to illumination that has been cut off for a P-type CdTe sample 0.5 µm thick with SRV=1000 cm/s

Where the effective lifetime was found to be 24.7 ns. Once again, we see that as SRV increases the effective lifetime decreases.

When the thickness was increased to 5 μm, we found

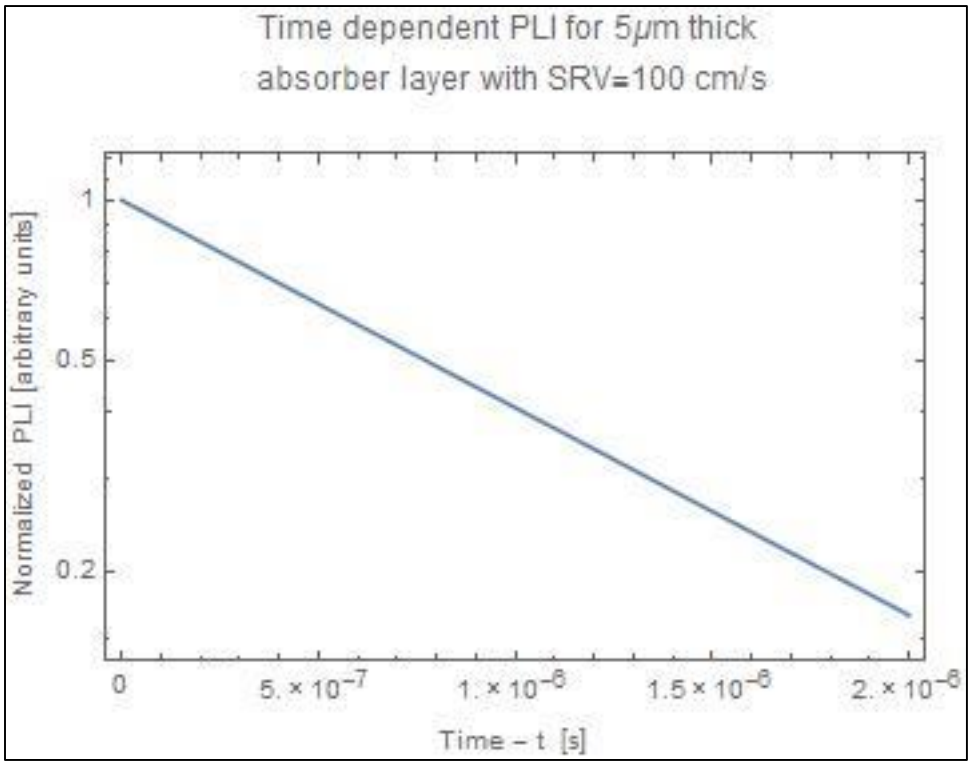

Figure 31. PL response to illumination that has been cut off for a P-type CdTe sample 5 µm thick with SRV=100 cm/s

Where the effective lifetime was found to be 1.11 μs.

And when the SRV was increased, we found

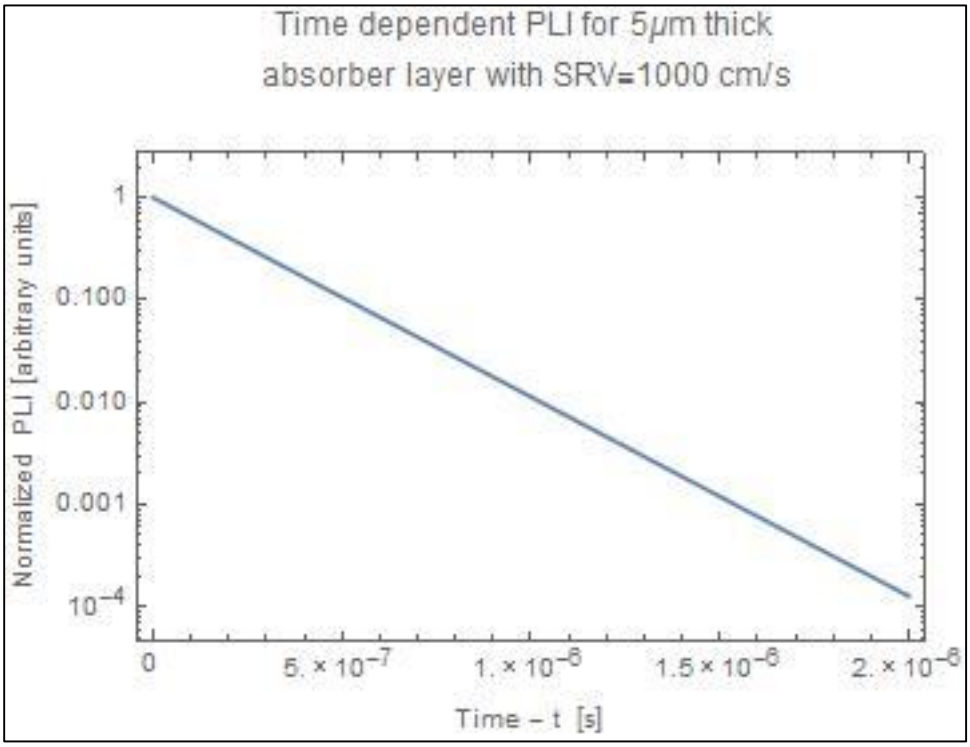

Figure 32. PL response to illumination that has been cut off for a P-type CdTe sample 5 μm thick with SRV=1000 cm/s

Where the effective lifetime was found to be 0.22 μs. There are a few things to note here. First, once again we see confirmation that as SRV increases, the effective lifetime of the sample decreases. We also note, that once again we see that as the layer thickness increases, the effective lifetime increases as well. The third thing to note is that the effective lifetimes for holes and electrons in N-type and P-type CdTe, respectively, are approximately equal despite the differences in their mobilities. It is worth noting that in the last scenario studied for both types, we see that the hole lifetime is slightly higher than the electron lifetime in the same scenario, again related to the higher minority electron drift velocity. However it is not significant, indicating the samples are surface

limited even with SRV = 100 cm/s. For every scenario above, we see that if PL is plotted on a log scale we should expect a linear response with time, despite the multi-exponential decay that we expect at the onset. This confirms our definition of the effective lifetime not significantly depending on higher root terms. The Mathematica codes used to generate these plots can be found in Appendices C through F.

By exploring the dynamics of the excess charge carriers in PLI (low-injection steady state) and TRPL (low-injection transient state) we are able to make conclusions about the PL response in both scenarios. For the Steady State, we conclude that as SRV increases, the excess carrier concentration and PL decrease. For the Transient State, we conclude that as SRV increases, the PL decreases. We are also able to conclude that the effective lifetime is dominated by the first root, ϕ_0, while all others make little contribution, leading to a linear response of PL with time (when plotted logarithmically).[†]

[†] As stated at the beginning of this chapter, the flow of information presented here closely follows that found in textbooks, such as [32] and [33]

3. METHODS

Now that we have investigated the excess charge dynamics in PL, we can turn to a discussion of the characterization techniques used in this study. All of the techniques, except for Spectral Ellipsometry, are governed by PL dynamics. We will begin with the exception and discuss spectral ellipsometry.

3.1 Spectral Ellipsometry

Instead of measuring the PL response of a semiconductor, spectral ellipsometry measures the way incident light interacts with a material. At its core, spectral ellipsometry measures the change in polarization of reflected light incident on a thin-film sample, and compares this change to a model to extract materials properties. The properties, such as layer thickness, refractive index or dielectric constant, determine the exact nature of the change in polarization. This technique exploits the phase information, or polarization state, inherent in the incident and reflected light beams.

To describe in more detail, we need a working definition of light. Light is composed of many electromagnetic waves that can be described using Maxwell's equations. The result of Maxwell's equations give us two equations that totally describe an electromagnetic plane wave[12]

$$\tilde{E}(z,t) = E_0 e^{i(kz-\omega t+\delta)} \tag{121}$$

$$\tilde{B}(z,t) = \frac{E_0}{c} e^{i(kz-\omega t+\delta)} \tag{122}$$

Note how the above are complex values. The physical fields are the real parts of $\tilde{E}(z,t)$ and $\tilde{B}(z,t)$. Using Euler's formula to get the real portion of the expression above, we can describe the electric field as

$$E(z,t) = E_0 \cos(kz - \omega t + \delta) \tag{123}$$

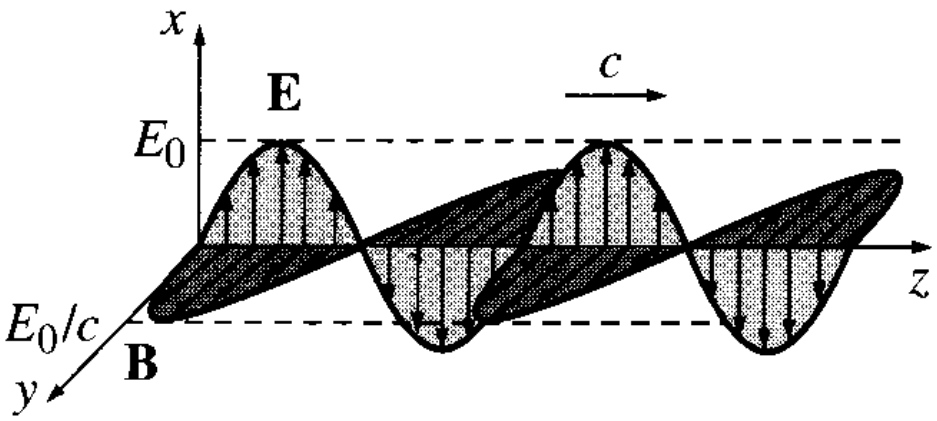

Figure 33. The physical electric and magnetic fields in an electromagnetic plane wave.[12]

Now we need to define polarized light. All light, regardless of its polarization can be described as the superposition of two orthogonal electromagnetic plane wave components. These electromagnetic plane waves are typically decomposed into an s component, which is perpendicular to the plane of incidence, and a p component, which is parallel to the plane of incidence. Depending on the phase difference between the s and p components, the light with be polarized differently. If the two components are in phase (the phase difference is zero), then the light is said to be linearly polarized. If the two components are out of phase by 90°, and their amplitudes are equal then the light is said

to be circularly polarized. Anywhere in between these two scenarios, the light is said to be elliptically polarized. See Fig. 34 below

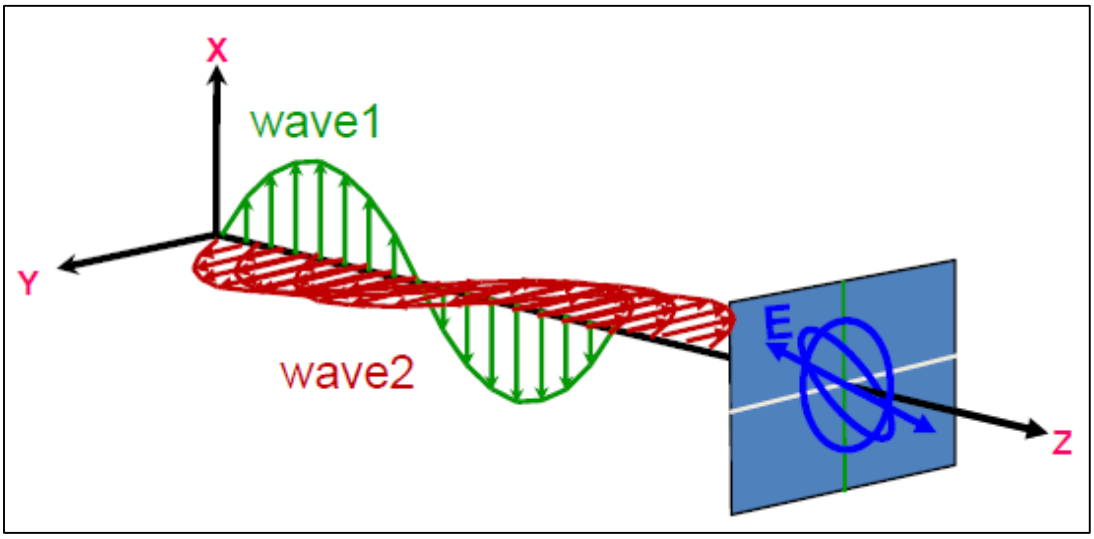

Figure 34. Depiction of polarization types. *Here we see a superposition of a p component with multiple s components, showing the different kinds of polarization. Copyright protected by Woollam company*

When light is incident on a material, the material differentiates between the s and p components, and interacts with the two differently. Ellipsometry measures this change in the s and p components after reflection. It does this by determining the complex reflectance ratio, ρ, which is defined as

$$\rho = \frac{\widetilde{R_p}}{\widetilde{R_s}} = \tan(\Psi)\, e^{i\Delta} \tag{124}$$

Where

$$\widetilde{R_p} = \frac{\tilde{E}_p^{reflected}}{\tilde{E}_p^{incident}} \tag{125}$$

$$\widetilde{R_s} = \frac{\tilde{E}_s^{reflected}}{\tilde{E}_s^{incident}} \tag{126}$$

And Ψ and Δ are the specific values that are measured by the instrument. From the relation of ρ above, we can see that Ψ describes the ratio of the amplitudes of the two polarized components, while Δ describes the phase difference between the two.[13]

To determine these values, a typical spectral ellipsometry setup consists of an incident light source that is linearly polarized, typically by using a polarizer, and is then passed through a compensator (typically a quarter-wave plate). After the light has reflected, it is then passed through a secondary polarizer, called an analyzer, and then falls onto the detector (see Fig. 35 below). The data that is collected is then compared to a model based on the sample being tested. Most of these models assume that the sample is composed of a discrete number of well-defined layers that are optically homogeneous and isotropic.

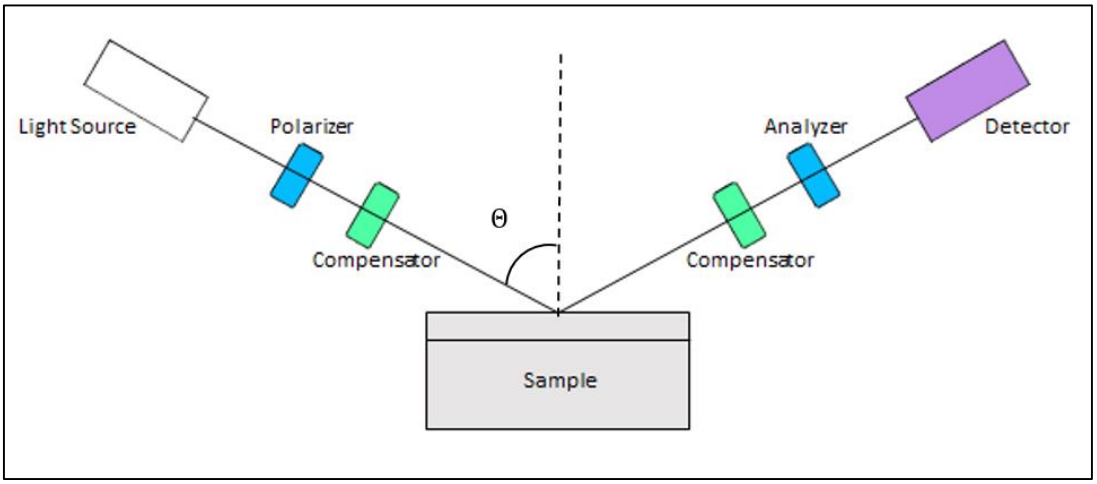

Figure 35. Typical setup for spectral ellipsometry measurements

These models attempt to fit the complex index of refraction, $\tilde{n}$, and the complex dielectric function, $\tilde{\epsilon}$, according to the optical response of the material being tested. These material properties are related through

$$\tilde{\epsilon} = \tilde{n}^2 \tag{127}$$

The complex index of refraction is defined as

$$\tilde{n} = n + ik \tag{128}$$

Where n is the real index of refraction and k is the extinction coefficient. The extinction coefficient is related to the absorption coefficient, α, through[14]

$$\alpha = \frac{4\,\pi\,k}{\lambda_0} \tag{129}$$

Where λ_0 is the wavelength of light in a vacuum. The complex dielectric function is defined as

$$\tilde{\epsilon} = \epsilon_1 + i\epsilon_2 \tag{130}$$

With this, we see that n, k, ϵ_1, and ϵ_2 are related by[15]

$$\tilde{\epsilon} = \epsilon_1 + i\epsilon_2 = \tilde{n}^2 = (n + ik)^2 = n^2 - k^2 + i2nk \tag{131}$$

Matching real and imaginary parts, we see that

$$\epsilon_1 = n^2 - k^2 \tag{132}$$

$$\epsilon_2 = 2nk \tag{133}$$

And by continuing to manipulate these complex values, we can also determine

$$n = \sqrt{\frac{|\tilde{\epsilon}| + \epsilon_1}{2}} \tag{134}$$

$$k = \sqrt{\frac{|\tilde{\epsilon}| - \epsilon_1}{2}} \tag{135}$$

Where $|\tilde{\epsilon}|$ is the complex modulus, defined as

$$|\tilde{\epsilon}| = \sqrt{\epsilon_1^2 + \epsilon_2^2} \tag{136}$$

The pairs of values, n, k, and ϵ_1, ϵ_2 must be consistent with the Kramers-Kronig relations, which connect the real and imaginary parts of any complex function that is analytic in the upper-half plane. To illustrate this, the Kramers-Kronig relations for ϵ_1 and ϵ_2 are given by

$$\epsilon_1(\omega) = 1 + \frac{2}{\pi} P \int_0^\infty \frac{\omega' \epsilon_2(\omega')}{\omega'^2 - \omega^2} d\omega' \tag{137}$$

$$\epsilon_2(\omega) = -\frac{2\omega}{\pi} P \int_0^\infty \frac{\epsilon_1(\omega') - 1}{\omega'^2 - \omega^2} d\omega' \tag{138}$$

From this we see that if we know either $\epsilon_1(\omega)$ or $\epsilon_2(\omega)$, then through the Kramers-Kronig relations we can determine the other, and through the relations above, we can also find n and k.[16,17] How these optical values are fit to the data is dependent on the type of model being used. A single measurement is often not enough to determine unique values for n, k and thickness for multiple layers. Hence, measurements are often taken at multiple wavelengths and angles which is then modeled to extract the desired quantities. This technique is called Variable Angle Spectroscopy.

For this study, a J.A. Woollam, variable angle Spectral Ellipsometer was used. The models used for the CdTe layers were available with the accompanying software. The model used for the CdMgTe layers, developed by Craig Swartz, was based on a collection of Cody-Lorentz oscillators, and the free parameters were fit to the ellipsometric data. The model used for CdMgTe DH structure, shown in Fig. 35 below, was an approximation of the sample structure. The model assumed a 10nm layer of CdTe on the top, followed by 30nm of CdMgTe, and the rest of the structure was approximated as a CdTe substrate. This should be an accurate model since the penetration of light in the material is limited by the absorption coefficient and the absorption depth (α^{-1}). The measurements were performed with visible light, meaning that the furthest light could penetrate the sample was about $0.2\mu m$, well before the second layer of CdMgTe.

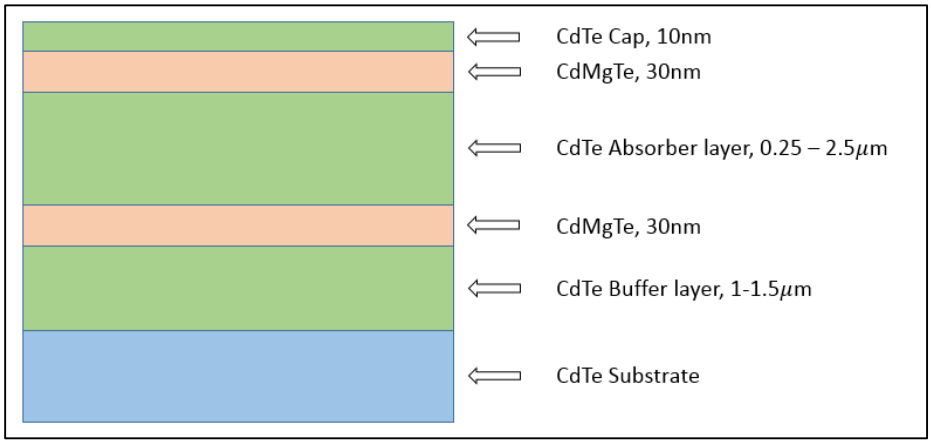

Figure 36. Typical structure of CdTe/CdMgTe Double Heterostructure as grown via MBE

The real and imaginary dielectric properties, as well as the layer thickness of the alloy barrier were extracted from this oscillator model, and the band gap was identified as a maximum in the real refractive index, as seen in Fig. 37 below.[18,19]

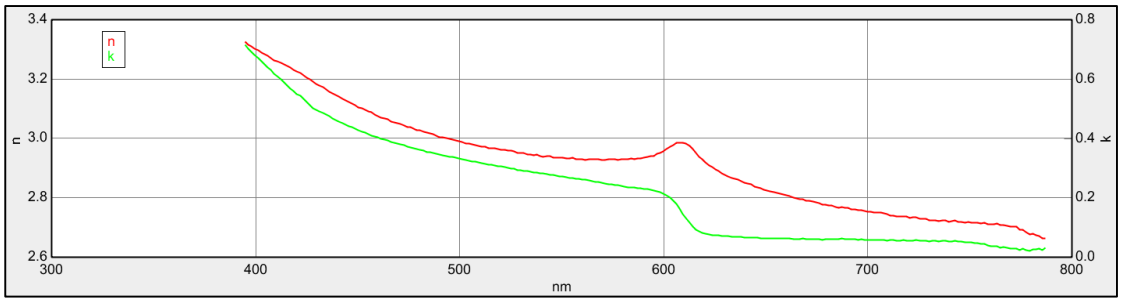

Figure 37. Typical optical constant data for DHs. *Here, the data for DH sample z373, $Cd_{1-x}Mg_xTe$ (x=0.33) at room temperature as measured by variable angle spectroscopic ellipsometry is shown, displaying a clear peak in the index of refraction near the band gap.*

Once the band gap was identified, Mg composition was then able to be determined based on results from Energy-dispersive X-ray Spectroscopy (EDS) measurements performed on a Scanning Electron Microscope (SEM) and Cathodoluminescence (CL) measurements taken by various other members of the research group here at Texas State on 1 μm thick CdMgTe samples. EDS measurements were used to determine the atomic percent of the Mg concentration within the samples, while CL measurements were used to determine the band gap energy of the same samples. Both EDS and CL measurements are highly time intensive and hard to obtain for thin layers such as those used for DH structures. By comparing the Mg concentration as gathered by EDS with the band gap energy as measured by CL, the following trend

was found for finding the x value of $Cd_{1-x}Mg_xTe$ alloys if the band gap energy was known

$$x = \frac{E_g - 1.503}{1.6085} \tag{139}$$

This trend was then compared with several other trends found in literature and was found to be in good agreement, as shown in Fig. 38 below. [20,21,22,23]

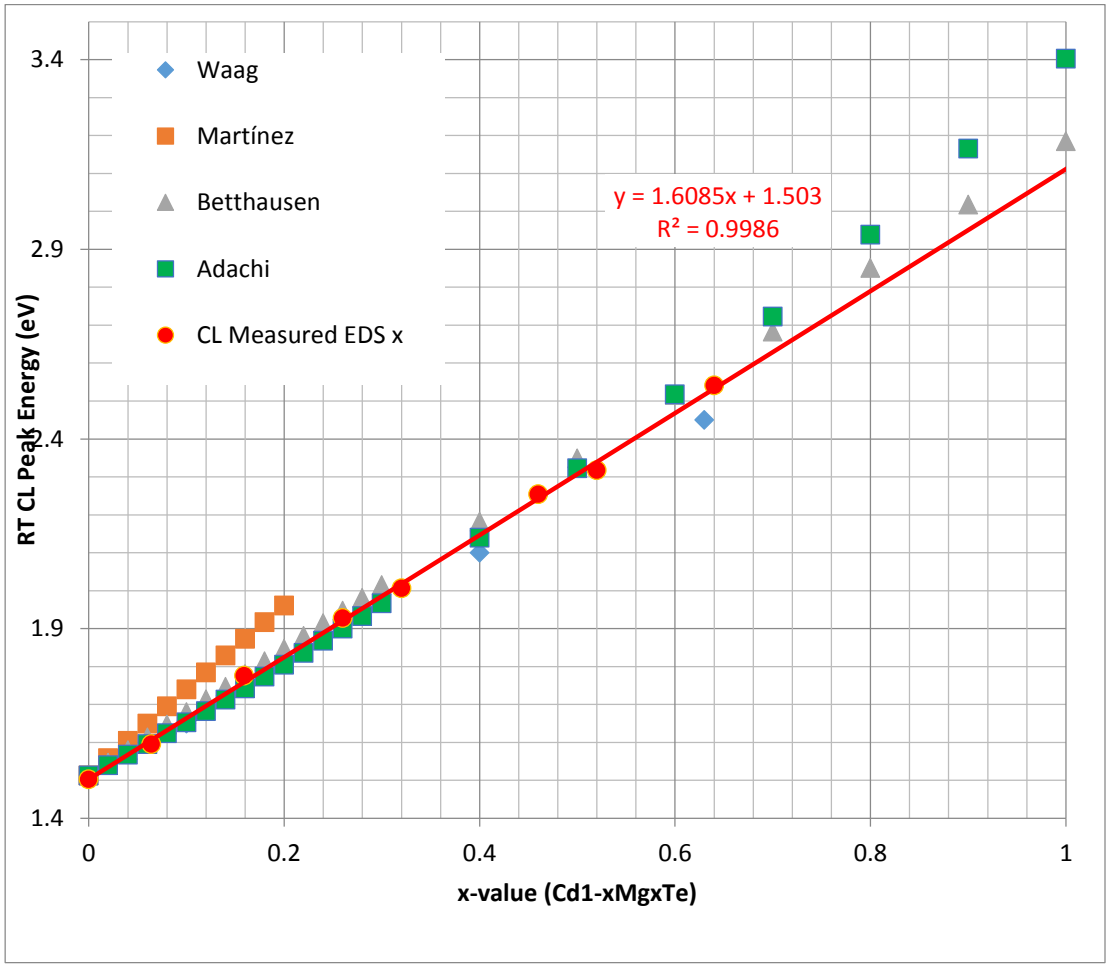

Figure 38. Determination of correlation between x-value and band gap energy of $Cd_{1-x}Mg_xTe$ alloys and comparison with other results found in literature. *Here, the trend shown in red was the determination found at Texas State, and was compared with others found in literature.* [20,21,2223]

The largest uncertainty in using ellipsometry in this way comes from the determination of the band gap energy from the peak in the index of refraction. As stated earlier, this peak occurs *near* the band gap energy. To make sure that the determination of the band gap energy was accurate enough for our purposes, the calculation of x value from the band gap as identified with ellipsometry was compared with the Mg concentration as determined by Atom Probe Tomography (APT), performed by Brian Gorman, et al., at Colorado School of Mines, and was found to be in good agreement, as indicated by the data in Fig. 39 below.

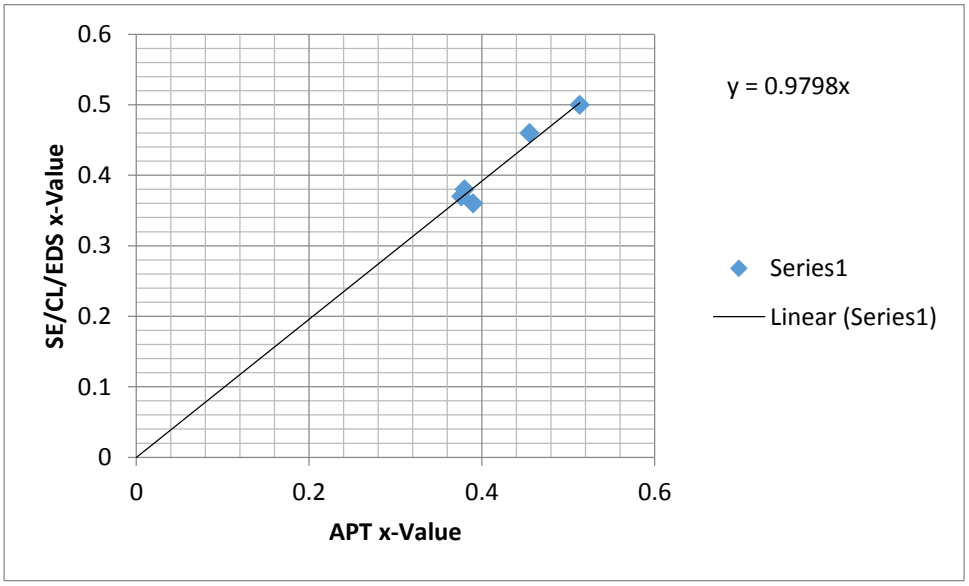

Figure 39. Comparison of x-value as determined by spectral ellipsometry and as determined by Atom Probe Tomography

Once satisfied that the Ellipsometry measurements accurate, they were performed by various members of the research group, including the author, and were used to determine that control of Mg composition during MBE growth had been accomplished.

The use of ellipsometry was motivated by the quick, and non-destructive nature of the measurement.

3.2 Confocal Photoluminescence

Confocal Photoluminescence (c-PL) Microscopy is an optical scanning point source imagining technology originally designed for biological applications but has proven to be quite useful in characterizing semiconductors as well[24]. Laser excitation of energy greater than the band gap of the semiconductor sample to be tested is used, which excites electrons into the conduction band and subsequently induces photoluminescence. Filters in the optical beam path filter out the reflected laser light, so that only photoluminescence is collected. A pinhole is placed in the beam path conjugate to the focal plane (hence the term confocal) and the collected luminescence is measured using a photomultiplier tube (PMT). A schematic of the optical beam path in confocal microscopy is shown below in Fig. 40. When using c-PL this way, a non-radiative defect map of the sample is created.

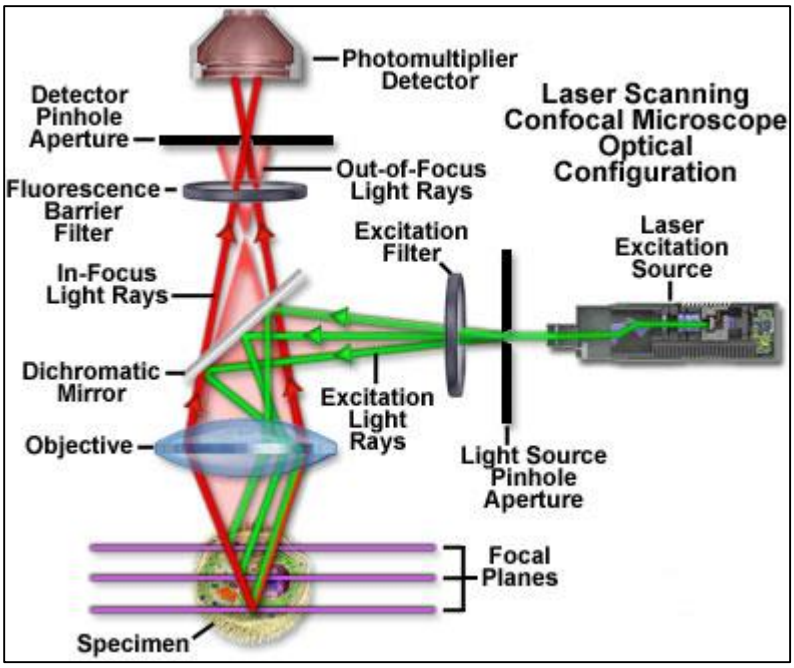

Figure 40. Optical beam path in typical confocal photoluminescence microscopy set up. [34]

C-PL has a couple of major advantages as a characterization technique. The first is that it is non-invasive, which is of particular importance to this study as CdTe is a very soft II-IV semiconductor and is prone to damage. The second is the inclusion of pinholes placed in the optical path that restrict out-of-focus luminescence from reaching the detector focal plane, significantly enhancing both lateral and depth resolution. The last advantage is the 3D capabilities. While the 3D feature is more heavily used in biological applications, it has limited applications in photovoltaic applications as well, limited by the optical absorption of the material.

An Olympus FluoView FV1000 confocal microscope was used to obtain the images presented here with the samples at room temperature. Initially, three laser diodes

of wavelengths 635nm (20 mW total output power of laser, (TP)), 559nm (15mW TP), and 405nm (50mW TP), and one Ar laser of wavelength 488nm (30mW TP) provided illumination of epitaxially grown CdTe on CdTe(211B) and InSb substrates. The power of these lasers was measured at the objective using a Thorlabs calibrated power meter. These measurements are not absolute, as the objectives used were oil immersive and no oil was used when the power was measured, and so, these are representative power measurements. These powers are recorded in Table 10. These lasers, in conjunction with an High Quality 710nm Long Pass (HQ710LP) Barrier filter were used to allow for panchromatic imaging of non-radiative defects in the sample.[25] Initially, a 40x magnification oil immersion UPLAPO objective lens with a Numerical Aperture (NA) of 1.0 was used.

In confocal microscopy, the spot size is typically defined as the diameter of the first Airy disc and can be calculated through the relation

$$D_A = \frac{1.22\lambda_{ex}}{NA} \tag{140}$$

Where D_A is the diameter of the first Airy disc, and λ_{ex} is the wavelength of the excitation source. The lateral optical resolution is typically defined as the radius of the first Airy disc

$$R_A = \frac{0.61\ \lambda_{ex}}{NA} \tag{141}$$

Where R_A is the lateral resolution, or the smallest discernible distance. The axial, or depth resolution can be calculated through the relation

$$R_d = \frac{1.5\, n\, \lambda_{ex}}{NA^2} \tag{142}$$

Where R_d is the depth resolution, and n is the index of refraction of the medium.[26] With this, we were able to determine that for the most common wavelength of excitation used, 635 nm, we achieved a lateral resolution of about 0.4μm using the 40x objective. While the above relation for the depth resolution is true for transparent samples, for opaque samples we must also consider Beer's law which relates the intensity of light to the depth of the sample through

$$I(x) = I_0 e^{-\alpha x} \tag{143}$$

Where $I(x)$ is the intensity, I_0 is the incident intensity, α is the absorption coefficient, and x is the depth into the sample. The absorption coefficient is wavelength and material dependent. The absorption spectrum for CdTe is shown in Fig 41. The characteristic absorption depth $(1/\alpha)$ at 635nm is approximately 0.2μm. The working depth resolution will end up being a convolution of the absorption depth and the depth resolution given above. We note that, the depth resolution was measured to be 0.25-0.5μm using a ZnTe sample and excitation wavelength of 405nm.The image size using the UPLAPO 40x objective was 800*800 [Pixels], and with a 2x digital zoom, the images corresponded to 158μm*158μm. The sampling speed was set to 200μs/Pixel. The voltage for the PMT was set as low as possible to allow for adequate imaging, typically around 200V.

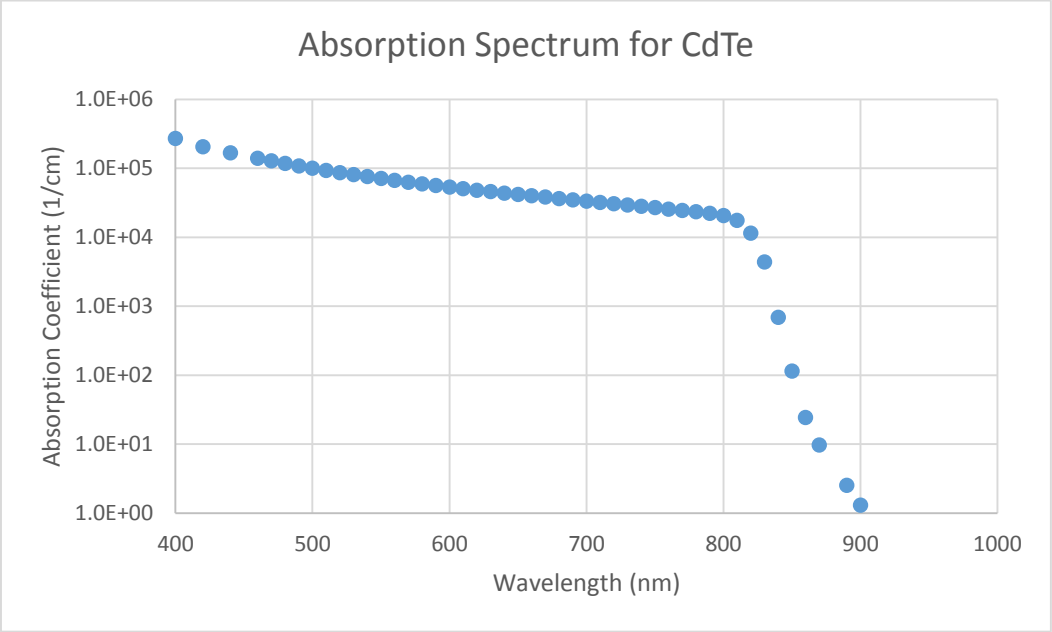

Figure 41. Plot of the absorption coefficient vs wavelength. *Data shown here was collected at FirstSolar*

Because CdTe was investigated using longer excitation wavelengths, resolution was increased further by switching to a 60x magnification oil immersion PlanApo objective lens with an NA of 1.40.[27] With this, the lateral resolution was improved to 0.27μm. An image taken with the 60x objective in conjunction with a 1.5x and 4x digital zoom produced images of approximately 140μm and 50μm on a side, respectively. The image size was set to 1024*1024 [Pixels] for a step size of approximately 137nm, which oversampled the resolution by about two times. To ensure that the brightest focal plane, which corresponds to the top of the sample, over the entire image size was captured, a sequence of images was taken at varying focal planes. Typical step size in depth was 0.20μm. After the sequence was taken, a sum of selected images was formed to create the brightest and best focused image over the entire image area. This image collection method took about 30 minutes per image, depending on how many images were included

in the sequence. For statistical soundness, images were typically taken at 5 or 6 different spots of a CdTe sample, putting the time spent characterizing a single sample at approximately 3 hours.

From the resolution geometry, the power density of the laser spots were determined. From this, the excess carrier concentration can also be determined. We have determined previously that in steady state, the recombination rate equals the generation rate. Recall that the radiative recombination rate R_L ($photons/cm^3 s$) is related to the carrier concentration through

$$R_L = B_{rad} np \tag{144}$$

Assuming radiative recombination dominates, with the power density (PD) known (W/cm^3), we divide this value by the energy of a photon to get the photon generation rate. The carrier concentrations in the above equation are composed of the equilibrium concentrations plus the excess carrier concentrations. So then, our expression can be re-written as

$$\frac{PD}{E_{photon}} = R_L = B_{rad}(n_0 + \Delta p)(p_0 + \Delta p) \tag{145}$$

$$\frac{PD}{E_{photon}} = R_L = B_{rad}[n_i^2 + \Delta p(n_0 + p_0 + \Delta p)] \tag{146}$$

At very high-injection, defined as the condition where $\Delta p \gg N$, where N is the background doping, then the Δp terms will dominate and the equilibrium concentrations will drop out. The intrinsic carrier concentration in CdTe is on the order of $10^5/cm^3$, and so will not make a significant contribution. We are left with

$$\frac{PD}{E_{photon}} = B_{rad}[\Delta p^2] \tag{147}$$

Which can be solved for the excess carriers to give

$$\Delta p = \sqrt{\frac{PD}{E_{photon}B_{rad}}} \tag{148}$$

Knowing that the background doping for CdTe is on the order of $10^{14}cm^{-3}$, then with the results shown in Table 10, we know that we are in fact working in the high-injection regime. This remains true for most doping levels examined as well.

Table 10. Calculated figures of merit for c-PL. *Here, calculations use the 60x objective with an NA of 1.4 mentioned previously*

Wavelength (nm)	Power at 100% (W)	R_A (cm)	D_A (cm)	Cylindrical Volume (cm^3)	Power Density (W/cm^3)	Carriers/cm^3
405	4.10E-05	1.76E-05	3.53E-05	4.89E-14	8.38E+08	4.13253E+18
488	2.30E-05	2.13E-05	4.25E-05	7.10E-14	3.24E+08	2.81972E+18
559	1.90E-05	2.44E-05	4.87E-05	9.32E-14	2.04E+08	2.39454E+18
635	1.27E-05	2.77E-05	5.53E-05	1.20E-13	1.06E+08	1.83682E+18

After image collection, images were uploaded as .bmp or .tif files and processed using the ImageJ program which is an open source image analysis program maintained by NIST.[28] By using a Fast Fourier Transform – Bandpass Filter to remove large intensity variations and enhance contrast, the program was able to identify dark spots within a certain inputted pixel size range, typically between 35 and 2 pixels. After this, a manual threshold was set on the image to identify point defects in the image. Then, upon using the Analyze Particles feature within the program, a count of the point defects was

performed on the image. By combining this spot count with the known area of the images, a non-radiative defect density (DD) was obtained. See Fig. 42 below.

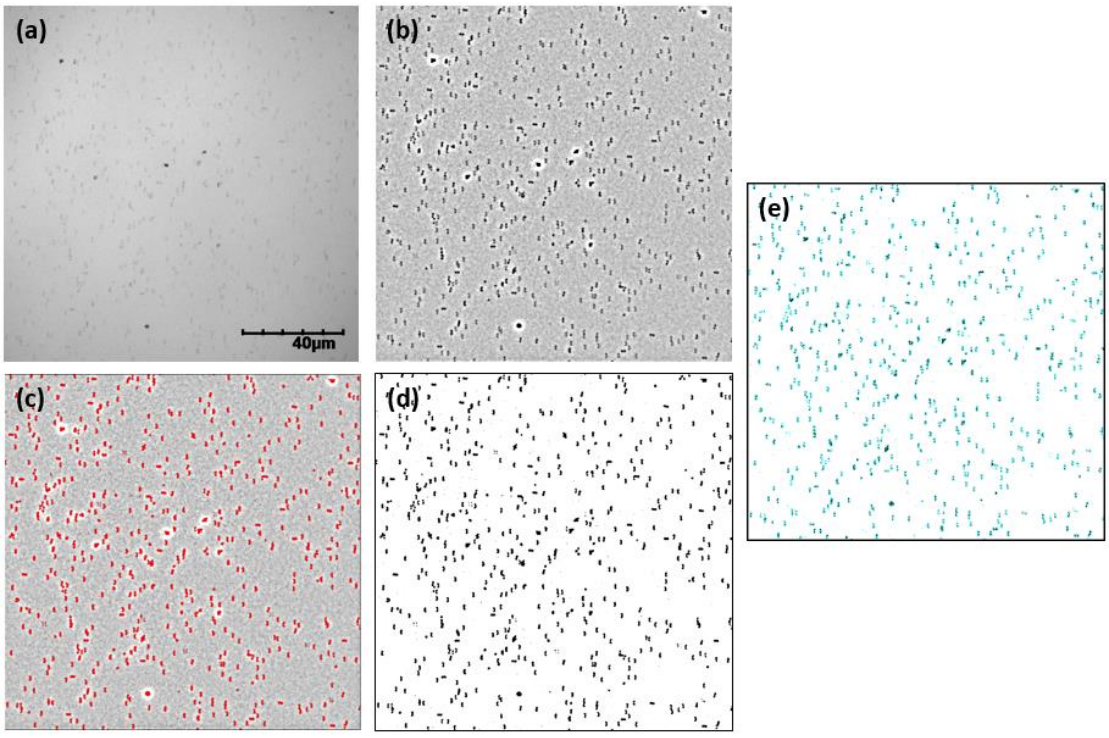

Figure 42. C-PL Image processing sequence using ImageJ. *(a) As measured c-PL image of CdMgTe DH. (b) Application of the Bandpass Filter. (c) Manually thresholding the image, seen in red. (d) Application of the threshold. (e) Application of the Analyze Particle feature, indicating what has been counted with a blue outline. Here, ImageJ detected 1148 particles, which translates to a DD of* $5.76x10^{6}/cm^{2}$

The above approach required significant collection time. To improve upon this method, a consultation with an Olympus technician occurred. After consultation, it was determined that image collection was not occurring at the optimal voltage for the PMT. Moving forward, the PMT was set near 500V, the optimal voltage for the greatest signal to noise ratio. With the PMT voltage increased, the number of lasers used to excite the samples could be reduced to the 559nm and 635nm laser diodes. It was also determined

that the image size of the images taken with the 60x objective and the 1.5x digital zoom should be increased to 2048*2048 [Pixels].

In an effort to cut down the amount of time it took to collect images, it was suggested that the sampling speed decrease to 2.0μs/Pixel and to introduce Line Kalman Integration in an effort to decrease noise. The Line Kalman Integration is a form of Kalman Filtering, which is a statistical filter that uses auto-regression of prior measurements to predict the present measurement and then corrects the estimate with a moving average as soon as the present measurement is available[29]. This integration measures a single line of the image a specified number of times, typically 4, and produces a weighted average of that line, based on the results of the measurements taken, where measurements with higher certainty are weighted more. The integration helps reduce the uncertainty in the measurement originating from the random nature of emission of photoluminescence. By modifying the image collection process in this way, imaging time was reduced from approximately 30 minutes an image to approximately 6 minutes an image for 1.5x images, and approximately 3 minutes for 4x images.

The images produced by the method described above gave valuable information about the crystalline quality of the CdTe samples that were grown via MBE. The first figure of merit was mentioned above, the DD. This gave a quantitative means of providing feedback to the MBE growers. Typical c-PL results are shown in Fig. 43.

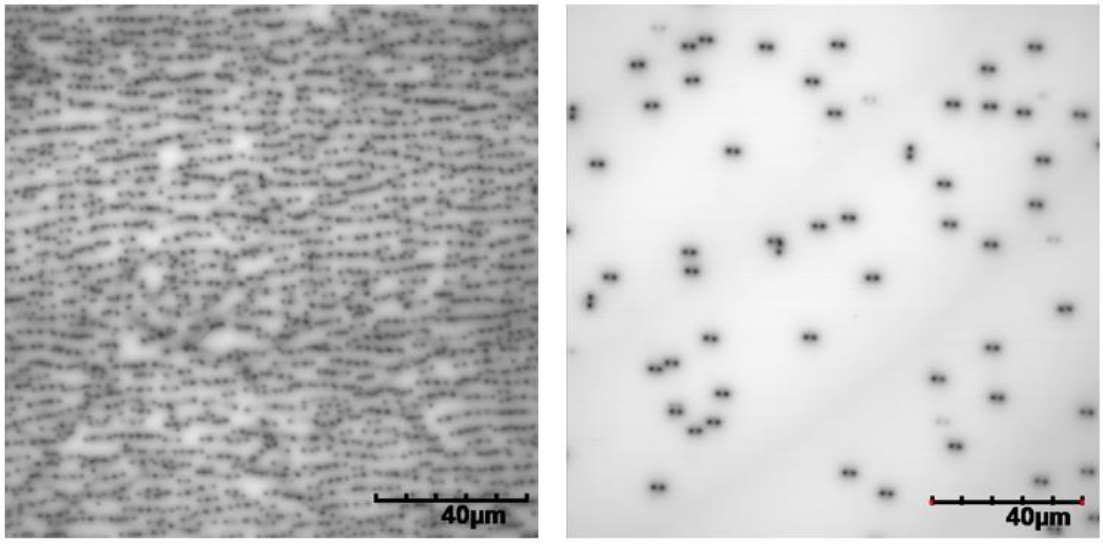

Figure 43. Typical c-PL images of two CdMgTe DH structures. *The left image has a DD in the low 10^7/cm^2, while the right has a DD in the mid 10^5/cm^2.*

These images were also able to provide information about the types of defects present in the sample, from point defects, to twins which were determined from a characteristic double-dark spot defect, and misfit dislocations. The presence of twin defects was confirmed through the acquisition of the Atomic Force Microscopy (AFM) image shown in Fig. 44.

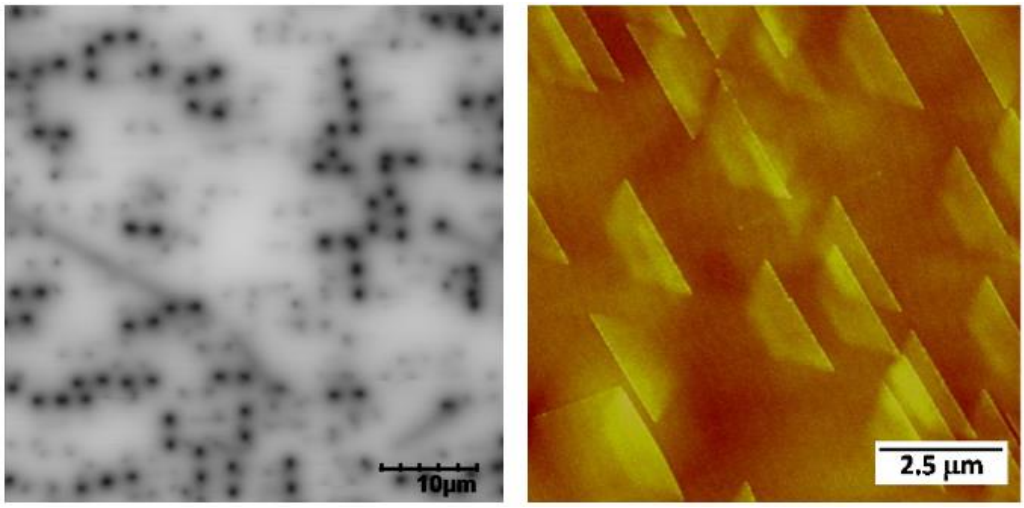

Figure 44. C-PL and AFM images confirming the presence of twin related defects*. The c-PL image on the right shows that this DH had a high concentration of the characteristic double dark spot defect. By comparing this with the AFM image which shows twinning defects rising from the surface of the sample, the presence of these defects was confirmed.*

As part of the study, CdTe/CdMgTe DHs were grown on various substrates including CdTe(100), CdTe(211B) and InSb(100). CdTe and InSb have a slight lattice mismatch, i.e. the atomic spacing between the two materials are not the same. This mismatch causes stress in the lattice, which in turn causes strain in the film. When the thickness of the film increases, it may become energetically favorable for misfit dislocations to form at the interface of the film and the substrate. The thickness at which this occurs is typically called the critical thickness[30]. Based on the number of misfit dislocations present in the c-PL image, it could be determined if the sample had exceeded the critical thickness when grown on InSb as seen in Fig. 45 (a). This critical thickness inhibited desired layer thicknesses within the DH structures, so alloying with small amounts of Se to create CdSeTe was done, creating CdSeTe/CgMgTe DHs in an effort to create to a better lattice match with InSb. Verification of successful lattice matching of CdSeTe was accomplished with c-PL, as seen in Fig. 45 (b).

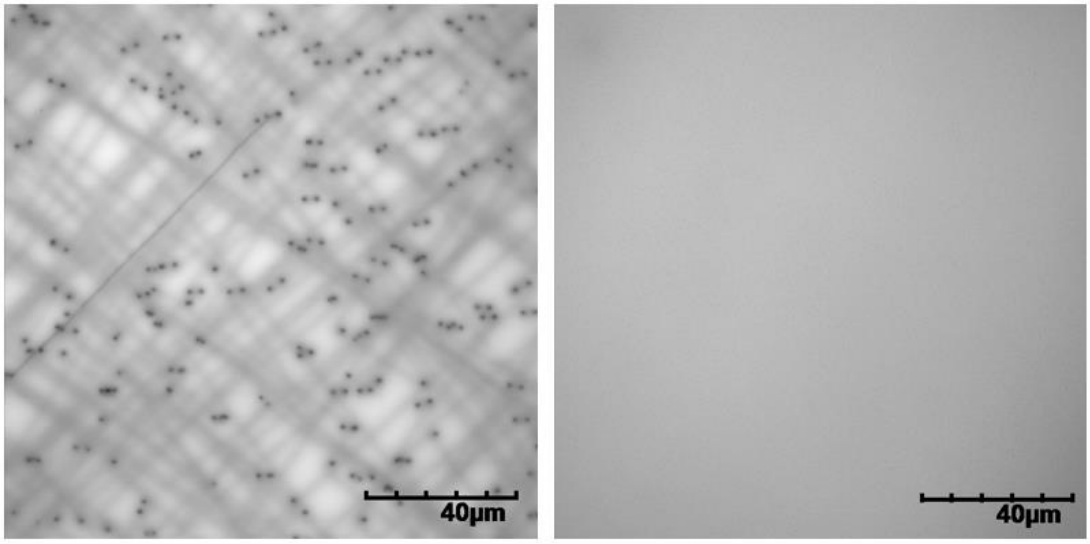

Figure 45. C-PL images for a DH that has exceeded critical thickness and a DH where lattice matching had been achieved. *(a) Left, c-PL image of CdTe/CdMgTe DH with an absorber layer 2 µm that has clearly exceeded critical thickness. (b) Right, lattice matched CdSeTe/CdMgTe DH with an absorber layer of 5µm.*

When used this way, c-PL can serve as an effective screening technique for determining the crystalline quality of epitaxially grown structures. The quantitative DD provided feedback for proceeding PL analysis. Specifically, the DD gave information on possible recombination mechanisms occurring in the sample, and allowed us to select low DD samples for evaluating fundamental recombination, without the complication of DD recombination.

3.3 Photoluminescence Intensity Measurements

Photoluminescence Intensity (PLI) Measurements share many of the same principles as c-PL, and are carried out in a similar manner. Laser excitation of energy greater than the band gap of the sample to be tested is used, which induces

photoluminescence. Filters in the optical beam path once again are used to filter out the reflected laser light, ensuring that only photoluminescence is collected and measured. By using a power meter to directly measure the power of the laser excitation, and by knowing the spot size of the laser, it is possible to study the PLI efficiency (the photoluminescence intensity divided by excitation intensity) as a function of excitation intensity.

PLI and c-PL share one major advantage, namely, that they are both non-invasive. This allows for multiple characterizations on a single sample, thereby allowing cross-referencing between multiple characterization techniques.

For PLI, excitation was initially provided by a COHERENT INNOVA 300 argon ion laser of 514 nm wavelength chopped at 400 Hz by a Stanford Research Systems Model SR540 Chopper Controller. A 6.5x objective lens focused the laser light onto an adjustable stage equipped with micrometers in both the x and y directions. The absolute excitation power was measured using a ThorLabs calibrated power meter. The photoluminescence was collected through the same objective, passed through optical filters to reject reflected laser light including Raman Edge, Long Pass and Short Pass filters, and focused onto a ThorLabs Si Amplified photodiode detector. The detector was then connected to a Stanford Research Systems SR510 Lock-in Amplifier which measured the voltage response of the Si detector corresponding to over 6 orders of magnitude in PL intensity. The photoluminescence intensity variation was then recorded as the laser intensity was varied with a series of calibrated neutral density (ND) filters that spanned 5 orders of magnitude in excitation intensity. The ND filters were mounted in two Filter Wheels, one containing ND 0, 0.3, 0.5, 0.8 plus a laser blocking plate, while

the other contained ND 0, 1, 2, 3, and 4. It should be noted that these ND values are not exact, but approximations to make measurement recording easier. An ND filter (also sometimes called Optical Density or OD) works to decrease the amount of light that passes through it. The following expression relates the optical density, d, with the incident intensity I_0 and the transmitted intensity

$$d = -\log\frac{I}{I_0} \tag{149}$$

The optical density is closely related to attenuation. To calibrate the ND filters, the ThorLabs power meter was placed on the stage, and the power with and without the filter was measured, allowing for an accurate determination of the ND of the filters. The use of this Filter Wheel allowed for controlled laser power variation over approximately 5 orders of magnitude. A schematic of the PLI set up is shown below in Fig. 46.

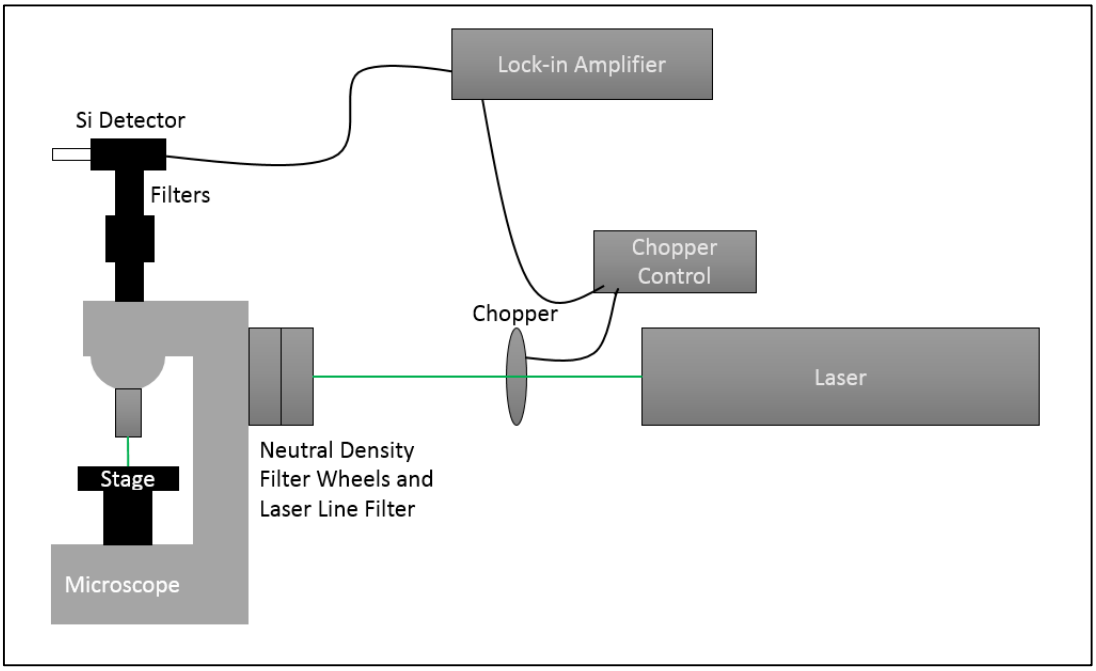

Figure 46. Schematic of initial PLI set up. *The excitation source runs through a chopper then through a series of neutral density filters, is reflected out of the microscope objective and lands on the sample. From there, it is reflected through the top of the microscope where it encounters a number of filters that block the excitation source, and only permit photoluminescence to pass and land on the detector. The lock-in amplifier, which is connected to the chopper in an effort to cut down on electrical noise, then reads the detection as a voltage.*

The schematic of the filters used before the detector are shown below.

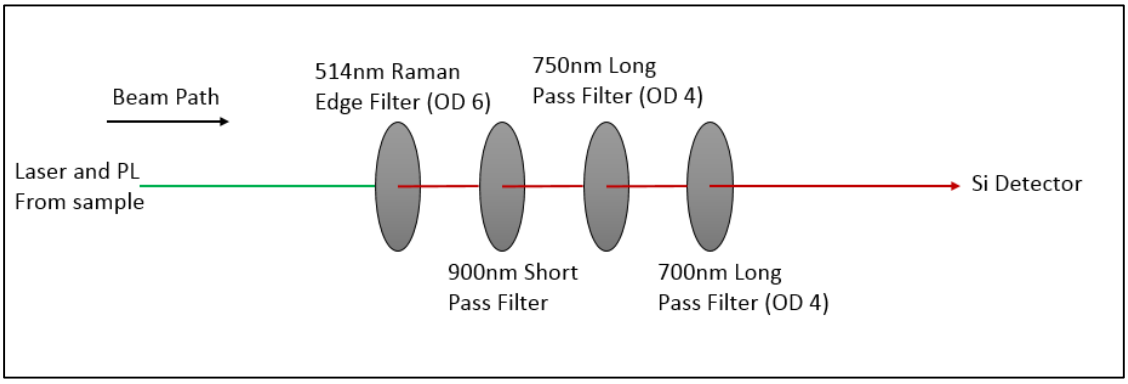

Figure 47. Depiction of filters used in PLI setup. *Diagram of the filters used to block the excitation source and allow transmission of the photoluminescence. The Raman Filter blocks the laser light, while the Pass filters block out any ambient light that may be passing through the beam path while simultaneously allowing transmission of the PL.*

The Raman Edge Filter had an OD of approximately 6, while the 750nm and 700nm Long Pass Filters had an optical density of 4, each. This means that at the detector, there is an overall OD of 14 in regards to the laser light. To demonstrate the effects of the Pass filters shown above, the measured PL spectrum for CdTe is shown below.

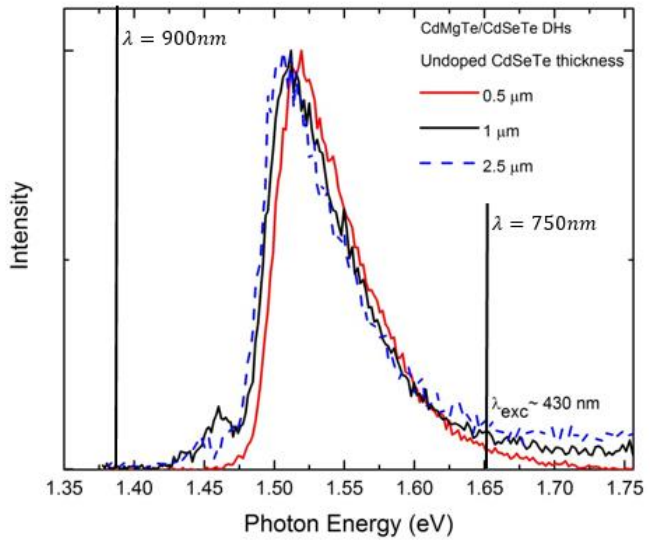

Figure 48. The PL spectra of undoped CdMgTe/CdSeTe DHs with 0.5 – 2.5μm absorber layer measured with 430nm excitation wavelength. *The vertical lines correspond to the wavelengths of the Pass filters. From here, we see that our filters act to block out any light that does not fall in the PL spectra of CdTe.*

From the Figure above, we see that the 750nm Long Pass Filter actually blocks a small fraction of the PL. This filter was included in the beam path anyways because the overall OD leading to the detector was not high enough without it, i.e. with an overall OD of 10 leading up to the detector from the Raman Edge and 700nm Long Pass Filters, laser light was still being detected. Once the inclusion of the 750nm Pass filter occurred, this was no longer the case.

Due to catastrophic equipment failure, a new laser was brought in to perform PLI measurements. This laser, a COHERENT INNOVA 90, also provided light of 514nm wavelength for excitation. One parameter of crucial importance to this measurement technique is the spot size of the excitation source. This parameter is important for analysis, which relies heavily on absolute knowledge of excitation intensity (W/cm^2). With the new laser in place, spot size measurements were taken by collecting the photoluminescence of a GaAs/AlGaAs DH calibration sample at 5 μm intervals up to and over the cleaved edge of the sample, simulating a moving knife edge measurement. This was done in both the x and y directions. This produced a symmetric erf intensity profile with respect to distance. With this data, it was then possible to determine local derivatives of the data, and fit a Gaussian curve using MATLAB. Using this technique it was determined that there was a FWHM Gaussian spot size of 120μm. An example of the data collected and the local derivatives of the data to show an approximate Gaussian curve are shown below in Fig. 49. Note that the limited range of the high precision micrometer on the stage did not allow measurement of the complete peak, but did provide enough data to accurately determine the spot shape and FWHM.

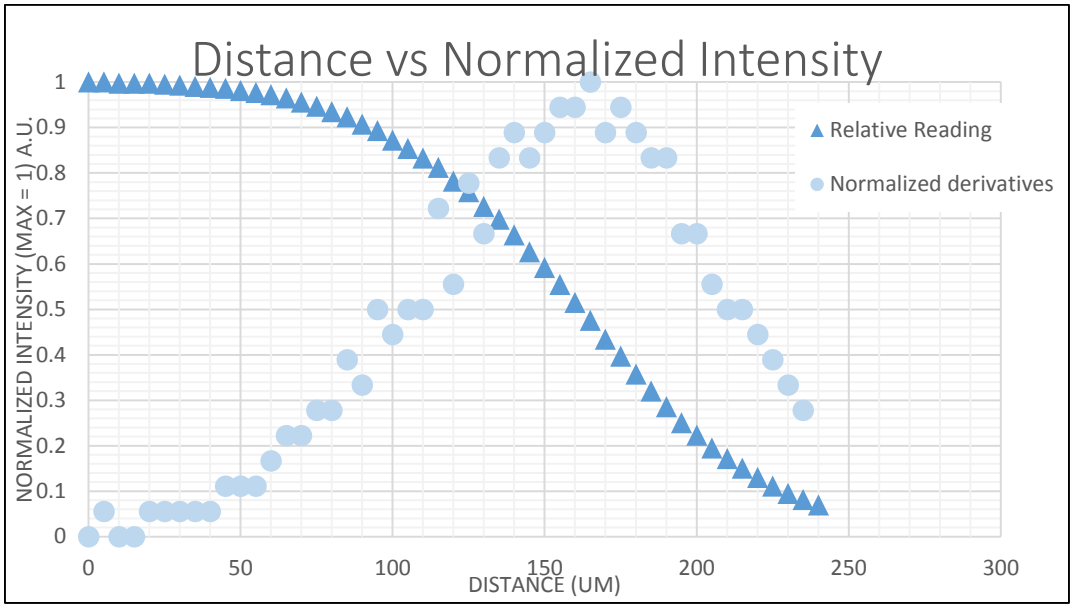

Figure 49. Spot Size measurement data. *Plot of the normalized intensity readings versus distance. The normalized data is shown here as the Relative Reading, while the local derivatives are shown as the Normalized derivatives.*

A Gaussian fit of the data above, performed using MATLAB, is shown below in Fig. 50.

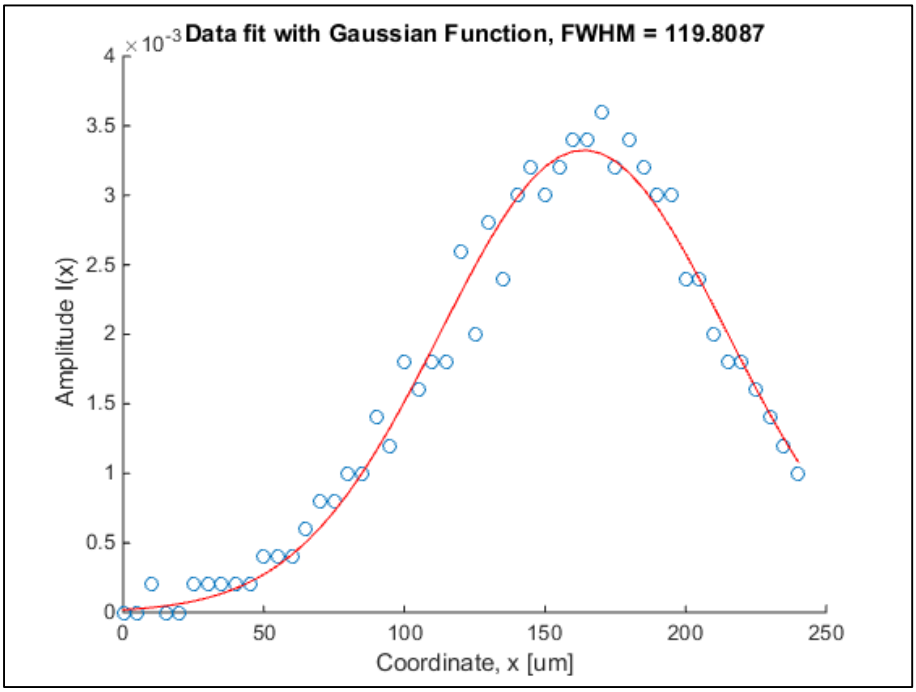

Figure 50. Gaussian fit of spot size measurement. *Fit of the local derivatives of the raw intensity data. Here, we see that the fit determined that the FWHM of the spot was approximately 120 µm.*

Because of the strong dependence on accurate input intensity that PLI analysis requires, a daily calibration routine was performed before measurements were taken. The goal of this calibration was to ensure consistency between measurements. To do this, the laser profile was checked to verify that it was in the Gaussian mode. Once confirmed, then the power of the laser on the stage was measured and adjusted if necessary to match an agreed upon value. After this, the laser alignment was checked using a calibration sample on the stage and removing the Si Detector from the setup, allowing the laser light to reflect through the top of the microscope onto the ceiling. The ceiling had a target that the laser was intended to align with. If the alignment was off, mirrors in the beam path were adjusted to correct the alignment. The target on the ceiling was very effective, as small changes in the beam path were exaggerated by the relatively large distance to the

ceiling, making this an accurate way to verify alignment. After alignment of the laser, the PL of one of two standard GaAs/AlGaAs DH calibration samples was made. Because the Lock-in Amplifier was connected to a chopper, it was important to make sure that the two devices were operating at the same frequency. It was also important to adjust the phase of the Lock-in to match the input signal from the Si Detector so that a maximum signal was being detected by the Lock-in Amplifier. The standard calibration sample was then measured in an agreed upon spot, and the value of the reading was checked. For consistency, this measurement was intended to produce the same value every time it was measured. If there was variation in the measurement, then slight adjustments to the laser alignment would be made, usually in the form of small changes in the stage height. If a change in stage height occurred, then the power of the laser at the stage would be re-measured to ensure that the change was not significant enough to change the excitation power. Once everything was determined consistent, then the sample to be tested would be placed on the stage, the Si Detector would be removed again, and alignment of the laser with the target on the ceiling would be verified for again. If it were misaligned due to a surface gradient on the sample, then adjustments to mirrors in the beam path would occur. Only by performing this strict calibration routine before every measurement were we able to determine efficiencies and accurately compare measurements for different samples. A standard procedure is detailed in Appendix G.

The two GaAs/AlGaAs DHs also served as a reference for determining internal quantum efficiency. These two GaAs samples were measured previously by others to have approximately 100% internal quantum efficiency. Others calculated the ratio to CdTe and the results agree that the best samples measured by PLI have 90-100% internal

quantum efficiency. Based on this, all PLI measurements were normalized so that the best samples mentioned above gave a normalized efficiency of 100%.

The initial setup could measure six orders of magnitude in PL intensity. It was determined that this was not sufficient for characterization of better samples. In order to improve the PLI setup, a Hamamatsu R943-02 PMT was added along with another Raman Edge Filter and more Long Pass Filters, a shutter to maintain a light-tight seal when not in use, and a Stanford Research Systems Model SR830 DSP Lock-in Amplifier with femto-amp detection capabilities. This allowed the use of the full range of the ND filter combinations and was accompanied by the addition of another ND filter in the optical beam path to modulate the laser power, as well as a small, right angle prism mirror to divert the beam path towards the PMT. A schematic of the PLI set up with these upgrades is shown below in Fig. 51.

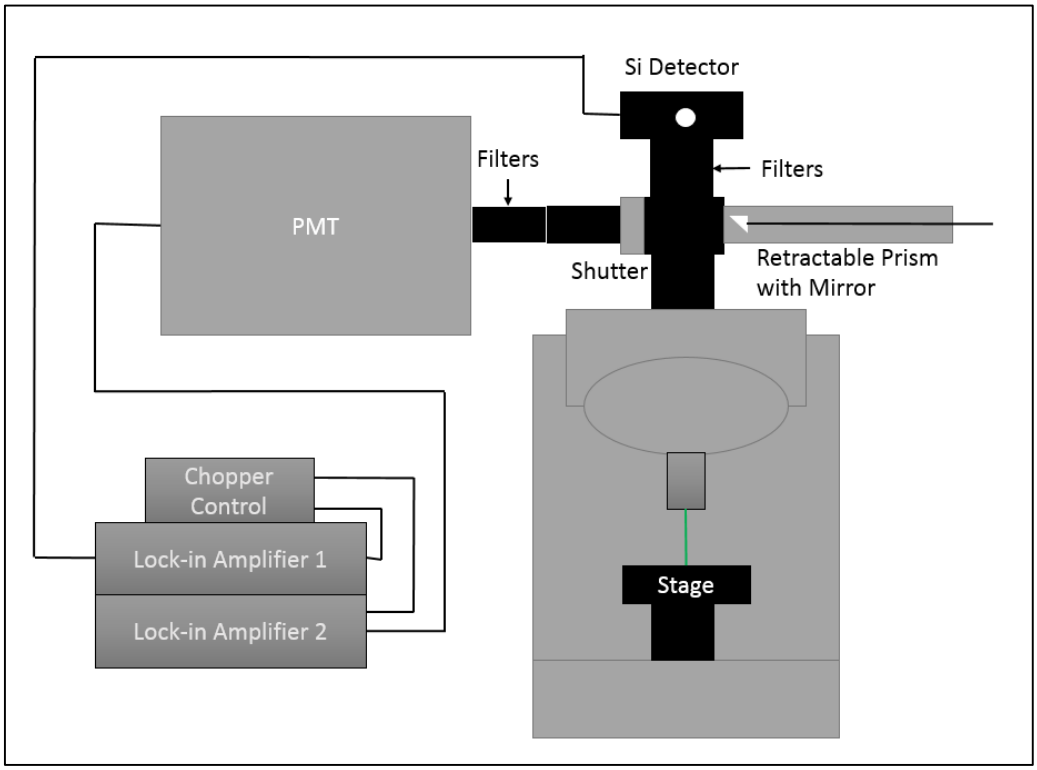

Figure 51. Schematic of upgraded PLI setup. *Note that the laser and chopper are not shown.*

A schematic of the filters used before the detector is shown below

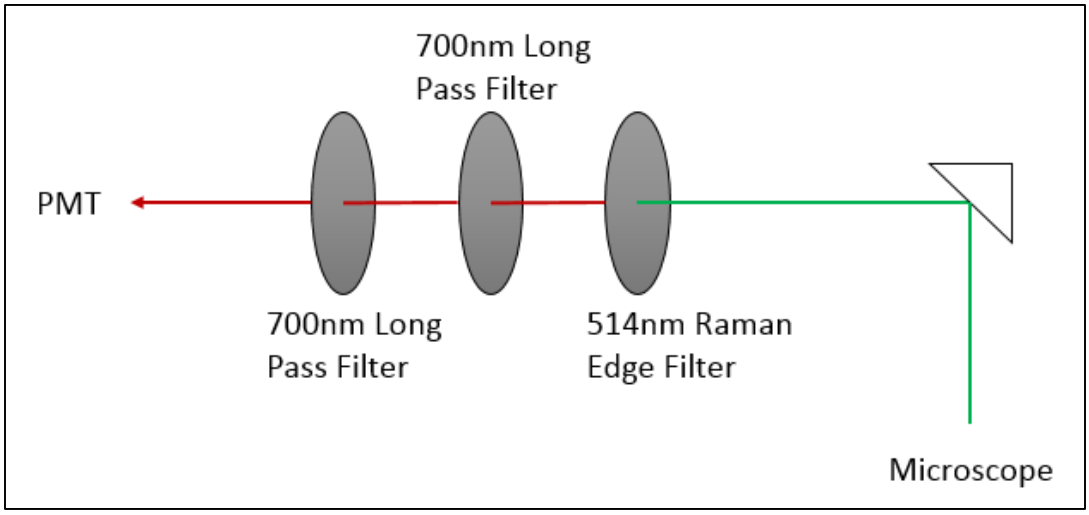

Figure 52. Diagram of filters used in the beam path leading to the PMT in PLI setup. *The Long Pass Filters reflect all light with wavelengths shorter than 700nm and allow transmission of all light with wavelengths longer than 700nm.*

It should be noted that the two Lock-In Amplifiers did not record measurements in the same units, i.e. one of them measured in volts while the other measured in amps. The PMT gain was sensitive to applied voltage, which could not be controlled absolutely. Because the gain on the PMT was not consistent, a unique conversion factor was needed for each sample. To determine this, a sample was measured at the lower range of good signal to noise ratio on the photodiode, and was then measured on the PMT with the same input intensity. This transition occurs at different excitation powers for each sample. By measuring the sample with the same excitation power using both devices, a conversion factor could be determined. These additions improved the range of varied laser intensity to 8 orders of magnitude and improved the range of PL detection to span 10 orders of magnitude.

With the addition of another ND Filter into the beam path that needed to be calibrated, it was decided that all of the ND filters should be calibrated again to determine accuracy for analysis purposes. It was found that a few of the filters had possibly changed since the initial calibration, and the new attenuation was recorded for analysis purposes. The actual values of the ND filters are recorded below in Table 11.

Table 11. Calibration of ND filters.

Marked ND	Input Intensity (mW)	Output Intensity (mW)	Attenuation	Actual ND
0	67.3	67.3	1	0
0.3	67.3	31.9	2.11	0.32
0.5	67.3	17.2	3.91	0.59
0.8	67.3	7.97	8.44	0.93
1	67.3	5.99	11.24	1.05
1.3	67.3	2.78	24.21	1.38
1.5	67.3	1.64	41.04	1.61
1.8	67.3	0.699	96.28	1.98
2	67.2	0.531	126.55	2.10
2.3	67.3	0.249	270.28	2.43
2.5	67.2	1.44E-01	466.99	2.67
2.8	67.2	6.28E-02	1070.06	3.03
3	67.2	4.63E-02	1451.40	3.16
3.3	67.2	2.21E-02	3040.72	3.48
3.5	67.2	1.21E-02	5567.52	3.75
3.8	67.2	5.67E-03	11851.85	4.07
4	67.2	8.30E-03	8096.39	3.91
4.3	67.3	4.00E-03	16825.00	4.23
4.5	67.2	2.19E-03	30684.93	4.49
4.8	67.2	1.09E-03	61651.38	4.79
In Beam path				
3	67.2	5.62E-02	1195.73	3.08
3.3	67.7	2.66E-02	2545.11	3.41

Figure 53. Image of the upgraded PLI setup.

The data obtained by the method described above gave information about the radiative efficiency of CdTe samples. The PL efficiency was then plotted versus the excitation intensity to determine trends in structures. The trends in PLI efficiency can reveal information about interface trap states and energies. A screenshot of the Excel file that was used for analysis is shown below.

Date	3/16/2015							Sample #	Z-373 Remeasure	Las.Power	210 mW
laser power on stage					0.073	W					
within FWHM					70.0%		between 85% and 15 % of intensity				
FWHM					120	microns					
Power density (ND=0)					4.52E+02	W/cm2					
Sample transmittance				@514 nm (laser)	1.000				Norm factor	0.00708	
				@1455 nm (Peak PL)	1.000						
Single detector											
ND	Time (s)	Raw PL signal (mV)	Gain (dB)	Integrated PL signal (mV)	P0' (W/cm2)	Normal. PL	OD factors	efficiency	Norm Eff		
0	1	2.91	0	2.91E+00	4.52E+02	2.91E+00		6.44E-03	9.09E-01		
0.3	1	1.33	0	1.33E+00	2.14E+02	1.33E+00		6.21E-03	8.77E-01		
0.5	1	0.727	0	7.27E-01	1.16E+02	7.27E-01		6.29E-03	8.89E-01		
0.8	1	2.97E-01	0	2.97E-01	5.35E+01	2.97E-01		5.55E-03	7.84E-01		
1	1	2.20E-01	0	2.20E-01	4.02E+01	2.20E-01		5.47E-03	7.72E-01		
1.3	1	9.06E-02	0	9.06E-02	1.87E+01	9.06E-02		4.85E-03	6.85E-01		
1.5	1	4.42E-02	0	4.42E-02	1.10E+01	4.42E-02		4.01E-03	5.67E-01		
1.8	1	1.52E-02	0	1.52E-02	4.69E+00	1.52E-02		3.24E-03	4.57E-01		
2	1	9.62E-03	0	9.62E-03	3.57E+00	9.62E-03		2.69E-03	3.80E-01		
2.3	1	3.08E-03	0	3.08E-03	1.67E+00	3.08E-03		1.84E-03	2.60E-01		
2.5	1	3.58	70	1.20E-03	9.68E-01	1.20E-03		1.24E-03	1.75E-01		
2.8	1	7.85E-01	70	2.63E-04	4.22E-01	2.63E-04		6.22E-04	8.78E-02		
3	1	4.30E-01	70	1.44E-04	3.11E-01	1.44E-04		4.62E-04	6.52E-02		
3.3	1	9.61E-02	70	3.21E-05	1.49E-01	3.21E-05		2.16E-04	3.05E-02		
3.5	1	2.53E-02	70	8.45E-06	8.12E-02	8.45E-06		1.04E-04	1.47E-02		
3.8	1	4.81E-03		1.61E-06	3.81E-02	1.61E-06		4.22E-05	5.96E-03		
4	1	1.06E-02		3.54E-06	5.58E-02	3.54E-06		6.35E-05	8.96E-03		
4.3	1	2.43E-03		8.14E-07	2.69E-02	8.14E-07		3.03E-05	4.28E-03		
4.5	1	8.49E-04		2.84E-07	1.47E-02	2.84E-07		1.93E-05	2.72E-03		
4.8	1	1.95E-04		6.52E-08	7.33E-03	6.52E-08		8.89E-06	1.26E-03		
5	1	5.20E-05		1.74E-08	2.99E-03	1.74E-08		5.82E-06	8.22E-04		
5.3	1	1.38E-05		4.60E-09	1.42E-03	4.60E-09		3.25E-06	4.59E-04		
5.5	1	5.48E-06		1.83E-09	7.63E-04	1.83E-09		2.40E-06	3.39E-04		
5.8	1			0.00E+00	3.54E-04	0.00E+00		0.00E+00	0.00E+00		
6	1			0.00E+00	2.60E-04	0.00E+00		0.00E+00	0.00E+00		
6.3	1			0.00E+00	1.23E-04	0.00E+00		0.00E+00	0.00E+00		
6.5	1				6.66E-05	0.00E+00		0.00E+00	0.00E+00		
6.8	1				3.08E-05	0.00E+00		0.00E+00	0.00E+00		

Figure 54. Screenshot of Excel sheet used for PLI analysis. *Here, all measurements are corrected for any sort of gain used while measuring. The efficiency is determined by dividing the PL by the input power. The normalized efficiency is then found by multiplying the previous result by a common normalization factor based on the best samples measured.*

For these calculations, first all measurements were corrected for any sort of gain used while measuring. In the above, you will notice that at ND 3.8, a record of the gain used stopped. This is because at this point the switch to the PMT occurred. Up to three previous point were then re-measured with the PMT, and the conversion factor used to necessary to connect the PMT and Si Detector measurements was calculated. This occurred at the lower end of the Si Detector range with a gain of 70 dB, thus the PMT measurements were treated with the same gain and corrected accordingly. After this, the corrected PL measurements were divided by the input intensity to determine the

efficiency of the sample. From there, the efficiencies were normalized using a common factor based on the best CdTe samples that were determined to have 90-100% internal quantum efficiency. A typical PL curve exhibits an "S" shaped curve like the one shown below

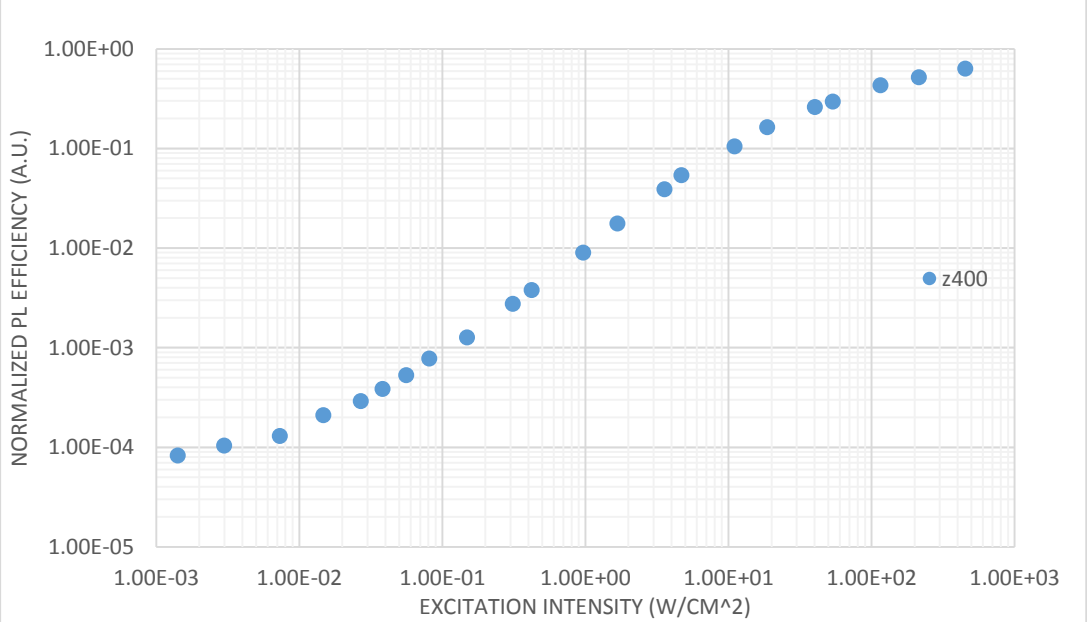

Figure 55. Normalized PL Efficiency vs Excitation Intensity for sample z400. *This particular sample had a 2 µm thick absorber layer and was grown on InSb(100), and was slightly alloyed with Se for lattice matching, making this a CdSeTe/CdSeMgTe DH. Note that on this (and all PLI plots) the PL is normalized by excitation intensity.*

At the low end of the curve where it begins to flatten out, we are considering the low-injection condition. Here, surface recombination dominates and the lifetime and surface recombination velocity are well defined. At the high end of the curve where it begins to flatten out again, we are considering high-injection conditions and the PL of the sample is beginning to reach the radiative limit. The sample is also approaching 100% internal quantum efficiency and radiative recombination dominates. In between the two,

the physics of the PL is complicated and dominated by a mix of non-linear effects. With the data supplied by the author, another member of the research team, Craig Swartz, was able to model the behavior of the PL and was able to determine sample specific material parameters such as interface trap density and the energy of the traps. The basic trends and concepts of the PLI response is shown below in Fig. 56.

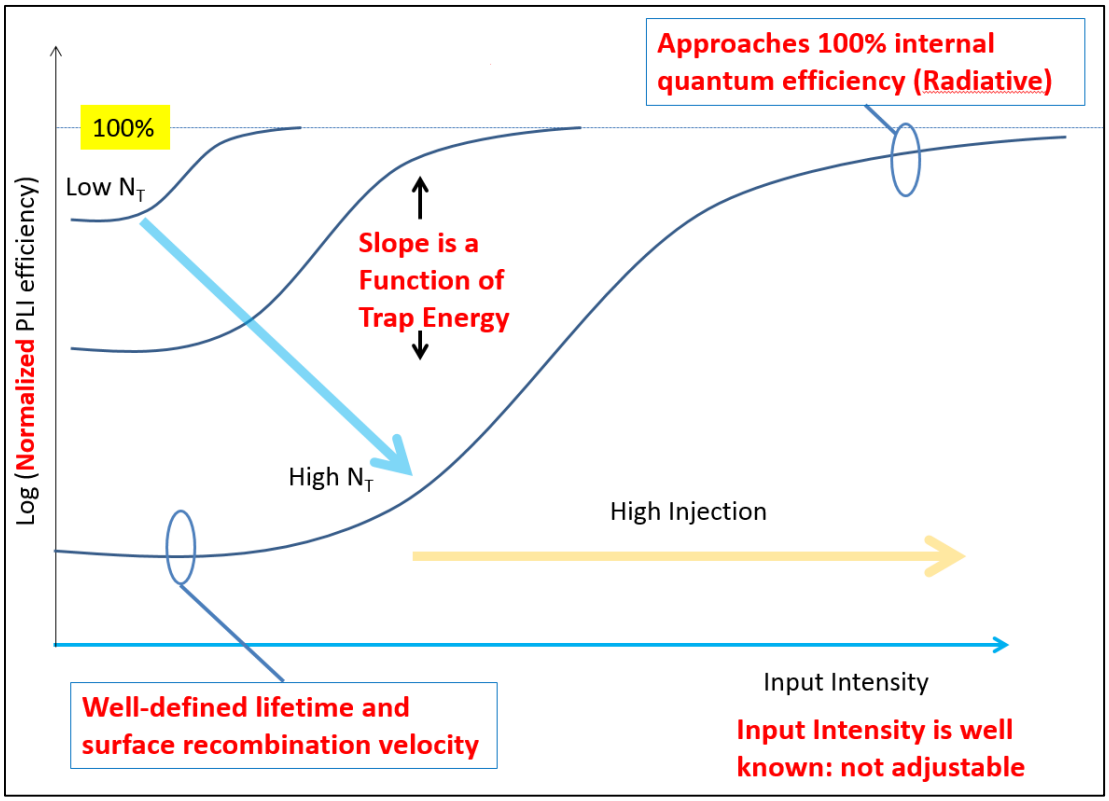

Figure 56. Basic Concepts of PLI Curve. *At low input intensity, we are in the low-injection condition where there is a well-defined carrier lifetime and surface recombination velocity. As we move to higher intensities, we transition into high-injection conditions, where the PL response approaches 100% internal quantum efficiency and radiative recombination dominates.*

Here we see that as the interface state density increases, the PL response decreases and becomes more varied, which makes sense because there are more traps contributing to

non-radiative recombination. We also see that the slope of the curve is a function of the energy of the interface state traps.

3.4 Time-Resolved Photoluminescence

Vital to this study was Time-Resolved Photoluminescence (TRPL) measurements performed by Logan Hancock and Sandeep Sohal here at Texas State University in Dr. Holtz' lab, and TRPL measurements performed by collaborators at the National Renewable Energies Laboratory (NREL). TRPL is another characterization technique that exploits the principles of semiconductor physics. Laser excitation of energy greater than the band gap energy is used, and the subsequent photoluminescence emission is collected and measured, this time with respect to time.

TRPL aims to measure the time-response of a single photon that has been emitted from a semiconductor via PL. Because PL emission is dominated by quantum mechanics, which is probabilistic in nature, TRPL requires many successive measurements for statistical accuracy.[31] This is analogous to nuclear decay, in the sense that we know that when one half-life of an unstable isotope has passed, only half of the material will remain. However, we cannot say precisely *when* the decay will occur. To achieve the many measurements need for TRPL, a pulsed laser source is used for excitation, typically pulsed on the order of 100s of kHz. As with the previous PL characterization methods described earlier, care is taken to filter out all laser light to make sure that only PL emission is detected.

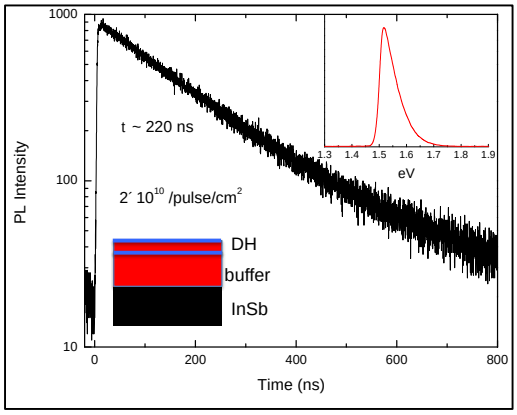

Figure 57. Room-temperature PL data for CdMnTe/CdTe. *Spectrum (inset) and decay curve. (Figure courtesy of Dr. Holz' group)*

TRPL measurements are used to explore the lifetimes of minority carriers in semiconductors. Here are Texas State, TRPL measurements used an excitation source with 430 nm wavelength, produced by a system of lasers in conjunction with a second-harmonic generator. The PL is then passed through a spectrometer equipped with a PMT. The TRPL measurements are performed using the time-correlated single photon counting (TCSPC) technique with a PMT that has a response time of approximately 150 ps. The optical injection is varied using Neutral Density filters and ranges from $1x10^{10}$ to $3x10^{11}$ photons/pulse/cm^2. At NREL, these measurements were performed using a regenerative, amplified Yb:KGW laser system that was tuned to 640 nm with 0.3 ps pulses at a repetition rate of 1.1MHz, in conjunction with an avalanche photodiode detector and TCSPC. The excitation intensity varied, but was kept at low-injection conditions of less than 10^{12} photons/cm^2.

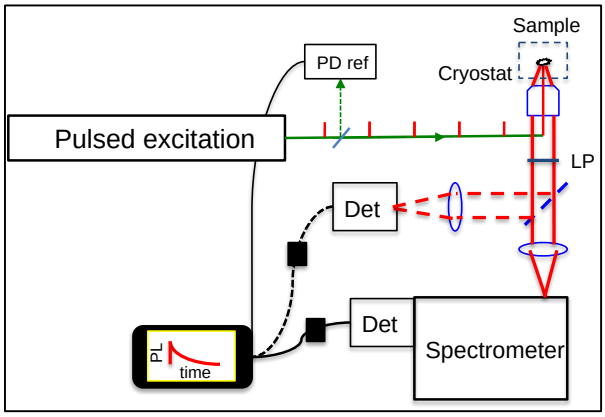

Figure 58. Depiction of major elements of TRPL measurement apparatus. *Light may either be spectroscopically analyzed or measured directly at the detector. (Figure courtesy of Dr. Holtz' group)*

For sufficiently low defect density (<10^6 cm^{-2}), if the TRPL is monitored for a long enough time and the sample is thin enough that carriers are able to diffuse to the back surface, then the excess carriers are approximately uniformly distributed in the sample volume, to form a quasi-equilibrium scenario. In this case, the lifetime is given by

$$\frac{1}{\tau_{eff}} = \frac{1}{\tau_{bulk}} + \left(\frac{d}{S_1 + S_2} + \frac{d^2}{\pi^2 D}\right)^{-1} \tag{150}$$

Where D is the diffusion coefficient, d is the sample or layer thickness, and S_1 and S_2 are the surface recombination velocities at the two interfaces. If we assume that the two surfaces are identical, then this reduces to

$$\frac{1}{\tau_{eff}} = \frac{1}{\tau_{bulk}} + \left(\frac{d}{2S} + \frac{d^2}{\pi^2 D}\right)^{-1} \tag{151}$$

The last term is the diffusion transit time. For the samples under investigation here, namely N and P-type CdTe with layer thicknesses of 0.5 and 5 μm, the transit time is

negligible and need not be considered in lifetime determination. A table of values for these samples is given below, where the diffusion transit time is defined as

$$DTT = \left(\frac{d^2}{\pi^2 D}\right) \tag{152}$$

Table 12. Diffusive transit times for various CdTe samples under investigation.

For P-Type CdTe ($D_e = 25.88\ cm^2/s$)	Diffusive Transit Time (DTT)
d = 0.5 μm	DTT = 9.8 ps
d = 5 μm	DTT = 978.8 ps
For N-Type ($D_h = 2.588\ cm^2/s$)	
d = 0.5 μm	DTT = 97.8 ps
d = 5 μm	DTT = 9.8 ns

We can immediately see that the majority of these values are negligible. The only one that may not be is the value for the N-type sample that is 5 μm thick. However, in comparison to the bulk lifetime which in these samples is 2 μs, 10 ns is also negligible. This means that in the first 10 ns, the excess charge carriers are still "settling" into equilibrium and may affect the very beginning of the decay, but will not affect in the long term. Thus, this reduces further to

$$\frac{1}{\tau_{eff}} = \frac{1}{\tau_{bulk}} + \frac{2S}{d} \tag{153}$$

The quasi-equilibrium state mentioned above will occur after a diffusion transit time, so this is a reasonable assumption. Note that this expression tells us that the effective lifetime τ_{eff} will always be shorter than the bulk lifetime, unless there is no surface recombination. It the minority carrier diffusion length and the sample dimension are comparable, then carriers are more likely to recombine at the surface than through bulk

processes. However, if the minority carrier diffusion length is many times the layer thickness, then a more uniform distribution of carriers will occur, and the carriers can reflect more of a bulk-like decay. Shown below are several TRPL measurements for CdTe and CdSeTe DHs that have been fit using the relation above.

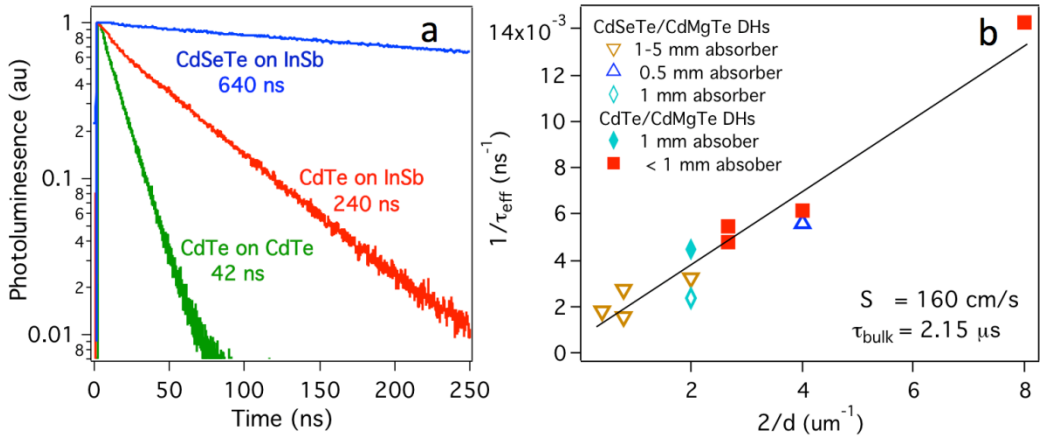

Figure 59. Determination of lifetimes and SRV for various DHs*. (a) TRPL measurements for CdTe and CdSeTe DHs with high lifetimes. (b) Effective recombination rate plotted against 2/d used to extract τ_{bulk} and SRV. (Figure to be published)*

The minority carrier lifetime is so important to the study of the viability of CdTe, and any semiconducting material used in photovoltaic applications, because it is related to the open circuit voltage of a solar cell through the relation

$$V_{oc} = \frac{kT}{q}\, ln\left(\frac{g_0\, N_d \tau_p}{n_i^2}\right) \tag{154}$$

Where N_d is the majority carrier concentration, n_i is the intrinsic carrier concentration, g_o is the generation rate and τ_p is the minority carrier lifetime. This in turn is important because V_{oc} is related to efficiency of a cell through

$$\eta = \frac{V_{oc} J_{sc} FF}{Input\ Power} \tag{155}$$

Where FF is the Fill Factor, which is related to the maximum power point voltage and current, and J_{sc} is the short-circuit current density. With this, we can say that a long measurement lifetime should be a good indicator of device efficiency.

4. RESULTS

Now that we have given a thorough description of the measurement techniques used in this study, we can discuss the results. To begin, the PL of "bare" CdTe was recorded. Bare CdTe refers to either a bare CdTe substrate, or CdTe that has been grown on a substrate, with no other layers. These results were then compared with similar measurements done on GaAs, and AlGaAs/GaAs DHs.

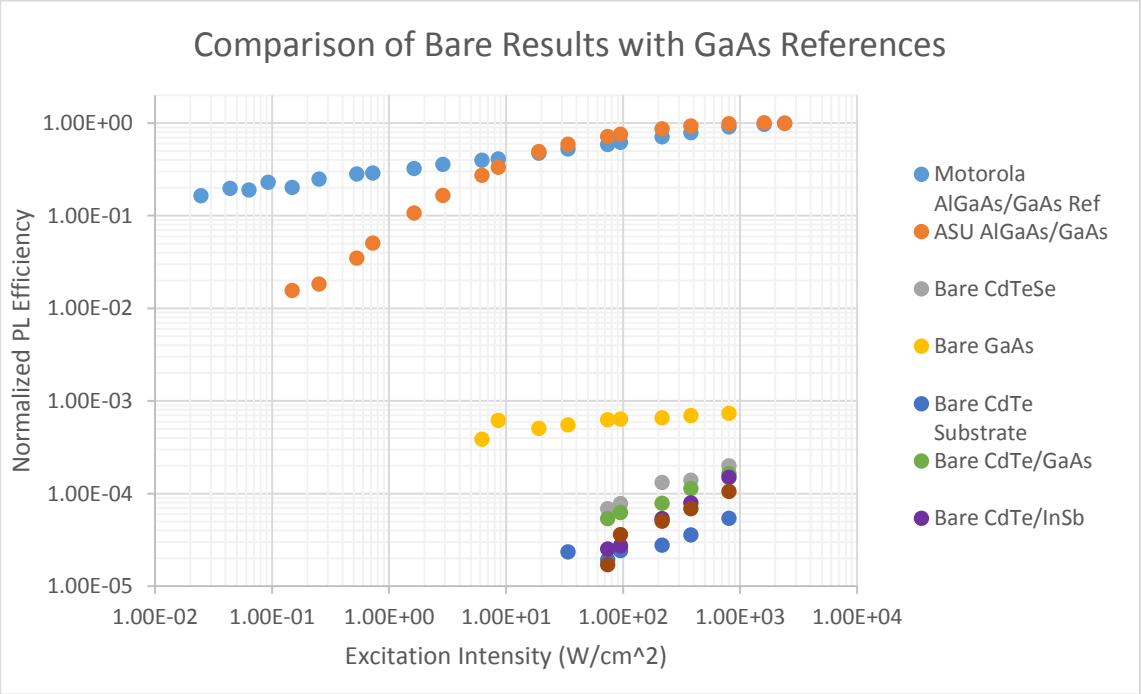

Figure 60. PLI Efficiency vs input Intensity for various Bare CdTe samples and various GaAs samples for comparison.

In general, we see very poor PL efficiency of CdTe, maxing out around 2E-4, regardless of substrate. Note how the jump between the bare GaAs and the DHs is three orders of magnitude. It was these vastly different results for the GaAs samples that inspired the

proceeding work on DHs for CdTe in this study. After this, SHs were grown on CdTe(211) substrates using CdMgTe as a barrier.

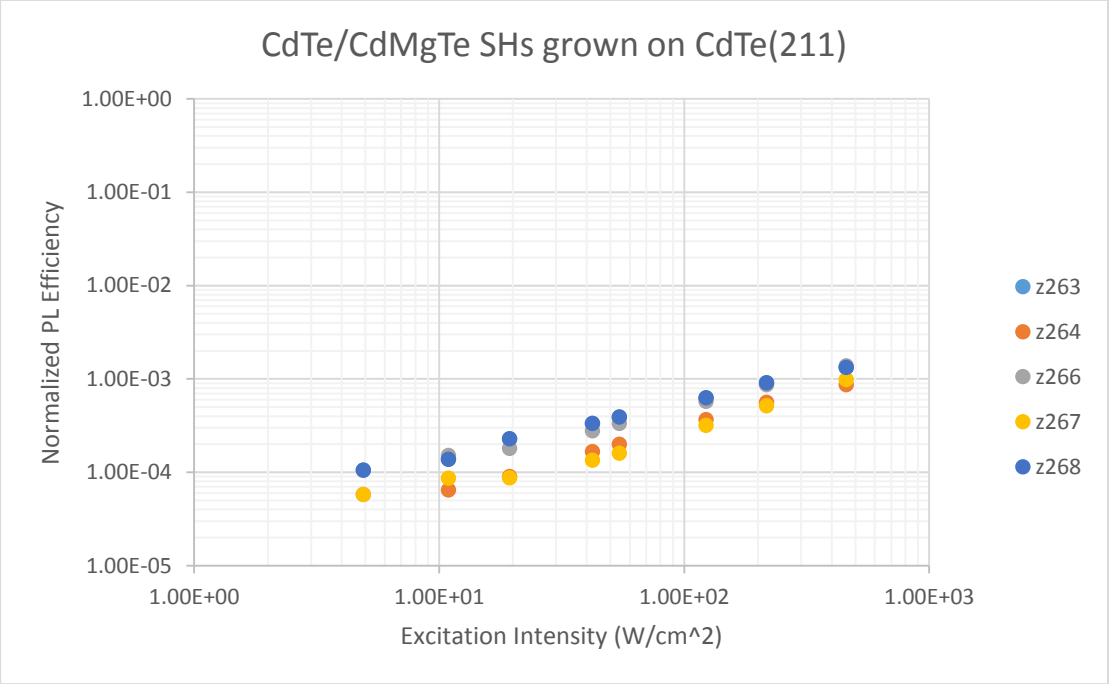

Figure 61. PLI Efficiency vs input Intensity for the first few SH structures grown on CdTe(211).

With the introduction of a CdMgTe barrier, we see the PL efficiency increase by an order of magnitude, suggesting that the exposed CdTe surface in the bare CdTe results was a source of non-radiative recombination. After this, growth experiments were performed in an effort to improve PL.

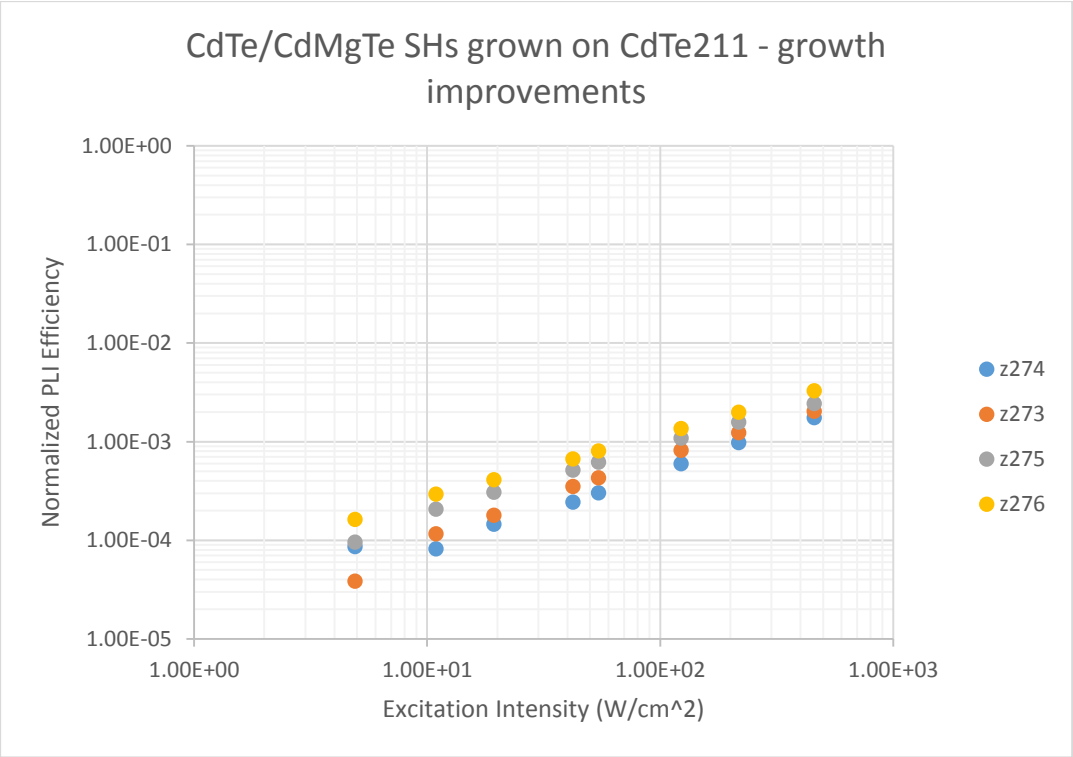

Figure 62. PLI Efficiency vs input Intensity for SH structures with growth improvements.

These growth experiments included substrate preparation methods, annealing the substrate before growth as well as heating the substrate during growth at different temperatures and varying the over pressure within the chamber during growth. With this, an increase in efficiency by a factor of about 3 was seen. After this, the first DHs were grown.

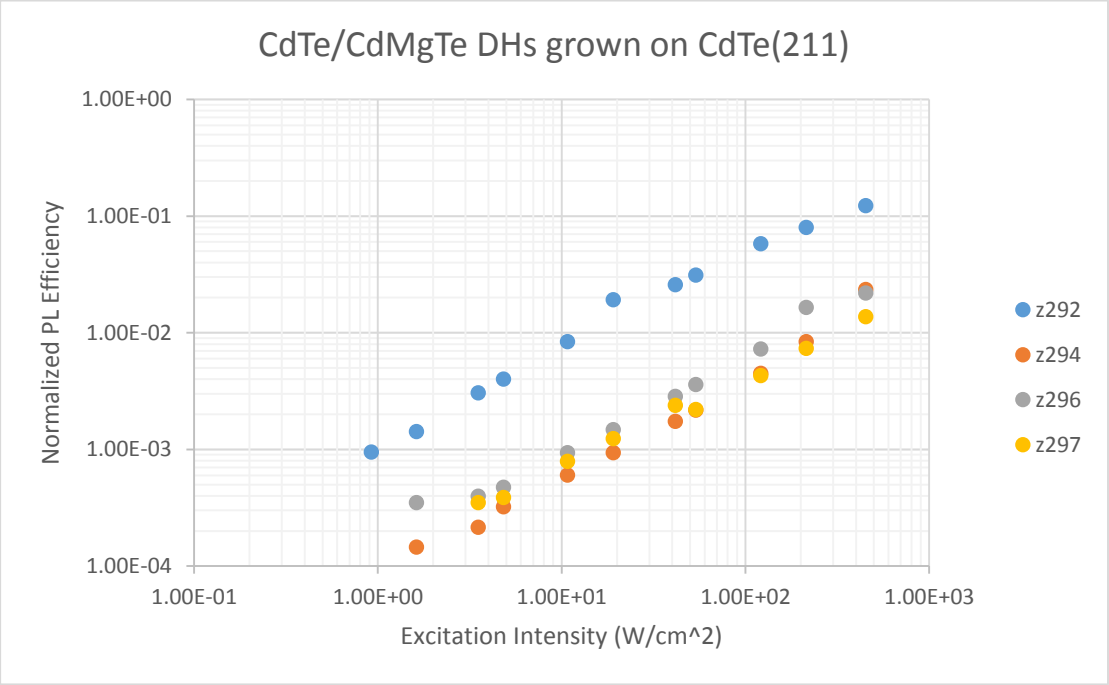

Figure 63. PLI Efficiency vs input Intensity for the first few DH structures grown on CdTe(211). *Here we see an increase in PL efficiency by two orders of magnitude.*

With the introduction of a second CdMgTe barrier layer, we see the PL efficiency jump by two orders of magnitude, indicating that the homoepitaxial interface was also a source of non-radiative recombination. All of the samples here have the same layer structure except for one: a 200nm buffer layer of CdTe, followed by a 20nm layer of CdMgTe, then a 1μm layer of CdTe, followed by a 30nm layer of CdMgTe, with a 30nm cap of CdTe. Z292 varied from this structure, but the only difference was the thickness of the buffer layer, which was 1μm. The order of magnitude difference implies that there are issues at the homoepitaxial interface that distance seems to help with. The next set of DHs was grown on CdZnTe.

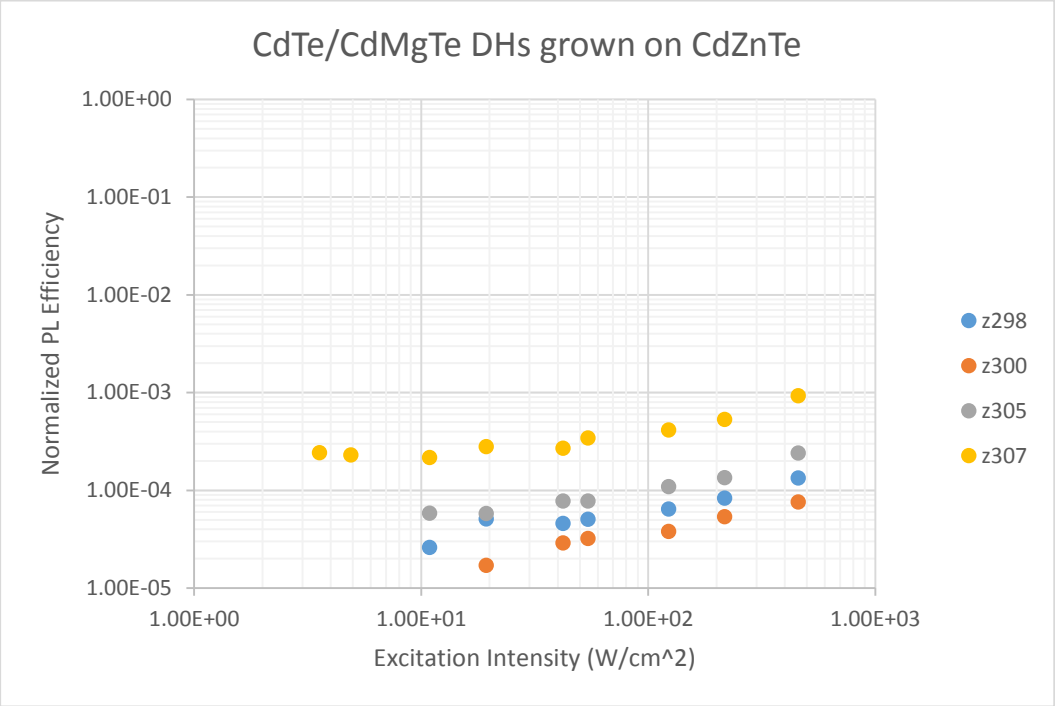

Figure 64. PLI Efficiency vs input Intensity for DHs grown on CdZnTe.

Because the preparation of CdTe substrates before growth was time intensive, an investigation of other viable substrates to be grown on was performed, starting with CdZnTe. Due to the decrease in PL by two orders of magnitude, CdZnTe was not used as a substrate again until after doping investigations were complete and growth of device structures was investigated (not covered in this study).

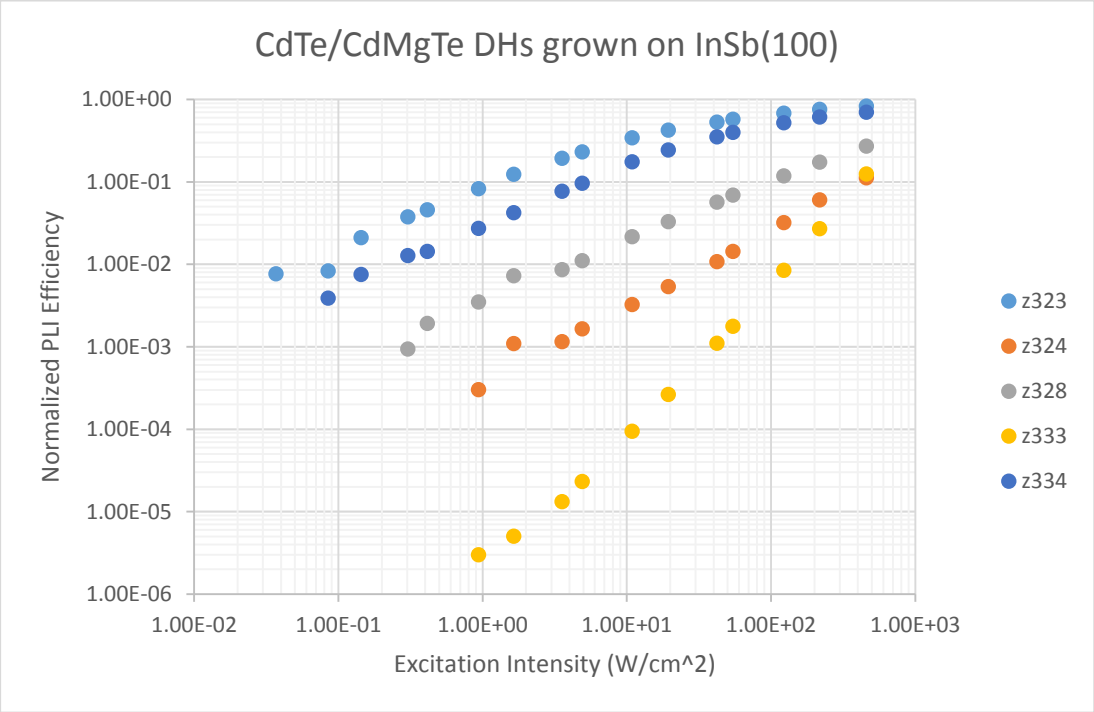

Figure 65. PLI Efficiency vs input Intensity for DHs grown on InSb(100).

The next substrate investigated was InSb(100), which produced an increase in PL efficiency by a factor of about 5. DHs grown on InSb(100) also resulted in a marked decrease in DD as visible by c-PL. The DD for the best InSb growths were 2 orders of magnitude lower than the best CdTe growths. From here, the investigation focused heavily on DHs grown on InSb(100).

The supplied PL data was then used to model the PL response in CdTe, using a numerical model developed by Craig Swartz. This was done using an approach based on a distribution of interfacial states across the band gap. The continuity equations for generation, recombination (including radiative and SRH), drift, and diffusion are solved for the steady-state condition by a finite difference method. Field effects, including the charging of interface states, are incorporated by self-consistent iteration with Poisson's

equation. The intensity dependence of photo carrier density, and hence PL signal intensity, can then be found as a function of the interface state density.

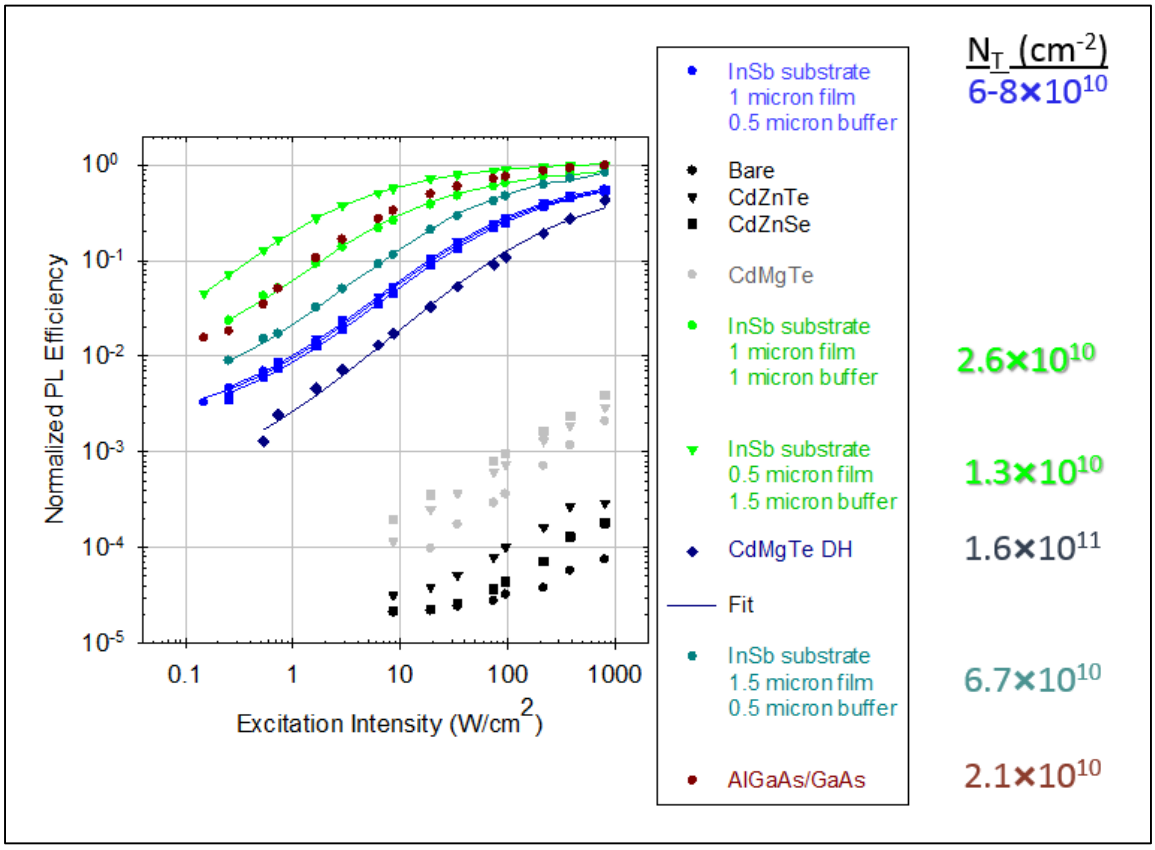

Figure 66. Modeling work for DHs with varying buffer layer thickness. *The interface state densities N_t for each sample are shown to the right.*

The modeling work showed a correlation between the PL efficiency and the interface state density. As N_t decreased, the efficiency of the DH increased at lower injection levels, causing the onset of the S shape to be delayed.

To investigate the effects of the substrate/epilayer interface on the carrier lifetime, TRPL measurements were performed on samples with varying buffer layer thickness.

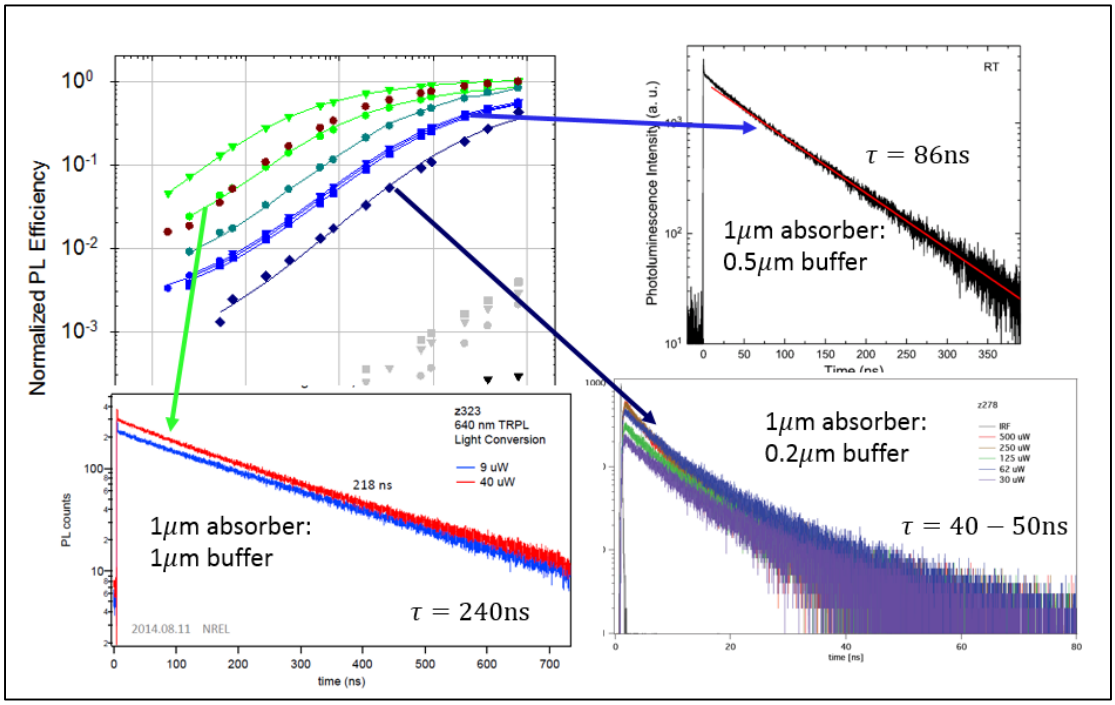

Figure 67. Comparison of PLI and TRPL for DHs with varying buffer thickness*. Here we see that PL intensity and TRPL lifetime increase with increased buffer layer thickness*

It was found that increasing the buffer layer thickness had a significant impact on the lifetimes as measured by TRPL. Here we see that as the buffer was made thicker, the lifetime of the sample increased. This can be explained by the accompanying decrease in the number of interface states found for each sample through PLI modeling. When the buffer layer was changed from 0.2μm to 1.0μm, the interface states changed by approximately one order of magnitude, down to $1.3\ x\ 10^{10}\ cm^{-2}$, suggesting that the homoepitaxial interface is a significant source of interface traps.

Using only the interface trap state density N_t as determined by fitting the PLI data, the time response of photo-generated carriers was simulated. This simulation shows

a decay consistent with the time response as measured by TRPL. Here, the response was simulated and measured for different input intensities.

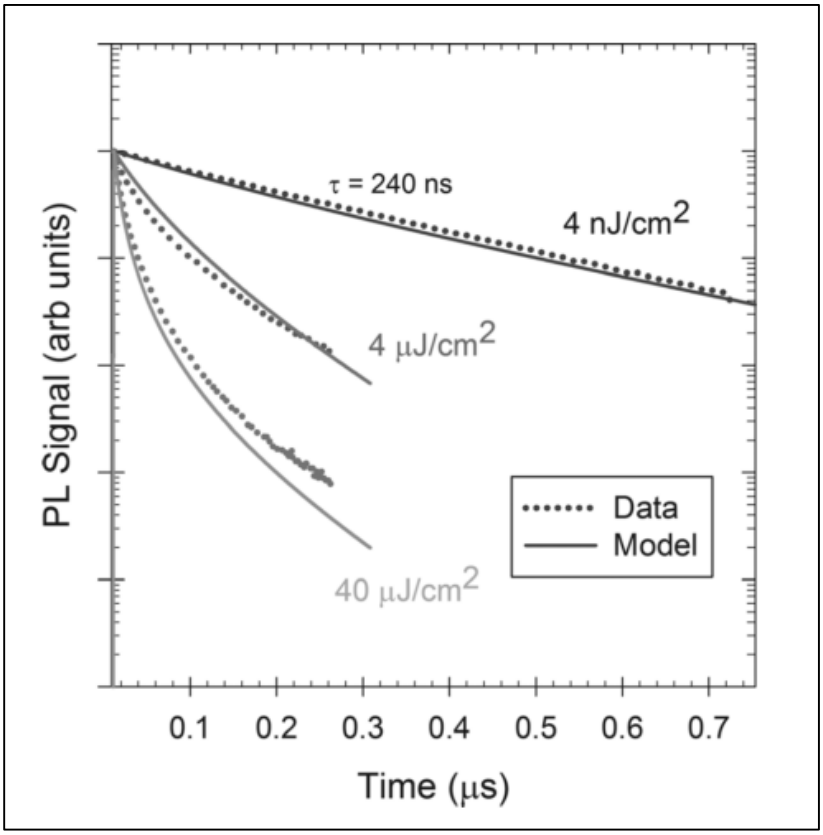

Figure 68. TRPL response simulation. *The trap parameters resulting from the PLI data were used to simulate the time dependent distribution of carriers after a pulse of photo-generated electron-hole pairs – without the use of any additional parameters. Here, we see good agreement between the simulation and the response as measured by TRPL.*

It should be noted that there are multiple values of the radiative recombination coefficient for CdTe reported in the literature. However, when the higher values were used, such as $5x10^{-9}\ cm^3/s$, it was found that either the PLI or the TRPL could be modeled, but not both. Only by using a radiative recombination coefficient of $B_{rad} = 1x10^{-10}\ cm^3/s$,

were both PLI and TRPL able to be successfully modeled, suggesting that this is the true value for CdTe[4].

In the previous investigation, the total layer thicknesses were limited by the critical thickness that arises from the slight lattice mismatch of CdTe and InSb. In an effort to create thicker layers, Sellenium alloying (~1%) was introduced to the CdTe layers for a better lattice match.

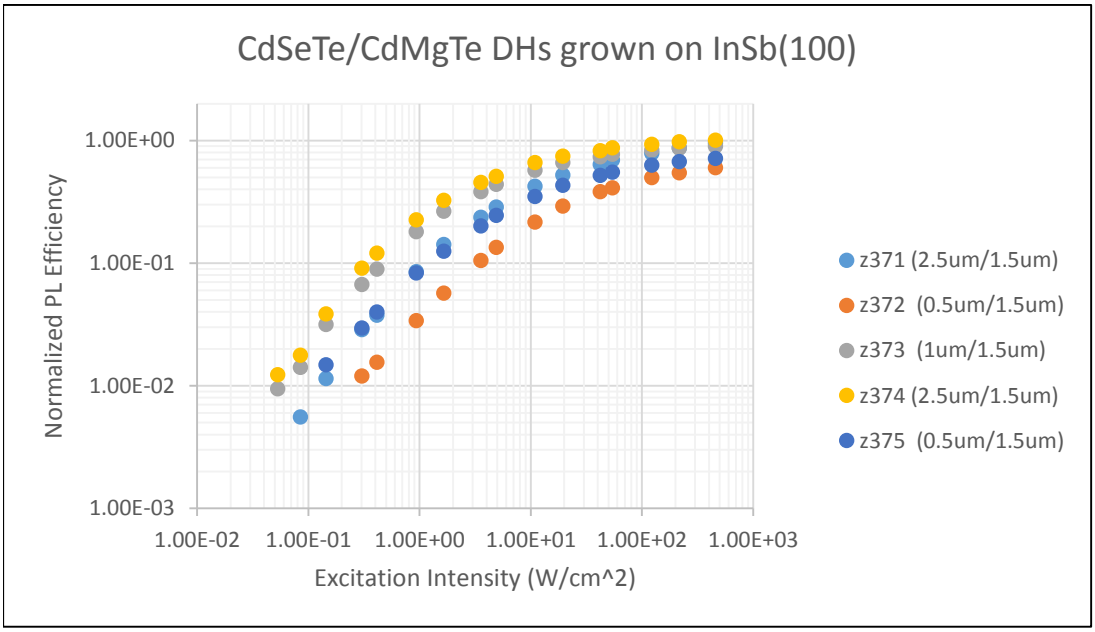

Figure 69. PLI Efficiency vs input Intensity for DHs grown on InSb(100) with Se alloying for lattice matching.

With the determination that a thicker buffer layer produced better PLI and carrier lifetimes, the buffer layer was held constant at 1.5μm and the absorber layer was allowed to vary. Here, we see that as the absorber layer increases, the PLI increases as well, in agreement with our predictions from the Steady State investigations. It was also seen that

the efficiency of the samples was still fairly high at the limits of detection in our set up. It was at this point that the introduction of a PMT occurred to produce a wider range of signal detection. This is also when the original laser used failed, and the new laser was brought in. Once these changes to the set up occurred, the above series was re-measured.

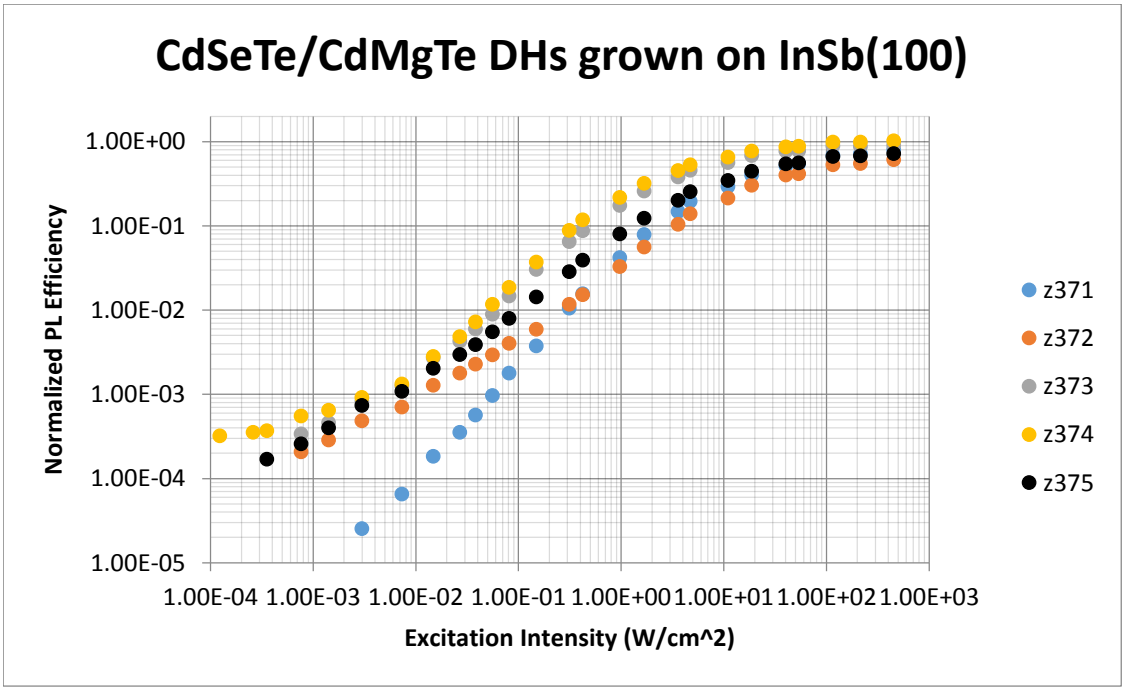

Figure 70. PLI Efficiency vs input Intensity for the same DHs as in Fig. 69, but with increased detection range as provided by the inclusion of a PMT in the PL set up.

It is here that we finally start to see the bottom of the S shape of the PL response. These measurements were then compared with TRPL measurements.

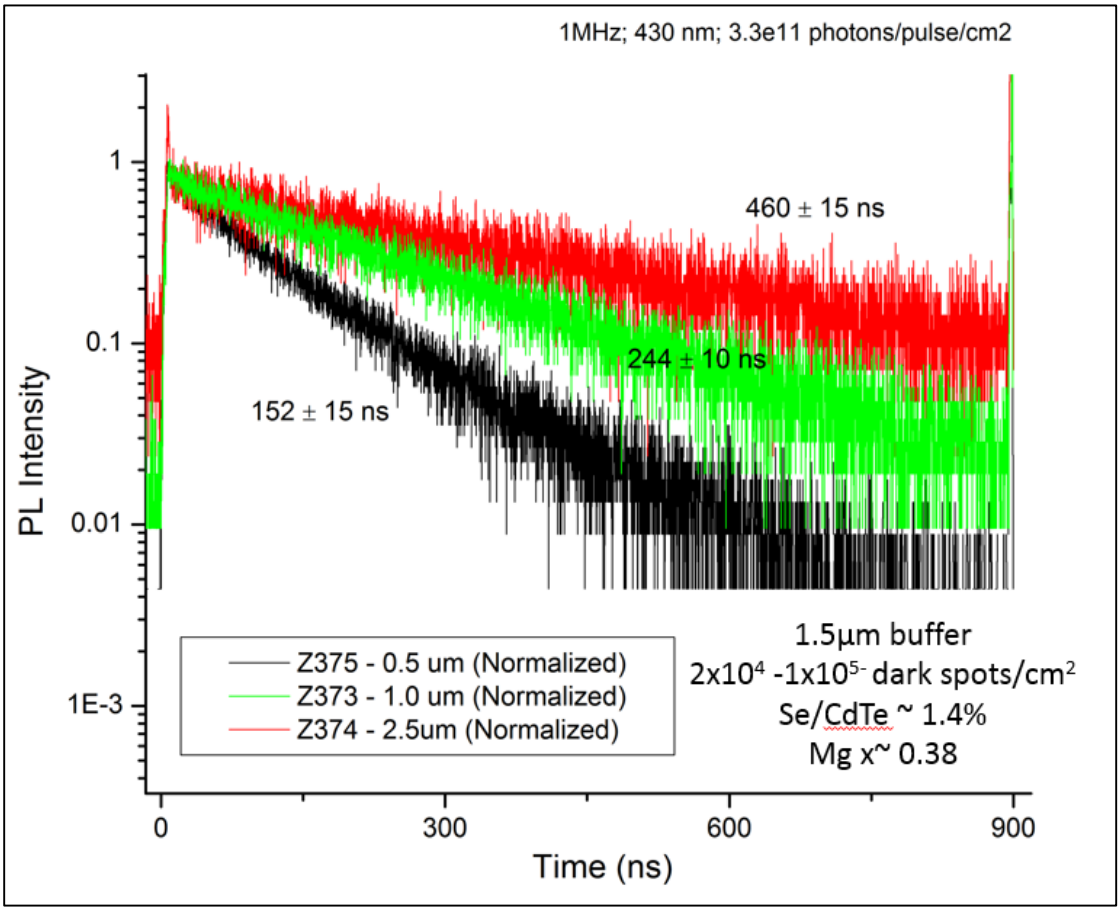

Figure 71. TRPL measurements for DHs with varying active layer thickness. *Here we see the TRPL measurements of previous the DHs, showing increased lifetime with increased active layer thickness*

Here we see that as the active layer thickness increases, the measured lifetime also increases, in agreement with our predictions from the Transient State investigations. As the active layer is increased, the carriers interact less with the surface, contributing to a smaller SRV, leading to a longer lifetime.

Before doping experiments, the last investigation performed was of the correlation between TRPL lifetimes and DD as measured by c-PL.

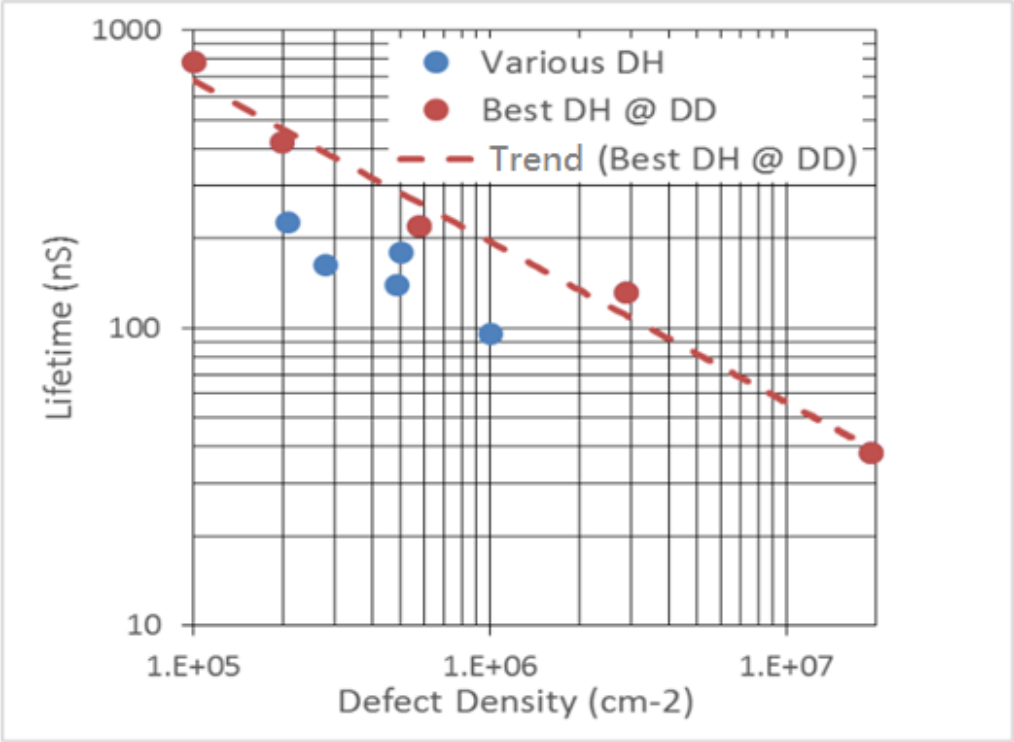

Figure 72. TRPL lifetime vs DD as measured by c-PL

The red trendline is illustrative of what is possible in terms of lifetime at a given DD. Carrier lifetimes at a given DD for CdTe are approximately 10 times that of a GaAs DH at the same DD, indicating that CdTe is more tolerant to defects than GaAs.

After these investigations, doping experiments were performed. The doping species investigated at Texas State was Iodine, a group IIV element that tends to substitute for Te in CdTe, making it an n-type dopant. A simultaneous investigation of Indium doping was performed at ASU, where it was found that there was a threshold of doping concentration after which the PL signal would drop off dramatically, indicating that non-radiative recombination was dominating. A similar investigation was performed

on Iodine, where no such threshold was seen, indicating that CdTe can be doped at higher levels using Iodine than Indium.

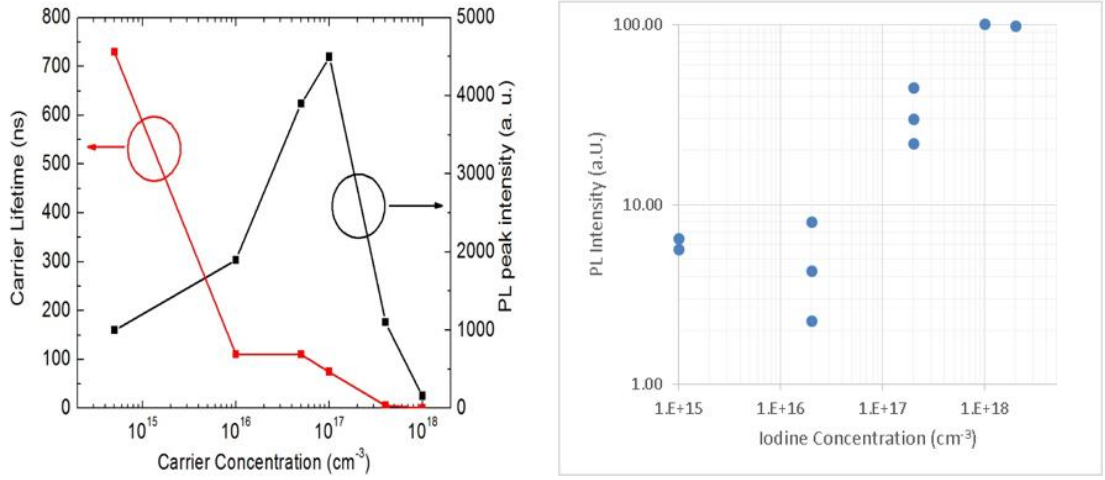

Figure 73. Comparison of Indium and Iodine doping effects on PL signal. *On the left we see the ASU investigation of Indium doping, with a clear threshold at which PL response drops dramatically. On the right is a similar investigation performed on Iodine where no such threshold is seen.*

Here, the differences in PL signal for a given Iodine doping concentration can be attributed to different active layer thicknesses. For the doped series with a concentration of $2x10^{16}\ cm^{-3}$, the lowest signal response corresponds to the sample with the thinnest active layer, while the highest signal response corresponds to the sample with the thickest active layer, in agreement with our predictions from the Steady State investigations.

After this, an investigation of the effects of different doping concentrations on PL signal was performed. To begin, a set layer structure was determined and the doping levels were allowed to vary.

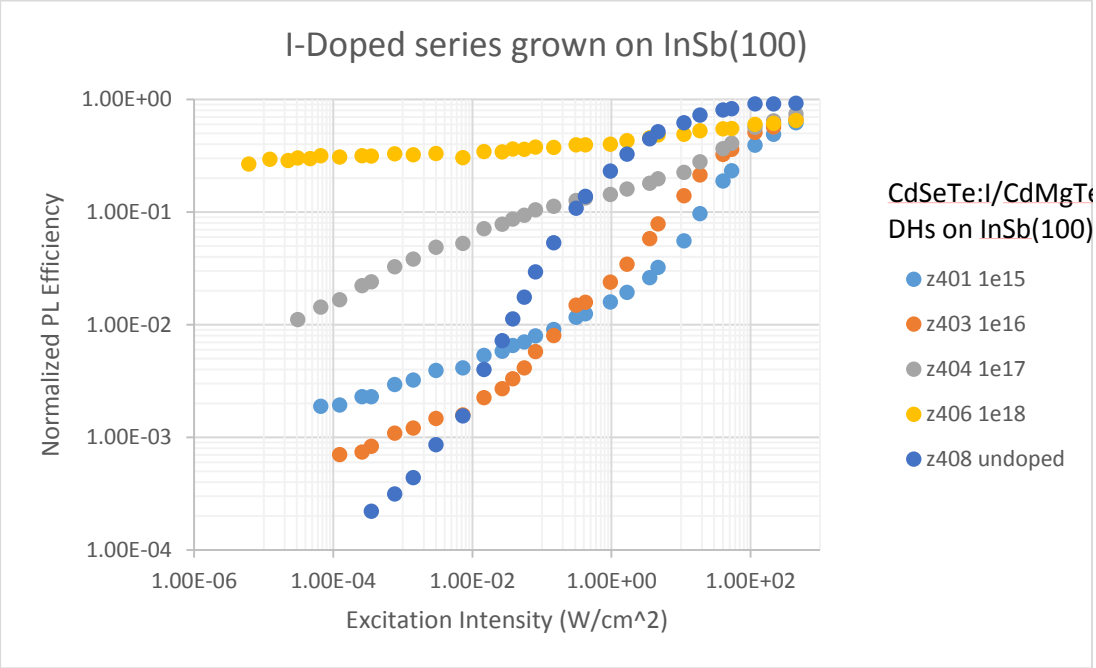

Figure 74. PLI Efficiency vs input Intensity for the first I-doped series of DHs.

Here, all samples had a 2μm absorber layer and a 1.5μm buffer layer, and only the concentration of doping was varied. We see that the PL response loses some of the characteristic S shape of the curve, most prominently at the higher levels of doping. This makes sense because we have doped so heavily that radiative recombination will dominate throughout due to its quadratic dependence on the total carrier concentration. The doping concentration was verified using Hall measurements performed by other members of the research group here at Texas State. The next series of doped samples had all of the same parameters except for the thickness of the absorber layer, which was decreased to 1μm.

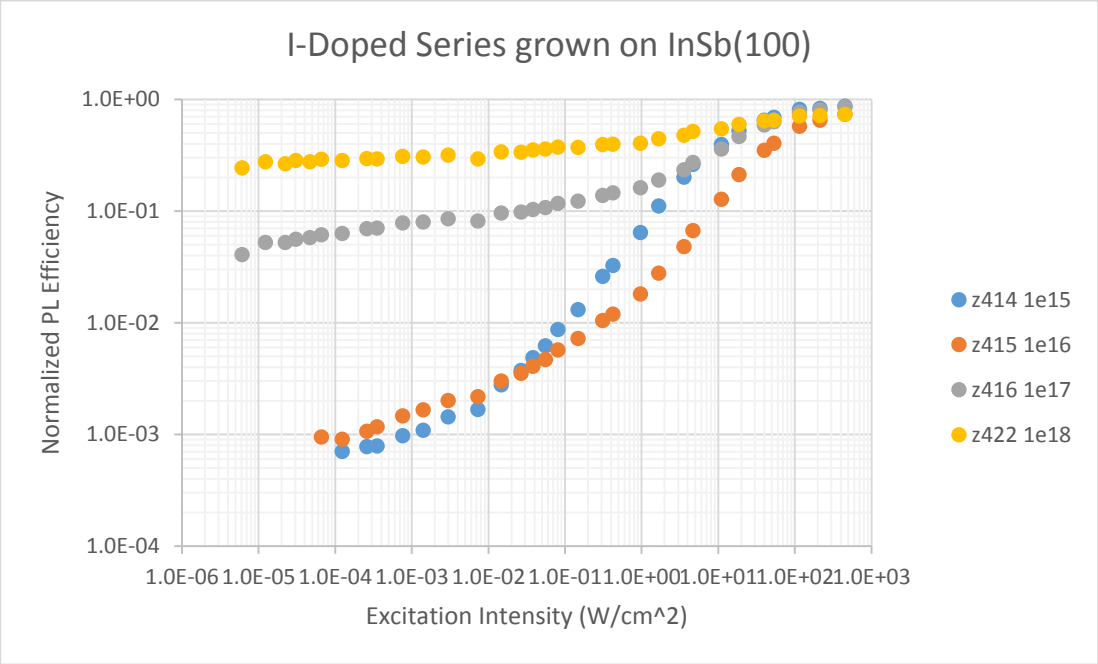

Figure 75. PLI Efficiency vs input Intensity for the second series of I-doped DHs*. Here, we have a thinner absorber layer than the first series*

Here, the loss in shape is a little more pronounced at higher doping concentrations, but less pronounced at lower concentrations, but in general, we see that same trends as the first series. The last series to be investigated was a doped series where the doping concentration was held constant and the absorber layer thickness was allowed vary.

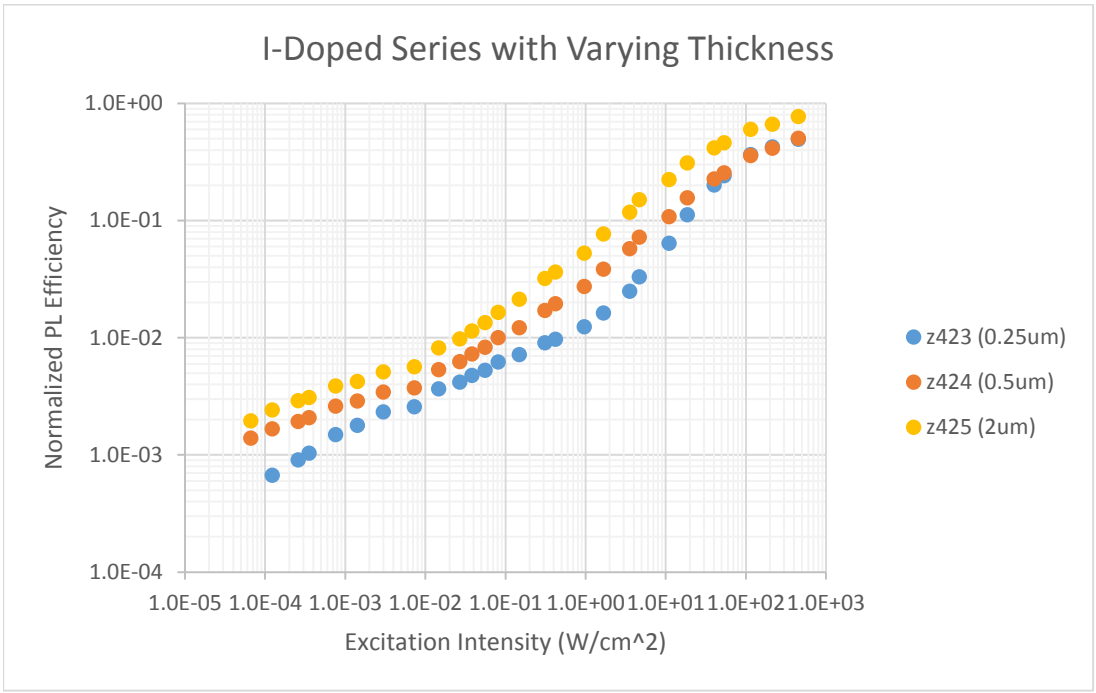

Figure 76. PLI Efficiency vs input Intensity for DHs with the same level of I-doping, with different absorber layer thicknesses.

Here, all samples have a buffer thickness of 1.5μm and are doped at $1x10^{16}/cm^3$. In this case, we see the clearest confirmation that as the active layer thickness increases, so does PLI as predicted earlier during our discussion of excess charge carrier dynamics in low-injection steady state.

5. CONCLUSIONS

To begin, Spectral Ellipsometry and c-PL were demonstrated to be effective screening techniques for determining Mg compostion and crystalline quality respectively. With the use of c-PL, information on DD and types of defects present could be obtained, and it could be determined if the critical thickness had been exceeded or if lattice matching had been achieved. These quick characterization techniques were able to provide a fast feedback loop for MBE growers, allowing for the sheer volume of samples that were grown during this study (over 250). It was also found that the bare CdTe surface and the homoepitaxial interface are significant sources of interface trap states, both of which can be passivated through the use of DHs. It was found that the homoepitaxial interface seems to have a greater than expected effect on lifetime, suggesting significant non-radiative recombination is taking place. By approaching the characterization of CdTe in a similar manner as to what was done in early studies of GaAs, it was determined that interfacial recombination is a significant source of non-radiative recombination in CdTe. With the use of the DH structures grown in this study, some of the longest bulk lifetimes for CdTe have been measured, putting to rest the issue of short lifetimes as "intrinsic" in CdTe. Through the study of lifetime versus DD it was found that CdTe is more tolerant of defects than GaAs. Successful simultaneous modeling of PLI and TRPL indicated that the radiative recombination coefficient of CdTe is[4] $B_{rad} = 1x10^{-10}\ cm^3/s$. It was also demonstrated that Iodine can be used as a viable n-type dopant for CdTe. With this, we conclude that CdTe is a viable material for PV applications. Future work on CdTe should focus on the other challenges with this

material; namely, the difficulties with p-type doping and the formation of an ohmic contact.

APPENDIX SECTION

APPENDIX A: MATHEMATICA CODES FOR STEADY STATE CALCULATIONS OF N-TYPE CDTE

Steady State Calculations
N-type CdTe – exploring excess carrier profiles and PLI with varying SRV values.

```
(*For Length = 5um*)
Clear[x];
x0=5*^-4; (*cm*)
tp=2*^-6; (*s*)
kb=1.38*^-23; (*J/K*)
T=300; (*K*)
q=1.6*^-19;(*C*)
mobp=100; (*cm^2/Vs*)
Dp=mobp*kb*T/q;(*cm^2/s*)
Lp=Sqrt[Dp*tp]; (*cm*)
s0=0;
s1=1;
s2=10;
s3=100;
s4=1000;
s5=10000;
delp0[x_]:=1-(s0*Cosh[x/Lp])/(s0*Cosh[x0/(2*Lp)]+Dp/Lp*Sinh[x0/(2*Lp)]);
delp1[x_]:=1-(s1*Cosh[x/Lp])/(s1*Cosh[x0/(2*Lp)]+Dp/Lp*Sinh[x0/(2*Lp)]);
delp2[x_]:=1-(s2*Cosh[x/Lp])/(s2*Cosh[x0/(2*Lp)]+Dp/Lp*Sinh[x0/(2*Lp)]);
delp3[x_]:=1-(s3*Cosh[x/Lp])/(s3*Cosh[x0/(2*Lp)]+Dp/Lp*Sinh[x0/(2*Lp)]);
delp4[x_]:=1-(s4*Cosh[x/Lp])/(s4*Cosh[x0/(2*Lp)]+Dp/Lp*Sinh[x0/(2*Lp)]);
delp5[x_]:=1-(s5*Cosh[x/Lp])/(s5*Cosh[x0/(2*Lp)]+Dp/Lp*Sinh[x0/(2*Lp)]);
Plot[{delp0[x],delp1[x],delp2[x], delp3[x], delp4[x], delp5[x]},{x,-x0/2,x0/2},
PlotRange->{0,1}, PlotLegends->{"s=0", "s=1", "s=10", "s=100", "s=1000",
"s=10000"}]
LogPlot[{delp0[x],delp1[x],delp2[x], delp3[x], delp4[x], delp5[x]},{x,-x0/2,x0/2},
PlotRange->{0,1}, PlotLegends->{"s=0", "s=1 cm/s", "s=10 cm/s", "s=100 cm/s",
"s=1000 cm/s", "s=10,000 cm/s"},Frame->True, FrameTicks-
>{{{0.010,0.05,0.1,0.5,1},None},{{0,{-5*^-4/2,"- x0/2"},{5*^-4/2,"
x0/2"}},None}},FrameLabel->{"x","(Δp(x))/(g' τp)"},
 PlotLabel->"Excess Carrier Concentration Profile for 5μm thick absorber layer
  "]


PLI0[x_]:=Integrate[delp0[x],{x, -x0/2,x0/2}];
PLI1[x_]:=Integrate[delp1[x],{x, -x0/2,x0/2}];
PLI2[x_]:=Integrate[delp2[x],{x, -x0/2,x0/2}];
PLI3[x_]:=Integrate[delp3[x],{x, -x0/2,x0/2}];
PLI4[x_]:=Integrate[delp4[x],{x, -x0/2,x0/2}];
```

```
PLI5[x_]:=Integrate[delp5[x],{x, -x0/2,x0/2}];

w=1/PLI0[x];

Print["Normalized PLI0 = ", w*PLI0[x]];
Print["Normalized PLI1 = ", w*PLI1[x]];
Print["Normalized PLI2 = ", w*PLI2[x]];
Print["Normalized PLI3 = ", w*PLI3[x]];
Print["Normalized PLI4 = ", w*PLI4[x]];
Print["Normalized PLI5 = ", w*PLI5[x]];

ListLogLogPlot[{{s0,w*PLI0[x]},{s1,w*PLI1[x]},{s2,w*PLI2[x]},{s3,w*PLI3[x]},{s4,
w*PLI4[x]},{s5,w*PLI5[x]}},Frame->True,FrameLabel->{"Surface Recombination
Velocity [cm/s]","Normalized PLI [arbitrary units]"},
 PlotLabel->"Normalized PLI vs SRV for 5µm thick absorber layer
  "]

Print["Dp = ", Dp];
Print["Lp = ",Lp];
{
```

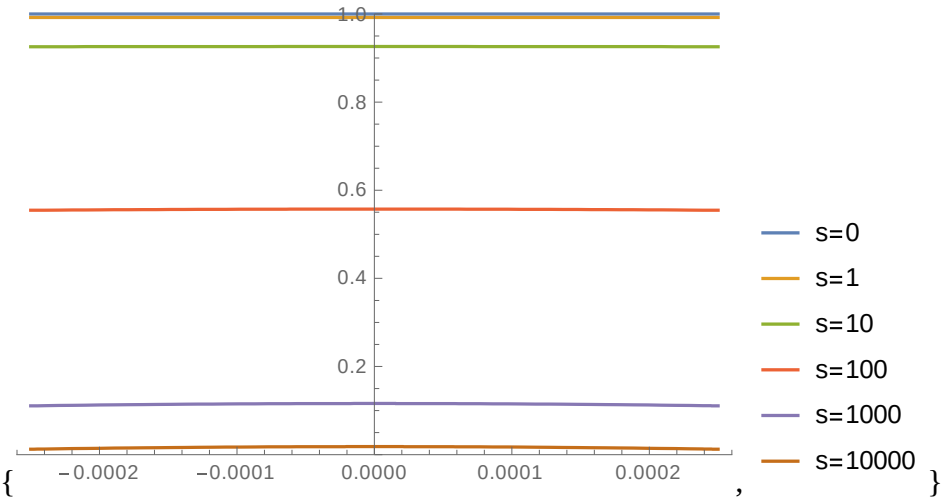


```
{                                                                    ,                }
}
{
```

Excess Carrier Concentration Profile for 5μm thick absorber layer

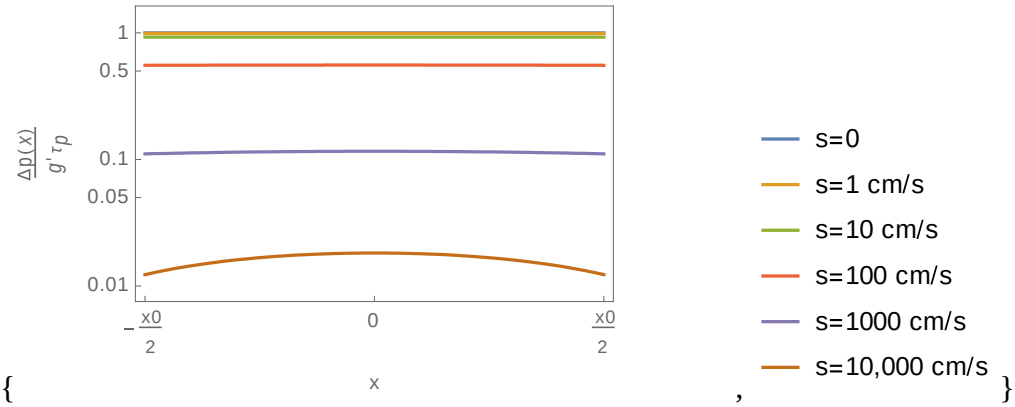

{ , }
}
Normalized PLI0 = 1.
Normalized PLI1 = 0.992064
Normalized PLI2 = 0.925948
Normalized PLI3 = 0.556349
Normalized PLI4 = 0.114278
Normalized PLI5 = 0.016254

Normalized PLI vs SRV for 5μm thick absorber layer

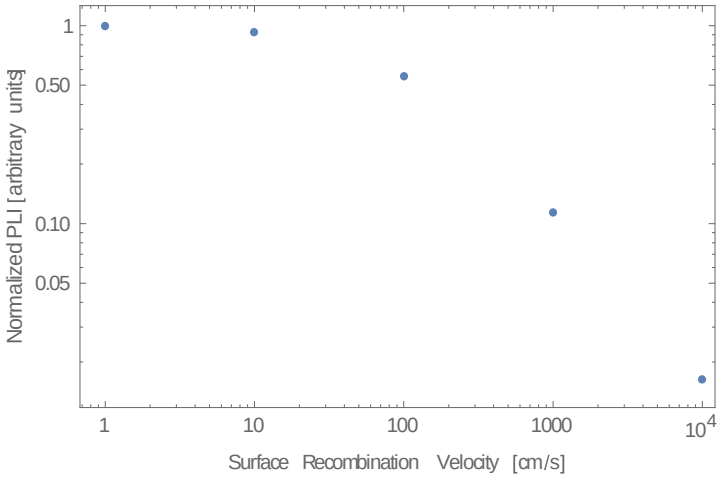

Dp = 2.5875
Lp = 0.00227486

(*For length equal to 0.5um*)
Clear[x];
x0=0.5*^-4; (*cm*)
tp=2*^-6; (*s*)
kb=1.38*^-23; (*J/K*)
T=300; (*K*)
q=1.6*^-19;(*C*)
mobp=100; (*cm^2/Vs*)

```
Dp=mobp*kb*T/q;(*cm^2/s*)
Lp=Sqrt[Dp*tp]; (*cm*)
s0=0;
s1=1;
s2=10;
s3=100;
s4=1000;
s5=10000;
delp0[x_]:=1-(s0*Cosh[x/Lp])/(s0*Cosh[x0/(2*Lp)]+Dp/Lp*Sinh[x0/(2*Lp)]);
delp1[x_]:=1-(s1*Cosh[x/Lp])/(s1*Cosh[x0/(2*Lp)]+Dp/Lp*Sinh[x0/(2*Lp)]);
delp2[x_]:=1-(s2*Cosh[x/Lp])/(s2*Cosh[x0/(2*Lp)]+Dp/Lp*Sinh[x0/(2*Lp)]);
delp3[x_]:=1-(s3*Cosh[x/Lp])/(s3*Cosh[x0/(2*Lp)]+Dp/Lp*Sinh[x0/(2*Lp)]);
delp4[x_]:=1-(s4*Cosh[x/Lp])/(s4*Cosh[x0/(2*Lp)]+Dp/Lp*Sinh[x0/(2*Lp)]);
delp5[x_]:=1-(s5*Cosh[x/Lp])/(s5*Cosh[x0/(2*Lp)]+Dp/Lp*Sinh[x0/(2*Lp)]);
Plot[{delp0[x],delp1[x],delp2[x], delp3[x], delp4[x], delp5[x]},{x,-x0/2,x0/2},
PlotRange->{0,1}, PlotLegends->{"s=0", "s=1", "s=10", "s=100", "s=1000",
"s=10000"}]
LogPlot[{delp0[x],delp1[x],delp2[x], delp3[x], delp4[x], delp5[x]},{x,-x0/2,x0/2},
PlotRange->{0,1}, PlotLegends->{"s=0", "s=1 cm/s", "s=10 cm/s", "s=100 cm/s",
"s=1000 cm/s", "s=10,000 cm/s"},Frame->True, FrameTicks-
>{{{0.010,0.05,0.1,0.5,1},None},{{0,{-0.5*^-4/2,"- x0/2"},{0.5*^-4/2,"
x0/2"}},None}},FrameLabel->{"x","(Δp(x))/(g' τp)"},
 PlotLabel->"Excess Carrier Concentration Profile
   for 0.5μm thick absorber layer
  "]
PLI0[x_]:=Integrate[delp0[x],{x, -x0/2,x0/2}];
PLI1[x_]:=Integrate[delp1[x],{x, -x0/2,x0/2}];
PLI2[x_]:=Integrate[delp2[x],{x, -x0/2,x0/2}];
PLI3[x_]:=Integrate[delp3[x],{x, -x0/2,x0/2}];
PLI4[x_]:=Integrate[delp4[x],{x, -x0/2,x0/2}];
PLI5[x_]:=Integrate[delp5[x],{x, -x0/2,x0/2}];

w=1/PLI0[x];

Print["Normalized PLI0 = ", w*PLI0[x]];
Print["Normalized PLI1 = ", w*PLI1[x]];
Print["Normalized PLI2 = ", w*PLI2[x]];
Print["Normalized PLI3 = ", w*PLI3[x]];
Print["Normalized PLI4 = ", w*PLI4[x]];
Print["Normalized PLI5 = ", w*PLI5[x]];

ListLogLogPlot[{{s0,w*PLI0[x]},{s1,w*PLI1[x]},{s2,w*PLI2[x]},{s3,w*PLI3[x]},{s4,
w*PLI4[x]},{s5,w*PLI5[x]}},Frame->True,FrameLabel->{"Surface Recombination
Velocity [cm/s]","Normalized PLI [arbitrary units]"},
 PlotLabel->"Normalized PLI vs SRV for 0.5μm thick absorber layer
  "]
```

```
Print["Dp = ", Dp];
Print["Lp = ",Lp];
{
```

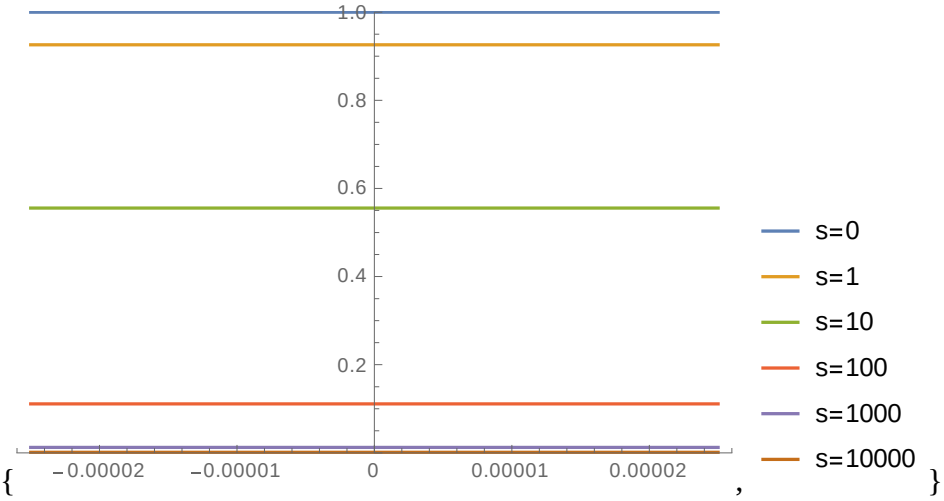


```
{ , }
}
{
```

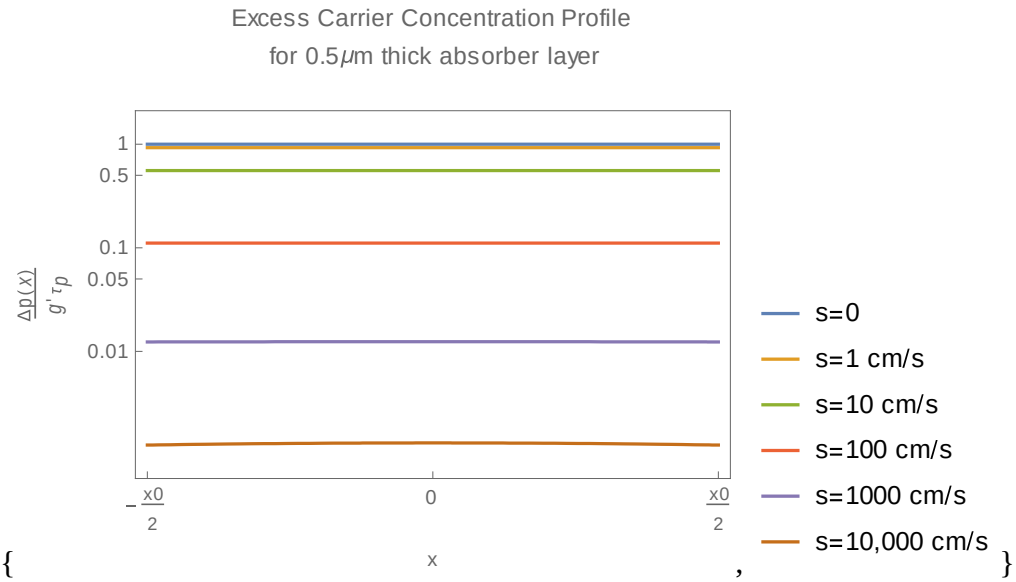


```
{ , }
}
Normalized PLI0 =  1.
Normalized PLI1 =  0.925926
Normalized PLI2 =  0.555564
Normalized PLI3 =  0.111143
Normalized PLI4 =  0.0123849
Normalized PLI5 =  0.00128859
```

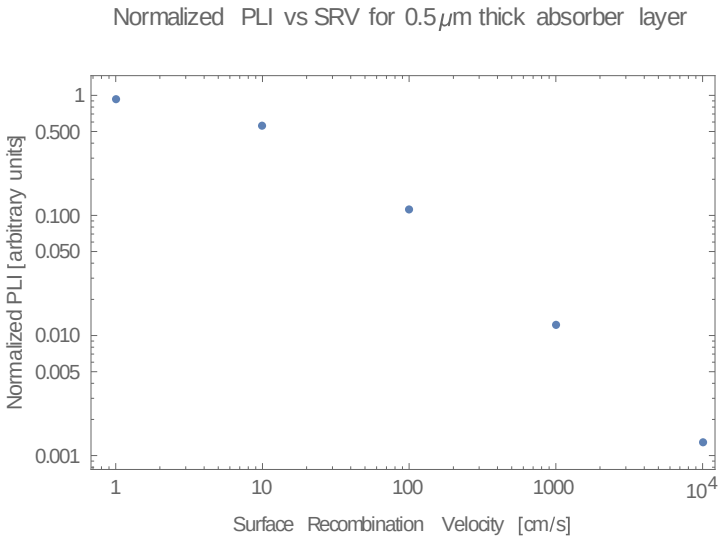

Dp = 2.5875
Lp = 0.00227486

APPENDIX B: MATHEMATICA CODES FOR STEADY STATE CALCULATIONS OF P-TYPE CDTE

Steady State Calculations
P-type CdTe – exploring excess carrier profile and PLI with various SRV values

```
(*For length = 5um*)
Clear[x];
x0=5*^-4; (*cm*)
tn=2*^-6; (*s*)
kb=1.38*^-23; (*J/K*)
T=300; (*K*)
q=1.6*^-19;(*C*)
mobn=1000; (*cm^2/Vs*)
Dn=mobn*kb*T/q;(*cm^2/s*)
Ln=Sqrt[Dn*tn]; (*cm*)
s0=0;
s1=1;
s2=10;
s3=100;
s4=1000;
s5=10000;
deln0[x_]:=1-(s0*Cosh[x/Ln])/(s0*Cosh[x0/(2*Ln)]+Dn/Ln*Sinh[x0/(2*Ln)]);
deln1[x_]:=1-(s1*Cosh[x/Ln])/(s1*Cosh[x0/(2*Ln)]+Dn/Ln*Sinh[x0/(2*Ln)]);
deln2[x_]:=1-(s2*Cosh[x/Ln])/(s2*Cosh[x0/(2*Ln)]+Dn/Ln*Sinh[x0/(2*Ln)]);
deln3[x_]:=1-(s3*Cosh[x/Ln])/(s3*Cosh[x0/(2*Ln)]+Dn/Ln*Sinh[x0/(2*Ln)]);
deln4[x_]:=1-(s4*Cosh[x/Ln])/(s4*Cosh[x0/(2*Ln)]+Dn/Ln*Sinh[x0/(2*Ln)]);
deln5[x_]:=1-(s5*Cosh[x/Ln])/(s5*Cosh[x0/(2*Ln)]+Dn/Ln*Sinh[x0/(2*Ln)]);
Plot[{deln0[x],deln1[x],deln2[x], deln3[x], deln4[x], deln5[x]},{x,-x0/2,x0/2},
PlotRange->{0,1}, PlotLegends->{"s=0", "s=1", "s=10", "s=100", "s=1000",
"s=10000"}]
LogPlot[{deln0[x],deln1[x],deln2[x], deln3[x], deln4[x], deln5[x]},{x,-x0/2,x0/2},
PlotRange->{0,1}, PlotLegends->{"s=0", "s=1 cm/s", "s=10 cm/s", "s=100 cm/s",
"s=1000 cm/s", "s=10,000 cm/s"},Frame->True, FrameTicks-
>{{{0.010,0.05,0.1,0.5,1},None},{{0,{-5*^-4/2,"- x0/2"},{5*^-4/2,"
x0/2"}},None}},FrameLabel->{"x","(Δp(x))/(g' τp)"},
 PlotLabel->"Excess Carrier Concentration Profile for 5μm thick absorber layer
  "]


PLI0[x_]:=Integrate[deln0[x],{x, -x0/2,x0/2}];
PLI1[x_]:=Integrate[deln1[x],{x, -x0/2,x0/2}];
PLI2[x_]:=Integrate[deln2[x],{x, -x0/2,x0/2}];
PLI3[x_]:=Integrate[deln3[x],{x, -x0/2,x0/2}];
PLI4[x_]:=Integrate[deln4[x],{x, -x0/2,x0/2}];
PLI5[x_]:=Integrate[deln5[x],{x, -x0/2,x0/2}];
```

```
w=1/PLI0[x];

Print["Normalized PLI0 = ", w*PLI0[x]];
Print["Normalized PLI1 = ", w*PLI1[x]];
Print["Normalized PLI2 = ", w*PLI2[x]];
Print["Normalized PLI3 = ", w*PLI3[x]];
Print["Normalized PLI4 = ", w*PLI4[x]];
Print["Normalized PLI5 = ", w*PLI5[x]];

ListLogLogPlot[{{s0,w*PLI0[x]},{s1,w*PLI1[x]},{s2,w*PLI2[x]},{s3,w*PLI3[x]},{s4,
w*PLI4[x]},{s5,w*PLI5[x]}},Frame->True,FrameLabel->{"Surface Recombination
Velocity [cm/s]","Normalized PLI [arbitrary units]"},
 PlotLabel->"Normalized PLI vs SRV for 5µm thick absorber layer
  "]

Print["Dn = ", Dn];
Print["Ln = ", Ln];
{
```

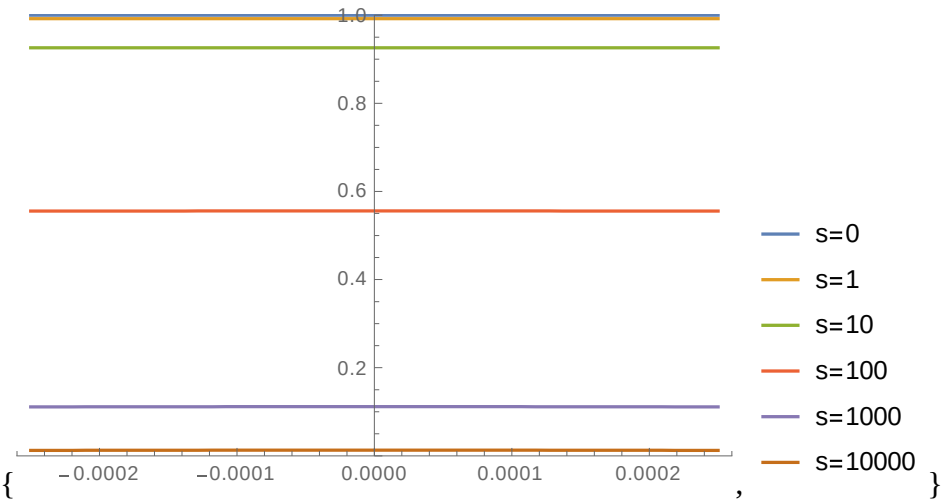


```
{                                                                    }
}
{
```

Excess Carrier Concentration Profile for 5μm thick absorber layer

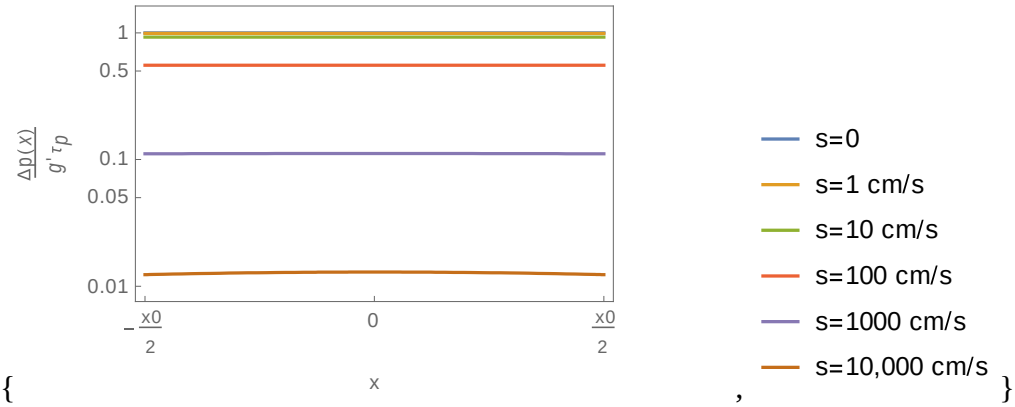

{ , }
}
Normalized PLI0 = 1.
Normalized PLI1 = 0.992064
Normalized PLI2 = 0.925928
Normalized PLI3 = 0.555635
Normalized PLI4 = 0.111429
Normalized PLI5 = 0.0127382

Normalized PLI vs SRV for 5μm thick absorber layer

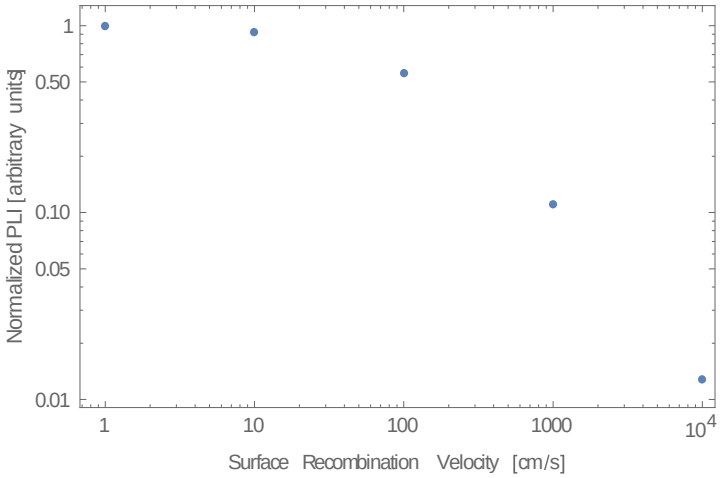

Dn = 25.875
Ln = 0.00719375

(*For length = 0.5um*)
Clear[x];
x0=0.5*^-4; (*cm*)
tn=2*^-6; (*s*)
kb=1.38*^-23; (*J/K*)
T=300; (*K*)
q=1.6*^-19;(*C*)
mobn=1000; (*cm^2/Vs*)

```
Dn=mobn*kb*T/q;(*cm^2/s*)
Ln=Sqrt[Dn*tn]; (*cm*)
s0=0;
s1=1;
s2=10;
s3=100;
s4=1000;
s5=10000;
deln0[x_]:=1-(s0*Cosh[x/Ln])/(s0*Cosh[x0/(2*Ln)]+Dn/Ln*Sinh[x0/(2*Ln)]);
deln1[x_]:=1-(s1*Cosh[x/Ln])/(s1*Cosh[x0/(2*Ln)]+Dn/Ln*Sinh[x0/(2*Ln)]);
deln2[x_]:=1-(s2*Cosh[x/Ln])/(s2*Cosh[x0/(2*Ln)]+Dn/Ln*Sinh[x0/(2*Ln)]);
deln3[x_]:=1-(s3*Cosh[x/Ln])/(s3*Cosh[x0/(2*Ln)]+Dn/Ln*Sinh[x0/(2*Ln)]);
deln4[x_]:=1-(s4*Cosh[x/Ln])/(s4*Cosh[x0/(2*Ln)]+Dn/Ln*Sinh[x0/(2*Ln)]);
deln5[x_]:=1-(s5*Cosh[x/Ln])/(s5*Cosh[x0/(2*Ln)]+Dn/Ln*Sinh[x0/(2*Ln)]);
Plot[{deln0[x],deln1[x],deln2[x], deln3[x], deln4[x], deln5[x]},{x,-x0/2,x0/2},
PlotRange->{0,1}, PlotLegends->{"s=0", "s=1", "s=10", "s=100", "s=1000",
"s=10000"}]
LogPlot[{deln0[x],deln1[x],deln2[x], deln3[x], deln4[x], deln5[x]},{x,-x0/2,x0/2},
PlotRange->{0,1}, PlotLegends->{"s=0", "s=1 cm/s", "s=10 cm/s", "s=100 cm/s",
"s=1000 cm/s", "s=10,000 cm/s"},Frame->True, FrameTicks-
>{{{0.010,0.05,0.1,0.5,1},None},{{0,{-0.5*^-4/2,"- x0/2"},{0.5*^-4/2,"
x0/2"}},None}},FrameLabel->{"x","(Δp(x))/(g' τp)"},
 PlotLabel->"Excess Carrier Concentration Profile
  for 0.5μm thick absorber layer
  "]
PLI0[x_]:=Integrate[deln0[x],{x, -x0/2,x0/2}];
PLI1[x_]:=Integrate[deln1[x],{x, -x0/2,x0/2}];
PLI2[x_]:=Integrate[deln2[x],{x, -x0/2,x0/2}];
PLI3[x_]:=Integrate[deln3[x],{x, -x0/2,x0/2}];
PLI4[x_]:=Integrate[deln4[x],{x, -x0/2,x0/2}];
PLI5[x_]:=Integrate[deln5[x],{x, -x0/2,x0/2}];

w=1/PLI0[x];

Print["Normalized PLI0 = ", w*PLI0[x]];
Print["Normalized PLI1 = ", w*PLI1[x]];
Print["Normalized PLI2 = ", w*PLI2[x]];
Print["Normalized PLI3 = ", w*PLI3[x]];
Print["Normalized PLI4 = ", w*PLI4[x]];
Print["Normalized PLI5 = ", w*PLI5[x]];

ListLogLogPlot[{{s0,w*PLI0[x]},{s1,w*PLI1[x]},{s2,w*PLI2[x]},{s3,w*PLI3[x]},{s4,
w*PLI4[x]},{s5,w*PLI5[x]}},Frame->True,FrameLabel->{"Surface Recombination
Velocity [cm/s]","Normalized PLI [arbitrary units]"},
 PlotLabel->"Normalized PLI vs SRV for 0.5μm thick absorber layer
  "]
```

```
Print["Dn = ", Dn];
Print["Ln = ", Ln];
{
```

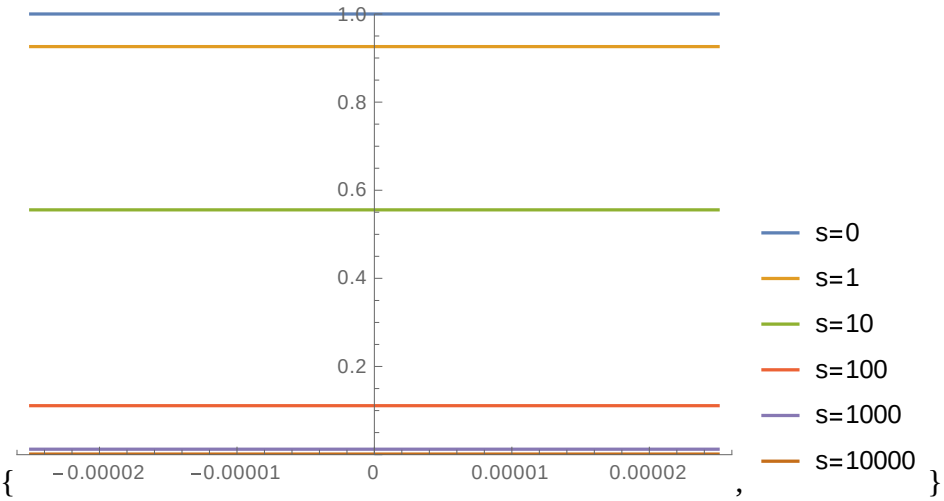


```
{ , }
}
{
```

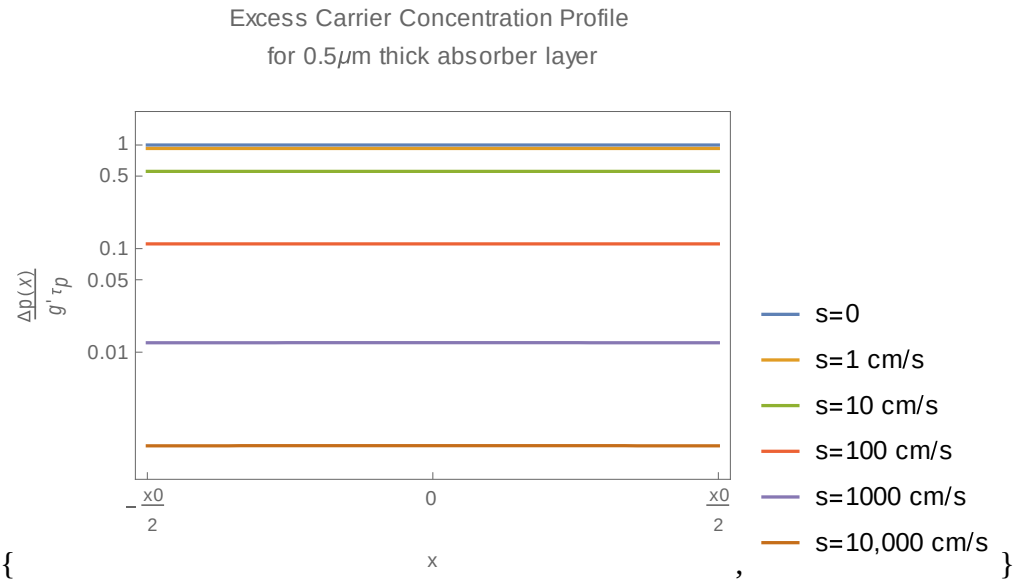


```
{ , }
}
Normalized PLI0 =  1.
Normalized PLI1 =  0.925926
Normalized PLI2 =  0.555556
Normalized PLI3 =  0.111114
Normalized PLI4 =  0.0123496
Normalized PLI5 =  0.00125246
```

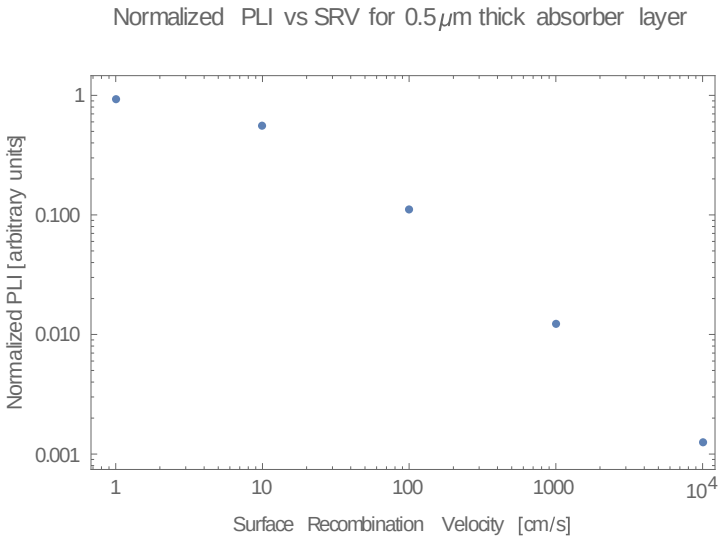

Dn = 25.875
Ln = 0.00719375

APPENDIX C: MATHEMATICA CODES FOR TRANSIENT STATE CALCULATIONS OF N-TYPE CDTE FOR DETERMINATION OF TERMS

Transient State Calculations
N-type CdTe - Plotting excess carrier profile to determine appropriate number of terms

```
ClearSystemCache[];
Clear[x];

(*For length = 5um*)
x0=5.*^-4; (*cm*)
mobp=100; (*cm^2/Vs*)
kb=1.38*^-23; (*J/K*)
T=300; (*K*)
q=1.6*^-19; (*C*)
Dp=mobp*kb*T/q;(*cm^2/s*)
tp=2*^-6; (*s*)
s0=0; (*cm/s*)
s1=1; (*cm/s*)
s2=20; (*cm/s*)
s3=50; (*cm/s*)
s4=100; (*cm/s*)
s5=1000; (*cm/s*)
x=y*x0/2;
LHS1[x_]:=Piecewise[{{Cot[x],0<=x<Pi}}]; (*must be unitless, therefore y is 1/um*)
LHS2[x_]:=Piecewise[{{Cot[x],Pi<=x<2*Pi}}];
LHS3[x_]:=Piecewise[{{Cot[x],2*Pi<=x<4*Pi}}];
LHS4[x_]:=Piecewise[{{Cot[x],4*Pi<=x<6*Pi}}];
LHS5[x_]:=Piecewise[{{Cot[x],6*Pi<=x<8*Pi}}];
RHS1[x_]:=x*(2*Dp/(s1*x0));
RHS2[x_]:=x*(2*Dp/(s2*x0));
RHS3[x_]:=x*(2*Dp/(s3*x0));
RHS4[x_]:=x*(2*Dp/(s4*x0));
RHS5[x_]:=x*(2*Dp/(s5*x0));

Plot[{Cot[x],RHS1[x], RHS2[x], RHS3[x], RHS4[x], RHS5[x]},{x,0,3*Pi}, PlotRange-
>{-2,100},  PlotLegends->{"ctnx", "s=1", "s=20","s=50", "s=100", "s=1000"}, Ticks-
>{{0,Pi/2,Pi,3*Pi/2, 2*Pi},{}}]


x1=FindRoot[LHS1[x]==RHS5[x],{x,0.1}][[1,2]];
x2=FindRoot[LHS2[x]==RHS5[x],{x,Pi}][[1,2]];
x3=FindRoot[LHS3[x]==RHS5[x],{x,2*Pi}][[1,2]];
```

```
x4=FindRoot[LHS4[x]==RHS5[x],{x,4*Pi}][[1,2]];
x5=FindRoot[LHS5[x]==RHS5[x],{x,6*Pi}][[1,2]];

r1=2*x1/x0;
r2=2*x2/x0;
r3=2*x3/x0;
r4=2*x4/x0;
r5=2*x5/x0;

Clear[g];
Clear[t];
t=0;
g=1;

Ar1=(2*r1)/(r1*x0+Sin[r1*x0])*Integrate[g*Cos[r1*z],{z,-x0/2,x0/2}] ;
Ar2=(2*r2)/(r2*x0+Sin[r2*x0])*Integrate[g*Cos[r2*z],{z,-x0/2,x0/2}] ;
Ar3=(2*r3)/(r3*x0+Sin[r3*x0])*Integrate[g*Cos[r3*z],{z,-x0/2,x0/2}] ;
Ar4=(2*r4)/(r4*x0+Sin[r4*x0])*Integrate[g*Cos[r4*z],{z,-x0/2,x0/2}] ;
Ar5=(2*r5)/(r5*x0+Sin[r5*x0])*Integrate[g*Cos[r5*z],{z,-x0/2,x0/2}] ;

u1[w_]:=Ar1*Exp[-r1^2*Dp*t]*Cos[r1*w];
u2[w_]:=Ar2*Exp[-r2^2*Dp*t]*Cos[r2*w];
u3[w_]:=Ar3*Exp[-r3^2*Dp*t]*Cos[r3*w];
u4[w_]:=Ar4*Exp[-r4^2*Dp*t]*Cos[r4*w];
u5[w_]:=Ar5*Exp[-r5^2*Dp*t]*Cos[r5*w];

v1[w_]:=u1[w];
v2[w_]:=v1[w]+u2[w];
v3[w_]:=v2[w]+u3[w];
v4[w_]:=v3[w]+u4[w];
v5[w_]:=v4[w]+u5[w];

delp1[w_]:=Exp[-t/tp]*v1[w];
delp2[w_]:=Exp[-t/tp]*v2[w];
delp3[w_]:=Exp[-t/tp]*v3[w];
delp4[w_]:=Exp[-t/tp]*v4[w];
delp5[w_]:=Exp[-t/tp]*v5[w];

(*For SRV=100*)
xx1=FindRoot[LHS1[x]==RHS4[x],{x,0.1}][[1,2]];
xx2=FindRoot[LHS2[x]==RHS4[x],{x,Pi}][[1,2]];
xx3=FindRoot[LHS3[x]==RHS4[x],{x,2*Pi}][[1,2]];
xx4=FindRoot[LHS4[x]==RHS4[x],{x,4*Pi}][[1,2]];
xx5=FindRoot[LHS5[x]==RHS4[x],{x,6*Pi}][[1,2]];

rr1=2*xx1/x0;
```

```
rr2=2*xx2/x0;
rr3=2*xx3/x0;
rr4=2*xx4/x0;
rr5=2*xx5/x0;

Aar1=(2*rr1)/(rr1*x0+Sin[rr1*x0])*Integrate[g*Cos[rr1*z],{z,-x0/2,x0/2}] ;
Aar2=(2*rr2)/(rr2*x0+Sin[rr2*x0])*Integrate[g*Cos[rr2*z],{z,-x0/2,x0/2}] ;
Aar3=(2*rr3)/(rr3*x0+Sin[rr3*x0])*Integrate[g*Cos[rr3*z],{z,-x0/2,x0/2}] ;
Aar4=(2*rr4)/(rr4*x0+Sin[rr4*x0])*Integrate[g*Cos[rr4*z],{z,-x0/2,x0/2}] ;
Aar5=(2*rr5)/(rr5*x0+Sin[rr5*x0])*Integrate[g*Cos[rr5*z],{z,-x0/2,x0/2}] ;

uu1[w_]:=Aar1*Exp[-rr1^2*Dp*t]*Cos[rr1*w];
uu2[w_]:=Aar2*Exp[-rr2^2*Dp*t]*Cos[rr2*w];
uu3[w_]:=Aar3*Exp[-rr3^2*Dp*t]*Cos[rr3*w];
uu4[w_]:=Aar4*Exp[-rr4^2*Dp*t]*Cos[rr4*w];
uu5[w_]:=Aar5*Exp[-rr5^2*Dp*t]*Cos[rr5*w];

vv1[w_]:=uu1[w];
vv2[w_]:=vv1[w]+uu2[w];
vv3[w_]:=vv2[w]+uu3[w];
vv4[w_]:=vv3[w]+uu4[w];
vv5[w_]:=vv4[w]+uu5[w];

ddelp1[w_]:=Exp[-t/tp]*vv1[w];
ddelp2[w_]:=Exp[-t/tp]*vv2[w];
ddelp3[w_]:=Exp[-t/tp]*vv3[w];
ddelp4[w_]:=Exp[-t/tp]*vv4[w];
ddelp5[w_]:=Exp[-t/tp]*vv5[w];

(*Print[Style["ddelp1[w] = ", Bold,Blue], ddelp1[w]];
Print[Style["ddelp2[w] = ", Bold,Blue], ddelp2[w]];
Print[Style["ddelp3[w] = ", Bold,Blue], ddelp3[w]];
Print[Style["ddelp4[w] = ", Bold,Blue], ddelp4[w]];
Print[Style["ddelp5[w] = ", Bold,Blue], ddelp5[w]];

Print[Style["delp1[w] = ", Bold,Blue], delp1[w]];
Print[Style["delp2[w] = ", Bold,Blue], delp2[w]];
Print[Style["delp3[w] = ", Bold,Blue], delp3[w]];
Print[Style["delp4[w] = ", Bold,Blue], delp4[w]];
Print[Style["delp5[w] = ", Bold,Blue], delp5[w]];*)


Plot[{ddelp1[w],ddelp2[w], ddelp3[w],ddelp4[w],ddelp5[w]},{w,-x0/2,x0/2},PlotRange-
>{0.9988,1.002}, PlotLegends->{"Δp(x,0) - 1 term", "Δp(x,0) - 2 terms", "Δp(x,0) - 3
terms", "Δp(x,0) - 4 terms", "Δp(x,0) - 5 terms"}, LabelStyle->Directive[Bold, Black],
```

```
 Frame->True,FrameTicks-
>{{{0.999,0.9995,1.0,1.0005,1.0010,1.0015,1.002},None},{{0,{-5*^-4/2,"-2.5
μm"},{5*^-4/2,"2.5 μm"}},None}},FrameLabel->{"x","Δp(x,0)"},
 PlotLabel->"Excess Carrier profile
  at t = 0 s with SRV = 100 cm/s
  "]
Plot[{ddelp1[w],ddelp2[w], ddelp3[w],ddelp4[w],ddelp5[w]},{w,-x0/2,x0/2},PlotRange-
>{0,1.5}, PlotLegends->{"Δp(x,0) - 1 term", "Δp(x,0) - 2 terms", "Δp(x,0) - 3 terms",
"Δp(x,0) - 4 terms", "Δp(x,0) - 5 terms"},PlotLabel->"SRV=100", LabelStyle-
>Directive[Bold, Black]]
Print["Let n = 1/alphan^2*Dp"];
Print[Style["n1 = ", Bold,Blue],1/(rr1^2*Dp)];
Print[Style["n2 = ", Bold,Blue], 1/(rr2^2*Dp)];
Print[Style["n3 = ", Bold,Blue], 1/(rr3^2*Dp)];
Print[Style["n4 = ", Bold,Blue], 1/(rr4^2*Dp)];
Print[Style["n5 = ", Bold,Blue], 1/(rr5^2*Dp)];



Plot[{delp1[w],delp2[w], delp3[w],delp4[w],delp5[w]},{w,-x0/2,x0/2},PlotRange-
>{0.988,1.02},PlotLegends->{"Δp(x,0) - 1 term", "Δp(x,0) - 2 terms", "Δp(x,0) - 3
terms", "Δp(x,0) - 4 terms", "Δp(x,0) - 5 terms"}, LabelStyle->Directive[Bold, Black],
 Frame->True,FrameTicks->{{{0.99,0.995,1.0,1.005,1.010,1.015,1.02},None},{{0,{-
5*^-4/2,"-2.5 μm"},{5*^-4/2,"2.5 μm"}},None}},FrameLabel->{"x","Δp(x,0)"},
 PlotLabel->"Excess Carrier profile
  at t = 0 s with SRV = 1000 cm/s
  "]
Plot[{delp1[w],delp2[w], delp3[w],delp4[w],delp5[w]},{w,-x0/2,x0/2},PlotRange-
>{0,1.5},PlotLegends->{"Δp(x,0) - 1 term", "Δp(x,0) - 2 terms", "Δp(x,0) - 3 terms",
"Δp(x,0) - 4 terms", "Δp(x,0) - 5 terms"},PlotLabel->"SRV=1000", LabelStyle-
>Directive[Bold, Black]]
Print["Let n = 1/alphan^2*Dp"];
Print[Style["n1 = ", Bold,Blue], 1/(r1^2*Dp)];
Print[Style["n2 = ", Bold,Blue], 1/(r2^2*Dp)];
Print[Style["n3 = ", Bold,Blue], 1/(r3^2*Dp)];
Print[Style["n4 = ", Bold,Blue], 1/(r4^2*Dp)];
Print[Style["n5 = ", Bold,Blue], 1/(r5^2*Dp)];

{
```

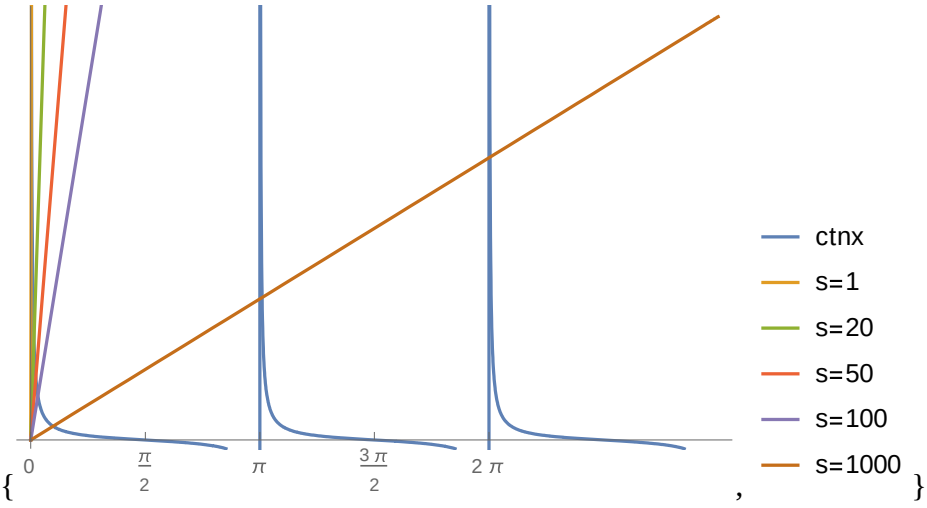
0
π/2
π
3π/2
2π
ctnx
s=1
s=20
s=50
s=100
s=1000

{ , }

}

{

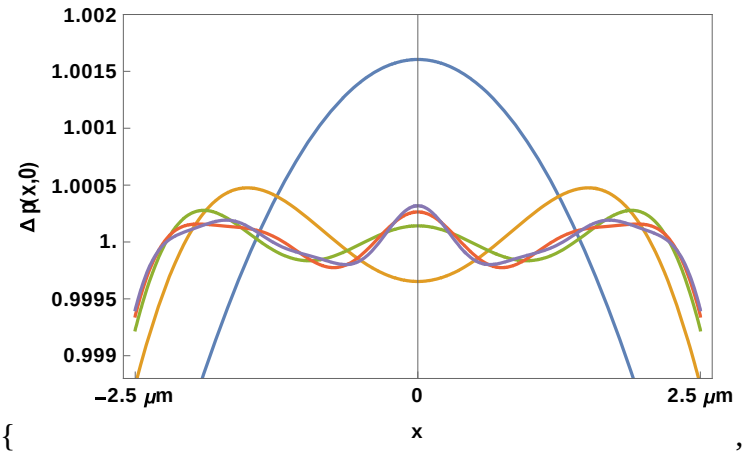
Excess Carrier profile
at t = 0 s with SRV = 100 cm/s
1.002
1.0015
1.001
1.0005
1.
0.9995
0.999
Δ p(x,0)
−2.5 μm
0
2.5 μm
x
Δp(x,0) – 1 term
Δp(x,0) – 2 terms
Δp(x,0) – 3 terms
Δp(x,0) – 4 terms
Δp(x,0) – 5 terms

{ , }

}

{

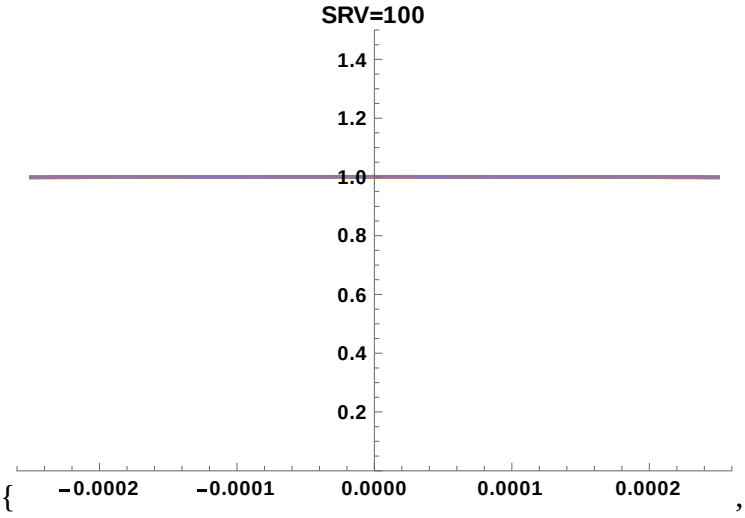
SRV=100
1.4
1.2
1.0
0.8
0.6
0.4
0.2
−0.0002
−0.0001
0.0000
0.0001
0.0002
Δp(x,0) – 1 term
Δp(x,0) – 2 terms
Δp(x,0) – 3 terms
Δp(x,0) – 4 terms
Δp(x,0) – 5 terms

{ , }

}
Let n = 1/alphan^2*Dp
n1 = $2.50806*10^{-6}$
n2 = $2.44259*10^{-9}$
n3 = $6.11544*10^{-10}$
n4 = $1.52942*10^{-10}$
n5 = $6.79788*10^{-11}$
{

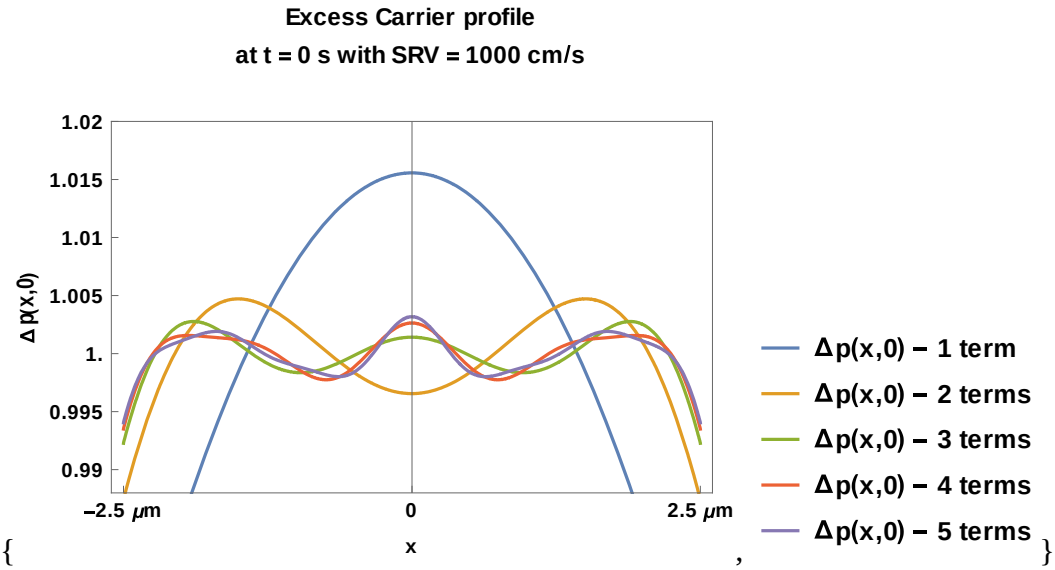

}
{
}
{

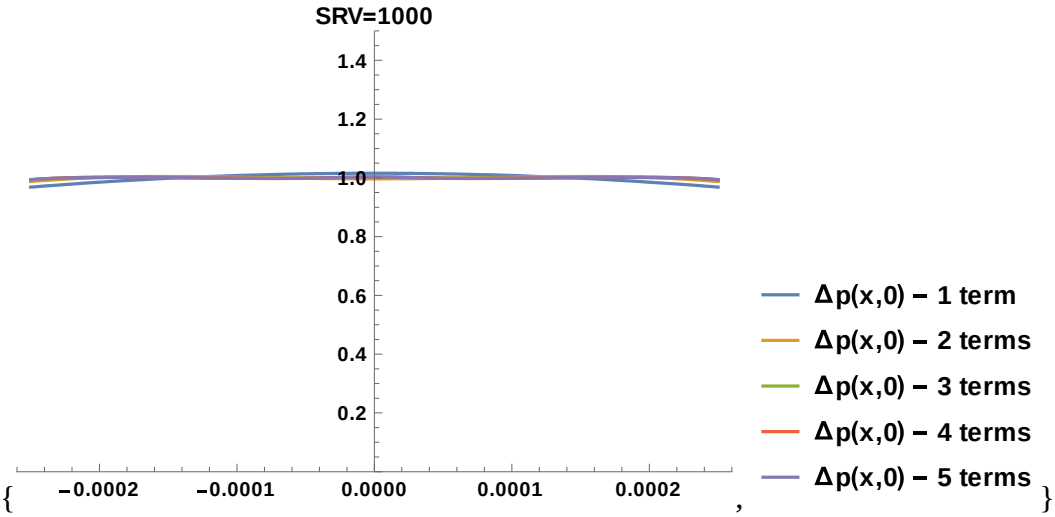

}
Let n = 1/alphan^2*Dp
n1 = $2.58102*10^{-7}$
n2 = $2.40061*10^{-9}$
n3 = $6.08867*10^{-10}$
n4 = $1.52774*10^{-10}$
n5 = $6.79456*10^{-11}$

```
(*For length = 0.5um*)
x0=0.5*^-4;

x1=FindRoot[LHS1[x]==RHS5[x],{x,0.1}][[1,2]];
x2=FindRoot[LHS2[x]==RHS5[x],{x,Pi}][[1,2]];
x3=FindRoot[LHS3[x]==RHS5[x],{x,2*Pi}][[1,2]];
x4=FindRoot[LHS4[x]==RHS5[x],{x,4*Pi}][[1,2]];
x5=FindRoot[LHS5[x]==RHS5[x],{x,6*Pi}][[1,2]];

r1=2*x1/x0;
r2=2*x2/x0;
r3=2*x3/x0;
r4=2*x4/x0;
r5=2*x5/x0;

Clear[g];
Clear[t];
t=0;
g=1;

Ar1=(2*r1)/(r1*x0+Sin[r1*x0])*Integrate[g*Cos[r1*z],{z,-x0/2,x0/2}] ;
Ar2=(2*r2)/(r2*x0+Sin[r2*x0])*Integrate[g*Cos[r2*z],{z,-x0/2,x0/2}] ;
Ar3=(2*r3)/(r3*x0+Sin[r3*x0])*Integrate[g*Cos[r3*z],{z,-x0/2,x0/2}] ;
Ar4=(2*r4)/(r4*x0+Sin[r4*x0])*Integrate[g*Cos[r4*z],{z,-x0/2,x0/2}] ;
Ar5=(2*r5)/(r5*x0+Sin[r5*x0])*Integrate[g*Cos[r5*z],{z,-x0/2,x0/2}] ;

u1[w_]:=Ar1*Exp[-r1^2*Dp*t]*Cos[r1*w];
u2[w_]:=Ar2*Exp[-r2^2*Dp*t]*Cos[r2*w];
u3[w_]:=Ar3*Exp[-r3^2*Dp*t]*Cos[r3*w];
u4[w_]:=Ar4*Exp[-r4^2*Dp*t]*Cos[r4*w];
u5[w_]:=Ar5*Exp[-r5^2*Dp*t]*Cos[r5*w];

v1[w_]:=u1[w];
v2[w_]:=v1[w]+u2[w];
v3[w_]:=v2[w]+u3[w];
v4[w_]:=v3[w]+u4[w];
v5[w_]:=v4[w]+u5[w];

delp1[w_]:=Exp[-t/tp]*v1[w];
delp2[w_]:=Exp[-t/tp]*v2[w];
delp3[w_]:=Exp[-t/tp]*v3[w];
delp4[w_]:=Exp[-t/tp]*v4[w];
delp5[w_]:=Exp[-t/tp]*v5[w];

(*For SRV=100*)
xx1=FindRoot[LHS1[x]==RHS4[x],{x,0.1}][[1,2]];
```

```
xx2=FindRoot[LHS2[x]==RHS4[x],{x,Pi}][[1,2]];
xx3=FindRoot[LHS3[x]==RHS4[x],{x,2*Pi}][[1,2]];
xx4=FindRoot[LHS4[x]==RHS4[x],{x,4*Pi}][[1,2]];
xx5=FindRoot[LHS5[x]==RHS4[x],{x,6*Pi}][[1,2]];

rr1=2*xx1/x0;
rr2=2*xx2/x0;
rr3=2*xx3/x0;
rr4=2*xx4/x0;
rr5=2*xx5/x0;

Aar1=(2*rr1)/(rr1*x0+Sin[rr1*x0])*Integrate[g*Cos[rr1*z],{z,-x0/2,x0/2}] ;
Aar2=(2*rr2)/(rr2*x0+Sin[rr2*x0])*Integrate[g*Cos[rr2*z],{z,-x0/2,x0/2}] ;
Aar3=(2*rr3)/(rr3*x0+Sin[rr3*x0])*Integrate[g*Cos[rr3*z],{z,-x0/2,x0/2}] ;
Aar4=(2*rr4)/(rr4*x0+Sin[rr4*x0])*Integrate[g*Cos[rr4*z],{z,-x0/2,x0/2}] ;
Aar5=(2*rr5)/(rr5*x0+Sin[rr5*x0])*Integrate[g*Cos[rr5*z],{z,-x0/2,x0/2}] ;

uu1[w_]:=Aar1*Exp[-rr1^2*Dp*t]*Cos[rr1*w];
uu2[w_]:=Aar2*Exp[-rr2^2*Dp*t]*Cos[rr2*w];
uu3[w_]:=Aar3*Exp[-rr3^2*Dp*t]*Cos[rr3*w];
uu4[w_]:=Aar4*Exp[-rr4^2*Dp*t]*Cos[rr4*w];
uu5[w_]:=Aar5*Exp[-rr5^2*Dp*t]*Cos[rr5*w];

vv1[w_]:=uu1[w];
vv2[w_]:=vv1[w]+uu2[w];
vv3[w_]:=vv2[w]+uu3[w];
vv4[w_]:=vv3[w]+uu4[w];
vv5[w_]:=vv4[w]+uu5[w];

ddelp1[w_]:=Exp[-t/tp]*vv1[w];
ddelp2[w_]:=Exp[-t/tp]*vv2[w];
ddelp3[w_]:=Exp[-t/tp]*vv3[w];
ddelp4[w_]:=Exp[-t/tp]*vv4[w];
ddelp5[w_]:=Exp[-t/tp]*vv5[w];

(*Print[Style["ddelp1[w] = ", Bold,Blue], ddelp1[w]];
Print[Style["ddelp2[w] = ", Bold,Blue], ddelp2[w]];
Print[Style["ddelp3[w] = ", Bold,Blue], ddelp3[w]];
Print[Style["ddelp4[w] = ", Bold,Blue], ddelp4[w]];
Print[Style["ddelp5[w] = ", Bold,Blue], ddelp5[w]];

Print[Style["delp1[w] = ", Bold,Blue], delp1[w]];
Print[Style["delp2[w] = ", Bold,Blue], delp2[w]];
Print[Style["delp3[w] = ", Bold,Blue], delp3[w]];
Print[Style["delp4[w] = ", Bold,Blue], delp4[w]];
Print[Style["delp5[w] = ", Bold,Blue], delp5[w]];*)
```

```
Plot[{ddelp1[w],ddelp2[w], ddelp3[w],ddelp4[w],ddelp5[w]},{w,-x0/2,x0/2},PlotRange-
>{0.99988,1.0002}, PlotLegends->{"Δp(x,0) - 1 term", "Δp(x,0) - 2 terms", "Δp(x,0) - 3
terms", "Δp(x,0) - 4 terms", "Δp(x,0) - 5 terms"}, LabelStyle->Directive[Bold, Black],
 Frame->True,FrameTicks-
>{{{0.9999,0.99995,1.0,1.00005,1.00010,1.00015,1.0002},None},{{0,{-0.5*^-4/2,"-0.25
μm"},{0.5*^-4/2,"0.25 μm"}},None}},FrameLabel->{"x","Δp(x,0)"},
 PlotLabel->"Excess Carrier profile
  at t = 0 s with SRV = 100 cm/s
  "]
Plot[{ddelp1[w],ddelp2[w], ddelp3[w],ddelp4[w],ddelp5[w]},{w,-x0/2,x0/2},PlotRange-
>{0,1.1}, PlotLegends->{"Δp(x,0) - 1 term", "Δp(x,0) - 2 terms", "Δp(x,0) - 3 terms",
"Δp(x,0) - 4 terms", "Δp(x,0) - 5 terms"},PlotLabel->"SRV=100", LabelStyle-
>Directive[Bold, Black]]
Print["Let n = 1/alphan^2*Dp"];
Print[Style["n1 = ", Bold,Blue],1/(rr1^2*Dp)];
Print[Style["n2 = ", Bold,Blue], 1/(rr2^2*Dp)];
Print[Style["n3 = ", Bold,Blue], 1/(rr3^2*Dp)];
Print[Style["n4 = ", Bold,Blue], 1/(rr4^2*Dp)];
Print[Style["n5 = ", Bold,Blue], 1/(rr5^2*Dp)];



Plot[{delp1[w],delp2[w], delp3[w],delp4[w],delp5[w]},{w,-x0/2,x0/2},PlotRange-
>{0.9988,1.002},PlotLegends->{"Δp(x,0) - 1 term", "Δp(x,0) - 2 terms", "Δp(x,0) - 3
terms", "Δp(x,0) - 4 terms", "Δp(x,0) - 5 terms"}, LabelStyle->Directive[Bold, Black],
 Frame->True,FrameTicks-
>{{{0.999,0.9995,1.0,1.0005,1.0010,1.0015,1.002},None},{{0,{-0.5*^-4/2,"-0.25
μm"},{0.5*^-4/2,"0.25 μm"}},None}},FrameLabel->{"x","Δp(x,0)"},
 PlotLabel->"Excess Carrier profile
  at t = 0 s with SRV = 1000 cm/s
  "]
Plot[{delp1[w],delp2[w], delp3[w],delp4[w],delp5[w]},{w,-x0/2,x0/2},PlotRange-
>{0,1.1},PlotLegends->{"Δp(x,0) - 1 term", "Δp(x,0) - 2 terms", "Δp(x,0) - 3 terms",
"Δp(x,0) - 4 terms", "Δp(x,0) - 5 terms"},PlotLabel->"SRV=1000", LabelStyle-
>Directive[Bold, Black]]
Print["Let n = 1/alphan^2*Dp"];
Print[Style["n1 = ", Bold,Blue], 1/(r1^2*Dp)];
Print[Style["n2 = ", Bold,Blue], 1/(r2^2*Dp)];
Print[Style["n3 = ", Bold,Blue], 1/(r3^2*Dp)];
Print[Style["n4 = ", Bold,Blue], 1/(r4^2*Dp)];
Print[Style["n5 = ", Bold,Blue], 1/(r5^2*Dp)];


{
```

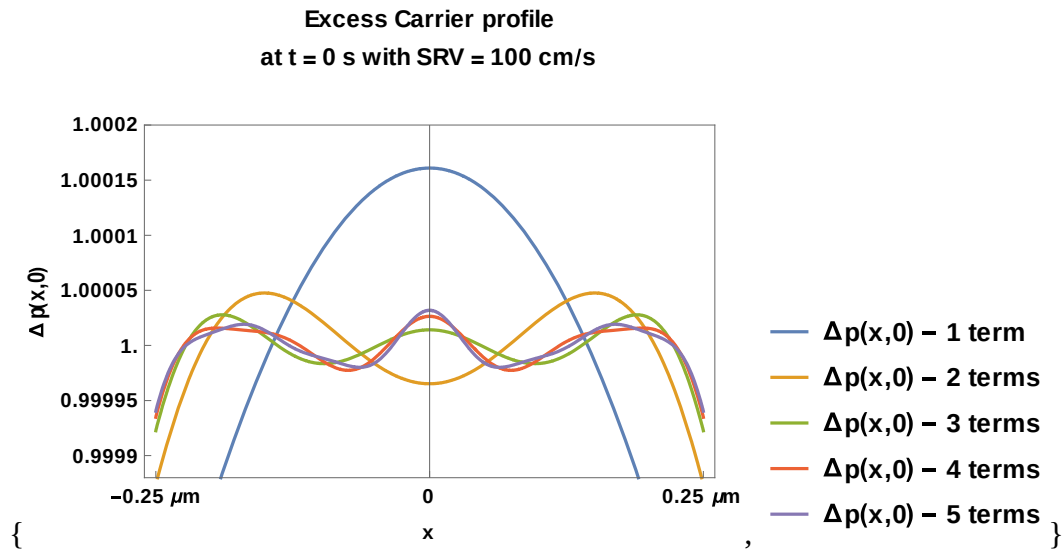

{

}

{

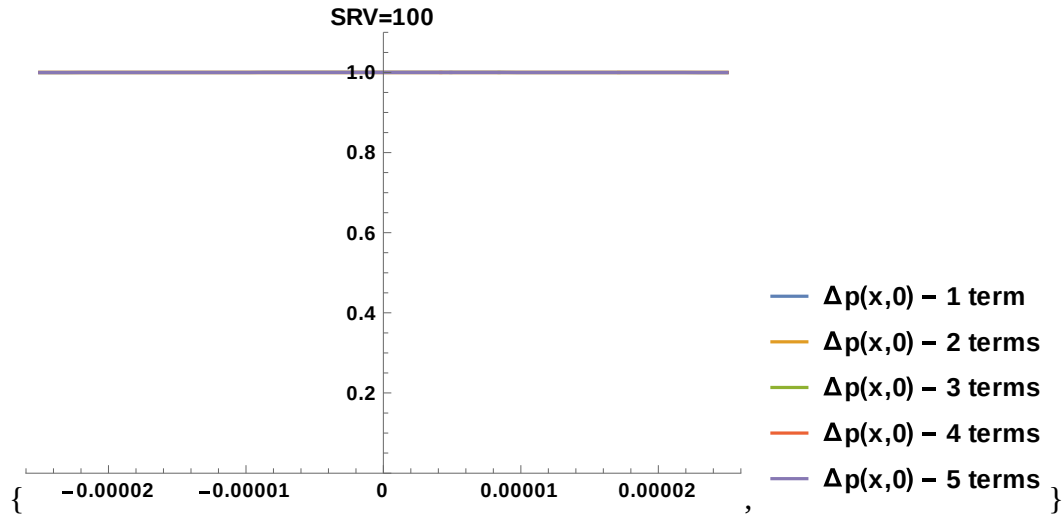

{

}

Let n = 1/alphan^2*Dp

n1 = $2.50081*10^{-7}$

n2 = $2.44689*10^{-11}$

n3 = $6.11813*10^{-12}$

n4 = $1.52959*10^{-12}$

n5 = $6.79822*10^{-13}$

{

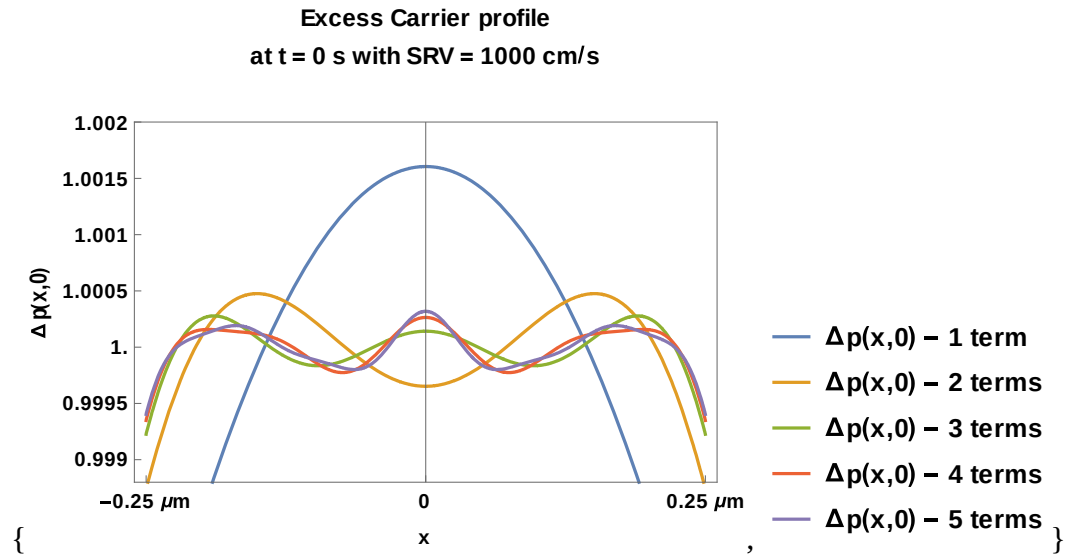

{

}

{

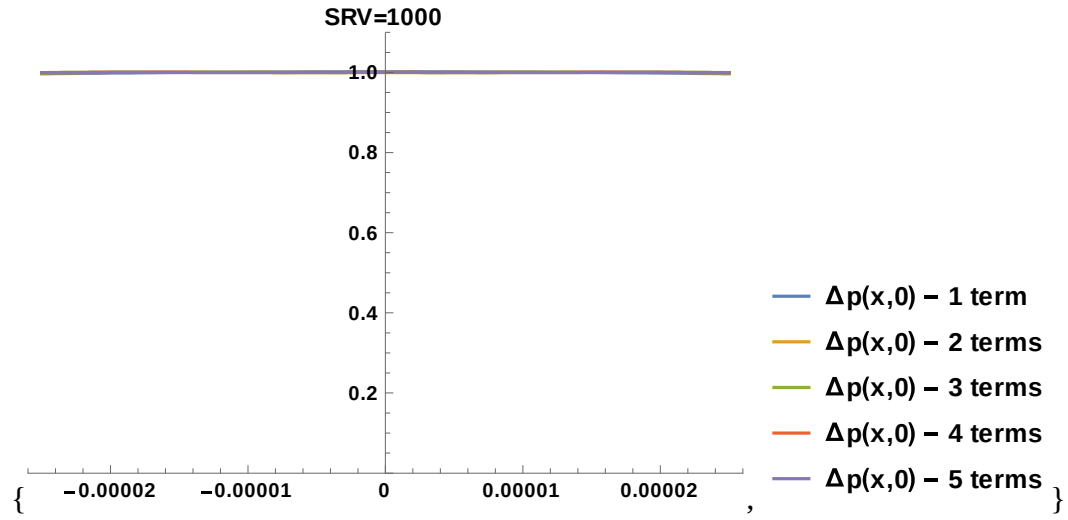

{ , }

}

Let n = 1/alphan^2*Dp

n1 = $2.50806*10^{-8}$

n2 = $2.44259*10^{-11}$

n3 = $6.11544*10^{-12}$

n4 = $1.52942*10^{-12}$

n5 = $6.79788*10^{-13}$

APPENDIX D: MATHEMATICA CODES FOR TRANSIENT STATE CALCULATIONS OF P-TYPE CDTE FOR DETERMINATION OF TERMS

Transient State Calculations
P-type CdTe - Plotting excess carrier profile to determine appropriate number of terms.

```
ClearSystemCache[];
Clear[x];

(*For length = 5um*)
x0=5.*^-4; (*cm*)
mobn=1000; (*cm^2/Vs*)
kb=1.38*^-23; (*J/K*)
T=300; (*K*)
q=1.6*^-19; (*C*)
Dn=mobn*kb*T/q;(*cm^2/s*)
tn=2*^-6; (*s*)
s0=0; (*cm/s*)
s1=1; (*cm/s*)
s2=20; (*cm/s*)
s3=50; (*cm/s*)
s4=100; (*cm/s*)
s5=1000; (*cm/s*)
x=y*x0/2;
LHS1[x_]:=Piecewise[{{Cot[x],0<=x<Pi}}]; (*must be unitless, therefore y is 1/um*)
LHS2[x_]:=Piecewise[{{Cot[x],Pi<=x<2*Pi}}];
LHS3[x_]:=Piecewise[{{Cot[x],2*Pi<=x<4*Pi}}];
LHS4[x_]:=Piecewise[{{Cot[x],4*Pi<=x<6*Pi}}];
LHS5[x_]:=Piecewise[{{Cot[x],6*Pi<=x<8*Pi}}];
RHS1[x_]:=x*(2*Dn/(s1*x0));
RHS2[x_]:=x*(2*Dn/(s2*x0));
RHS3[x_]:=x*(2*Dn/(s3*x0));
RHS4[x_]:=x*(2*Dn/(s4*x0));
RHS5[x_]:=x*(2*Dn/(s5*x0));

(*Plot[{Cot[x],RHS1[x], RHS2[x], RHS3[x], RHS4[x], RHS5[x]},{x,0,3*Pi},
PlotRange□{-2,100},  PlotLegends□{"ctnx", "s=1", "s=20","s=50", "s=100", "s=1000"},
Ticks□{{0,Pi/2,Pi,3*Pi/2, 2*Pi},{}}]*)


x1=FindRoot[LHS1[x]==RHS5[x],{x,0.1}][[1,2]];
x2=FindRoot[LHS2[x]==RHS5[x],{x,Pi}][[1,2]];
x3=FindRoot[LHS3[x]==RHS5[x],{x,2*Pi}][[1,2]];
x4=FindRoot[LHS4[x]==RHS5[x],{x,4*Pi}][[1,2]];
x5=FindRoot[LHS5[x]==RHS5[x],{x,6*Pi}][[1,2]];
```

```
r1=2*x1/x0;
r2=2*x2/x0;
r3=2*x3/x0;
r4=2*x4/x0;
r5=2*x5/x0;

Clear[g];
Clear[t];
t=0;
g=1;

Ar1=(2*r1)/(r1*x0+Sin[r1*x0])*Integrate[g*Cos[r1*z],{z,-x0/2,x0/2}] ;
Ar2=(2*r2)/(r2*x0+Sin[r2*x0])*Integrate[g*Cos[r2*z],{z,-x0/2,x0/2}] ;
Ar3=(2*r3)/(r3*x0+Sin[r3*x0])*Integrate[g*Cos[r3*z],{z,-x0/2,x0/2}] ;
Ar4=(2*r4)/(r4*x0+Sin[r4*x0])*Integrate[g*Cos[r4*z],{z,-x0/2,x0/2}] ;
Ar5=(2*r5)/(r5*x0+Sin[r5*x0])*Integrate[g*Cos[r5*z],{z,-x0/2,x0/2}] ;

u1[w_]:=Ar1*Exp[-r1^2*Dn*t]*Cos[r1*w];
u2[w_]:=Ar2*Exp[-r2^2*Dn*t]*Cos[r2*w];
u3[w_]:=Ar3*Exp[-r3^2*Dn*t]*Cos[r3*w];
u4[w_]:=Ar4*Exp[-r4^2*Dn*t]*Cos[r4*w];
u5[w_]:=Ar5*Exp[-r5^2*Dn*t]*Cos[r5*w];

v1[w_]:=u1[w];
v2[w_]:=v1[w]+u2[w];
v3[w_]:=v2[w]+u3[w];
v4[w_]:=v3[w]+u4[w];
v5[w_]:=v4[w]+u5[w];

delp1[w_]:=Exp[-t/tn]*v1[w];
delp2[w_]:=Exp[-t/tn]*v2[w];
delp3[w_]:=Exp[-t/tn]*v3[w];
delp4[w_]:=Exp[-t/tn]*v4[w];
delp5[w_]:=Exp[-t/tn]*v5[w];

(*For SRV=100*)
xx1=FindRoot[LHS1[x]==RHS4[x],{x,0.1}][[1,2]];
xx2=FindRoot[LHS2[x]==RHS4[x],{x,Pi}][[1,2]];
xx3=FindRoot[LHS3[x]==RHS4[x],{x,2*Pi}][[1,2]];
xx4=FindRoot[LHS4[x]==RHS4[x],{x,4*Pi}][[1,2]];
xx5=FindRoot[LHS5[x]==RHS4[x],{x,6*Pi}][[1,2]];

rr1=2*xx1/x0;
rr2=2*xx2/x0;
rr3=2*xx3/x0;
rr4=2*xx4/x0;
```

```
rr5=2*xx5/x0;

Aar1=(2*rr1)/(rr1*x0+Sin[rr1*x0])*Integrate[g*Cos[rr1*z],{z,-x0/2,x0/2}] ;
Aar2=(2*rr2)/(rr2*x0+Sin[rr2*x0])*Integrate[g*Cos[rr2*z],{z,-x0/2,x0/2}] ;
Aar3=(2*rr3)/(rr3*x0+Sin[rr3*x0])*Integrate[g*Cos[rr3*z],{z,-x0/2,x0/2}] ;
Aar4=(2*rr4)/(rr4*x0+Sin[rr4*x0])*Integrate[g*Cos[rr4*z],{z,-x0/2,x0/2}] ;
Aar5=(2*rr5)/(rr5*x0+Sin[rr5*x0])*Integrate[g*Cos[rr5*z],{z,-x0/2,x0/2}] ;

uu1[w_]:=Aar1*Exp[-rr1^2*Dn*t]*Cos[rr1*w];
uu2[w_]:=Aar2*Exp[-rr2^2*Dn*t]*Cos[rr2*w];
uu3[w_]:=Aar3*Exp[-rr3^2*Dn*t]*Cos[rr3*w];
uu4[w_]:=Aar4*Exp[-rr4^2*Dn*t]*Cos[rr4*w];
uu5[w_]:=Aar5*Exp[-rr5^2*Dn*t]*Cos[rr5*w];

vv1[w_]:=uu1[w];
vv2[w_]:=vv1[w]+uu2[w];
vv3[w_]:=vv2[w]+uu3[w];
vv4[w_]:=vv3[w]+uu4[w];
vv5[w_]:=vv4[w]+uu5[w];

ddelp1[w_]:=Exp[-t/tn]*vv1[w];
ddelp2[w_]:=Exp[-t/tn]*vv2[w];
ddelp3[w_]:=Exp[-t/tn]*vv3[w];
ddelp4[w_]:=Exp[-t/tn]*vv4[w];
ddelp5[w_]:=Exp[-t/tn]*vv5[w];

(*Print[Style["ddelp1[w] = ", Bold,Blue], ddelp1[w]];
Print[Style["ddelp2[w] = ", Bold,Blue], ddelp2[w]];
Print[Style["ddelp3[w] = ", Bold,Blue], ddelp3[w]];
Print[Style["ddelp4[w] = ", Bold,Blue], ddelp4[w]];
Print[Style["ddelp5[w] = ", Bold,Blue], ddelp5[w]];

Print[Style["delp1[w] = ", Bold,Blue], delp1[w]];
Print[Style["delp2[w] = ", Bold,Blue], delp2[w]];
Print[Style["delp3[w] = ", Bold,Blue], delp3[w]];
Print[Style["delp4[w] = ", Bold,Blue], delp4[w]];
Print[Style["delp5[w] = ", Bold,Blue], delp5[w]];*)

Plot[{ddelp1[w],ddelp2[w], ddelp3[w],ddelp4[w],ddelp5[w]},{w,-x0/2,x0/2},PlotRange-
>{0.99988,1.0002}, PlotLegends->{"Δp(x,0) - 1 term", "Δp(x,0) - 2 terms", "Δp(x,0) - 3
terms", "Δp(x,0) - 4 terms", "Δp(x,0) - 5 terms"}, LabelStyle->Directive[Bold, Black],
 Frame->True,FrameTicks-
>{{{0.9999,0.99995,1.0,1.00005,1.00010,1.00015,1.0002},None},{{0,{-5*^-4/2,"-2.5
μm"},{5*^-4/2,"2.5 μm"}},None}},FrameLabel->{"x","Δp(x,0)"},
 PlotLabel->"Excess Carrier profile
  at t = 0 s with SRV = 100 cm/s
```

```
 "]
Plot[{ddelp1[w],ddelp2[w], ddelp3[w],ddelp4[w],ddelp5[w]},{w,-x0/2,x0/2},PlotRange-
>{0,1.5}, PlotLegends->"Expressions",PlotLabel->"SRV=100",LabelStyle-
>Directive[Bold, Purple]]
Print[Style["n1 = ", Bold,Blue],1/(rr1^2*Dn)];
Print[Style["n2 = ", Bold,Blue], 1/(rr2^2*Dn)];
Print[Style["n3 = ", Bold,Blue], 1/(rr3^2*Dn)];
Print[Style["n4 = ", Bold,Blue], 1/(rr4^2*Dn)];
Print[Style["n5 = ", Bold,Blue], 1/(rr5^2*Dn)];


Plot[{delp1[w],delp2[w], delp3[w],delp4[w],delp5[w]},{w,-x0/2,x0/2},PlotRange-
>{0.9988,1.002},PlotLegends->{"Δp(x,0) - 1 term", "Δp(x,0) - 2 terms", "Δp(x,0) - 3
terms", "Δp(x,0) - 4 terms", "Δp(x,0) - 5 terms"}, LabelStyle->Directive[Bold, Black],
 Frame->True,FrameTicks-
>{{{0.999,0.9995,1.0,1.0005,1.0010,1.0015,1.002},None},{{0,{-5*^-4/2,"-2.5
μm"},{5*^-4/2,"2.5 μm"}},None}},FrameLabel->{"x","Δp(x,0)"},
 PlotLabel->"Excess Carrier profile
  at t = 0 s with SRV = 1000 cm/s
  "]
Plot[{delp1[w],delp2[w], delp3[w],delp4[w],delp5[w]},{w,-x0/2,x0/2},PlotRange-
>{0,1.5},PlotLegends->"Expressions",PlotLabel->"SRV=1000",LabelStyle-
>Directive[Bold, Purple]]
Print[Style["n1 = ", Bold,Blue], 1/(r1^2*Dn)];
Print[Style["n2 = ", Bold,Blue], 1/(r2^2*Dn)];
Print[Style["n3 = ", Bold,Blue], 1/(r3^2*Dn)];
Print[Style["n4 = ", Bold,Blue], 1/(r4^2*Dn)];
Print[Style["n5 = ", Bold,Blue], 1/(r5^2*Dn)];

{
```

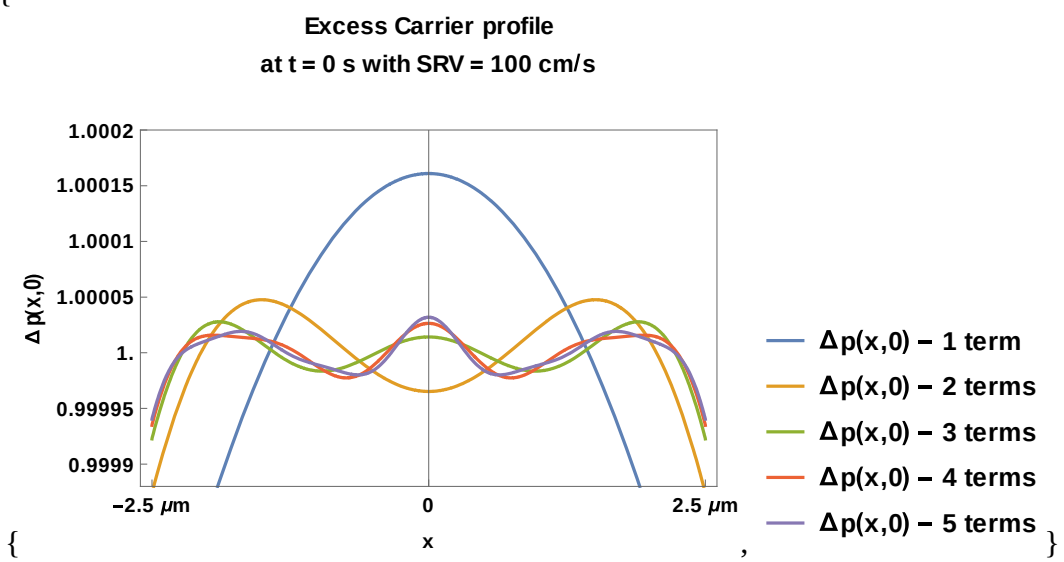


```
{                                                                    ,          }
}
```

{

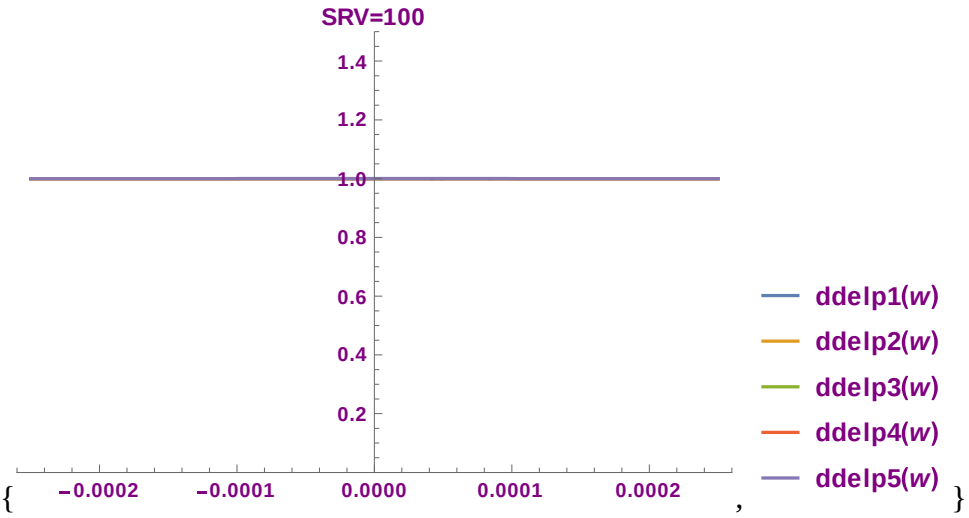

}

n1 = $2.50081*10^{-6}$
n2 = $2.44689*10^{-10}$
n3 = $6.11813*10^{-11}$
n4 = $1.52959*10^{-11}$
n5 = $6.79822*10^{-12}$

{

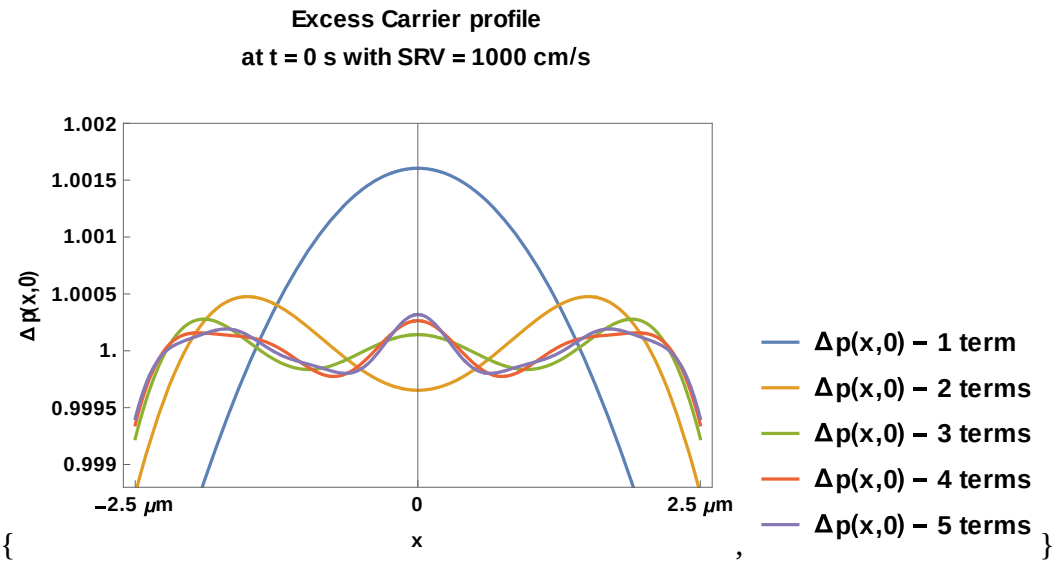

}

{

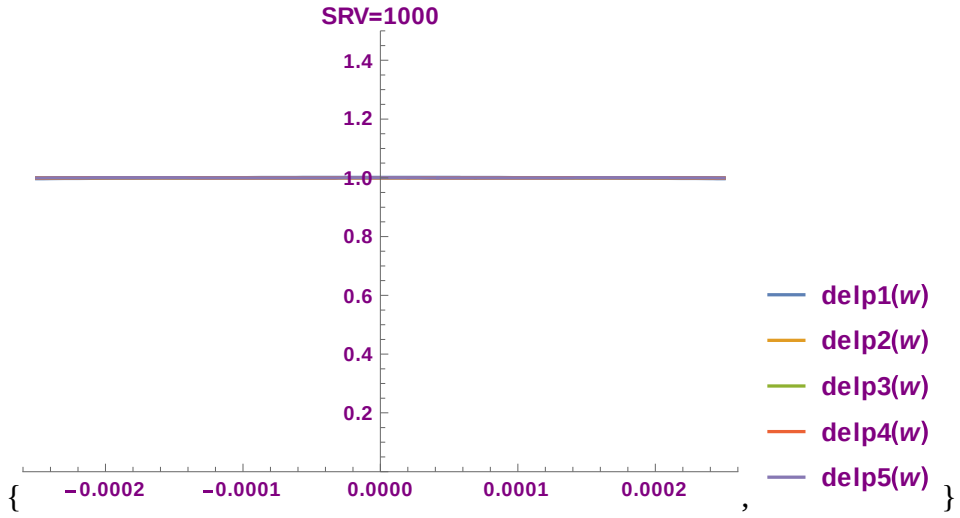

{ , }

}

n1 = $2.50806*10^{-7}$
n2 = $2.44259*10^{-10}$
n3 = $6.11544*10^{-11}$
n4 = $1.52942*10^{-11}$
n5 = $6.79788*10^{-12}$

(*For length = 0.5um*)
x0=0.5*^-4;

x1=FindRoot[LHS1[x]==RHS5[x],{x,0.1}][[1,2]];
x2=FindRoot[LHS2[x]==RHS5[x],{x,Pi}][[1,2]];
x3=FindRoot[LHS3[x]==RHS5[x],{x,2*Pi}][[1,2]];
x4=FindRoot[LHS4[x]==RHS5[x],{x,4*Pi}][[1,2]];
x5=FindRoot[LHS5[x]==RHS5[x],{x,6*Pi}][[1,2]];

r1=2*x1/x0;
r2=2*x2/x0;
r3=2*x3/x0;
r4=2*x4/x0;
r5=2*x5/x0;

Clear[g];
Clear[t];
t=0;
g=1;

Ar1=(2*r1)/(r1*x0+Sin[r1*x0])*Integrate[g*Cos[r1*z],{z,-x0/2,x0/2}] ;
Ar2=(2*r2)/(r2*x0+Sin[r2*x0])*Integrate[g*Cos[r2*z],{z,-x0/2,x0/2}] ;
Ar3=(2*r3)/(r3*x0+Sin[r3*x0])*Integrate[g*Cos[r3*z],{z,-x0/2,x0/2}] ;
Ar4=(2*r4)/(r4*x0+Sin[r4*x0])*Integrate[g*Cos[r4*z],{z,-x0/2,x0/2}] ;
Ar5=(2*r5)/(r5*x0+Sin[r5*x0])*Integrate[g*Cos[r5*z],{z,-x0/2,x0/2}] ;

```
u1[w_]:=Ar1*Exp[-r1^2*Dn*t]*Cos[r1*w];
u2[w_]:=Ar2*Exp[-r2^2*Dn*t]*Cos[r2*w];
u3[w_]:=Ar3*Exp[-r3^2*Dn*t]*Cos[r3*w];
u4[w_]:=Ar4*Exp[-r4^2*Dn*t]*Cos[r4*w];
u5[w_]:=Ar5*Exp[-r5^2*Dn*t]*Cos[r5*w];

v1[w_]:=u1[w];
v2[w_]:=v1[w]+u2[w];
v3[w_]:=v2[w]+u3[w];
v4[w_]:=v3[w]+u4[w];
v5[w_]:=v4[w]+u5[w];

delp1[w_]:=Exp[-t/tn]*v1[w];
delp2[w_]:=Exp[-t/tn]*v2[w];
delp3[w_]:=Exp[-t/tn]*v3[w];
delp4[w_]:=Exp[-t/tn]*v4[w];
delp5[w_]:=Exp[-t/tn]*v5[w];

(*For SRV=100*)
xx1=FindRoot[LHS1[x]==RHS4[x],{x,0.1}][[1,2]];
xx2=FindRoot[LHS2[x]==RHS4[x],{x,Pi}][[1,2]];
xx3=FindRoot[LHS3[x]==RHS4[x],{x,2*Pi}][[1,2]];
xx4=FindRoot[LHS4[x]==RHS4[x],{x,4*Pi}][[1,2]];
xx5=FindRoot[LHS5[x]==RHS4[x],{x,6*Pi}][[1,2]];

rr1=2*xx1/x0;
rr2=2*xx2/x0;
rr3=2*xx3/x0;
rr4=2*xx4/x0;
rr5=2*xx5/x0;

Aar1=(2*rr1)/(rr1*x0+Sin[rr1*x0])*Integrate[g*Cos[rr1*z],{z,-x0/2,x0/2}] ;
Aar2=(2*rr2)/(rr2*x0+Sin[rr2*x0])*Integrate[g*Cos[rr2*z],{z,-x0/2,x0/2}] ;
Aar3=(2*rr3)/(rr3*x0+Sin[rr3*x0])*Integrate[g*Cos[rr3*z],{z,-x0/2,x0/2}] ;
Aar4=(2*rr4)/(rr4*x0+Sin[rr4*x0])*Integrate[g*Cos[rr4*z],{z,-x0/2,x0/2}] ;
Aar5=(2*rr5)/(rr5*x0+Sin[rr5*x0])*Integrate[g*Cos[rr5*z],{z,-x0/2,x0/2}] ;

uu1[w_]:=Aar1*Exp[-rr1^2*Dn*t]*Cos[rr1*w];
uu2[w_]:=Aar2*Exp[-rr2^2*Dn*t]*Cos[rr2*w];
uu3[w_]:=Aar3*Exp[-rr3^2*Dn*t]*Cos[rr3*w];
uu4[w_]:=Aar4*Exp[-rr4^2*Dn*t]*Cos[rr4*w];
uu5[w_]:=Aar5*Exp[-rr5^2*Dn*t]*Cos[rr5*w];

vv1[w_]:=uu1[w];
vv2[w_]:=vv1[w]+uu2[w];
```

```
vv3[w_]:=vv2[w]+uu3[w];
vv4[w_]:=vv3[w]+uu4[w];
vv5[w_]:=vv4[w]+uu5[w];

ddelp1[w_]:=Exp[-t/tn]*vv1[w];
ddelp2[w_]:=Exp[-t/tn]*vv2[w];
ddelp3[w_]:=Exp[-t/tn]*vv3[w];
ddelp4[w_]:=Exp[-t/tn]*vv4[w];
ddelp5[w_]:=Exp[-t/tn]*vv5[w];

(*Print[Style["ddelp1[w] = ", Bold,Blue], ddelp1[w]];
Print[Style["ddelp2[w] = ", Bold,Blue], ddelp2[w]];
Print[Style["ddelp3[w] = ", Bold,Blue], ddelp3[w]];
Print[Style["ddelp4[w] = ", Bold,Blue], ddelp4[w]];
Print[Style["ddelp5[w] = ", Bold,Blue], ddelp5[w]];

Print[Style["delp1[w] = ", Bold,Blue], delp1[w]];
Print[Style["delp2[w] = ", Bold,Blue], delp2[w]];
Print[Style["delp3[w] = ", Bold,Blue], delp3[w]];
Print[Style["delp4[w] = ", Bold,Blue], delp4[w]];
Print[Style["delp5[w] = ", Bold,Blue], delp5[w]];*)

Plot[{ddelp1[w],ddelp2[w], ddelp3[w],ddelp4[w],ddelp5[w]},{w,-x0/2,x0/2},PlotRange-
>{0.99988,1.0002}, PlotLegends->{"Δp(x,0) - 1 term", "Δp(x,0) - 2 terms", "Δp(x,0) - 3
terms", "Δp(x,0) - 4 terms", "Δp(x,0) - 5 terms"}, LabelStyle->Directive[Bold, Black],
 Frame->True,FrameTicks-
>{{{0.9999,0.99995,1.0,1.00005,1.00010,1.00015,1.0002},None},{{0,{-0.5*^-4/2,"-0.25
μm"},{0.5*^-4/2,"0.25 μm"}},None}},FrameLabel->{"x","Δp(x,0)"},
 PlotLabel->"Excess Carrier profile
  at t = 0 s with SRV = 100 cm/s
  "]
Plot[{ddelp1[w],ddelp2[w], ddelp3[w],ddelp4[w],ddelp5[w]},{w,-x0/2,x0/2},PlotRange-
>{0,1.5}, PlotLegends->"Expressions",PlotLabel->"SRV=100",LabelStyle-
>Directive[Bold, Purple]]
Print[Style["n1 = ", Bold,Blue],1/(rr1^2*Dn)];
Print[Style["n2 = ", Bold,Blue], 1/(rr2^2*Dn)];
Print[Style["n3 = ", Bold,Blue], 1/(rr3^2*Dn)];
Print[Style["n4 = ", Bold,Blue], 1/(rr4^2*Dn)];
Print[Style["n5 = ", Bold,Blue], 1/(rr5^2*Dn)];


Plot[{delp1[w],delp2[w], delp3[w],delp4[w],delp5[w]},{w,-x0/2,x0/2},PlotRange-
>{0.9988,1.002},PlotLegends->{"Δp(x,0) - 1 term", "Δp(x,0) - 2 terms", "Δp(x,0) - 3
terms", "Δp(x,0) - 4 terms", "Δp(x,0) - 5 terms"}, LabelStyle->Directive[Bold, Black],
```

```
 Frame->True,FrameTicks-
>{{{0.999,0.9995,1.0,1.0005,1.0010,1.0015,1.002},None},{{0,{-0.5*^-4/2,"-0.25
µm"},{0.5*^-4/2,"0.25 µm"}},None}},FrameLabel->{"x","Δp(x,0)"},
 PlotLabel->"Excess Carrier profile
  at t = 0 s with SRV = 1000 cm/s
  "]
Plot[{delp1[w],delp2[w], delp3[w],delp4[w],delp5[w]},{w,-x0/2,x0/2},PlotRange-
>{0,1.5},PlotLegends->"Expressions",PlotLabel->"SRV=1000",LabelStyle-
>Directive[Bold, Purple]]
Print[Style["n1 = ", Bold,Blue], 1/(r1^2*Dn)];
Print[Style["n2 = ", Bold,Blue], 1/(r2^2*Dn)];
Print[Style["n3 = ", Bold,Blue], 1/(r3^2*Dn)];
Print[Style["n4 = ", Bold,Blue], 1/(r4^2*Dn)];
Print[Style["n5 = ", Bold,Blue], 1/(r5^2*Dn)];
```

{

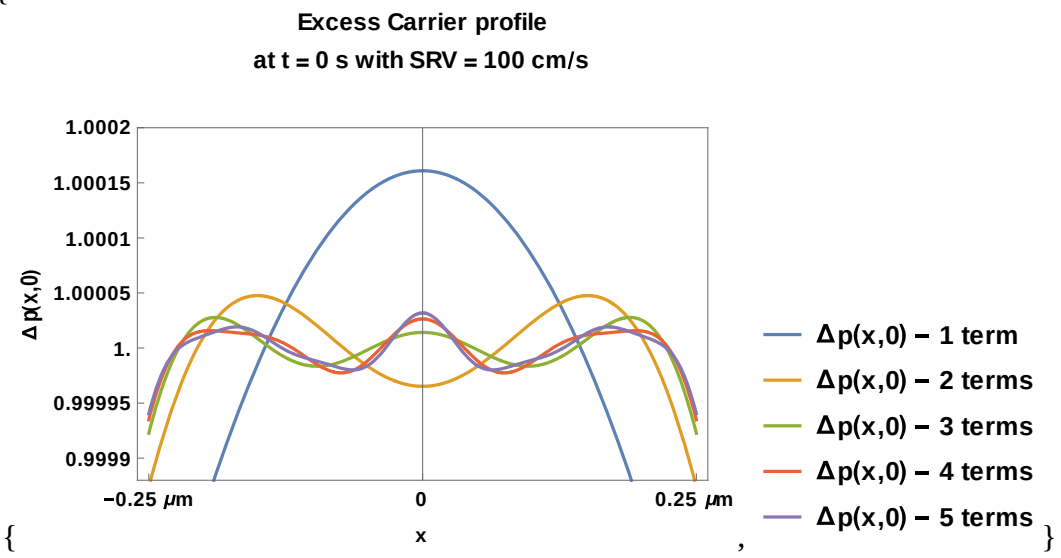

{ , }

}

{

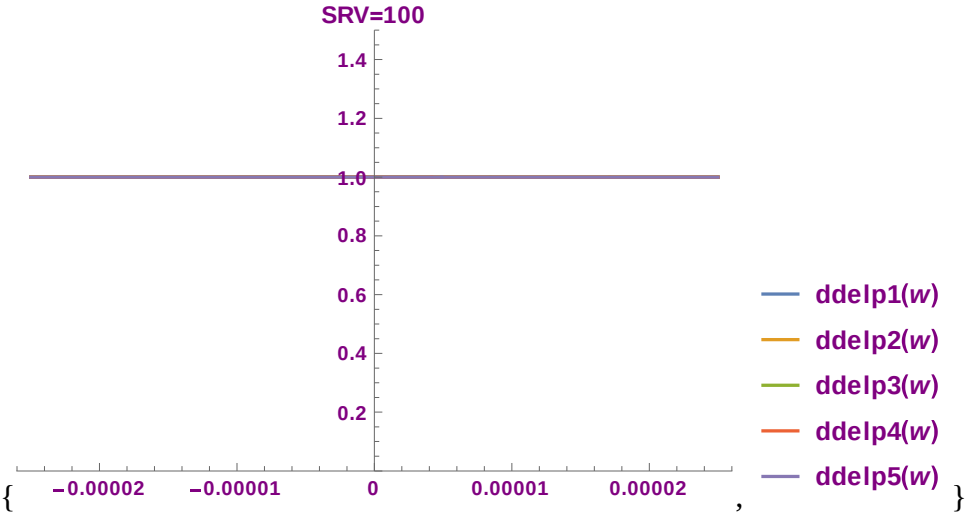

{ , }

}

n1 = $2.50081*10^{-7}$

n2 = $2.44689*10^{-11}$

n3 = $6.11813*10^{-12}$

n4 = $1.52959*10^{-12}$

n5 = $6.79822*10^{-13}$

{

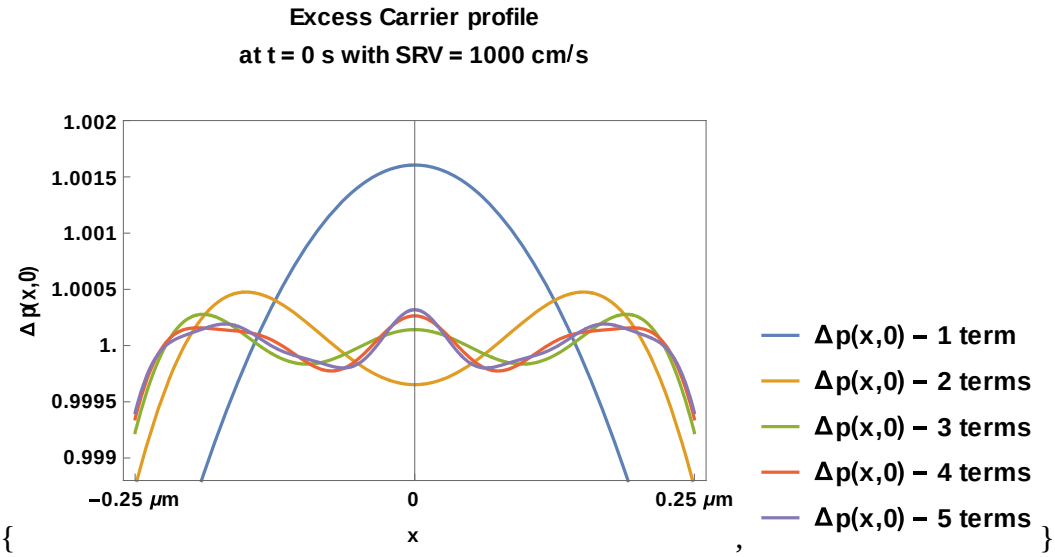

{ , }

}

{

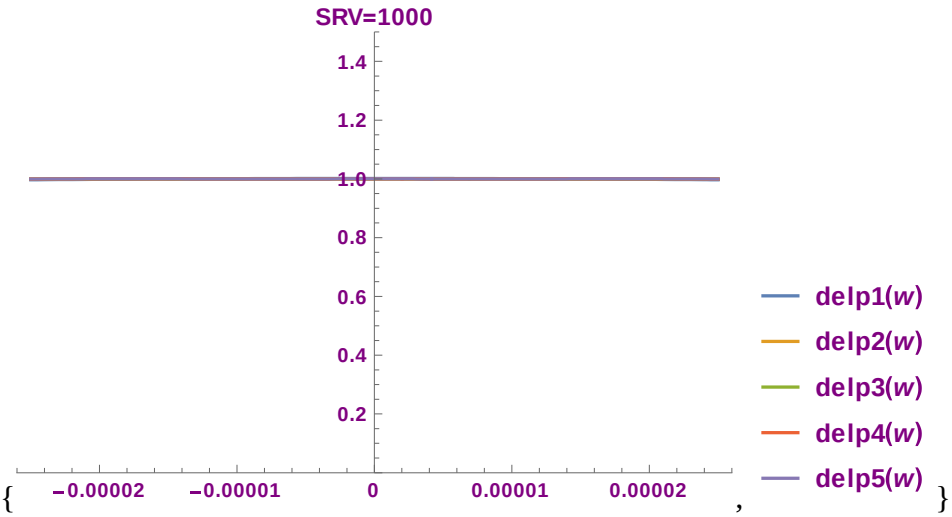

{ , }

}

n1 = $2.50806*10^{-8}$

n2 = $2.44259*10^{-11}$

n3 = $6.11544*10^{-12}$

n4 = $1.52942*10^{-12}$

n5 = $6.79788*10^{-13}$

APPENDIX E: MATHEMATICA CODES FOR TRANSIENT STATE CALCULATIONS OF N-TYPE CDTE FOR DETERMINATION OF TIME RESPONSE OF PHOTOLUMINESCENCE

Transient State Calculations
N-type CdTe – Plotting Time Response of Photoluminescence

```
ClearSystemCache[];
Clear[x];
Clear[g];
Clear[t];
Clear[w];

(*For length = 5um*)
x0=5.0*^-4; (*cm*)
mobp=100; (*cm^2/Vs*)
kb=1.38*^-23; (*J/K*)
T=300; (*K*)
q=1.6*^-19; (*C*)
Dp=mobp*kb*T/q;(*cm^2/s*)
tp=2*^-6; (*s*)
s0=0; (*cm/s*)
s1=1; (*cm/s*)
s2=20; (*cm/s*)
s3=50; (*cm/s*)
s4=100; (*cm/s*)
s5=1000; (*cm/s*)
x=y*x0/2;
LHS1[x_]:=Piecewise[{{Cot[x],0<=x<Pi}}]; (*must be unitless, therefore y is 1/um*)
LHS2[x_]:=Piecewise[{{Cot[x],Pi<=x<2*Pi}}];
LHS3[x_]:=Piecewise[{{Cot[x],2*Pi<=x<4*Pi}}];
LHS4[x_]:=Piecewise[{{Cot[x],4*Pi<=x<6*Pi}}];
LHS5[x_]:=Piecewise[{{Cot[x],6*Pi<=x<8*Pi}}];
RHS1[x_]:=x*(2*Dp/(s1*x0));
RHS2[x_]:=x*(2*Dp/(s2*x0));
RHS3[x_]:=x*(2*Dp/(s3*x0));
RHS4[x_]:=x*(2*Dp/(s4*x0));
RHS5[x_]:=x*(2*Dp/(s5*x0));

(*Plot[{Cot[x],RHS4[x], RHS5[x]},{x,0,3*Pi}, PlotRange□{-2,100},
Exclusions□{0,Pi,2*Pi},
Frame□True,FrameTicks□{{{0,None},None},{{0,Pi/2,Pi,3*Pi/2,
2*Pi,5*Pi/2},None}},PlotLegends□{"ctn((α x0)/2)",  "s=100 cm/s", "s=1000cm/s"},
FrameLabel□{"(α x0)/2","f((α x0)/2)"},
PlotLabel□"Intersections of Curves,
N-type CdTe
```

"]*)

g=1;

x1=FindRoot[LHS1[x]==RHS5[x],{x,0.1}][[1,2]];
x2=FindRoot[LHS2[x]==RHS5[x],{x,Pi}][[1,2]];
x3=FindRoot[LHS3[x]==RHS5[x],{x,2*Pi}][[1,2]];
x4=FindRoot[LHS4[x]==RHS5[x],{x,4*Pi}][[1,2]];
x5=FindRoot[LHS5[x]==RHS5[x],{x,6*Pi}][[1,2]];

r1=2*x1/x0;
r2=2*x2/x0;
r3=2*x3/x0;
r4=2*x4/x0;
r5=2*x5/x0;

Ar1=(2*r1)/(r1*x0+Sin[r1*x0])*Integrate[g*Cos[r1*z],{z,-x0/2,x0/2}] ;
Ar2=(2*r2)/(r2*x0+Sin[r2*x0])*Integrate[g*Cos[r2*z],{z,-x0/2,x0/2}] ;
Ar3=(2*r3)/(r3*x0+Sin[r3*x0])*Integrate[g*Cos[r3*z],{z,-x0/2,x0/2}] ;
Ar4=(2*r4)/(r4*x0+Sin[r4*x0])*Integrate[g*Cos[r4*z],{z,-x0/2,x0/2}] ;
Ar5=(2*r5)/(r5*x0+Sin[r5*x0])*Integrate[g*Cos[r5*z],{z,-x0/2,x0/2}] ;

u1[w_,t_]:=Ar1*Exp[-r1^2*Dp*t]*Cos[r1*w];
u2[w_,t_]:=Ar2*Exp[-r2^2*Dp*t]*Cos[r2*w];
u3[w_,t_]:=Ar3*Exp[-r3^2*Dp*t]*Cos[r3*w];
u4[w_,t_]:=Ar4*Exp[-r4^2*Dp*t]*Cos[r4*w];
u5[w_,t_]:=Ar5*Exp[-r5^2*Dp*t]*Cos[r5*w];

v1[w_,t_]:=u1[w,t];
v2[w_,t_]:=v1[w,t]+u2[w,t];
v3[w_,t_]:=v2[w,t]+u3[w,t];
v4[w_,t_]:=v3[w,t]+u4[w,t];
v5[w_,t_]:=v4[w,t]+u5[w,t];

delp1[w_,t_]:=Exp[-t/tp]*v1[w,t];
delp2[w_,t_]:=Exp[-t/tp]*v2[w,t];
delp3[w_,t_]:=Exp[-t/tp]*v3[w,t];
delp4[w_,t_]:=Exp[-t/tp]*v4[w,t];
delp5[w_,t_]:=Exp[-t/tp]*v5[w,t];

I1[w_,t_]:=Integrate[delp1[w,t],{w,-x0/2,x0/2}];
I2[w_,t_]:=Integrate[delp2[w,t],{w,-x0/2,x0/2}];
I3[w_,t_]:=Integrate[delp3[w,t],{w,-x0/2,x0/2}];
I4[w_,t_]:=Integrate[delp4[w,t],{w,-x0/2,x0/2}];I5[w_,t_]:=Integrate[delp5[w,t],{w,-x0/2,x0/2}];

```
(*For SRV=100*)
xx1=FindRoot[LHS1[x]==RHS4[x],{x,0.1}][[1,2]];
xx2=FindRoot[LHS2[x]==RHS4[x],{x,Pi}][[1,2]];
xx3=FindRoot[LHS3[x]==RHS4[x],{x,2*Pi}][[1,2]];
xx4=FindRoot[LHS4[x]==RHS4[x],{x,4*Pi}][[1,2]];
xx5=FindRoot[LHS5[x]==RHS4[x],{x,6*Pi}][[1,2]];

rr1=2*xx1/x0;
rr2=2*xx2/x0;
rr3=2*xx3/x0;
rr4=2*xx4/x0;
rr5=2*xx5/x0;

Aar1=(2*rr1)/(rr1*x0+Sin[rr1*x0])*Integrate[g*Cos[rr1*z],{z,-x0/2,x0/2}] ;
Aar2=(2*rr2)/(rr2*x0+Sin[rr2*x0])*Integrate[g*Cos[rr2*z],{z,-x0/2,x0/2}] ;
Aar3=(2*rr3)/(rr3*x0+Sin[rr3*x0])*Integrate[g*Cos[rr3*z],{z,-x0/2,x0/2}] ;
Aar4=(2*rr4)/(rr4*x0+Sin[rr4*x0])*Integrate[g*Cos[rr4*z],{z,-x0/2,x0/2}] ;
Aar5=(2*rr5)/(rr5*x0+Sin[rr5*x0])*Integrate[g*Cos[rr5*z],{z,-x0/2,x0/2}] ;

uu1[w_,t_]:=Aar1*Exp[-rr1^2*Dp*t]*Cos[rr1*w];
uu2[w_,t_]:=Aar2*Exp[-rr2^2*Dp*t]*Cos[rr2*w];
uu3[w_,t_]:=Aar3*Exp[-rr3^2*Dp*t]*Cos[rr3*w];
uu4[w_,t_]:=Aar4*Exp[-rr4^2*Dp*t]*Cos[rr4*w];
uu5[w_,t_]:=Aar5*Exp[-rr5^2*Dp*t]*Cos[rr5*w];

vv1[w_,t_]:=uu1[w,t];
vv2[w_,t_]:=vv1[w,t]+uu2[w,t];
vv3[w_,t_]:=vv2[w,t]+uu3[w,t];
vv4[w_,t_]:=vv3[w,t]+uu4[w,t];
vv5[w_,t_]:=vv4[w,t]+uu5[w,t];

ddelp1[w_,t_]:=Exp[-t/tp]*vv1[w,t];
ddelp2[w_,t_]:=Exp[-t/tp]*vv2[w,t];
ddelp3[w_,t_]:=Exp[-t/tp]*vv3[w,t];
ddelp4[w_,t_]:=Exp[-t/tp]*vv4[w,t];
ddelp5[w_,t_]:=Exp[-t/tp]*vv5[w,t];


II1[w_,t_]:=Integrate[ddelp1[w,t],{w,-x0/2,x0/2}];
II2[w_,t_]:=Integrate[ddelp2[w,t],{w,-x0/2,x0/2}];
II3[w_,t_]:=Integrate[ddelp3[w,t],{w,-x0/2,x0/2}];
II4[w_,t_]:=Integrate[ddelp4[w,t],{w,-x0/2,x0/2}];II5[w_,t_]:=Integrate[ddelp5[w,t],{w,-
x0/2,x0/2}];

(*Print[Style["r1 = " , Bold, Blue],r1, Style["
```

```
Ar1 = " , Bold, Blue],Ar1, Style["
u1[w,t] = "  , Bold, Blue], u1[w,t],Style["
v1[w,t] = "  , Bold, Blue], v1[w,t]];
Print[Style["r2 = " , Bold, Blue],r2, Style["
Ar2 = " , Bold, Blue],Ar2, Style["
u2[w,t] = "  , Bold, Blue], u2[w,t],Style["
v2[w,t] = "  , Bold, Blue], v2[w,t]];
Print[Style["r3 = " , Bold, Blue],r3, Style["
Ar3 = " , Bold, Blue],Ar3, Style["
u3[w,t] = "  , Bold, Blue], u3[w,t],Style["
v3[w,t] = "  , Bold, Blue], v3[w,t]];*)
(*Print[Style["Excess Carrier Profile (SRV=100) = ", Bold, Blue],ddelp5[w,t]];
Print[Style["I1 = ", Bold, Blue], II1[w,t]];
Print[Style["I2 = ", Bold, Blue], II2[w,t]];
Print[Style["I3 = ", Bold, Blue], II3[w,t]];
Print[Style["I4 = ", Bold, Blue], II4[w,t]];Print[Style["I5 = ", Bold, Blue], II5[w,t]];*)
pp=1/II5[w,0];

LogPlot[pp*II5[w,t],{t,0,2000*^-9},Frame->True,FrameLabel->{"Time - t
[s]","Normalized PLI [arbitrary units]"},
 PlotLabel->"Time dependent PLI for 5μm thick
  absorber layer with SRV=100 cm/s
  "]
Print[Style["τeff = ", Bold, Blue], ((1/tp)+rr1^2*Dp)^(-1)];

p=1/I5[w,0];
(*Print[Style["Excess Carrier Profile (SRV=1000) = ", Bold, Blue],delp5[w,t]];
Print[Style["I1 = ", Bold, Blue], I1[w,t]];
Print[Style["I2 = ", Bold, Blue], I2[w,t]];
Print[Style["I3 = ", Bold, Blue], I3[w,t]];
Print[Style["I4 = ", Bold, Blue], I4[w,t]];Print[Style["I5 = ", Bold, Blue], I5[w,t]];*)
LogPlot[p*I5[w,t],{t,0,2000*^-9},Frame->True,FrameLabel->{"Time - t
[s]","Normalized PLI [arbitrary units]"},
 PlotLabel->"Time dependent PLI for 5μm thick
  absorber layer with SRV=1000 cm/s
  "]
Print[Style["τeff = ", Bold, Blue], ((1/tp)+r1^2*Dp)^(-1)];
```

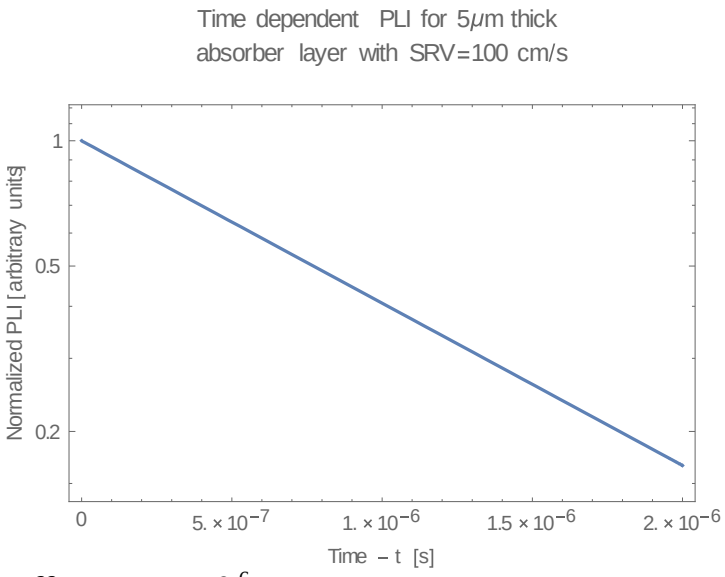

τeff = $1.1127*10^{-6}$

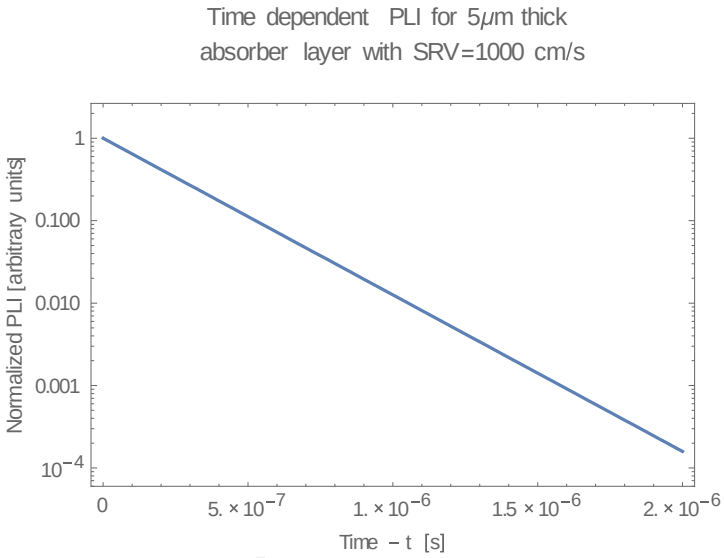

τeff = $2.28601*10^{-7}$

(*For length = 0.5um*)
x0 = 0.5*^-4;

```
x1=FindRoot[LHS1[x]==RHS5[x],{x,0.1}][[1,2]];
x2=FindRoot[LHS2[x]==RHS5[x],{x,Pi}][[1,2]];
x3=FindRoot[LHS3[x]==RHS5[x],{x,2*Pi}][[1,2]];
x4=FindRoot[LHS4[x]==RHS5[x],{x,4*Pi}][[1,2]];
x5=FindRoot[LHS5[x]==RHS5[x],{x,6*Pi}][[1,2]];

r1=2*x1/x0;
r2=2*x2/x0;
r3=2*x3/x0;
```

```
r4=2*x4/x0;
r5=2*x5/x0;

Ar1=(2*r1)/(r1*x0+Sin[r1*x0])*Integrate[g*Cos[r1*z],{z,-x0/2,x0/2}] ;
Ar2=(2*r2)/(r2*x0+Sin[r2*x0])*Integrate[g*Cos[r2*z],{z,-x0/2,x0/2}] ;
Ar3=(2*r3)/(r3*x0+Sin[r3*x0])*Integrate[g*Cos[r3*z],{z,-x0/2,x0/2}] ;
Ar4=(2*r4)/(r4*x0+Sin[r4*x0])*Integrate[g*Cos[r4*z],{z,-x0/2,x0/2}] ;
Ar5=(2*r5)/(r5*x0+Sin[r5*x0])*Integrate[g*Cos[r5*z],{z,-x0/2,x0/2}] ;

u1[w_,t_]:=Ar1*Exp[-r1^2*Dp*t]*Cos[r1*w];
u2[w_,t_]:=Ar2*Exp[-r2^2*Dp*t]*Cos[r2*w];
u3[w_,t_]:=Ar3*Exp[-r3^2*Dp*t]*Cos[r3*w];
u4[w_,t_]:=Ar4*Exp[-r4^2*Dp*t]*Cos[r4*w];
u5[w_,t_]:=Ar5*Exp[-r5^2*Dp*t]*Cos[r5*w];

v1[w_,t_]:=u1[w,t];
v2[w_,t_]:=v1[w,t]+u2[w,t];
v3[w_,t_]:=v2[w,t]+u3[w,t];
v4[w_,t_]:=v3[w,t]+u4[w,t];
v5[w_,t_]:=v4[w,t]+u5[w,t];

delp1[w_,t_]:=Exp[-t/tp]*v1[w,t];
delp2[w_,t_]:=Exp[-t/tp]*v2[w,t];
delp3[w_,t_]:=Exp[-t/tp]*v3[w,t];
delp4[w_,t_]:=Exp[-t/tp]*v4[w,t];
delp5[w_,t_]:=Exp[-t/tp]*v5[w,t];


I1[w_,t_]:=Integrate[delp1[w,t],{w,-x0/2,x0/2}];
I2[w_,t_]:=Integrate[delp2[w,t],{w,-x0/2,x0/2}];
I3[w_,t_]:=Integrate[delp3[w,t],{w,-x0/2,x0/2}];
I4[w_,t_]:=Integrate[delp4[w,t],{w,-x0/2,x0/2}];I5[w_,t_]:=Integrate[delp5[w,t],{w,-
x0/2,x0/2}];

(*For SRV=100*)
xx1=FindRoot[LHS1[x]==RHS4[x],{x,0.1}][[1,2]];
xx2=FindRoot[LHS2[x]==RHS4[x],{x,Pi}][[1,2]];
xx3=FindRoot[LHS3[x]==RHS4[x],{x,2*Pi}][[1,2]];
xx4=FindRoot[LHS4[x]==RHS4[x],{x,4*Pi}][[1,2]];
xx5=FindRoot[LHS5[x]==RHS4[x],{x,6*Pi}][[1,2]];

rr1=2*xx1/x0;
rr2=2*xx2/x0;
rr3=2*xx3/x0;
rr4=2*xx4/x0;
rr5=2*xx5/x0;
```

```
Aar1=(2*rr1)/(rr1*x0+Sin[rr1*x0])*Integrate[g*Cos[rr1*z],{z,-x0/2,x0/2}] ;
Aar2=(2*rr2)/(rr2*x0+Sin[rr2*x0])*Integrate[g*Cos[rr2*z],{z,-x0/2,x0/2}] ;
Aar3=(2*rr3)/(rr3*x0+Sin[rr3*x0])*Integrate[g*Cos[rr3*z],{z,-x0/2,x0/2}] ;
Aar4=(2*rr4)/(rr4*x0+Sin[rr4*x0])*Integrate[g*Cos[rr4*z],{z,-x0/2,x0/2}] ;
Aar5=(2*rr5)/(rr5*x0+Sin[rr5*x0])*Integrate[g*Cos[rr5*z],{z,-x0/2,x0/2}] ;

uu1[w_,t_]:=Aar1*Exp[-rr1^2*Dp*t]*Cos[rr1*w];
uu2[w_,t_]:=Aar2*Exp[-rr2^2*Dp*t]*Cos[rr2*w];
uu3[w_,t_]:=Aar3*Exp[-rr3^2*Dp*t]*Cos[rr3*w];
uu4[w_,t_]:=Aar4*Exp[-rr4^2*Dp*t]*Cos[rr4*w];
uu5[w_,t_]:=Aar5*Exp[-rr5^2*Dp*t]*Cos[rr5*w];

vv1[w_,t_]:=uu1[w,t];
vv2[w_,t_]:=vv1[w,t]+uu2[w,t];
vv3[w_,t_]:=vv2[w,t]+uu3[w,t];
vv4[w_,t_]:=vv3[w,t]+uu4[w,t];
vv5[w_,t_]:=vv4[w,t]+uu5[w,t];

ddelp1[w_,t_]:=Exp[-t/tp]*vv1[w,t];
ddelp2[w_,t_]:=Exp[-t/tp]*vv2[w,t];
ddelp3[w_,t_]:=Exp[-t/tp]*vv3[w,t];
ddelp4[w_,t_]:=Exp[-t/tp]*vv4[w,t];
ddelp5[w_,t_]:=Exp[-t/tp]*vv5[w,t];


II1[w_,t_]:=Integrate[ddelp1[w,t],{w,-x0/2,x0/2}];
II2[w_,t_]:=Integrate[ddelp2[w,t],{w,-x0/2,x0/2}];
II3[w_,t_]:=Integrate[ddelp3[w,t],{w,-x0/2,x0/2}];
II4[w_,t_]:=Integrate[ddelp4[w,t],{w,-x0/2,x0/2}];II5[w_,t_]:=Integrate[ddelp5[w,t],{w,-
x0/2,x0/2}];

(*Print[Style["r1 = " , Bold, Blue],r1, Style["
Ar1 = " , Bold, Blue],Ar1, Style["
u1[w,t] = "  , Bold, Blue], u1[w,t],Style["
v1[w,t] = "  , Bold, Blue], v1[w,t]];
Print[Style["r2 = " , Bold, Blue],r2, Style["
Ar2 = " , Bold, Blue],Ar2, Style["
u2[w,t] = "  , Bold, Blue], u2[w,t],Style["
v2[w,t] = "  , Bold, Blue], v2[w,t]];
Print[Style["r3 = " , Bold, Blue],r3, Style["
Ar3 = " , Bold, Blue],Ar3, Style["
u3[w,t] = "  , Bold, Blue], u3[w,t],Style["
v3[w,t] = "  , Bold, Blue], v3[w,t]];*)
(*Print[Style["Excess Carrier Profile (SRV=100) = ", Bold, Blue],ddelp5[w,t]];
Print[Style["I1 = ", Bold, Blue], II1[w,t]];
```

```
Print[Style["I2 = ", Bold, Blue], II2[w,t]];
Print[Style["I3 = ", Bold, Blue], II3[w,t]];
Print[Style["I4 = ", Bold, Blue], II4[w,t]];Print[Style["I5 = ", Bold, Blue], II5[w,t]];*)
pp=1/II5[w,0];

LogPlot[pp*II5[w,t],{t,0,2000*^-9},Frame->True,FrameLabel->{"Time - t
[s]","Normalized PLI [arbitrary units]"},
 PlotLabel->"Time dependent PLI for 0.5μm thick
  absorber layer with SRV=100 cm/s
  "]
Print[Style["τeff = ", Bold, Blue], ((1/tp)+rr1^2*Dp)^(-1)];

p=1/I5[w,0];
(*Print[Style["Excess Carrier Profile (SRV=1000) = ", Bold, Blue],delp5[w,t]];
Print[Style["I1 = ", Bold, Blue], I1[w,t]];
Print[Style["I2 = ", Bold, Blue], I2[w,t]];
Print[Style["I3 = ", Bold, Blue], I3[w,t]];
Print[Style["I4 = ", Bold, Blue], I4[w,t]];Print[Style["I5 = ", Bold, Blue], I5[w,t]];*)
LogPlot[p*I5[w,t],{t,0,2000*^-9},Frame->True,FrameLabel->{"Time - t
[s]","Normalized PLI [arbitrary units]"},
 PlotLabel->"Time dependent PLI for 0.5μm thick
  absorber layer with SRV=1000 cm/s
  "]
Print[Style["τeff = ", Bold, Blue], ((1/tp)+r1^2*Dp)^(-1)];
```

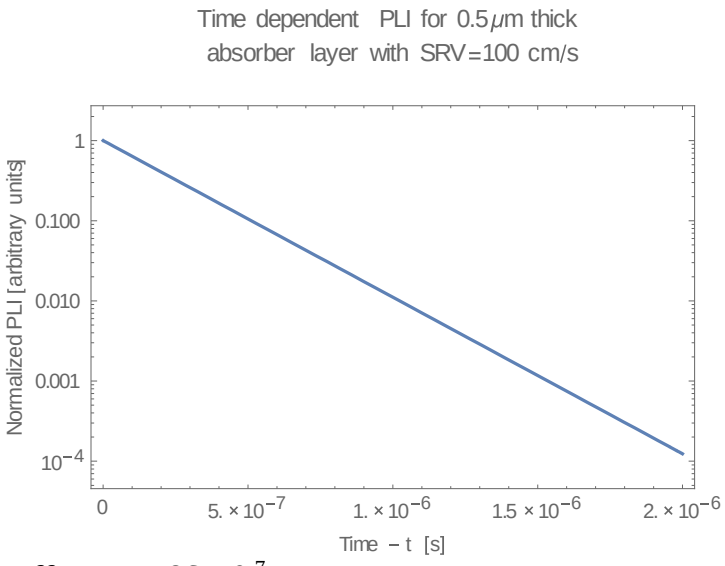

τeff = $2.22286*10^{-7}$

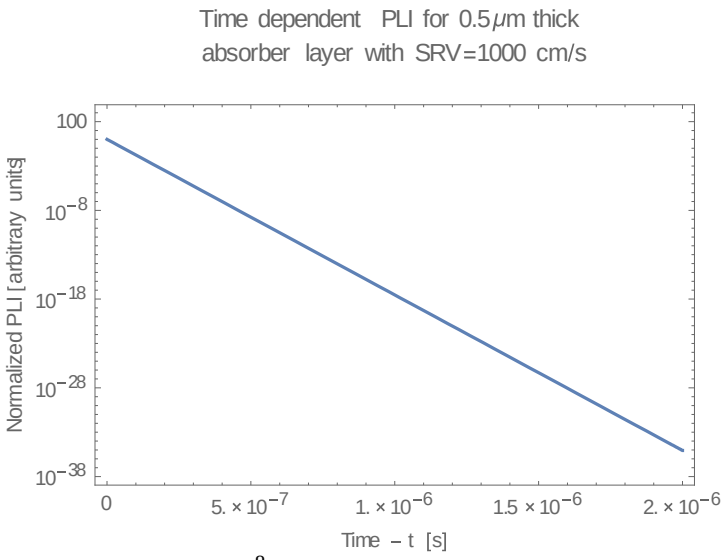

τeff = 2.47699*10^{-8}

APPENDIX F: MATHEMATICA CODES FOR TRANSIENT STATE CALCULATIONS OF P-TYPE CDTE FOR DETERMINATION OF TIME RESPONSE OF PHOTOLUMINESCENCE

Transient State Calculations
P-type CdTe - Plotting Time Response of Photoluminescence

```
ClearSystemCache[];
Clear[x];
Clear[g];
Clear[t];
Clear[w];

(*For length = 5um*)
x0=5.*^-4; (*cm*)
mobn=1000; (*cm^2/Vs*)
kb=1.38*^-23; (*J/K*)
T=300; (*K*)
q=1.6*^-19; (*C*)
Dn=mobn*kb*T/q;(*cm^2/s*)
tn=2*^-6; (*s*)
s0=0; (*cm/s*)
s1=1; (*cm/s*)
s2=20; (*cm/s*)
s3=50; (*cm/s*)
s4=100; (*cm/s*)
s5=1000; (*cm/s*)
x=y*x0/2;
LHS1[x_]:=Piecewise[{{Cot[x],0<=x<Pi}}]; (*must be unitless, therefore y is 1/um*)
LHS2[x_]:=Piecewise[{{Cot[x],Pi<=x<2*Pi}}];
LHS3[x_]:=Piecewise[{{Cot[x],2*Pi<=x<4*Pi}}];
LHS4[x_]:=Piecewise[{{Cot[x],4*Pi<=x<6*Pi}}];
LHS5[x_]:=Piecewise[{{Cot[x],6*Pi<=x<8*Pi}}];
RHS1[x_]:=x*(2*Dn/(s1*x0));
RHS2[x_]:=x*(2*Dn/(s2*x0));
RHS3[x_]:=x*(2*Dn/(s3*x0));
RHS4[x_]:=x*(2*Dn/(s4*x0));
RHS5[x_]:=x*(2*Dn/(s5*x0));

(*Plot[{Cot[x], RHS4[x], RHS5[x]},{x,0,3*Pi}, PlotRange□{-2,100},
Exclusions□{0,Pi,2*Pi},
Frame□True,FrameTicks□{{{0,None},None},{{0,Pi/2,Pi,3*Pi/2,
2*Pi,5*Pi/2},None}},PlotLegends□{"ctn((α x0)/2)",  "s=100 cm/s", "s=1000cm/s"},
FrameLabel□{"(α x0)/2","f((α x0)/2)"},
PlotLabel□"Intersections of Curves,
P-type CdTe
```

"]*)

g=1;

x1=FindRoot[LHS1[x]==RHS5[x],{x,0.1}][[1,2]];
x2=FindRoot[LHS2[x]==RHS5[x],{x,Pi}][[1,2]];
x3=FindRoot[LHS3[x]==RHS5[x],{x,2*Pi}][[1,2]];
x4=FindRoot[LHS4[x]==RHS5[x],{x,4*Pi}][[1,2]];
x5=FindRoot[LHS5[x]==RHS5[x],{x,6*Pi}][[1,2]];

r1=2*x1/x0;
r2=2*x2/x0;
r3=2*x3/x0;
r4=2*x4/x0;
r5=2*x5/x0;

Ar1=(2*r1)/(r1*x0+Sin[r1*x0])*Integrate[g*Cos[r1*z],{z,-x0/2,x0/2}] ;
Ar2=(2*r2)/(r2*x0+Sin[r2*x0])*Integrate[g*Cos[r2*z],{z,-x0/2,x0/2}] ;
Ar3=(2*r3)/(r3*x0+Sin[r3*x0])*Integrate[g*Cos[r3*z],{z,-x0/2,x0/2}] ;
Ar4=(2*r4)/(r4*x0+Sin[r4*x0])*Integrate[g*Cos[r4*z],{z,-x0/2,x0/2}] ;
Ar5=(2*r5)/(r5*x0+Sin[r5*x0])*Integrate[g*Cos[r5*z],{z,-x0/2,x0/2}] ;

u1[w_,t_]:=Ar1*Exp[-r1^2*Dn*t]*Cos[r1*w];
u2[w_,t_]:=Ar2*Exp[-r2^2*Dn*t]*Cos[r2*w];
u3[w_,t_]:=Ar3*Exp[-r3^2*Dn*t]*Cos[r3*w];
u4[w_,t_]:=Ar4*Exp[-r4^2*Dn*t]*Cos[r4*w];
u5[w_,t_]:=Ar5*Exp[-r5^2*Dn*t]*Cos[r5*w];

v1[w_,t_]:=u1[w,t];
v2[w_,t_]:=v1[w,t]+u2[w,t];
v3[w_,t_]:=v2[w,t]+u3[w,t];
v4[w_,t_]:=v3[w,t]+u4[w,t];
v5[w_,t_]:=v4[w,t]+u5[w,t];

delp1[w_,t_]:=Exp[-t/tn]*v1[w,t];
delp2[w_,t_]:=Exp[-t/tn]*v2[w,t];
delp3[w_,t_]:=Exp[-t/tn]*v3[w,t];
delp4[w_,t_]:=Exp[-t/tn]*v4[w,t];
delp5[w_,t_]:=Exp[-t/tn]*v5[w,t];

I1[w_,t_]:=Integrate[delp1[w,t],{w,-x0/2,x0/2}];
I2[w_,t_]:=Integrate[delp2[w,t],{w,-x0/2,x0/2}];
I3[w_,t_]:=Integrate[delp3[w,t],{w,-x0/2,x0/2}];
I4[w_,t_]:=Integrate[delp4[w,t],{w,-x0/2,x0/2}];I5[w_,t_]:=Integrate[delp5[w,t],{w,-x0/2,x0/2}];

```
(*For SRV=100*)
xx1=FindRoot[LHS1[x]==RHS4[x],{x,0.1}][[1,2]];
xx2=FindRoot[LHS2[x]==RHS4[x],{x,Pi}][[1,2]];
xx3=FindRoot[LHS3[x]==RHS4[x],{x,2*Pi}][[1,2]];
xx4=FindRoot[LHS4[x]==RHS4[x],{x,4*Pi}][[1,2]];
xx5=FindRoot[LHS5[x]==RHS4[x],{x,6*Pi}][[1,2]];

rr1=2*xx1/x0;
rr2=2*xx2/x0;
rr3=2*xx3/x0;
rr4=2*xx4/x0;
rr5=2*xx5/x0;

Aar1=(2*rr1)/(rr1*x0+Sin[rr1*x0])*Integrate[g*Cos[rr1*z],{z,-x0/2,x0/2}] ;
Aar2=(2*rr2)/(rr2*x0+Sin[rr2*x0])*Integrate[g*Cos[rr2*z],{z,-x0/2,x0/2}] ;
Aar3=(2*rr3)/(rr3*x0+Sin[rr3*x0])*Integrate[g*Cos[rr3*z],{z,-x0/2,x0/2}] ;
Aar4=(2*rr4)/(rr4*x0+Sin[rr4*x0])*Integrate[g*Cos[rr4*z],{z,-x0/2,x0/2}] ;
Aar5=(2*rr5)/(rr5*x0+Sin[rr5*x0])*Integrate[g*Cos[rr5*z],{z,-x0/2,x0/2}] ;

uu1[w_,t_]:=Aar1*Exp[-rr1^2*Dn*t]*Cos[rr1*w];
uu2[w_,t_]:=Aar2*Exp[-rr2^2*Dn*t]*Cos[rr2*w];
uu3[w_,t_]:=Aar3*Exp[-rr3^2*Dn*t]*Cos[rr3*w];
uu4[w_,t_]:=Aar4*Exp[-rr4^2*Dn*t]*Cos[rr4*w];
uu5[w_,t_]:=Aar5*Exp[-rr5^2*Dn*t]*Cos[rr5*w];

vv1[w_,t_]:=uu1[w,t];
vv2[w_,t_]:=vv1[w,t]+uu2[w,t];
vv3[w_,t_]:=vv2[w,t]+uu3[w,t];
vv4[w_,t_]:=vv3[w,t]+uu4[w,t];
vv5[w_,t_]:=vv4[w,t]+uu5[w,t];

ddelp1[w_,t_]:=Exp[-t/tn]*vv1[w,t];
ddelp2[w_,t_]:=Exp[-t/tn]*vv2[w,t];
ddelp3[w_,t_]:=Exp[-t/tn]*vv3[w,t];
ddelp4[w_,t_]:=Exp[-t/tn]*vv4[w,t];
ddelp5[w_,t_]:=Exp[-t/tn]*vv5[w,t];


II1[w_,t_]:=Integrate[ddelp1[w,t],{w,-x0/2,x0/2}];
II2[w_,t_]:=Integrate[ddelp2[w,t],{w,-x0/2,x0/2}];
II3[w_,t_]:=Integrate[ddelp3[w,t],{w,-x0/2,x0/2}];
II4[w_,t_]:=Integrate[ddelp4[w,t],{w,-x0/2,x0/2}];II5[w_,t_]:=Integrate[ddelp5[w,t],{w,-
x0/2,x0/2}];

(*Print[Style["r1 = " , Bold, Blue],r1, Style["
```

```
Ar1 = " , Bold, Blue],Ar1, Style["
u1[w,t] = "  , Bold, Blue], u1[w,t],Style["
v1[w,t] = "  , Bold, Blue], v1[w,t]];
Print[Style["r2 = " , Bold, Blue],r2, Style["
Ar2 = " , Bold, Blue],Ar2, Style["
u2[w,t] = "  , Bold, Blue], u2[w,t],Style["
v2[w,t] = "  , Bold, Blue], v2[w,t]];
Print[Style["r3 = " , Bold, Blue],r3, Style["
Ar3 = " , Bold, Blue],Ar3, Style["
u3[w,t] = "  , Bold, Blue], u3[w,t],Style["
v3[w,t] = "  , Bold, Blue], v3[w,t]];
Print[Style["Excess Carrier Profile (SRV=100) = ", Bold, Blue],ddelp5[w,t]];
Print[Style["I1 = ", Bold, Blue], II1[w,t]];
Print[Style["I2 = ", Bold, Blue], II2[w,t]];
Print[Style["I3 = ", Bold, Blue], II3[w,t]];
Print[Style["I4 = ", Bold, Blue], II4[w,t]];Print[Style["I5 = ", Bold, Blue], II5[w,t]];*)
pp=1/II5[w,0];

LogPlot[pp*II5[w,t],{t,0,2000*^-9},Frame->True,FrameLabel->{"Time - t
[s]","Normalized PLI [arbitrary units]"},
 PlotLabel->"Time dependent PLI for 5μm thick
  absorber layer with SRV=100 cm/s
  "]
Print[Style["τeff = ", Bold, Blue], ((1/tn)+rr1^2*Dn)^(-1)];

p=1/I5[w,0];

(*Print[Style["Excess Carrier Profile (SRV=1000) = ", Bold, Blue],delp5[w,t]];
Print[Style["I1 = ", Bold, Blue], I1[w,t]];
Print[Style["I2 = ", Bold, Blue], I2[w,t]];
Print[Style["I3 = ", Bold, Blue], I3[w,t]];
Print[Style["I4 = ", Bold, Blue], I4[w,t]];Print[Style["I5 = ", Bold, Blue], I5[w,t]];*)
LogPlot[p*I5[w,t],{t,0,2000*^-9},Frame->True,FrameLabel->{"Time - t
[s]","Normalized PLI [arbitrary units]"},
 PlotLabel->"Time dependent PLI for 5μm thick
  absorber layer with SRV=1000 cm/s
  "]
Print[Style["τeff = ", Bold, Blue], ((1/tn)+r1^2*Dn)^(-1)];
```

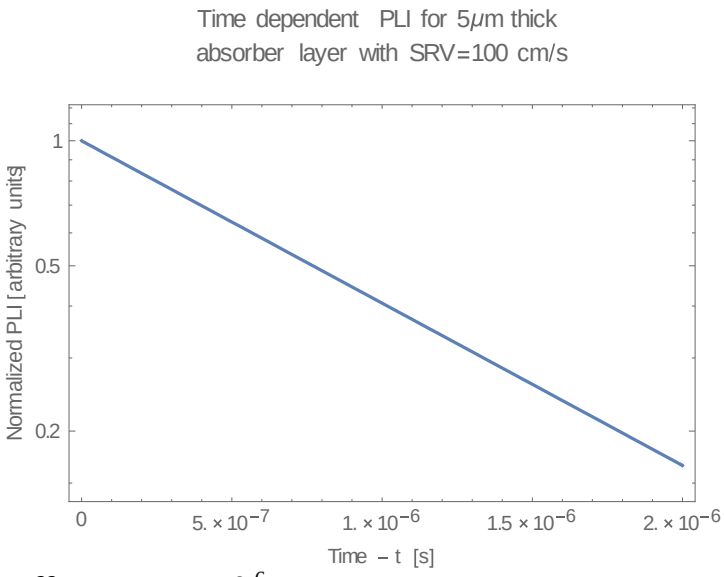

τeff = $1.11127*10^{-6}$

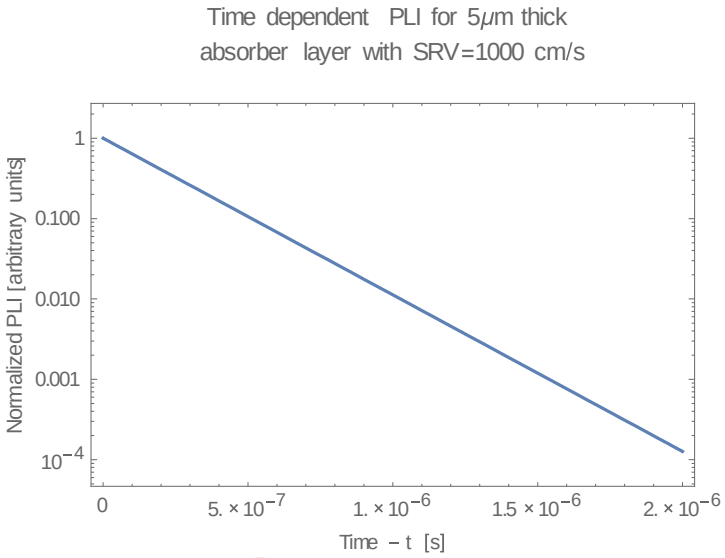

τeff = $2.22859*10^{-7}$

(*For length = 0.5um*)

```
x0=0.5*^-4;

x1=FindRoot[LHS1[x]==RHS5[x],{x,0.1}][[1,2]];
x2=FindRoot[LHS2[x]==RHS5[x],{x,Pi}][[1,2]];
x3=FindRoot[LHS3[x]==RHS5[x],{x,2*Pi}][[1,2]];
x4=FindRoot[LHS4[x]==RHS5[x],{x,4*Pi}][[1,2]];
x5=FindRoot[LHS5[x]==RHS5[x],{x,6*Pi}][[1,2]];

r1=2*x1/x0;
r2=2*x2/x0;
r3=2*x3/x0;
```

```
r4=2*x4/x0;
r5=2*x5/x0;

Ar1=(2*r1)/(r1*x0+Sin[r1*x0])*Integrate[g*Cos[r1*z],{z,-x0/2,x0/2}] ;
Ar2=(2*r2)/(r2*x0+Sin[r2*x0])*Integrate[g*Cos[r2*z],{z,-x0/2,x0/2}] ;
Ar3=(2*r3)/(r3*x0+Sin[r3*x0])*Integrate[g*Cos[r3*z],{z,-x0/2,x0/2}] ;
Ar4=(2*r4)/(r4*x0+Sin[r4*x0])*Integrate[g*Cos[r4*z],{z,-x0/2,x0/2}] ;
Ar5=(2*r5)/(r5*x0+Sin[r5*x0])*Integrate[g*Cos[r5*z],{z,-x0/2,x0/2}] ;

u1[w_,t_]:=Ar1*Exp[-r1^2*Dn*t]*Cos[r1*w];
u2[w_,t_]:=Ar2*Exp[-r2^2*Dn*t]*Cos[r2*w];
u3[w_,t_]:=Ar3*Exp[-r3^2*Dn*t]*Cos[r3*w];
u4[w_,t_]:=Ar4*Exp[-r4^2*Dn*t]*Cos[r4*w];
u5[w_,t_]:=Ar5*Exp[-r5^2*Dn*t]*Cos[r5*w];

v1[w_,t_]:=u1[w,t];
v2[w_,t_]:=v1[w,t]+u2[w,t];
v3[w_,t_]:=v2[w,t]+u3[w,t];
v4[w_,t_]:=v3[w,t]+u4[w,t];
v5[w_,t_]:=v4[w,t]+u5[w,t];

delp1[w_,t_]:=Exp[-t/tn]*v1[w,t];
delp2[w_,t_]:=Exp[-t/tn]*v2[w,t];
delp3[w_,t_]:=Exp[-t/tn]*v3[w,t];
delp4[w_,t_]:=Exp[-t/tn]*v4[w,t];
delp5[w_,t_]:=Exp[-t/tn]*v5[w,t];


I1[w_,t_]:=Integrate[delp1[w,t],{w,-x0/2,x0/2}];
I2[w_,t_]:=Integrate[delp2[w,t],{w,-x0/2,x0/2}];
I3[w_,t_]:=Integrate[delp3[w,t],{w,-x0/2,x0/2}];
I4[w_,t_]:=Integrate[delp4[w,t],{w,-x0/2,x0/2}];I5[w_,t_]:=Integrate[delp5[w,t],{w,-
x0/2,x0/2}];

(*For SRV=100*)
xx1=FindRoot[LHS1[x]==RHS4[x],{x,0.1}][[1,2]];
xx2=FindRoot[LHS2[x]==RHS4[x],{x,Pi}][[1,2]];
xx3=FindRoot[LHS3[x]==RHS4[x],{x,2*Pi}][[1,2]];
xx4=FindRoot[LHS4[x]==RHS4[x],{x,4*Pi}][[1,2]];
xx5=FindRoot[LHS5[x]==RHS4[x],{x,6*Pi}][[1,2]];

rr1=2*xx1/x0;
rr2=2*xx2/x0;
rr3=2*xx3/x0;
rr4=2*xx4/x0;
rr5=2*xx5/x0;
```

```
Aar1=(2*rr1)/(rr1*x0+Sin[rr1*x0])*Integrate[g*Cos[rr1*z],{z,-x0/2,x0/2}] ;
Aar2=(2*rr2)/(rr2*x0+Sin[rr2*x0])*Integrate[g*Cos[rr2*z],{z,-x0/2,x0/2}] ;
Aar3=(2*rr3)/(rr3*x0+Sin[rr3*x0])*Integrate[g*Cos[rr3*z],{z,-x0/2,x0/2}] ;
Aar4=(2*rr4)/(rr4*x0+Sin[rr4*x0])*Integrate[g*Cos[rr4*z],{z,-x0/2,x0/2}] ;
Aar5=(2*rr5)/(rr5*x0+Sin[rr5*x0])*Integrate[g*Cos[rr5*z],{z,-x0/2,x0/2}] ;

uu1[w_,t_]:=Aar1*Exp[-rr1^2*Dn*t]*Cos[rr1*w];
uu2[w_,t_]:=Aar2*Exp[-rr2^2*Dn*t]*Cos[rr2*w];
uu3[w_,t_]:=Aar3*Exp[-rr3^2*Dn*t]*Cos[rr3*w];
uu4[w_,t_]:=Aar4*Exp[-rr4^2*Dn*t]*Cos[rr4*w];
uu5[w_,t_]:=Aar5*Exp[-rr5^2*Dn*t]*Cos[rr5*w];

vv1[w_,t_]:=uu1[w,t];
vv2[w_,t_]:=vv1[w,t]+uu2[w,t];
vv3[w_,t_]:=vv2[w,t]+uu3[w,t];
vv4[w_,t_]:=vv3[w,t]+uu4[w,t];
vv5[w_,t_]:=vv4[w,t]+uu5[w,t];

ddelp1[w_,t_]:=Exp[-t/tn]*vv1[w,t];
ddelp2[w_,t_]:=Exp[-t/tn]*vv2[w,t];
ddelp3[w_,t_]:=Exp[-t/tn]*vv3[w,t];
ddelp4[w_,t_]:=Exp[-t/tn]*vv4[w,t];
ddelp5[w_,t_]:=Exp[-t/tn]*vv5[w,t];


II1[w_,t_]:=Integrate[ddelp1[w,t],{w,-x0/2,x0/2}];
II2[w_,t_]:=Integrate[ddelp2[w,t],{w,-x0/2,x0/2}];
II3[w_,t_]:=Integrate[ddelp3[w,t],{w,-x0/2,x0/2}];
II4[w_,t_]:=Integrate[ddelp4[w,t],{w,-x0/2,x0/2}];II5[w_,t_]:=Integrate[ddelp5[w,t],{w,-
x0/2,x0/2}];

(*Print[Style["r1 = " , Bold, Blue],r1, Style["
Ar1 = " , Bold, Blue],Ar1, Style["
u1[w,t] = "  , Bold, Blue], u1[w,t],Style["
v1[w,t] = "  , Bold, Blue], v1[w,t]];
Print[Style["r2 = " , Bold, Blue],r2, Style["
Ar2 = " , Bold, Blue],Ar2, Style["
u2[w,t] = "  , Bold, Blue], u2[w,t],Style["
v2[w,t] = "  , Bold, Blue], v2[w,t]];
Print[Style["r3 = " , Bold, Blue],r3, Style["
Ar3 = " , Bold, Blue],Ar3, Style["
u3[w,t] = "  , Bold, Blue], u3[w,t],Style["
v3[w,t] = "  , Bold, Blue], v3[w,t]];
Print[Style["Excess Carrier Profile (SRV=100) = ", Bold, Blue],ddelp5[w,t]];
Print[Style["I1 = ", Bold, Blue], II1[w,t]];
```

```
Print[Style["I2 = ", Bold, Blue], II2[w,t]];
Print[Style["I3 = ", Bold, Blue], II3[w,t]];
Print[Style["I4 = ", Bold, Blue], II4[w,t]];Print[Style["I5 = ", Bold, Blue], II5[w,t]];*)
pp=1/II5[w,0];

LogPlot[pp*II5[w,t],{t,0,2000*^-9},Frame->True,FrameLabel->{"Time - t
[s]","Normalized PLI [arbitrary units]"},
 PlotLabel->"Time dependent PLI for 0.5µm thick
  absorber layer with SRV=100 cm/s
  "]
Print[Style["τeff = ", Bold, Blue], ((1/tn)+rr1^2*Dn)^(-1)];

p=1/I5[w,0];

(*Print[Style["Excess Carrier Profile (SRV=1000) = ", Bold, Blue],delp5[w,t]];
Print[Style["I1 = ", Bold, Blue], I1[w,t]];
Print[Style["I2 = ", Bold, Blue], I2[w,t]];
Print[Style["I3 = ", Bold, Blue], I3[w,t]];
Print[Style["I4 = ", Bold, Blue], I4[w,t]];Print[Style["I5 = ", Bold, Blue], I5[w,t]];*)
LogPlot[p*I5[w,t],{t,0,2000*^-9},Frame->True,FrameLabel->{"Time - t
[s]","Normalized PLI [arbitrary units]"},
 PlotLabel->"Time dependent PLI for 0.5µm thick
  absorber layer with SRV=1000 cm/s
  "]
Print[Style["τeff = ", Bold, Blue], ((1/tn)+r1^2*Dn)^(-1)];
```

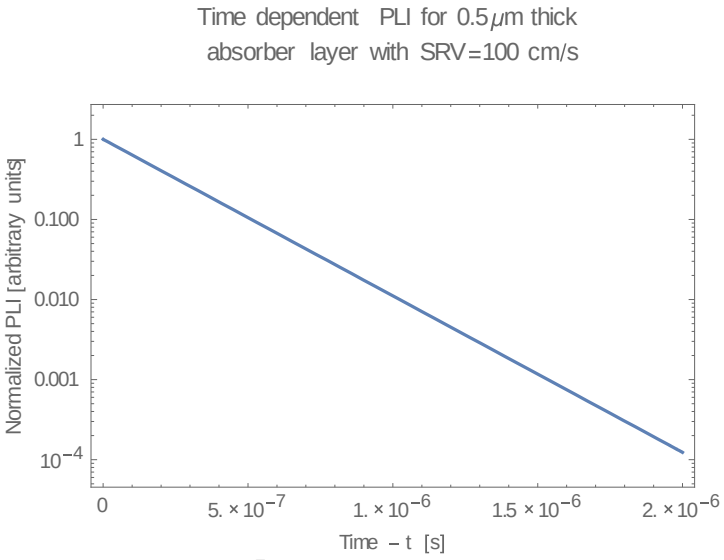

τeff = $2.22229*10^{-7}$

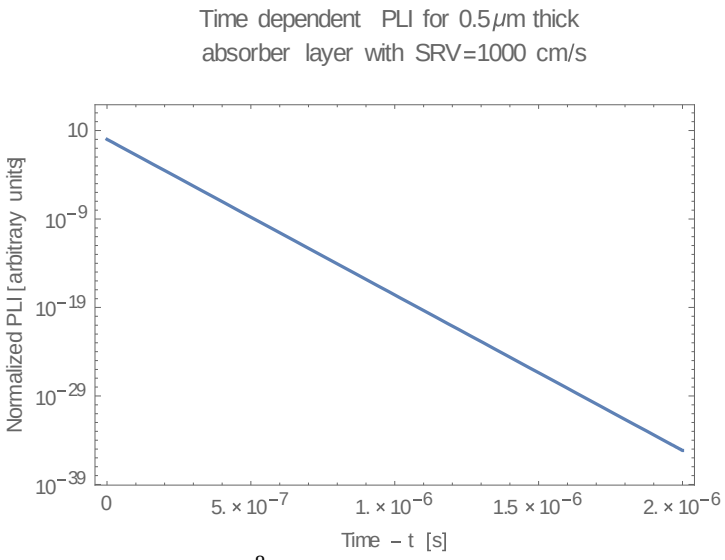

τeff = 2.46992*10^{-8}

APPENDIX G: STANDARD OPERATING PROCEDURE FOR PHOTOLUMINESCENCE INTENSITY MEASUREMENTS.

Photoluminescence Intensity (PLI) measurement SOP

1. First, check the circuit breaker to ensure that the MPL laser and Chiller breakers are on

Figure 1: Circuit breaker indicating the appropriate circuits that must be on

2. Check the chiller water level and add water from nearby Ozarka gallon bottle.
3. Ensure that the LED on the LIGHT button is off before turning on the COHERENT INNOVA 300 laser emission controller.

First, you need to check the laser beam. To do this, move the beam aperture shown below all the way towards the beam path

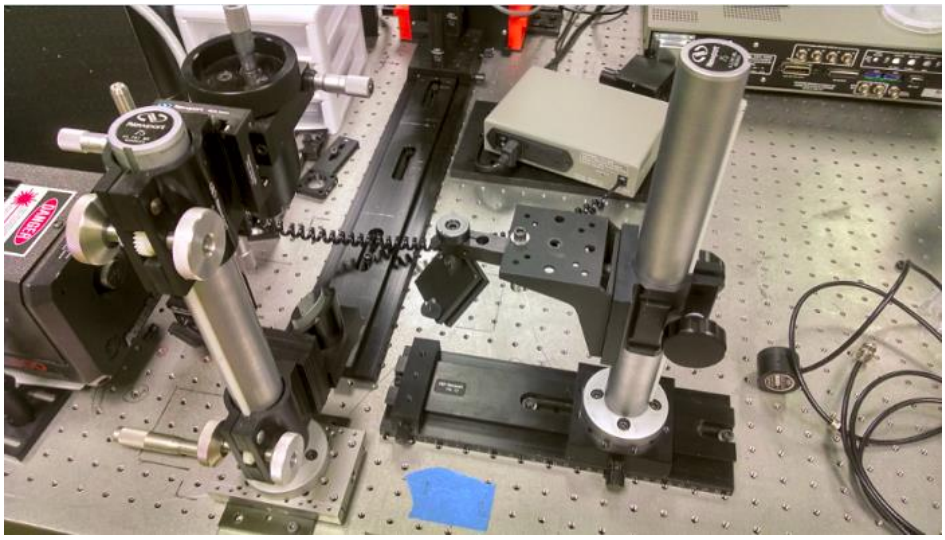

You will know if you have done this correctly when the beam appears on the door. If it doesn't, check to make sure that there is nothing blocking the beam path. Now, you can use the two knobs on the back of the COHERENT INNOVA 300 laser shown below to adjust the beam.

Sweep the lower knob through its entire range and try to center the laser within this range.
The upper knob allows you to adjust the symmetry of the beam. You want the beam to be as circularly symmetric as possible.

For PLI measurements, you want to operate around 30.0Amps and 0.210W. You can adjust the current by pressing the up and down arrows on the laser controller. Once the current is around 30.0A, press the LIGHT button. The LED above it should turn on. This feature allows you to set the power output of the laser and allow the current to vary. Set the power to 0.210W. If you do not get the desired power output in the range of 30-40A, then you probably need to adjust the laser beam as described above again.

4. Next, power on the ORIEL instruments Filter Wheel Controllers using the switch located on the back of the boxes. See picture below

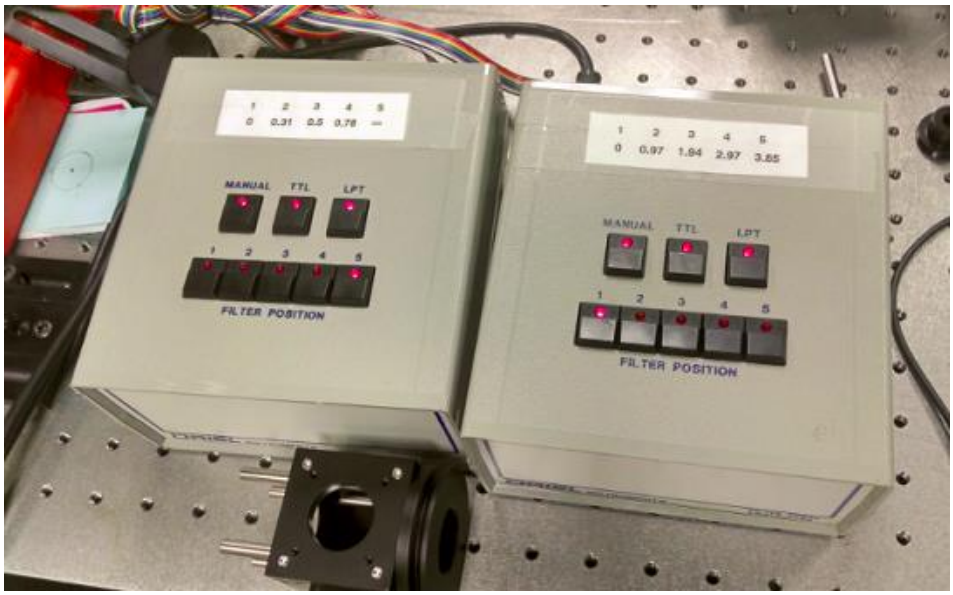

These filters allow the user to reduce the intensity of the incoming laser by applying different Neutral Density Filters to the incoming beam. Each filter position is labeled with its Neutral density. The following expressions relate the optical density, d, with the incident intensity, I_0, and the intensity after the filter.

$$d = -log\frac{I}{I_0}$$

$$Fractional\ transmittance\ \frac{I}{I_0} = 10^{-d}$$

Now select the desired filters. To start, use Filter Position 1 on both devices (this is called ND 0).

5. Next turn on the ThorLabs Power monitor shown below

This device allows the user to check the laser intensity at the stage. The device should read roughly 73mW with Filter Position 1 selected on both devices at the stage.

6. At this point, the laser should be exiting the microscope from the objective. Place one of the calibration samples on the stage. Carefully remove the Si Detector on top of the microscope and let it hang as shown.

Now, laser light is exiting the top of the microscope. Look up. You should see the beam hitting the circle on the ceiling as shown below.

When the beam fills the inner circle, the radius of the spot to be measured is 90μm. If the beam is not centered, you will have to adjust the beam using the knobs indicated below on the beam path aperture**. Checking the spot size for every sample placed on the stage is one of the most crucial steps for accurate measurements**. When checking the spot size, always ensure that the Si Detector is off before removing it from the microscope.

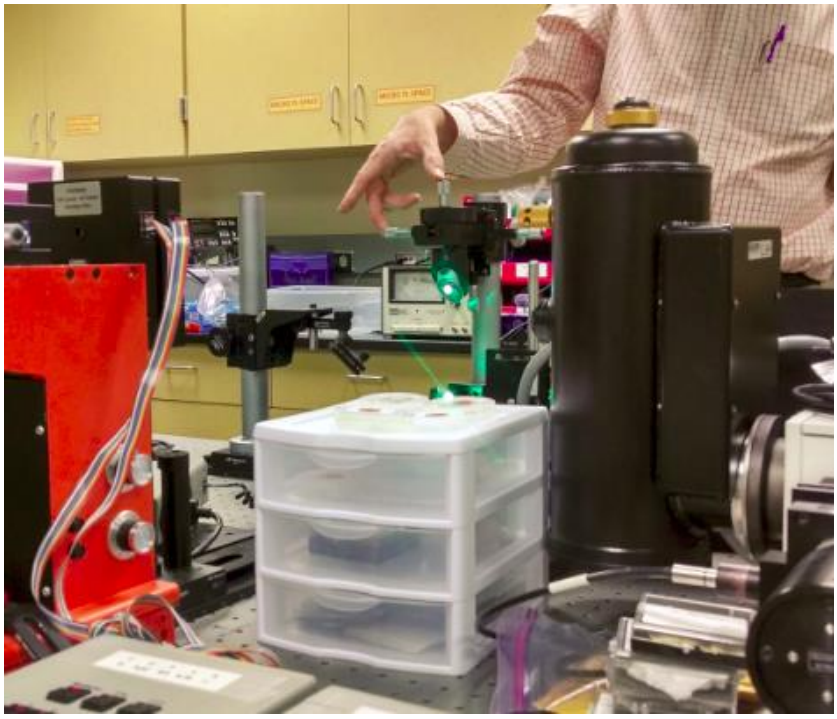

7. Next turn on the Thorlab Si Amplified Detector located on top of the microscope shown below. It is important to turn on the DC adaptor first, then the detector, otherwise you risk damaging the detector.

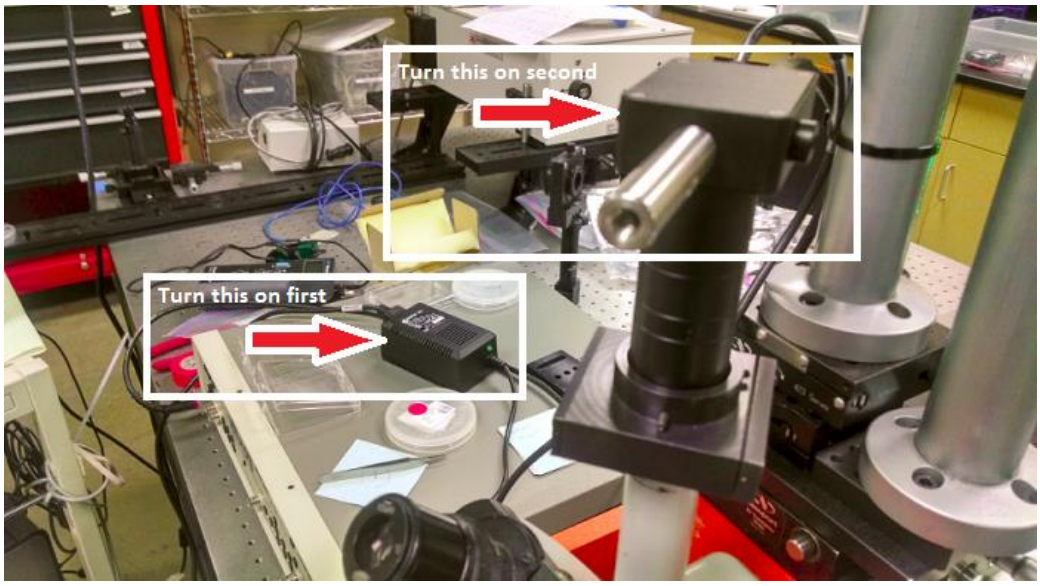

To adjust the dB at which the amplifier is operating, the location of the hole on the dial indicates which gain it is operating at. See figure below

Here, the Si Detector is set to 0dB.

8. Next, turn on the Stanford Research Systems Model SR540 Chopper Controller

This device controls the reference frequency for the SR510 Lock-in Amplifier. Due to the electronics and lights in the room, optical measurements will pick up large noise spikes at 60Hz and 120Hz. Because of this, the reference frequency should not be a multiple of these values.

9. Now turn on the Stanford Research Systems SR510 Lock-in Amplifier

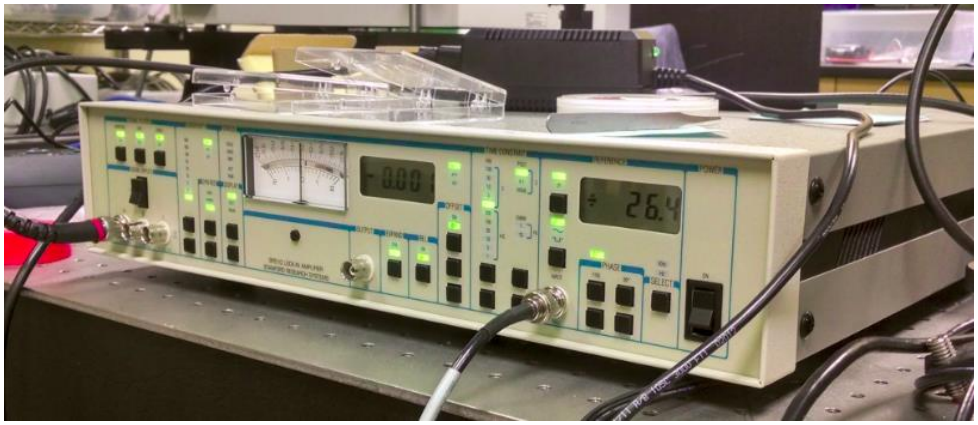

The bottom left-most corner of this display controls the measurement mode.

A – Voltage Mode
A-B – Voltage Mode with background subtracted
I – Current Mode.

For our purposes, we work in A – Voltage Mode. Directly above this is the signal filter controls.
All filters, BANDPASS, LINE, and LINEx2, should have IN highlighted. In the SENSITIVITY section of the display, you should start out in the 1mV range. In the TIME CONSTANT section of the display, you should start with the PRE and POST delays set to 1s. In the REFERENCE section of the display, with Hz selected, the device should display the reference frequency from the SR540 Chopper Control. The frequencies on the Lock-In Amplifier and the Chopper should be within 1 or 2 Hz of each other and the frequency displayed on the Lock-In Amplifier should be stable.

10. At this point, we are ready for calibration. With a calibration sample on the stage, select DEG in the REFERENCE section of the display on the Lock-In Amplifier using the button marked SELECT. The right most display will display an angle and the left display will show a voltage reading. Under the PHASE section of the display, hit the button marked 90°. This will shift the angle displayed by 90° and show a different voltage display. Using the buttons marked FINE, adjust the angle so that the voltage reading is as close to zero as possible. There are two calibration samples that can be used. The first looks like

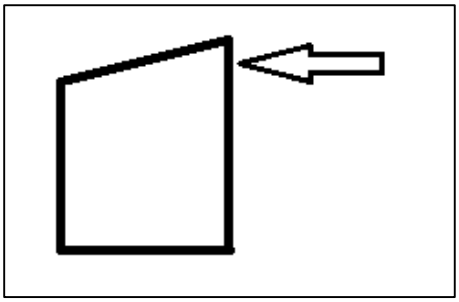

In the corner of the sample indicated, you should get a reading of about 0.6mV. The second sample looks like

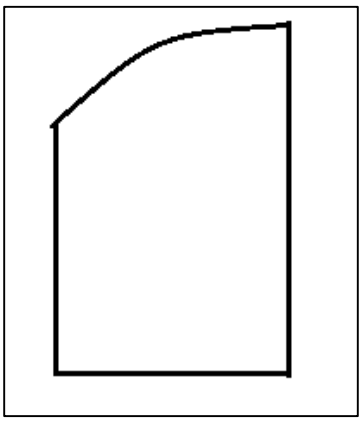

This sample is much bigger than the first and in the center should give a reading between 0.495mV and 0.500mV so long as you avoid the dirty parts. In order to achieve these readings you may have to adjust the stage height and the beam location if they have not already been adjusted. If the beam is in the proper place and you still do not achieve the correct readings, try adjusting the power of the laser on the COHERENT INNOVA 300 laser emission controller until the desired reading is obtained. Once these readings have been obtained, then we are ready to start measuring.

11. Now, with the sample to be measured on the stage, first check that the beam is still centered in the circle on the ceiling (turn off Si Detector before removing from the microscope). **This is one of the most important steps in obtaining accurate readings**. Try not to expose the sample to the full intensity of the laser (Filter Position 1 on both boxes) for very long as this could damage the sample if it is unstable. A good practice to minimize damage to the sample is to use the Filter marked ∞ between measurements and when you are not checking the beam location and size. This filter is basically a barrier that blocks all laser light from entering the microscope.

    If the beam is off center, then use ND 1.0 (Filter position 1 on the box on the left and Filter position 2 on the box on the right) to center the beam. This is less damaging to the sample and helps you to see if the beam is centered. Then use ND 0 to make sure the beam size is correct. Once the beam is centered and the appropriate size, cycle through all of the Optical Density Filters and record the filter, the Lock-In Amplifier reading, the Lock-In Amplifier scale (sensitivity), the Gain on the Si Detector, and the Time Constants used for each reading. As you increase the Optical Density, less light is coming through the laser so you will have to adjust the sensitivity as you go. Start with the Si Detector Gain set to 0dB, but if a good reading cannot be obtained, switch it to 70dB.

12. Once all measurements have been taken, the shutdown procedure is the reverse of the start up procedure.

REFERENCES

[1] www.ise.fraunhofer.de, *Fraunhofer Institute for Solar Energy Systems ISE* (2014).

[2] S. Esterly, *2013 Renewable Energy Data Book (Book), NREL (National Renewable Energy Laboratory)* (2013).

[3] SunShot U.S. Department of Energy, U.S. Dep. Energy 69 (2012).

[4] C.H. Swartz, M. Edirisooriya, E.G. LeBlanc, O.C. Noriega, P. a. R.D. Jayathilaka, O.S. Ogedengbe, B.L. Hancock, M. Holtz, T.H. Myers, and K.N. Zaunbrecher, Appl. Phys. Lett. **105**, 222107 (2014).

[5] W. Shockley and H.J. Queisser, J. Appl. Phys. **32**, 510 (1961).

[6] A. Luque and S. Hegedus, *Handbook of Photovoltaic Science and Engineering* (2011).

[7] G. Fonthal, L. Tirado-Mejía, J.I. Marín-Hurtado, H. Ariza-Calderón, and J.G. Mendoza-Alvarez, J. Phys. Chem. Solids **61**, 579 (2000).

[8] J. Wang and M. Isshiki, *Springer Handbook of Electronic and Photonic Materials* (2007).

[9] Z. Fang, X.C. Wang, H.C. Wu, C.Z. Zhao, Z. Fang, X.C. Wang, H.C. Wu, and C.Z. Zhao, Int. J. Photoenergy **2011**, 1 (2011).

[10] B.L. Williams, J.D. Major, L. Bowen, L. Phillips, G. Zoppi, I. Forbes, and K. Durose, Sol. Energy Mater. Sol. Cells **124**, 31 (2014).

[11] Z.I. Alferov, Rev. Mod. Phys. **73**, 767 (2001).

[12] D. Griffiths and R. College, *Introduction to Electrodynamics* (1999).

[13] D. Gonçalves and E.A. Irene, Quim. Nova **25**, 794 (2002).

[14] E. Hecht, *Optics* (Addison-Wesley, 2002).

[15] F. Wooten, *Optical Properties of Solids* (Academic Press, 1972).

[16] J.D. Jackson, *Classical Electrodynamics Third Edition* (1999).

[17] G.B. Arfken, H.J. Weber, and F.E. Harris, *Mathematical Methods for Physicists, Sixth Edition: A Comprehensive Guide* (2005).

[18] D. Poelman and J. Vennik, J. Phys. D. Appl. Phys. **21**, 1004 (1988).

[19] J. Chu and A. Sher, *Physics and Properties of Narrow Gap Semiconductors* (Springer Science & Business Media, 2007).

[20] A. Waag, H. Heinke, S. Scholl, C.R. Becker, and G. Landwehr, J. Cryst. Growth **131**, 607 (1993).

[21] C. Betthausen, Spin Effects in High- and Low-Field Magnetotransport Experiments in Semimagnetic Cd 1 − X Mn X Te Heterostructures, 2012.

[22] O. Martinez, Mater. Chem. Phys. **132**, 559 (2012).

[23] S. Adachi, *Properties of Group-IV, III-V and II-VI Semiconductors* (John Wiley & Sons, 2005).

[24] S.W. Paddock, Biotechniques **27**, 992 (1999).

[25] J. Chai, O.C. Noriega, a. Dedigama, J.J. Kim, a. a. Savage, K. Doyle, C. Smith, N. Chau, J. Pena, J.H. Dinan, D.J. Smith, and T.H. Myers, J. Electron. Mater. **42**, 3090 (2013).

[26] R.H. Webb, Reports Prog. Phys. **59**, 427 (1996).

[27] D.W. Piston, Biol. Bull. **195**, 1 (1998).

[28] M.D. Abràmoff, P.J. Magalhães, and S.J. Ram, Biophotonics Int. **11**, 36 (2004).

[29] J.A. Conchello and J.W. Lichtman, Nat Methods **2**, 920 (2005).

[30] J. Matthews, *Epitaxial Growth* (Academic Press, New York, 1975).

[31] M. Wahl (PicoQuant GmbH), Tech. Note 1 (2014).

[32] R.K. Ahrenkiel, *Minority Carriers In III-V Semiconductors: Physics and Applications* (Elsevier, 1993).

[33] J.P. McKelvey, *Solid State and Semiconductor Physics* (Krieger Publishing Company, 1966).

[34] M.E. Dailley, S.L. Shaw, J.R. Swedlow, P.D. Andrews, M.F. Langhorst, and M.W. Davidson, (n.d.).